Planar Electromagnetic Bandgap Structures and Applications

Md. Nurunnabi Mollah

School of Electrical & Electronic Engineering

A thesis submitted to the Nanyang Technological University
in fulfillment of the requirement for the degree of
Doctor of Philosophy

2005

Statement of Originality

I hereby certify that the content of this thesis is the result of work done by me and has not been submitted for a higher degree to any other University or Institution.

Date

Md. Nurunnabi Mollah

Acknowledgments

It gives me a lot pleasure to convey my heartfelt gratitude to Assistant Professor Dr. Nemai C Karmakar for his continuous and constant guidance throughout my research work toward Ph.D degree. I received continuous motivation and suggestions from him regularly. In my academic life, I am proud of having such a dynamic and punctual supervisor. His contributions and encouragements I cannot repay. After submission of my first draft to the university I missed him as he left NTU. Though he is now in Australia, I have received his continuous guidance. I would also like to appreciate Professor Dr. Yoon Soon Fatt, Vice-Dean (Research) and Professor Dr. Koh Soo Ngee, Division Head (communication engineering) for graciously giving of their time during candidature confirmation. I will remain grateful to them forever for their unbelievable support throughout my candidature.
I am very grateful to school of EEE due to giving me an excellent supervisor Associate Professor Jeffrey Shiang Fu in absence of Assistant Professor Nemai C Karmakar for me. I am highly pleased with him for his supports in all aspects. His sweet behavior has really provided a mental peace during my thesis corrections.

I am very grateful to Associate Professor Law Choi Look, Director, Positioning and Wireless Technology Centre (PWTC) for giving the facilities to support my research.

The completion of the directed research to obtain Ph.D degree is the outcome of hard work, perseverance, and the continued support of family, friends, and my fellow comrades-in-arms. Very special and cordial thanks go to Associate

Professor Hessan Quazi of Nanyang Business School (NBS) for his continuous support during my whole candidature. Mrs. Farida Quazi (the wife of Associate professor Hessan Quazi) took the part of my mother in all aspects during my whole candidature. I will remain grateful to them forever. I remember the affection, love and respect that I constantly received from the Bangladeshi NTU professors community. My special thanks goes to my mother-in-law Nasima Ara Begum who continuously motivated me from overseas for my degree. The author feels very deeply his late parents who always inspired him for higher education when they were alive in the world. Throughout my long journey simple word seems inadequate to express my gratitude to my brother G. Mowla and my beloved bhabi Mrs. Lima (G. Mowla's wife) to support and to guide me to come up to this level.

I will remain grateful to Prof. Dr. Koh Soo Ngee and Prof. Dr. Yoon Soon Fatt who extended their helping hands for candidature extensions and they became very generous to my ill health circumstances. I specially would like to thank Dr. Peter Yeo, Director of Gethin Jhones Clinic, NTU branch who helped me wholeheartedly regarding my health in different critical situations.

My thanks go to all technicians and staff of Communication Research Lab and Positioning and Wireless Technology Center (PWTC) for their assistance especially regarding fabrication and measurements for the prototype microstrip transmission lines, filters and antennas.

I convey my deepest appreciation to my spouse Asma Niger for her constant encouragements, unwavering devotion and deep patience with unconditional love

to complete my PhD degree. Endless affection goes to my daughter Marzan and son Raiyan for their patience who really missed me during their boyhood for the sake of my PhD degree.

Nanyang Technological University
School of Electrical and Electronic Engineering,
PhD Dissertation

Planar Electromagnetic Bandgap Structures and Applications

Student: Md. Nurunnabi Mollah Supervisor: Dr. Jeffrey S. Fu.

March 2005

Summary

With the emergence of novel wireless technologies, the demands for larger bandwidth, high efficiency and high capacity RF and microwave devices have been growing tremendously. To satisfy the demand novel materials, new processing techniques and refinement of existing devices have been evolving. Using electromagnetic bandgap (EBG) is a new technology to improve the performances of existing RF active and passive devices. EBG structures (EBGSs) are periodic structures, which exhibit distinct passband and stopband characteristics. The passband can be used as phase shifters and slow wave structures. The stopband characteristics can be used to suppress surface waves in dielectric media. Due to these unique properties, EBGSs find potential applications in many active and passive RF and microwave devices including antennas, filters, amplifiers and oscillators. Recently, the dispersion properties in passband of EBGSs are used in the phased array antennas for wide angle beam steering. Among various EBG configurations, planar EBGSs become most popular due to their low profile, ease of fabrication and integration with monolithic microwave integrated circuits (MMICs).

The thesis concerns the planar EBG structures in the forms of conventional circular and rectangular photonic bandgap structures (PBGSs) and defected ground structures (DGSs). Novel PBGSs in the form of non-uniform Binomial and *Chebyshev* distributions of unit PBG cells have been proposed. This novel PBGSs yield ripple free passband and wide stopband properties, which are very useful to suppress higher order harmonics in the bandpass filters. Next the chirped PBGSs are investigated that yield better passband return loss, low ripples and wider stopband than those for conventional PBGSs as well as non-uniform PBGSs mentioned earlier.

The parametric study of dumbbell shaped DGSs has been conducted with the gap width and length and the size of dumbbell slots. Three novel designs are proposed: non-uniform dumbbell shaped DGSs with *Chebyshev* distribution, hybrid DGS and PBG and modified hybrid DGS and PBG configurations. The novel designs outperform the conventional DGSs reported in the literature. The DGSs yield perfect LPF responses with negligible passband ripples and extremely wide stopband. The modified hybrid DGS and PBG configuration yields dual stopbands that can be used as a dual stopband filter.

The novel design are used in asymmetric coupled line bandpass filters, aperture coupled single band and dual-band patch antennas and finally in 4-element conventional and reconfigurable phased array antennas. For filters, PBGSs suppress second and third harmonics by about 40 dB. A comprehensive investigation of the number, filling factor and position of the PBGS under the filter has been conducted. The frequency response of the filter has been observed. This investigation is novel and illustrates the significance of PBGSs in suppression of higher order harmonics of the bandpass filters. It has been found that non-uniform distribution of PBGSs is more effective to suppress higher order harmonics than the conventional uniform PBGSs.

DGSs are very effective for simultaneous suppression of both 2^{nd} and 3^{rd} harmonics due to their very wide stopband performances. This phenomenon of DGSs has been demonstrated in various designs of asymmetric coupled line bandpass filters.

Finally, the passband phase properties of the PBG and DGS have been investigated. The comprehensive investigations of relative phase delays of PBGS and DGS assisted microstrip transmission lines have been performed. Such investigation is not found in the open literature. It is observed that DGSs yield much larger phase delay compared to a similar size PBG structure. Therefore, DGS assisted feed network can scan the beam over a wide angle. After thorough and satisfactory investigation of phase delays for PBGSs and DGSs, phased array theory is studied. The required phase delays for a 4-element phased array are calculated based on the element spacing and number of elements. A wide beam scanning up to approximately 60° is achieved with 0-8-16-24 DGS assisted corporate feed network for the 4-element patch antenna array. So far such wide angle scanning using DGS assisted beamforming network has not been reported in the open literature.

The recent demand for multi-band operation from a single antenna aperture has initiated reconfiguration antenna array development. To respond to the demand finally a reconfigurable phased array antenna has been proposed. The 4-element array is connected to 4 dummy patches via PIN diode switches. The effective length of the patch has been changed with the bias control voltages of the diodes. Theoretical simulation shows that frequency hopping and beam scanning at both frequencies are possible. The reconfigurable phased array antenna can work at 5.6 GHz and 8.65 GHz. At both frequencies beam scanning angles up to approximately 30° has been achieved. This finding is very significant for future multi-mission applications where compact and low cost designs are envisaged.

Table of Contents

List of Figures

List of Tables

List of Abbreviations

SAR	**Synthetic aperture radar**
AMTI	**Airborne moving target indication**
GMTI	**Ground moving target indication**
UAV	**Unmanned aerial vehicles**
FOPEN	**Foliage penetration**
FF	**Filling factor**
PBG	**Photonic bandgap**
PBGSs	**Photonic bandgap structures**
UPBGS	**Uniform PBGS**
B-PBGSs	**Binomially distributed PBGSs**
BPF	**Bandpass filter**
B-BPF	**B-PBGS assisted BPF**
PCB	**Printed circuit board**
PAE	**Power added efficiency**
DGS	**Defected ground structure**
TEM	**Transverse Electric and Magnetic**
CB-CPW	**Conductor backed-Coplanar waveguide**
MEMS	**Microelectromechanical system**
TM	**Transverse magnetic**
TE	**Transverse electric**
UC-PBG	**Uniplanar compact-photonic bandgap**
MIC	**Microwave integrated circuit**
MMIC	**Microwave monolithic integrated circuit**
EC	**Electromagnetic crystal**
EM	**Electromagnetic**
EBG	**Electromagnetic bandgap**
EBGS	**Electromagnetic bandgap structure**
PC	**Photonic crystal**
1-D, 2-D, 3-D	**One dimensional, two dimensional, three dimensional**
RF	**Radio frequency**
BW	**Bandwidth**
FET	**Field effect transistor**
VLSI	**Very large scale integration**
HRL	**Huges research lab**
RPM	**Reconfigurable patch module**
GARF	**General adaptive reconfigurable feed**
dB	**Decibel**
BW	**Bandwidth**
ACPA	**Aperture coupled patch antenna**
VSAT	**Very small aperture terminal**
CBS	**Conductor-backed slot**

LED	**Light emitting diode**
LPF	**Lowpass filter**
LO	**Local oscillator**
GPS	**Global positioning system**
HF	**High frequency**
VHF	**Very high frequency**
VNA	**Vector network analyzer**
MSAT	**Mobile satellite**
3-G	**Third generation**
HMIC	**Hybrid microwave integrated circuit**
MMIC	**Monolithic microwave integrated circuit**

List of Major Symbols

ε	Dielectric constant
γ	Propagation constant
β	Phase Constant
π	Pi = 3.1415927
ω	Angular frequency
k	Wave number (/m)

Chapter 1 Introduction

1.1 Planar Photonic Bandgap Structures (PBGSs)

Planar PBGSs are a class of periodic dielectrics, which are photonic analogs of the semiconductors. Electromagnetic (EM) waves behave in photonic substrates as electrons behave in semiconductors. Due to these characteristic PBGSs are known as EM bandgap structures (EBGSs). PBGSs exhibit wide band-pass and band-rejection properties at microwave and millimeter-wave frequencies and have offered tremendous applications in active and passive devices [1]-[12]. Introducing periodic perturbation such as dielectric rods, holes and patterns in waveguides and microstrip substrates forms PBG materials. While various configurations have been proposed in literature, only the planar etched PBG configurations are attracted much interest due to their ease of fabrication and integration with other circuits with photolithographic processes. The passband of PBGSs is used as slow wave medium that is useful for compact design. On the other hand the stopband is used to suppress the surface wave, leakage and spurious transmission [13] - [17]. Due to these unique properties of PBG structures, they find potential application in filter, antennas, waveguides, phased arrays and many other microwave devices and components.

In the conventional phased array antenna, solid-state phase shifters are used. They are expensive and the volume of the circuit increases with the number of switches. For beam steering [18] purpose PBGSs can play an important role. Thus PBG engineered structures are useful structures in microwave engineering. Inclusion of

PBGSs provides many advantageous features at a time such as compactness, surface wave suppression and beam steering capabilities in the design of a PBG assisted reconfigurable phased array antenna. Therefore attention will be paid to PBG designs in significant portions of this thesis. They will be implemented in antennas, filters, phased arrays and reconfigurable phased arrays.

Besides PBG structures, defected ground structures (DGSs) [19] will be focused. DGS differs from the PBG structures both in configuration and in principle of operations. DGSs are formed from 2-D regular square patterned PBGSs with narrow vertical slot connections. They are known as dumbbell shaped DGSs. In principle, PBGSs follow Bragg's condition [20] to generate the stopband. On the other hand the behavior of DGSs is controlled by current path around the DGS element. Both DGSs and PBGSs are termed as EBGSs. DGSs will be applied in second and third harmonics suppression of bandpass filter (BPF). Finally regular PBGSs and DGSs are applied in phased arrays. Additionally to these, reconfigurable phased array antennas are investigated and PBGSs in phase steering are implemented. Following sections describe the importance of reconfigurable microstrip antennas.

1.2 PBG Assisted Reconfigurable Microstrip Antenna

With the emergence of new technologies in wireless communications and their desired applications on a single platform, a single antenna aperture is required to perform multi-tasks at multiple frequency bands. The multi-mission role of a single aperture provides attractive features in technological point of view to afford an easier and charming scenario in the practical issues. The demand of the age has enforced the technology to be lighter, attractive and more compact to create a

special pace for itself to simplify our daily life. Multi-mission role has paved a new era in communication engineering. The switch over between tasks and frequency spectra must be dynamic such that high-speed communications could be established without any undesired delay and loss of information. A reconfigurable phased array antenna can only satisfy such specification requirements. In a reconfigurable phased array, the same antenna aperture can dynamically reconfigure itself for multiple frequency bands to perform various tasks.

To have a clear idea about multi mission role of a single aperture, a space based-radar system is a good example to enlighten its powerful vision. Here the satellite antenna can be dynamically reconfigured to provide synthetic aperture radar (SAR) at X-band, communications at L-band, airborne and ground moving target indication (AMTI/GMTI) at S-band. Another example is the Global Hawk unmanned aerial vehicles (UAV) where the antenna aperture provides communications from VHF to K-band, foliage penetration (FOPEN) radar from VHF to L-band and SAR at X-band. It is desirable to accomplish these functions with a single antenna. So if the antenna can be dynamically reconfigured, the multi functions can easily be achieved from the same antenna.

The switching over sub-bands provides multi-band facilities of an antenna that should have also the phase scanning capabilities to make it reconfigurable phased array antenna. These antennas may be electronically steerable [21], mechanically steerable [22] and electro-mechanically steerable [23]. The proposed antenna is an electronically steerable antenna. Electronically steered phased arrays are potential candidates to find many applications which include reconfigurable wireless and satellite communications networks, smart weapons, automobiles, airplanes and

radars. Beam steering is obtained with the linear variation of the phase between adjacent elements of an antenna array [24]. Electronic phase shifters obtain the phase variation. The number of phase shifters increases with the number of antenna elements in an array. So the use of huge number of phase shifters makes the device very bulky, expensive and unpleasant. For the proposed reconfigurable phased arrays, the microstrip antenna is considered as basic element and the array will be realized on a novel photonic bandgap (PBG) structured substrate.

Among various types of antennas to perform multi-band operations, microstrip patch antennas have been chosen. Microstrip antennas are widely used in high-performance aircraft, satellite and missile applications and spacecraft where size, weight, cost, performance, ease of installation and aerodynamic profile are constraints. They find applications in broad ranges of military, commercial and government applications due to their advantageous features such as lightweight, low profile, low cost, conformable to planar and nonplanar surfaces, compatible with hybrid microwave integrated circuit (HMIC), monolithic microwave integrated circuits (MMICs) and micro machined technology. They are very simple in design, mechanically robust when mounted on rigid surfaces and fabrication can easily be accomplished using modern printed-circuit technology. They are also very versatile in terms of resonant frequency, polarization, pattern and impedance under the consideration of a particular shape and mode selection.

Despite these dimensional advantages and versatilities microstrip patch antennas suffer from low gain, low power, low efficiency, narrow bandwidth, poor scan performance, spurious feed radiation and poor polarization purity. The crucial limitation is the inherent narrow bandwidth that is typically only a fraction of a

percent or at most a few percent. Only in limited applications, the narrow bandwidth is desirable such as government security systems. Thick substrates can be used to increase bandwidth (up to about 35 percent) and efficiency (up to 90 percent) [25]. However thick substrates stimulate surface wave propagations [26] that are not desirable as they do not couple with the space waves, rather they extract power from the total available power of direct radiation. They travel within the substrate and they are scattered at bends and surface discontinuities, such as the truncation of the dielectric and finite ground plane. These diffracted surface waves drastically degrade antenna efficiency; distort radiation patterns and polarization characteristics. The surface wave propagation is a crucial issue in microwave engineering that drastically degrades the performance of microwave devices and components. The available method of suppressing the surface wave is to use cavities [27]-[28].

The compact design is now the demand of the age. Substrates with high dielectric permittivity are potential candidate to minimize the size of the elements and suitable for establishing tightly bound fields to minimize undesired radiation and coupling. But the dielectric loss is higher and surface wave also propagates within the substrate. So the design with the substrates having higher value of dielectric constants is desirable for compact design having a management of enhancing the other performances of an antenna such as bandwidth (BW), return loss, gain and smoother radiation patterns [6], [29] etc.

The necessities of stacking for bandwidth enhancement and cavities for surface wave suppression in patch antennas can be alleviated by using PBGSs. PBGSs also ensure better performances of antennas in terms of BW, return loss, gain and

smoother pattern [5]. The compactness originates from higher valued dielectric substrates as well as from PBGSs.

PBGSs can improve the performance of microwave devices and components. PBG structured reconfigurable patch antenna yields improved performance that is highly demanding to mitigate the various requirements of important applications in our daily life. Modern age is dependent on the faster communications and the communications are enhanced with efficient antennas. Microstrip patch antennas have been replacing conventional bulky antennas in many commercial and military applications. Therefore the novel PBG assisted reconfigurable phased array antennas can easily find their potential applications [30]-[31] in the following areas:

- **Satellite Communications**

In the satellite communications the uplink and downlink operations are accomplished in different frequencies. So the dual frequency operations can be done with the application of reconfigurable antenna on a single-board.

- **Mobile Satellite (MSAT) Communications**

In the mobile satellite communications, the shaping of the beam-pattern and beam squinting against the obstacles to communicate with the satellites is also important issue. In this application PBG assisted phased array antenna is very good options.

- **Fleet Management**

Mobile satellite communications are used to monitor the large fleets of land vehicles, aircraft or ships, where reconfigurable phased array antennas play vital role.

- **Emergency Services**

Good communications irrespective of any terrain are only possible by mobile satellite communications supported by phased array antenna. During the period of emergency of a life, telemedicine facility can be available promptly by setting the quick communications. In such a situation PBG assisted wideband phased array antenna can find good application for large data of image transfer through satellites.

- **Civil Aviation and Aeronautical Services**

Presently HF/VHF radio communications are being used in these services. Considering the importance of service these types of radio communications may be replaced by GPS or MSAT.

- **Resource Development**

MSAT and GPS can be used for mining automation, oil and gas exploration companies, agriculture, and construction farms. In all cases headquarters can be communicated continuously by the mobile units through reconfigurable phased arrays.

- **3-G Wireless Communications**

3-G communication system is now available. In a handset all the useful activities are coming. But the different applications such as mobile communications, internet facilities, fax and data transferring need different frequency bands. So the different sub-bands provided by the reconfigurable antenna can fulfill all the requirements of the 3-G communication systems.

- **Manned Vehicles**

Positioning is an important research area to locate the objects and mapping certain geographic location. Manned vehicles can select the desired shortest and easiest path to reach the destination, which is covered in GPS application. In the long way the passenger can enjoy with direct broadcasting (DVS) TV using another bands of the same antenna aperture.

- **Unmanned Aerial Vehicles (UAV)**

In the global hawk UAV, the antenna aperture provides different communications in L, X and K-band in different applications.

In many ways reconfigurable phased array antennas are very much useful everywhere, every time showing their endless use in the whole world. The world has transformed to a global village due to unbelievable progress in communications where antennas play a very significant role. PBG structures enhance the performance of the antenna as well as all other microwave devices and components.

1.3 Significance of PBGS

PBG engineered structures may have different forms such as bumpy surface, corrugated surface, metal pad or high-impedance surface and planar PBG structures. Normally the ground plane is perturbed by PBGSs with different shape and different lattice structures. The shape may be uniform and non-uniform circular, square, rectangular, triangular patterned and the structures are named on the basis of the grid arrangement such as square, rectangular, triangular and honeycomb etc. Different shapes and sizes of PBGSs provide different S-parameter performances. The location of the PBG elements under the microstrip transmission line greatly influences the performance of the transmission line. However one of their main significances is their ability to generate stopband performance. Stopband is very useful to improve the performance of the microwave devices and components. For an example, to suppress of any unwanted transmission of signal the center of the stopband is chosen to be equal to the center of the unwanted signal. This concept is highly preferred for harmonic suppression of filter. For the improvement of antenna performance the PBG element is designed at the frequency of operation of the antenna. For the beam steering purpose the frequency of operation is chosen so that it remains within the passband of transmission line.

Another significance of PBGSs is their ability to provide slow-wave properties. For the compact design this property is used. Practically PBGSs can be used in amplifiers, mixers, filters, waveguides, antennas and many other devices to improve their performances.

1.4 Significance of DGS

The cell-separation (inter-element spacing) of conventional PBGS is approximately half-wavelength. So they need more space very often when they are designed at low frequency. Their integration with other circuits becomes difficult due to space limitation. Though it provides compactness than the normal designs, yet for more compactness PBGSs are not suitable candidate. Under such situation a uniplanar compact PBGS (UC-PBGS) has been proposed [32]. The UC-PBGS is complex in nature. The simpler way is to use DGS [33] in this context. DGSs are more compact than usual PBGS. They are more attractive and very simple to design. It can be seen that the conventional dumbbell shaped DGSs in conjunction with T-junction or cross-junction open stub yield excellent low pass filter (LPF) performance [33]. They are very compact in nature in the presence of open stub in the conductor plane. They provide very wide stopband.

1.5 Objective of the Thesis

The goal of this PhD thesis is to design novel PBG assisted microstrip transmission lines, filters, antennas, phased arrays and reconfigurable phased arrays. PBG assisted transmission lines are investigated to see their improved performance in terms of wider stopband and ripple free smoother transmission thorough the passband. In case of PBG assisted filter the bandgap property will be utilized in harmonic suppression. The EBG assisted microstrip patch antenna will be investigated to achieve improved performance in terms of return loss bandwidth, front to back lobe ratio (FBR), directivity and gain. The vital goal of this thesis is to design phased array antennas with the help of EBGSs. The beam will be steered

by controlling EBG elements that are located under the feed lines of the arrays. Reconfigurable phased array antennas will also be investigated. PBGSs will be implemented into the conventional lines, filters, antennas, phased arrays and reconfigurable phased arrays. The choice of the proper PBG structure is a vital issue to achieve better performance of the designed components for all the conventional designs. Therefore, the first goal is the proper selection of PBG units, which will yield distinct passband and stopband characteristics at the designed frequency. The PBGSs have different forms and their lattice structures are different. The investigations will be confined mainly to circular and square patterned PBG structures. Uniform PBG structures have constraints of filling factor (FF). FF is defined to be the volumetric ratio of one unit cell to single PBG element. FF controls the width and depth of the stopband [34]. The general concept of increasing the stopband is the enhancement of FF. But beyond some value of FF the passband transmission suffers from the worst performances. The passband contains huge ripples with large dimension of the PBG patterns. The passband return loss performance is also very poor. To alleviate these problems uniform circular PBGSs with optimized value of 0.25 is proposed [34]. Intensive investigation will be carried out on non-uniform PBG structures. In the case of non-uniform distributions PBG structures with Binomial [35] and *Chebyshev* distributions [36] will be investigated. The amplitudes of the PBG elements are calculated as per the coefficients of the distributions. For circular patterned PBGSs, the radius will be directly proportional to the coefficient of the distributions that is referred to as Type-A. Other distinct relationship will also be used where the coefficients are proportional to the area of PBG elements that is referred to as Type-B.

Next DGSs will be investigated. In the open literature researchers used UC-PBGS or DGSs [19], [32] to improve the performance of the LPF designs. Such structures/configurations need careful attention for both top and bottom layers of planar substrates. Attention will be devoted to develop wide bandgap and LPF performance by the perturbed ground plane only.

The project has the following objectives:

- Design of novel PBG elements that will provide broadband and distinct passband and stopband characteristics. In the present research the PBG elements with Binomial and *Chebyshev* distributions will be focused.
- Chirping technique will also be used to produce aperiodic structure, which will provide improved performance in terms of passband ripples and wider stopband. This is an alternate approach to implement non-uniform distributions of PBG unit cells in PBG array.
- DGS and a hybrid design of DGS-PBGS will also be investigated to achieve better performance
- Implementation of the PBG elements in the ground plane of microstrip patch antennas to investigate antenna performance
- Implementation of uniform and non-uniform circular PBG elements in harmonic suppression of band pass filter
- Implementation of dumbbell shaped DGS in harmonic suppression of band pass filter
- Implementation of the PBG elements under the feed networks of 4-elements array for beam steering purposes

- Implementation of DGS under the feed lines of a phased array antenna for beam steering purpose

- Implementation of relative phases in PCAAD to see the beam steering angle

- Development of a reconfigurable patch antenna array. In the array PIN diodes will be used to connect/disconnect the patches that will change the effective length of patch antennas to achieve different sub-bands from the same array. In the reconfigurable array, PBGSs will be used as phase shifters to build a reconfigurable phased array.

Once the individual components of the phased array are obtained with satisfactory performance, the final goal is to:

- Integrate the developed components into a complete reconfigurable phased array antenna perturbed by PBGSs/DGSs and finally test the complete array. A Vector network analyzer (VNA) will be used to test the return loss performance. Finally the radiation patterns will be measured in the anechoic chamber.

1.5.1 Proposed Array Configurations

Two different configurations are proposed (i) Reconfigurable Switched-Patch Array (c.f Fig. 1.1), and (ii) Switched-PBG lines. Finally It is proposed to combine these two techniques into a novel complete reconfigurable phased array as shown in Fig. 1.2.

1.5.1 Switched Patch Array

Fig. 1.1 shows a 4 × 4 element reconfigurable switched-patch array. When all the diodes are forward biased, the array is a 4 × 1 element linear array and operates at the lowest frequency. When the diodes of the middle row are reverse biased, the array is a 2 × 4 element array and operates at the middle frequency. When all the diodes are reverse biased the array is a 4 × 4 element planar array which operates at the highest frequency. Thus by changing the sequences of the bias voltage for the individual diodes many combinations of arrays at many frequencies can be achieved.

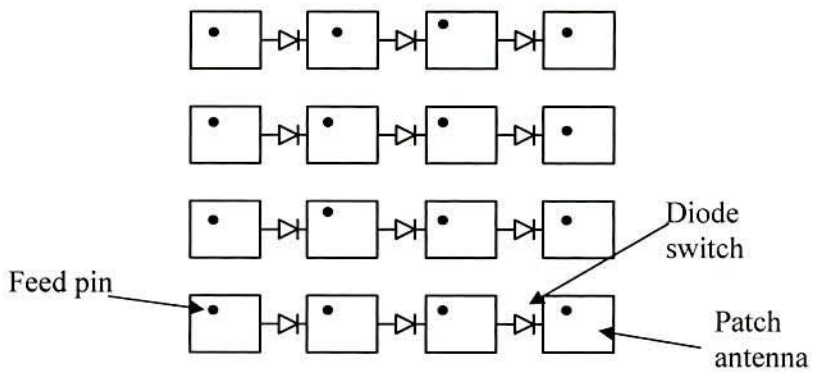

Fig. 1.1: A switched-patch antenna array for multi-band application.

1.5.2 Switched PBG Lines

In switched PBG lines, the phase transmission of the line changes with the number of PBG cells [18] under the lines. Thus using switched PBG cells under a transmission line is a novel idea of phase shifting. If the transmission line is used to excite the antenna elements in an array, a tunable antenna is achieved. The variation in number of PBG unit can be done by closing and opening the switches situated under the PBG structure or closing the PBG elements by conducting tapes.

It is worthwhile to mention that the PBG elements under the feed network are designed at central stopband frequency that is far away from the frequency of operation of the antenna. It should be ascertained that the passband provided by the PBG engineered microstrip line is wide enough so that the designed frequency of the antenna falls into the passband regions. This is the reason why the PBG elements sizes are not the same in all layers. Rather the sizes of the PBG elements under the feed network are smaller in size as they are designed at a higher frequency than the frequency of operation of the microstrip patch antenna.

1.5.3 Reconfigurable Phased Array

The proposed reconfigurable phased array, which is formed by integrating the switched patch elements on the top layer and the PBG lines as phase shifters in the bottom layers, is shown in Fig. 1.2. PBGSs under the feed network can be opened and closed by using PIN diode switches/conducting tape, which have not been shown in bottom layer of the proposed configuration. While the switched PBG lines yield the flexible phase shifts between individual elements, the diodes on the radiating layer yield multiples radiation. Thus a reconfigurable phased array antenna is achieved.

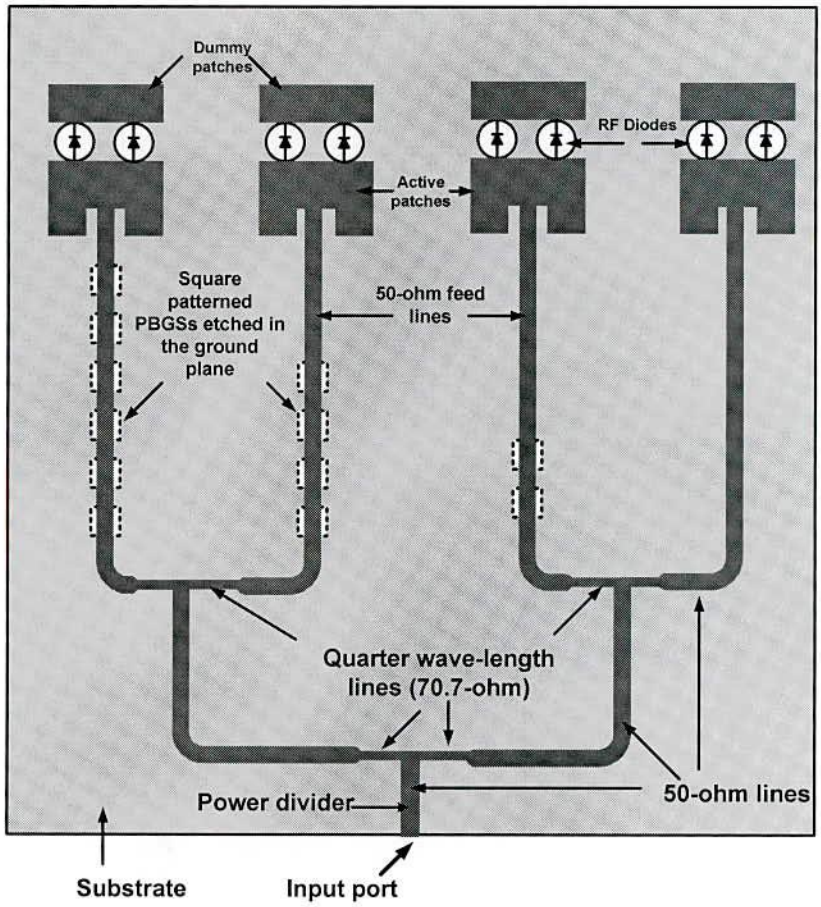

Fig. 1.2: A complete PBG assisted reconfigurable phased array antenna

1.6 Original Contributions

The following items are the original contributions stemmed from the thesis.

1. Implementation of 1-D PBGSs (Conventional PBGS and DGS) instead of 2-D PBGSs in case of beam steering of phased array antenna
2. Effect of number of PBGSs on S-parameter performance of PBG engineered microstrip transmission lines
3. Alleviation of the problem encountered from the optimized FF of PBG structure that is normally mentioned to be 0.25 for the conventional PBG element design.

4. The use of co-efficient of non-uniform distribution namely Binomial and *Chebyshev* distributions to calculate the amplitude of the PBG elements that are used to replace the conventional circular patterned PBG structures. The overall performances of PBG engineered structures are achieved with such distributions.
5. Novel chirping to yield improved performance
6. Low-pass filter syntheses are tremendously relaxed with such distributions.
7. Harmonic suppression of band pass filter (BPF) is seen to be superior in case of proposed structures compared to other standard result reported in the literature.
8. Investigation into non-uniform DGSs
9. Novel findings of Hybrid DGSs (Combination of DGS and PBGS)
10. Investigation into DGS assisted BPF that can suppress both second and third harmonics.
11. Improved performance of dual-band antennas in terms of return loss, gain and matching
12. Investigation of effect of number of PBG elements on antenna performances
13. Intensive investigation of relative phase properties of the PBG engineered lines that concern with filling factor, number of PBG elements and offset distances
14. Implementations of relative phase properties in beam steering of PBG assisted phased array antennas
15. Investigation into DGS assisted phased array antenna
16. Realization of PBG assisted reconfigurable phased array antenna

1.7 Thesis Outline

Followings are the out line of the thesis.

- In chapter 1, the introduction of the project is reported. This chapter elucidates the goal and proposition of the reconfigurable phased array's configurations.

- In chapter 2, a comprehensive literature survey on PBG structures and their applications into the microwave devices and components have been reported that results in the motivation, reasoning and the proposition of novel structures against the available structures in the literature.

- In chapter 3, the basic theory of periodic structures is presented. The design equations are presented. To get the idea about the passband-stopband phenomena of the EBGS, numerical result for dispersion diagram has been reported. This chapter shows some S-parameters performances of uniform circular and square patterned PBGSs. Their dependency on the number of uniform PBG elements has also been presented.

- In chapter 4, non-uniform PBGSs have been reported to see their improved performance over conventional regular PBGSs. Non-uniformity in amplitudes will be realized by implementing Binomial and *Chebyshev* distribution. On the other hand the non-uniformity in period (inter-element spacing) will be realized by chirping the elements in the design.

- In Chapter 5 the evolution from PBGS to DGS will be reported. The frequency properties of a unit cell of a dumbbell shaped DGS will be reported. The hybrid structures of DGS with *Chebyshev* distribution are proposed for LPF. Besides modified DGS will be reported to yield compact dual band performances.

- In chapter 6 PBG engineered antennas and filters will be demonstrated. The improved performances of aperture coupled patch antennas (ACPAs) will be reported in terms of return loss, gain and bandwidth performances. Conventional ACPAs and dual-band ACPAs will be investigated.

For filters mainly the performance of a coupled line BPF will be focused. The Binomially distributed PBGSs will be applied to suppress 2^{nd} and 3^{rd} harmonics. DGS will also be used in harmonic suppression. The important role of dumbbell shaped DGS in both 2^{nd} and 3^{rd} harmonic suppression will be reported.

- In chapter 7 phased properties of the microstrip transmission lines will be investigated intensively. Different parameters are mentioned that influence the phase properties of PBG engineered microstrip transmission line that will be helpful for phased array antenna design. The controlling parameters are used in the feed networks of a PBG assisted 4 by 1 feed network. Obtained phases are used in EM software PCAAD to see the beam steering of phased arrays. Then PBG assisted phased arrays and PBG assisted reconfigurable phased arrays are designed and simulated in EM software Zeland IE3D. Few prototypes are developed and tested. The performances are summarized for different parameters such as filling factor (FF), numbers and location of PBG elements. All the measured results of PBG assisted phased arrays and reconfigurable phased arrays have been summarized

- In chapter 8, conclusions and recommendation for future work have been presented.

Chapter 2 Literature Survey on PBG Assisted Microwave Devices

2.1 Introduction

A comprehensive literature survey on recent development of PBG structures and their applications to microwave devices including antennas has been reported in this chapter. PBG structures are found to play vital roles in enhancing the performance of the microwave components and devices. The stopband characteristic causes the dramatic improvement in the performance by suppressing surface waves, leakage and spurious transmission. FF is one of the important controlling factors to yield wider and distinct stopband that should be optimized to maintain a smoother transmission in the passband. In the literature for uniform circular patterned PBGSs, the optimized FF of 0.25 [34] is considered. This type of design is considered as a conventional PBG structure design. After carrying out the survey of beneficial effects of PBGSs, the reconfigurable phased array antennas reported in literature are presented. Finally a short briefing on motivation, reasoning and proposed proposition of PBGSs has been outlined.

2.2 PBG Structures

PBG structures are periodic in nature, which may be realized by drilling, cutting and etching on the metal or substrates. They may be formed in the ground plane or over the substrate. The transmission line can also be modified to form PBG characteristics without having any perturbation in the ground plane [37]-[38], [39]. This new idea can be extended to filter, antenna and other microwave component and devices where the complexity of packaging is minimized. The PBG

configuration is categorized as shown in Fig. 2.1. On the basis of dimension, PBG structures may be divided into 1-D, 2-D and 3-D PBGSs. Planar PBG structures and their applications to antennas has been reported in [46]. Following are the descriptions of different PBG structures.

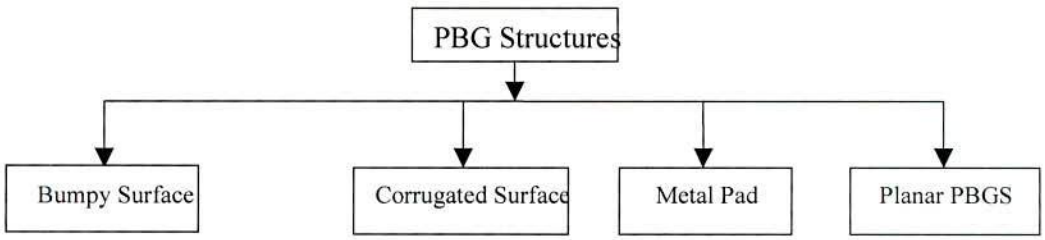

Fig. 2.1: Different PBG structures

- **Bumpy Surface**

Several configurations have been reported in the literature. The first structure is made by drilling a periodic pattern of holes in the substrate or etching a periodic pattern of circles in the ground plane. A bumpy metal sheet [40]-[41] has a narrow surface wave band-gap. Electric field wraps around the bumps at the upper edge of the band gap and the electric field also extends across the bumps at the lower edge of the band-gap, hence a slow wave structure is formed. Bumpy surface is shown in Fig. 2.2.

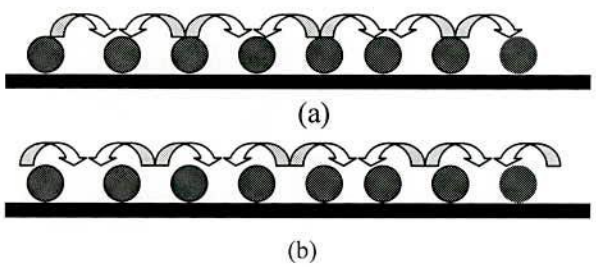

Fig. 2.2: Bumpy metal sheet: (a) electric field extends across the bumps at the lower edge and (b) electric field wraps around the bumps at the upper edge

- **Corrugated Surface**

A corrugated surface [42]-[43] is a metal slab into which a series of vertical slots are cut. The slots are narrow so that many of them fit within one wavelength across the slab. Each slot can be regarded as a parallel plate transmission line, running down into the slab, and shorted at the bottom. If the slots are one quarter-wavelength deep, then the short circuit at the bottom is transformed by the length of the slots into an open circuit at the top end. Thus the impedance at the top end is very high. In this situation the surface impedance is capacitive and transverse magnetic (TM) surface waves are forbidden. Furthermore, a plane wave polarized with the electric field perpendicular to the ridges will appear to be reflected with no phase reversal. Corrugated surface is shown in Fig. 2.3.

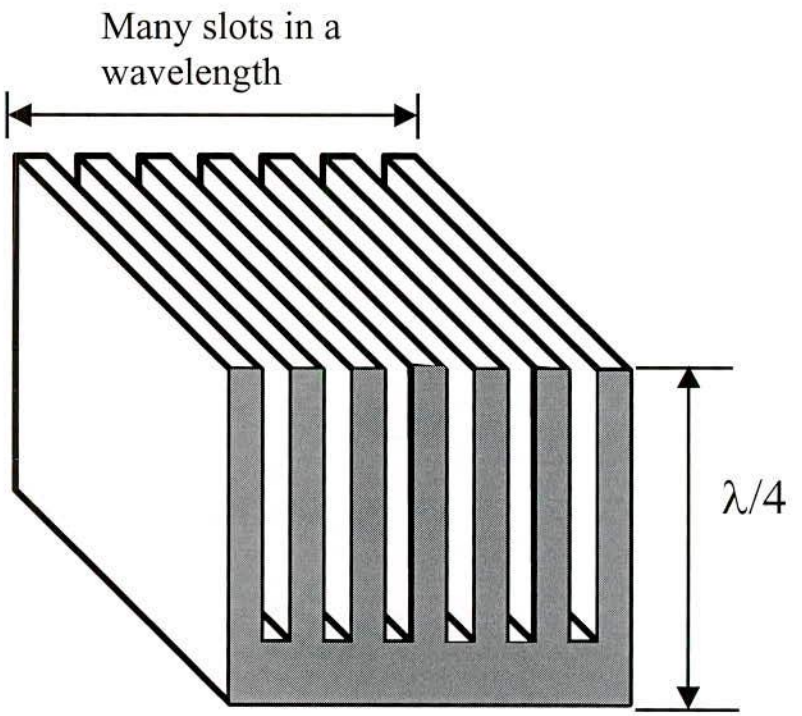

Fig. 2.3: Corrugated metal surface

- **Metal Pad or High-Impedance Surface**

A more effective and compact approach, compared to the corrugated surfaces, which makes use of a triangular or square lattice of metal pads connected to ground with vias, has been recently proposed and applied in [4] to enhance the gain of planar antennas. These structures are the first realization of planar compact electromagnetic crystals with a complete stop-band in the microwave range. This type of structure with a triangular lattice of hexagonal metal plates and square vias to ground is shown in Fig. 2.4.

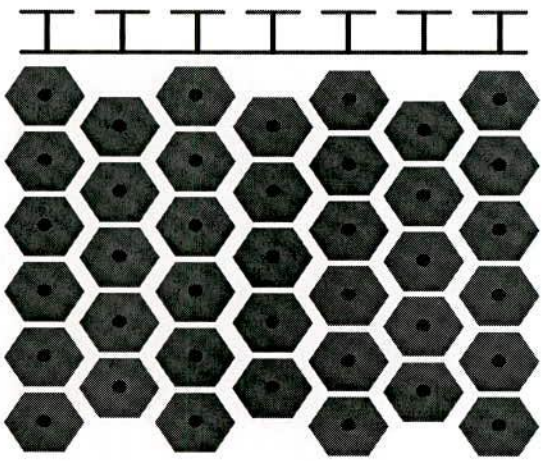

Fig. 2.4: Periodic metal connected to ground with via holes to yield high-impedance surface.

- **Planar PBG Structures**

The planar periodic PBG structures are normally etched in the ground plane. They may be of different forms on the basis of lattice structures. The lattice structure may be square, triangular, rectangular and honeycomb etc. The shape of the unit cell may also be square, rectangular, circular, triangular and sinusoidal etc. Researchers are continuing to develop different PBG structures to obtain better performance.

Uni-planar compact photonic Bandgap structure (UC-PBGS) [32] is shown in Fig. 2.5. Planar slow wave structures and low-leaky conductor backed coplanar waveguides (CPW) using UC-PBGS have been recently presented. Vias are not used in a UC-PBGS.

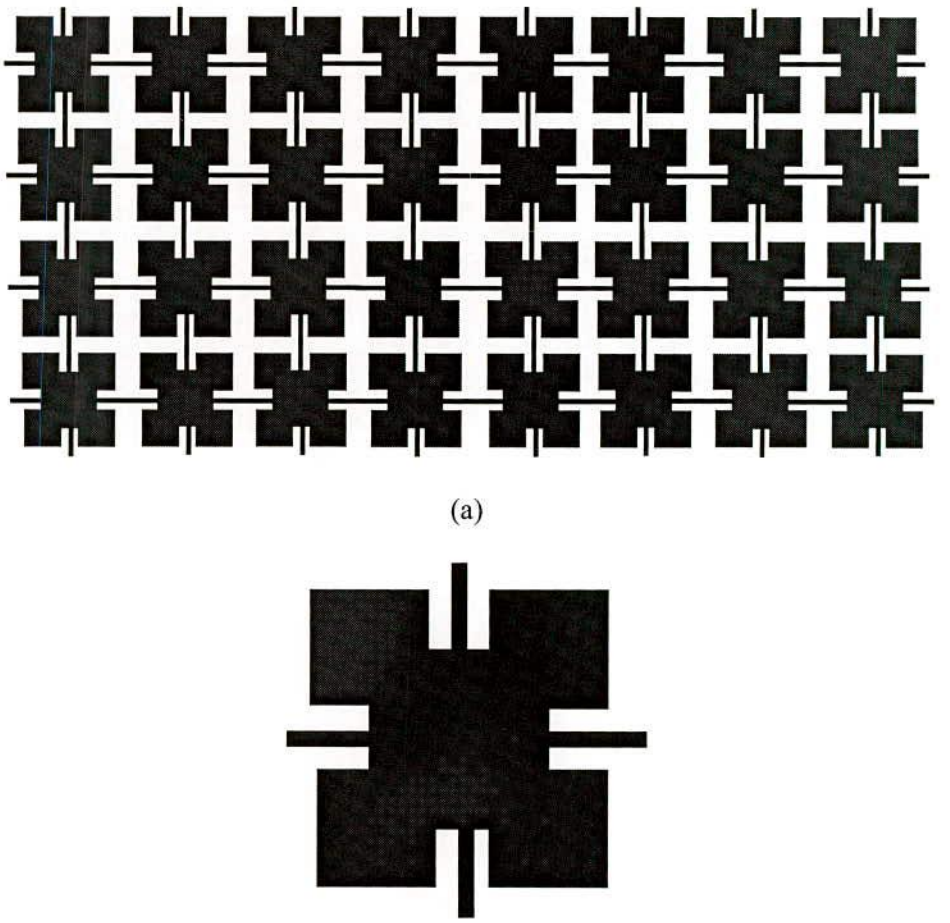

(a)

(b)

Fig. 2.5: (a) UC-PBG structure (b) Unit cell.

Advantages of this crystal are; simple, low-cost configuration and compatibility with MMIC photolithography. The UC-PBG structure, shown in Fig. 2.5, is a two-dimensional periodic lattice pattern on a dielectric substrate. The unit cell of the PBG lattice consists of square pads and narrow branches having inductive property, which is further, enhanced by insets. The PBG structure forms a

distributed LC network with a specific resonant frequency. At this frequency the periodic loading becomes an open circuit and an equivalent magnetic surface is created. Very recently a new simplified UC-PBGS in the form of square metal pads connected with thin lines has been proposed [12].

Few pictures are shown in this section to give the clear understanding about the lattice structures and shapes. Fig. 2.6 is a three dimensional view of a PBG engineered substrate. In the ground plane, uniform circular patterned PBG structures have been etched to realize an artificial (Photonic crystal) PC. This type of perturbation is truly responsible to generate unique characteristics. They provide stopband and passband that have many useful applications in microwave engineering. The radius of the circular slot is 'r' and the inter-element distance is 'a'. One of the important factors in PBG structure design is known as filling factor (FF). In case of uniform circular slots, the FF is r/a that can be understood from the Fig. 2.6. If the slots are square having their sides to be 'b' then FF is b/a. Lattice structures and shapes influence the performance of the structures [44]. The substrate being perturbed by triangular slots is shown in Fig. 2.7. In this figure though the slots are triangular but their lattice structure is square having same distance along x and y direction.

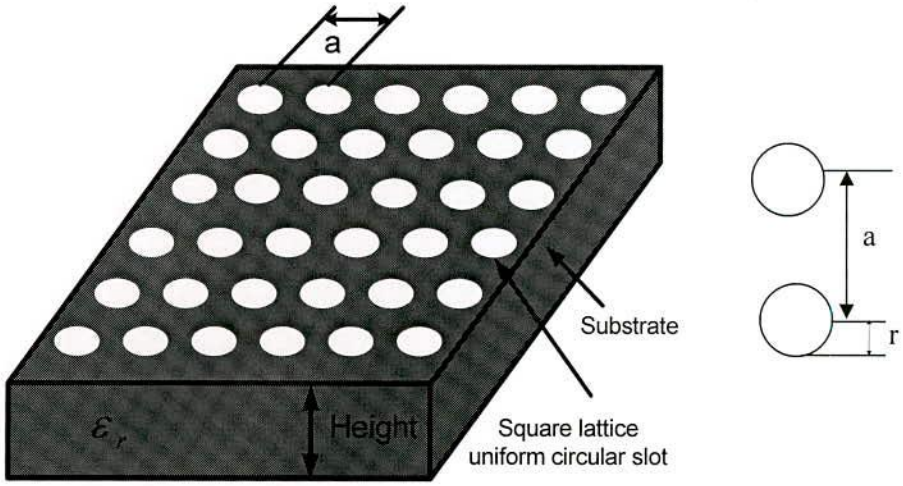

Fig. 2.6: Three-dimensional view of a substrate perturbed by uniform circular slots.

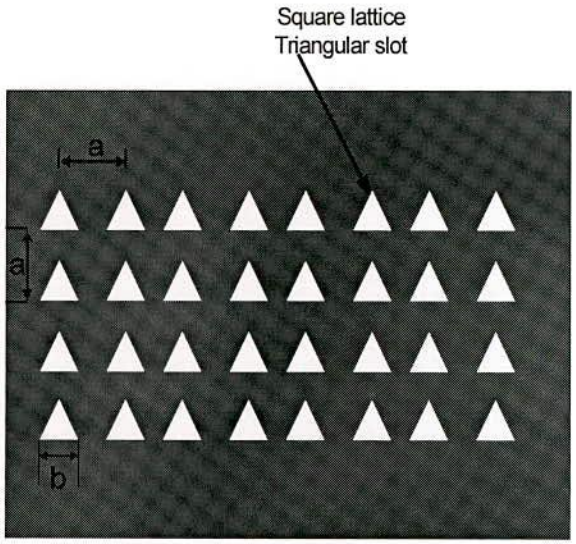

Fig. 2.7: Triangular slots with square lattice.

If triangular is equilateral then FF for this structure is b/a as shown in Fig. 2.7; where 'b' is the length of the arm of the triangle and 'a' is the inter-cell separation. The substrate perturbed by square slots is shown in Fig. 2.8. It can be seen from the figure that the square is having the length of all side of 'b' with inter-element spacing of 'a'. In this case the FF is also b/a.

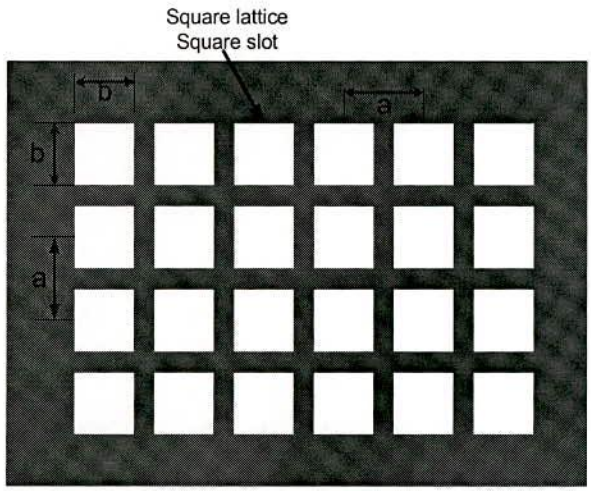

Fig. 2.8: The geometry of 2-D square slots having square lattice structure.

The uniform circular slots with different lattice structure are shown in below. It can be seen from Fig.2.9 that the slots are uniform circular and the lattice is square. This figure is same as Fig. 2.6. Only difference is their dimension. Fig. 2.6 is 3-D while Fig. 2.9 is 2-D. The circular slots with triangular lattice arrangement are shown in Fig. 2.10. From this figure it can be seen that their grids are in triangular form. But the period along the x direction is 'a' and along the y direction the slots rows maintain the same distance equal to period 'a'. It is suggested that triangular lattice can suppress the surface wave significantly. It is also encouraged to use non-equilateral triangular lattice for significant suppression of surface waves [16].

The lattice may be rectangular having different periods in x and y direction. This layout is more useful when PBGSs are required to design for dual band operations. Such geometry is proposed in VSAT antennas [45]. In VSAT antennas the dual band operations are needed for transmitting and receiving purposes.

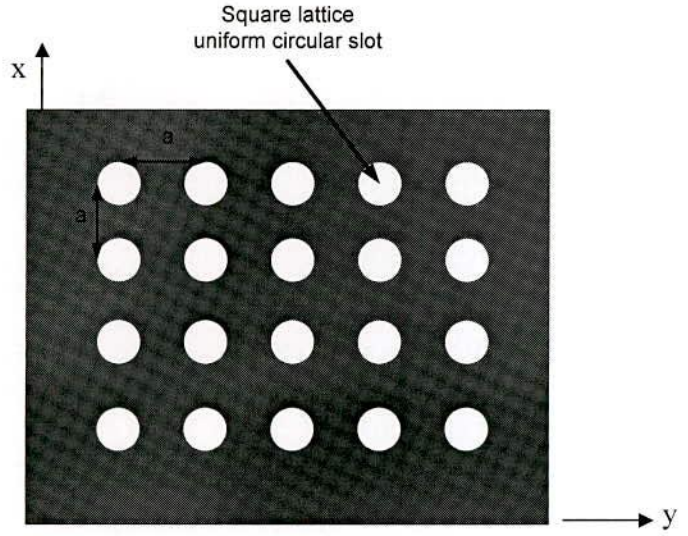

Fig. 2.9: 2-D geometry of a substrate having uniform circular slots with square lattice.

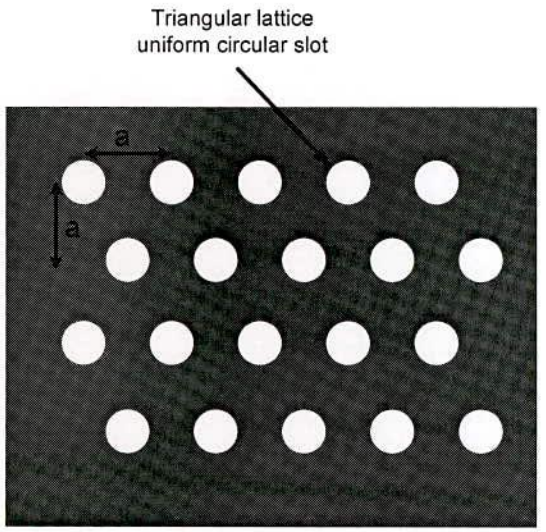

Fig. 2.10: Uniform circular slots with triangular lattice arrangement.

Normally conventional microstrip patch antenna operates at single frequency. The PBGSs are designed at the operating frequency. So in case of single frequency the lattice structures may be square or triangular. But in dual band operations the frequencies determine different periods resulting in a rectangular lattice. Such geometry with rectangular lattice is shown in Fig. 2.11.

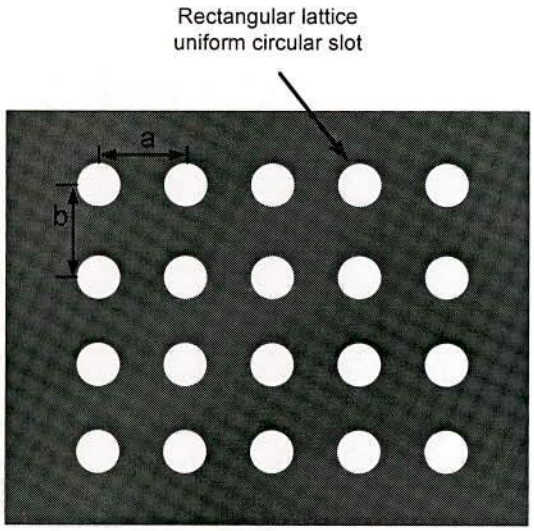

Fig. 2.11: Uniform circular slots with rectangular lattice.

2.2 Applications of PBG Structures in Microwave Devices

Due to the unique properties of PBG engineered structures, they find many applications in microwave components and devices. To realize microwave filters, mixers, antennas, power amplifiers, phased arrays etc. the stopband and passband created by the PBG structures to enhance performances of devices. Here the beneficial effects of PBGSs in different devices are discussed as shown in Fig. 2.12.

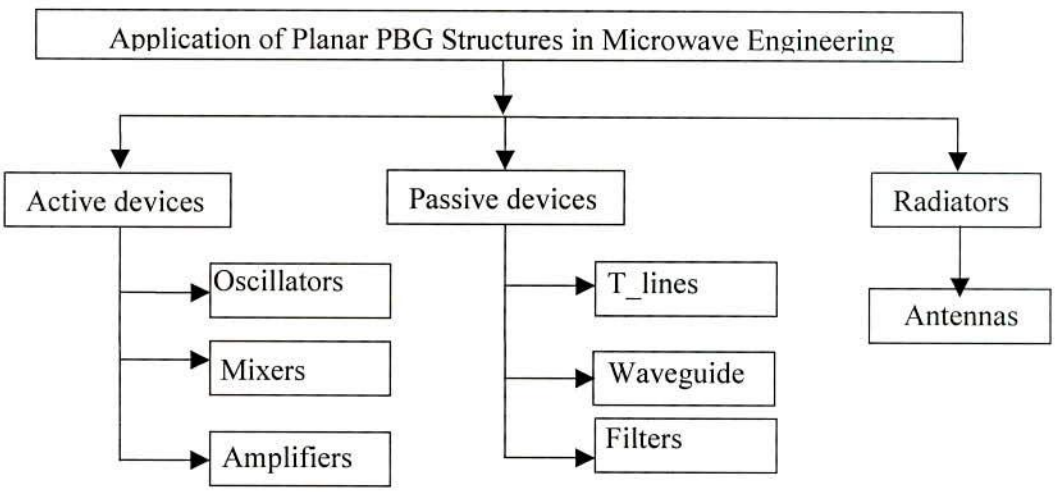

Fig. 2.12: Tree- structure of applications of planar PBGSs.

- **Low Noise Oscillator Design**

Y. Qian *et al.* [46] mentioned the design of passive and active components. Application of a high Q image guide resonator in an oscillator results a low noise oscillation. The defect mode concept in PBG structures has been utilized here. The schematic of a high Q resonator based on PBG defect - effect in an image guide is shown in [46]. It is interesting to note that a stop band for wave propagation is achieved when the condition "$\beta a = \pi$" is satisfied. On the other hand, a sharp high Q defect mode can be obtained when a cavity is formed in the middle of the PBG lattice with a length 'l' shown in [46]. Using a modulated Gaussian pulse placed outside the PBG grooves the image guide is excited. In this case 8.255 GHz is obtained as the peak frequency for transmission. Experimental investigation needs the design of a proper coupling scheme to launch and to measure the image guide mode. A microstrip-fed Yagi-Uda slot array is used in the design of an efficient transition for this purpose that is used for the measurement of S-parameters performances. The result shows the peak frequency to be 8.276 GHz, which is excellent (only 0.25% error). A reasonably high value of Qu = 697 is measured. Even though the RT/Duroid 6010 ($\tan \delta = 0.002$) is used for this experiment, it is not optimal as a low loss dielectric material for resonators.

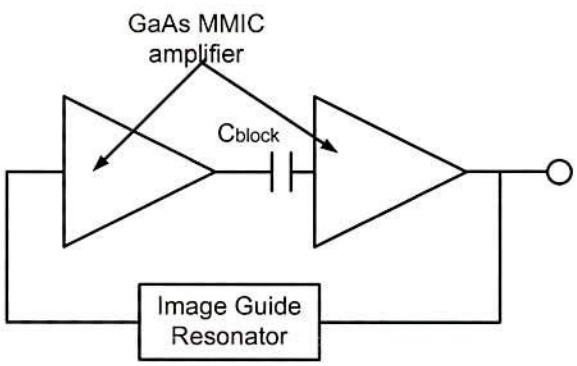

Fig. 2.13: Application of a high Q resonator in a low noise oscillator design.

In a low noise oscillator design, this type of an image guide resonator is very potential component to provide relatively pure spectrum. The resonator shown in Fig. 2.13 provides output power level of 8.5 dBm after the deduction of the co-axial cable loss. Noise level of about -102 dBc / Hz at 100 KHz offset is found.

- **Enhanced Spontaneous Emission LED by Microcavities**

PBG based microcavities [46] provide an LED with enhanced spontaneous emission. In the THz frequency range, the PBG based microcavities are outstanding candidates to achieve single mode, small volume resonators. These types of cavities are used to enhance spontaneous emission and to increase the efficiency of an LED. In Fig. 2.14, a high dielectric slab resides on a substrate with a much lower value of dielectric constant so that the electromagnetic energy of the guided modes is confined inside the high dielectric constant slab.

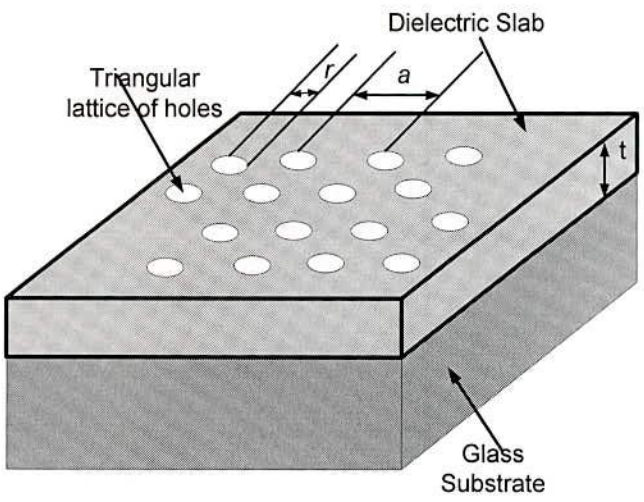

Fig. 2.14: Slab of higher dielectric constant light emitter material with a triangular array of holes lying on a lower dielectric constant substrate.

From the dispersion diagram of TE like mode for t/a = 0.33 and r/a = 0.40, a bandgap for the guided propagation is found in the range of 0.33c/a to 0.4c/a,

where c is the velocity of light. Defects realized by adding the appropriate volume of dielectric material is appreciated to support highly localized electromagnetic modes, whose frequency will fall within the range of the forbidden gap of the two dimensional crystal. The energy of this mode cannot couple to guided modes of the slab rather it resides around the defect which acts as micro cavity. In the design of LED, it is an excellent component where the confined energy is related in the active region of LED.

- **Broadband High Efficiency Power Amplifier**

The achievement of broadband harmonic tuning is typically cumbersome for active integrated antenna amplifiers and for power amplifiers in general. The technique of using periodic structure is actually suited for narrow band. So additional harmonic filtering is required which necessitates larger transmission stopbands. These types of larger stopbands can be achieved with the use of PBG ground plane. The proposed PBG assisted ground plane [47] for microstrip lines provides low loss, slow wave propagation at lower frequencies, and a wide distinctive stopband, as the frequency increases [48]. The implementation of PBG ground plane in power amplifiers results intrinsic, broadband harmonics without the need of any stub or filtering element. In the design of broadband power amplifier, the PBG periodic structure is integrated with a slot antenna where the periodic structure is used to tune the second harmonic. The measured power added efficiency (PAE) is better than 50% over an 8 % bandwidth (3.7 to 4.0 GHz) with second harmonic tuning only. If the combined approach [47] where the microstrip patch with shorting pins is used to tune the second harmonic and the periodic structure is used to tune out

the third for a class AB power amplifier, then PAE was 61% with output power of 21.9 dBm.

- **Efficient Transmitter Front-Ends Integrated with PBG Structures**

The tuning of second & third harmonics provides an efficient power amplifier. C.Y. Hang *et al.* [49] narrate a comparison between an amplifier assisted with a PBG microstrip line at the output, and the reference amplifier with a standard 50 Ω microstrip line of identical length. Comparing with the reference amplifier, it is reported that PBG assisted amplifier provides 10 % improvement in PAE and 13 dB increases, in output power. In addition PAE is better than 50 % from 3.32 to 3.62 GHz (8 % BW) for the PBG assisted amplifier and from 3.5 to 3.6 GHz (4 % BW) for the reference. The PBG structure provides 37 dB additional suppression for the 2^{nd} harmonic and at least 30 dB for the 3^{rd} harmonic. It is expected that the implementation of entire system on PBG ground plane may lead to very compact, high performance power amplifier for a wide range of wireless and microwave amplifiers.

- **Low Pass Filter (LPF)**

In this case, the UC-PBG structure shown in Fig. 2.5(a) is used in the ground plane to improve the performance of conventional LPF [34]. A small portion of the 50-ohm feed line is placed on the perforated ground plane (UC-PBG plane), the remaining being on the solid ground plane. Duroid substrate is used with $\varepsilon_r = 10.2$ and the thickness of the substrate is 25 mils. The width of the 50-ohm microstrip is 24 mils. The simulation result shows the wider stopband above 6 GHz and S_{21} is found to be below –30 dB for a wide frequency range. Within the stopband range,

the return loss is found to be about 0 dB indicating very little radiation loss which also verifies the PBG property. A stepped-impedance LPF with seven reactive elements has been chosen by [51].

From the comparison of PBG assisted and conventional filter, important findings are:

1) Maximum attenuation is increased from 20 dB to 58 dB due to the PBG application. 2) Spurious passband is completely suppressed. 3) The passband loss is comparable to the conventional LPF. 4) Application of PBG structure maintains matching conditions. 5) It does not increase the conductor loss.

- **Compact Microstrip Bandpass Filters (BPF)**

Conventional parallel-coupled band pass filters (BPF) need extra filters to suppress the spurious transmission that results the increase of insertion loss. It is reported [47] that the use of extra filters can be avoided by just applying PBG to obtain a compact microstrip BPF with intrinsic spurious rejection. The well-matched microstrip on the UC-PBG ground plane is suited as a low-loss transmission line. Generated spurious passbands at higher harmonics can be suppressed with the aid of PBGS as it provides a wide and deep stopband. The physical length of the filter circuit is reduced as well due to the slow-wave effect of the UC-PBG structure. Fig. 2.15 shows the schematic of a microstrip BPF on the UC-PBG ground.

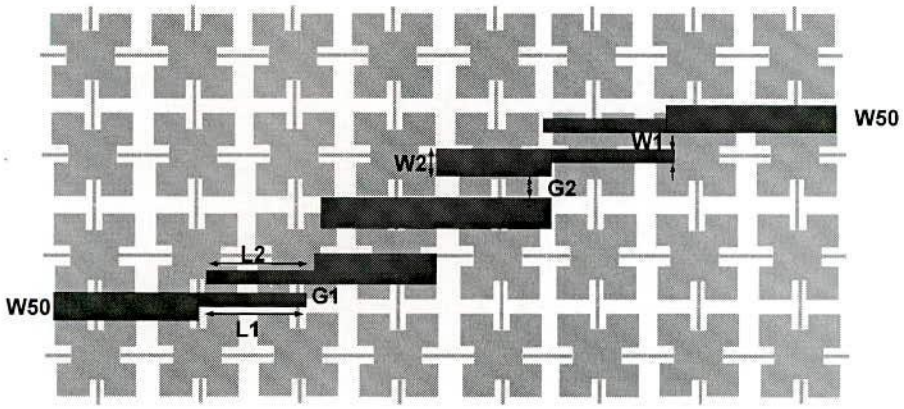

Fig. 2.15: Schematic diagram of a BPF over UC-PBG

The reference [51] narrates the standard design procedures of the parallel-coupled BPF. The requirements are [47]:

Center frequency = 6 GHz, W1= 17 mils, W2 = 21 mils, G1 = 8 mils, G2 = 28 mils. The width of microstrip feed lines = 24 mils (corresponding to 50-ohm transmission line).

Number of coupling sections = 4 (Four); a 0.5 dB equal-ripple response. The physical length of the coupled-line sections (L_1 and L_2) = 145 mils. This length is 20% shorter than that of a conventional quarter wavelength line.

At the frequency of 12 GHz and 17 GHz, transmissions co-efficient of a conventional BPF are seen to be –10 dB and -5 dB respectively. On the other hand the UC-PBG assisted filter provides the spurious suppression of 30-40 dB. Though the length of the microstrip resonator has been scaled accordingly to the slow-wave factor, but the coupling gap remains same, which results the increased fractional bandwidth (21.6 %) at 6 GHz center frequency. Like conventional BPF the coupling co-efficient can be optimized to improve the bandpass characteristics of the PBG assisted BPF. Including the effect of two SMA connectors, the minimum insertion loss of the PBG assisted filter is found to be 1.9 dB at 6.39 GHz.

- **Suppression of LO Leakage in a Mixer**

Conventional LPF needs many stages to reject LO leakage. However UC-PBG assisted filter [50] can be used to suppress this leakage in a drain mixer. The UC-PBG assisted filter is placed at the drain side to extract IF output as well as to reject the LO leakage.

It is mentioned that LO power has been injected into the drain more efficiently due to increase of conversion loss from 1 dB to 1.5 dB at lower levels in PBG assisted filter. It is reported that the PBG mixer suppresses LO leakage more than 10 dB.

- **PBG Filter without Packaging Problem**

Various types of PBG filters are very good candidates to offer passband and stopband properties. Normally PBG structure is etched on the ground plane. Due to packaging, shield effect is severe to degrade the performance of the filter. T. Akaline *et al.* [37] proposed a recent structure to improve this issue. The influence of the backside shield has been addressed here, which embeds the circuit when the filter is integrated in the microwave systems. Two patterned PBG structures have resulted in the improvement against the degraded performance due to the back shield. In this case, the top pattern is formed via a printed technology with five successive high and low impedance sections having width = 0.4 mm and 0.8 mm respectively. The backside ground plate is etched two holes of radius 3.5 mm with of 14.1 mm. The holes are under the high-impedance sections. The total length is 35.3 mm. S-parameters performance of PBG filter taking the effect of a shielding plate into account provides worst performance. On the other hand two-sided PBG filter provides better performance.

D. Nesic et al. [38] reported a unique PBG structure recently where sinusoidal variations have been implemented in characteristic impedance on the basis of the sinusoidal shaped microstrip line on the substrate. No etching in the ground plane was required. So the problem of packaging does not appear. It really stems the novelty on the solution of packaging problem in PBG structured component and devices.

- **Nonleaky CB-CPW**

In a conventional coplanar waveguide (CPW), an extra ground plane is normally used in its backside to increase mechanical strength, to realize mixed CPW microstrip circuits, or to provide a heat sink [52]. This type of conductor-backed CPW (CB-CPW) will excite the parallel plate mode resulting in the deterioration of CPW performance. Using posts to short the unwanted plate mode or using multi-layered substrate to shift the dispersion curve of the parallel-plate mode are the different approaches to solve the problem. The UC-PBGS is a promising candidate to stop this leakage due to its deep stopband characteristics. This can easily be etched in the top ground planes of a CB-CPW circuit without using any extra masks or via holes. Once the wave is launched the energy will leak along a definite angle providing a severe effect such as cross talk with neighboring circuits.

It is noted that the UC-PBG lattice is placed on the top ground plane. From the result it is seen that for the conventional CB-CPW, the significant leakage is observed at all frequencies and the insertion loss of a conventional CPW is found to be low below 13 GHz and starts rippling at higher frequencies for the reflections caused by the SMA connectors. Though power leakage is present in the passband (DC to 9 GHz) in the proposed CB-CPW but in the range of 9-14 GHz the

insertion loss has been found to increase significantly which is comparable to conventional CPW providing the information that the leakage has almost been suppressed. This type of novel CB-CPW may find its potential application to CPW-fed slot antennas.

- **PBG Applied to Antennas**

Potential application of PBG structures for improving antenna performance is now focused.

- **Phase Control of Plane Waves**

When an antenna is situated very close to a conducting surface, efficiency degrades due to out-of-phase image currents. It has been shown [1] that for a horizontal wire on a PBG substrate, the image currents are in phase with in the band-gap. When a probe-fed patch antenna is embedded in such a PBG structure, a smooth symmetric pattern with little backward radiation is observed. The efficiency of the patch antenna is also enhanced.

- **Gain Improvement**

In [6], the authors described a microstrip feed rectangular patch antenna with 52 mm width and 26 mm length. The substrate has a dielectric constant of $\varepsilon_r = 10$ and a size of 420 mm x 420 mm x 10 mm. The antenna is placed in the middle of the substrate. For the conventional design the gain was found to be -2 dB, but the gain was 7.5 dB when the antenna is etched on a PBG material. The back radiation was also reduced significantly indicating increased efficiency.

R. Coccioli *et al.* [5] described an aperture-coupled patch antenna on UC-PBG substrate. The antenna is designed at 12 GHz on a standard 1.27 mm thick substrate with $\varepsilon_r = 10.2$. The feed line is etched on a 0.64 mm thick substrate with $\varepsilon_r = 10.2$.

To increase coupling between the antenna and the feed line, a 0.38 mm wide and a 2.29 mm long H-shaped coupling slot is used. The length of radiating patch is 5.33 mm and the width is 2.54 mm. The effect of a finite substrate is taken into account. For a comparison, an identical patch surrounded by three periods of UC-PBGSs in each direction has also been etched on a finite substrate with the same dimensions. From the radiation pattern (not shown here) it is seen that the radiation patterns of the later are smoother than those of the standard antenna. The peak power received by the UC-PBG assisted patch in the broadside direction is 3 dB higher than that received by the reference patch. Together with smoother radiation patterns, this proves the effective suppression of surface waves and an increase in the radiation efficiency.

S. K. Sharma *et al.* [12] proposed a simplified UC-PBG structure to enhance the antenna performance. Instead of a complex PBG structure they have implemented the new UC-PBG structure without the inset in the structure as in the case of [5]. The use of lesser metal reduces the cost. 4, 5 and 6 grids patterned UC-PBG antennas show different performances. 4 and 6 grids UC-PBG antennas afford dual band gain with maximum gains of 5.24 and 3.95 dBi respectively. But 5 grids UC-PBG show single band gain with the maximum gain of 8.32 dBi at 12.5 GHz. But the reference antenna gain is found to be 2.89 dBi at 12.5 GHz. So the highest gain

is achieved from 5 grids UC-PBG structure. Though the gain is 3 times higher than the reference antenna but cross polarization increases here. Its peak however remains still below the acceptable -20 dB level. Front to back ratio raises from 12 dB to 18.92 dB for this novel simplified 5 grids PBG structure.

J.Y. Park *et al.* [53] described an improved low-profile cavity-backed slot antenna loaded with 2D UC-PBG reflector. They considered the cavity depth of the new antenna is 16 times thinner than that of a conventional $\lambda/4$ wavelength cavity slot antenna. The achievements include 1 dB higher gain than the reference antenna, good front-to-back ratio and no pattern distortion as compared to previous low-profile CBS antennas.

C. Caloz *et al.* [54] introduced a novel structure by stacking up 2 (or more) UC-PBG plates in the direction perpendicular to the plane of the substrate. This new structure has a merit of easy fabrication in contrast to other PBGSs like vias or dielectric inclusions. The periods of the lattice are 'a' and 'a/2' for the bottom and intermediate UC-PBG structures respectively. It has shown the overlapping effect of the stopband associated with each UC-PBG assisted plate results in a dramatic increase in the stop bandwidth preserving excellent transmission characteristics within the passband.

- **Directivity Improvement**

M. Qiu *et al.* [29] developed a high-directivity patch antenna with both PBG substrate and PBG cover. The dielectric constant of the substrate was $\varepsilon_r = 10$ and substrate thickness was 10 mm. The dimension of the patch was 32×18 mm. The

working frequency of the conventional patch antenna was 1.91 GHz. In the substrate medium, square lattice of air holes were used with period = 44 mm and radius of holes = 21 mm. The PBG substrate consists of 9 × 9 unit cells, with the middle five air holes unpunched to support the patch antenna. Thus the dimensions of the substrate are 396 ×396 mm ($L_x \times L_y$). But for the cover, PBG structure is a rectangular lattice (P_x = 60 mm, P_z = 48.5 mm), and the dielectric rods have a rectangular cross section (r_x = 27 mm, r_z = 23 mm). The dielectric constant was same. The distance between the substrate and the cover is chosen to be d = 60 mm. From the directivity radiation patterns for the conventional patch antenna and PBG antennas at a frequency of 1.95 GHz it is reported that the PBG assisted substrate can increase the directivity from 6.0 dB (conventional patch antenna) to 6.7 dB, and the PBG cover can increase the directivity from 6.0 to 13.0 dB. Directivity is raised to 17.1 dB due to the combination of the PBG substrate and PBG cover.

- **A Novel TEM Waveguide**

A novel TEM waveguide is very promising candidate as feeding structure of quasi-optical power combining amplifiers. The use of waveguide in power combining is very popular as the diffraction loss can be avoided in this case [55]. Though dielectric-loaded or oversized waveguides are often used in combined amplifier arrays for achieving uniform aperture field distribution [56] yet they are not suitable at small size due to not having any advantages over a conventional empty waveguide. High-dielectric constant material can improve the performance but it causes the bandwidth to be smaller. On the other hand, UC-PBG structure can be used to build a TEM waveguide with a uniform field distribution. Replacement of two sidewalls of a rectangular waveguide by UC-PBG structure constitutes TEM

waveguide providing PMC surface at the wider stopband. This structure can be fabricated on a thin substrate using a standard etching technique. The proposed PBG waveguide [57] produces a fairly uniform field distribution from 9.4 to 10.4 GHz and the phase velocity is found to be close to the speed of light that ensures TEM propagation. This type of waveguide also finds its application to TEM cells in EMC measurements.

2.4 Reconfigurable Antenna

There is a tremendous effort to dynamically reconfigure antennas to increase their functionality and widen their operating bandwidth to the point of "one does it all". Wideband and low loss switches ensure the antenna to reconfigure itself for multi-band applications. If the switches are varactor diodes, the change in reverse bias voltage also causes to operate the antenna in different frequencies within certain range of bias voltages. But the bandwidth is not high enough.

K. C. Gupta [58] proposed a reconfigurable rectangular ring slot antenna fed by a single slot line or CPW line. By varying the antenna length at two frequencies operation of a slot ring antenna has been proposed. For reconfiguration, 8 switches are used. Switching lengthens or shortens the antenna length. A sample antenna was designed with two operating frequencies being 3.0 and 8.3 GHz. At these two frequencies, the return losses were 17 dB and 22 dB respectively.

A. Fathy *et al.* [59] referred PIN junctions to generate solid-state plasmas, which are effectively implemented for reconfiguration of antennas. Injecting high dc currents into PIN junctions created plasma regions with relatively high

conductivity. A dipole antenna is segmented into 3 segments and utilized plasma generated regions to allow wide frequency coverage from 1 to 20 GHz.

Bernhard *et al.* [60] reported stacked reconfigurable antenna elements for space-based radar applications. They proposed two band applications. Lower band was 2.7-3.5 GHz and upper band was 7-9 GHz. For lower band operation, the upper band elements are disconnected via switches below the ground plane. In a stacked configuration, the upper band elements act as floating parasitic elements for the lower band elements. For the upper band application, lower band elements are grounded via switches so that the lower band elements act as the ground plane for the upper band elements.

- **Reconfigurable Phased Array**

Reconfigurable ground plane is achieved by varying the number of PBGSs in the ground plane. This concept leads to the idea that PBGSs can be used as beam-steerer. B. Elarman *et al.* [18] referred that the phase lag in a PBG engineered microstrip line is approximately proportional to the number of PBG elements in the structures. Based on this concept they designed a 4 × 1 array with reconfigurable ground plane. One feed line is always kept unperturbed that is represented by 0. The feed lines are perturbed with a distribution of 0-1-2-3, 0-2-4-8, 0-3-6-12, 0-4-8-16, 0-5-10-15 and 0-6-12-18. It is seen that the array is found to steer the beam in increments of approximately 6 degree.

2.5 Defected Ground Structure (DGS)

DGS is a new class of structure etched in the ground plane. It is new in terms of its principle of operation. It does not follow Bragg's condition to generate stopband

frequency. Rather the current path controls its stopband. A simple modification in a rectangular/square patterned PBGSs can develop dumbbell shape DGS [19], [61]. A narrow vertical slot connection between two rectangular / square patterned PBG elements give rise a dumbbell shaped DGS elements. In conventional PBG designs the central frequency is controlled by the inter-cell separation. On the other hand, the dimensions of DGS control the 3 dB attenuation point and the locations of the pole. One DGS element under 50-ohm line is show in Fig. 2.16.

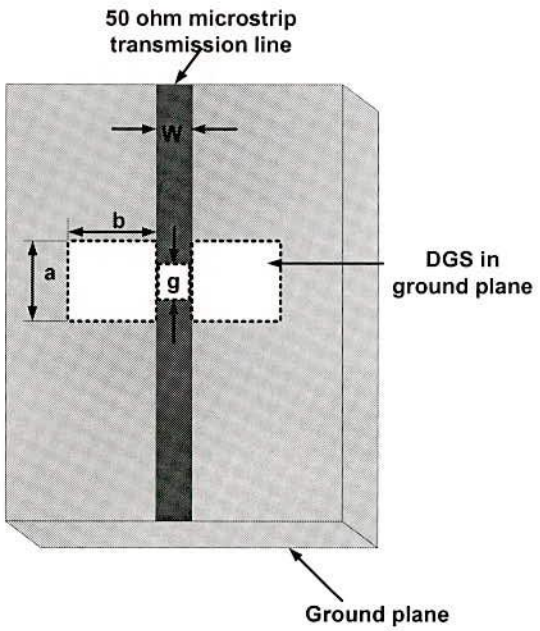

Fig. 2.16: One dumbbell shaped DGS element realized by vertical slot connection between two rectangular patterned PBGSs.

Ring patterned non-uniform dumbbell shaped DGS has been reported [62]. L. Garde *et al.* [62] proposed non-uniform ring patterned dumbbell shaped DGS to design LPF as PBGS with non-uniform distribution is proposed [35]. They have used DGS in the ground plane of a conventional LPF. The conventional LPF is implemented with transmission line obtained by the Richard's transformation that

yields different transmission with different impedances (High-Low impedance sections).

2.5.1 Application of DGS

- **DGS as a LPF**

Two designs for LPF having T-junction stub as well as cross-junction opened stub in conjunction with DGS is used in the ground plane. The T-junction and cross-junction open stub filters are realized by using only two DGS elements in the ground plane of LPF. Measured S-parameters performances have been compared for the fabricated DGS LPF with T-junction, cross-junction open stub, and conventional LPF. The attenuation characteristics for fabricated DGS assisted LPF show more than 20 dB filters up to 8 GHz. The measured insertion loss and return loss are less than 0.15 and 20 dB for fabricated DGS assisted LPF respectively. Besides this type of LPF, H. W. Liu *et al.* [63] proposed a novel fractal defected ground structure and its application to LPF.

2.6 Motivation, Reasoning and the Proposed Proposition of PBG Structures

From the intensive literature survey it is clear that the inclusion of PBGSs / DGSs improve the performance of microwave components and devices significantly. From the performance of novel 2-D PBG structures for microstrip lines it is obvious that the performance is hindered by the optimized value of FF. Even it can be seen from [34], the passband performance is very poor with the optimized FF. The performance with UC-PBGS is reported in [64]. So there exists a wider scope of research to find a newer model of PBG structures that will yield a very wider

and distinct stopband as well as a better passband with minimum ripple heights. The performance of the newer PBGSs for microstrip lines will be observed first and will be compared with the available performances in the literature. Newer DGSs is proposed to replace the conventional one. So the opportunities is being sought to use PBGS/DGS that yields better performances in terms return loss bandwidth, smoother transmission with minimum insertion loss, wider and distinct stopband performance. EBGS in the form PBGSs or DGSs are useful in many microwave devices and components. The conventional PBGSs / DGSs performances need to be improved. In such situation there are lots of research opportunities. This is the main motivation of the present research. The reasons of the present research work are to improve the performance conventional PBGSs/DGSs to be used in microwave devices and components. Both PBGSs and DGSs will be used in 1-D form to realize phased array antenna. This type of PBGS/DGS assisted phased array antenna is a novel idea in microwave community. The prime interests of the research may be mentioned as follows:

- **Non-uniform PBGSs**

From the comprehensive literature survey, it is found that that the researchers design PBGS with optimum filling factor of 0.25. Beyond this value degrades the performances of PBG assisted microstrip transmission line in terms of passband ripple height and return loss performance. The non-uniform distributions will be used to stretch the FF beyond the optimum filling factor and to improve the performances in terms of passband ripple height, better return loss showing impressive input matching including wider and distinct stopband.

Binomial and *Chebyshev* distribution will be used in calculating the amplitude the periodic structures. These configurations of PBGSs will stem better performance than conventional PBGSs. Beyond this, *Chebyshev* distribution will also be used in chirping technique. This chirping technique will show the superiority over the chirping technique available in the literature.

- **Metallic perturbed PBGSs**

In conventional circular patterned PBGSs if metallic perturbation is incorporated into the hole then it forms a ring patterned PBGSs. It facilitates the design in terms of aspect ratio (AR). The relationship of the performance with AR will be demonstrated. It is also believed that the application of *Chebyshev* distribution will further improve the performance.

It is observed that nobody has reported yet the effect of metallic perturbation into the conventional hole and in non-uniform PBGSs. The performance of uniform and non-uniform ring PBG structures will also be reported to use the aspect ratio facility. The detailed designs and performances of different proposed PBGSs for transmission lines will be explained in Chapter 4. In the literature all the reports are confined in low-pass region to investigate the passband performance. Nobody has reported to develop a ripple free passband in high frequency region. A nonuniform ring patterned PBGSs will be considered as a candidate for this purpose.

- **Non-uniform DGSs**

The conventional DGSs provide better performances than the conventional PBGSs. Specially in terms of wider stopband the conventional DGSs stems significant improvement over the regular conventional PBGSs. Therefore there is a scope to find the performance of DGSs with non-uniform distribution. As

Binomial distribution provides abrupt transition in size so attention will be confined to *Chebyshev* distribution. DGSs with *Chebyshev* distribution will provide better performance over the conventional DGSs reported in the literature.

- **Hybrid DGSs-PBGSs**

DGSs do not follow Bragg's condition, yet they may be distributed with a periodic distances. The location of attenuation poles can be controlled with the variation in DGS dimensions. The DGS is more compact design. So there is a scope to use interleaved PBGSs in the gap of periodic DGSs. This type of design will provide wider stopband than conventional DGSs and PBGSs. Even they are expected to be better than non-uniform DGSs also. Finally application of *Chebyshev* distribution in such hybrid design will provide further improvement. It is worthwhile to mention that both DGSs and PBGSs are actually EBGSs. So sometimes they will be referred to as EBGSs for convenience.

2.6.1 Applications of proposed configurations

Newly developed non-uniform PBGSs having Binomial and *Chebyshev* distribution will be applied to (i) suppress the harmonic suppression of BPF, (ii) realize improved LPF properties and (iii) develop dual stopband filter. Non-uniform DGS with *Chebyshev* distribution will also implemented to yield better LPF properties. Uniform ring patterned PBG elements will be applied to conventional aperture coupled patch antennas to investigate their performances. Uniform and non-uniform circular PBG elements will be used to improve the return loss performances in dual band antenna. Finally PBGS and DGS will be used to realize phased array antenna.

- **Applications to BPF**

Conventional PBGSs or PBGSs with non-uniform distribution generate stopband at a particular frequency. Second harmonic suppression may be attained significantly with the non-uniform PBGSs as they provide better performance than conventional ones. Uniform circular PBGS and non-uniform circular PBGS with Binomial distribution will be investigated to see their capabilities of harmonic suppression. To suppress the third harmonic along with second harmonic, the stopband should be enormously large so that they can cover both the harmonics. As PBGSs follow Bragg's condition to define the approximate center of the stopband frequency so they cannot generate enormous stopband suitable for third harmonic suppression. In this circumstance DGSs may be considered to be a vital candidate for both the second and third harmonic suppression.

- **Application to LPF**

All the available works on LPF are seen to use PBGSs/DGSs in the ground plane to improve the performance of conventional LPF. Such designs need to take care both in ground plane and in conductor plane. In the present research the non-uniform distribution of PBGSs and DGSs are considered to realize improved LPF performance without having any attention into conductor layer. Taking care of slots etched in the ground plane is only needed.

- **Application to dual stopband filter**

Attempt will be taken to design a dual stopband filter by PBGSs and DGSs. The dual stopband filter will be realized by conventional PBGSs designed at two frequencies. But this design is not compact as it consists of two sets of PBGSs. To

make it more compact, conventional DGSs with proper dimensions will provide a dual stopband filter. Besides hybrid designs with modified DGSs having interleaved PBGSs will also yield a compact dual stopband filter. *Chebyshev* distribution in the hybrid DGS-PBGS design will further improve the performance. All these designs are novel indeed.

- **Application to antennas**

PBGSs and DGSs will be applied to antenna to enhance the performance. The effect of PBGS on antenna performance will be investigated in terms of return loss, radiation pattern, gain, directivity and efficiency.

Uniform and non-uniform circular PBGSs are proposed to improve the input matching of a dual-band antenna. The non-uniform PBGSs are based on Binomial and *Chebyshev* distribution. Uniform PBGSs will be placed in the patch layer of an aperture coupled dual-band antenna. Antenna with double-layered uniform circular PBGSs (slot layer and patch layer of ACPA) will also be investigated to see the performance of input matching.

- **Application to PBG assisted phased array**

The phase properties of a transmission line perturbed by different numbers of PBG elements will be investigated. In addition to this, the dependency of the phase on the location of PBG elements and the FF will also be observed. Then different numbers of PBG elements with different FFs under the feed lines of an array will be used. Thus phased array using PBGSs will be achieved. DGSs will also be applied to see the beam steering angle. Finally PBGS will be used in reconfigurable phased array antenna.

In the proposed reconfigurable phased array antenna there are lot of scopes to use PBGSs in different layers. The important issue is to use 1-D PBGSs/DGSs under the feed network to steer the beam. To achieve wider range of beam steering angle DGS will be proposed. Investigation will also be carried to observe the compactness of DGS assisted 4-elements phased array design.

2.7 Conclusions

To understand the recent trend of PBGSs, the structures have been extensively studied. To find the areas of the applications of PBGSs in different RF passive and active devices and components, the literature of PBG applications to microwave devices and components have been investigated with significant attention. It can be seen that the literature supports the use of PBGSs to improve the performance of the microwave devices with vast applications mainly in antennas, LPFs and BPFs, amplifiers, oscillators and phased array. The literature survey on reconfigurable antenna has also been accomplished.

The conventional hole patterned PBGSs are found to have poor performance mainly in passband and their performances are hindered by the limiting value of FF. The alternatives in the form of hole and ring patterned PBGSs with non-uniform amplitudes based on Binomial and *Chebyshev distributions* have been proposed.

DGSs and its applications have also been surveyed. They draw more attention as they are compact in nature and provide promising performance than those for

conventional and non-uniform PBGSs. The usefulness of non-uniform DGSs with interleaved PBGSs is highlighted. Finally how the proposed designs will be applied in different RF passive devices has been reported. Main focuses are confined to the application of the proposed model to BPF, LPF, dual stopband filter, antenna, phased arrays and reconfigurable phased array antennas.

Chapter 3 Theory of PBGSs

3.1 Introduction

Recently PBGSs have occupied significant portions of microwave engineering literature to enhance the performance of many microwave devices and components. The nomenclature PBG is actually used in the optical communication. Recently they are scaled down to RF engineering. They are very old concepts in terms of periodic structures. PBG structures are periodic in nature. They originate from stopband and passband like periodic structures. To understand the stopband and passband phenomena in PBG structures, it is better to study the conventional periodic structure.

Waveguides and transmission lines loaded at periodic intervals with identical reactive elements are referred to as periodic structures [51]. This type of period structures yield two distinct properties, namely

(i) Passband – stopband characteristics; and

(ii) Stemming waves with phase velocity lower than the velocity of light in free space.

In the passband the EM is unattenuated along the structure. There may be some incidental conductor loss only. On the other hand, in the stopband the EM wave is totally attenuated so that it cannot propagate throughout the structure. This stopband – passband characteristics are very important to suppress the surface waves, a crucial issue in microwave engineering.

EM wave having the velocity lower than the velocity of light in free-space is called slow wave. Periodic perturbation in the ground plane provides periodic

discontinuity. Thus the slow wave property of the EM wave is achieved. Slow wave structures (SWSs) are promising candidates for compact design.

3.2 Periodic structures

3.2.1 Capacitively loaded transmission-line-circuit analysis:

A simple capacitively loaded transmission line can be analyzed to conceive the idea on periodic structures. The velocity of EM wave in a physically smooth transmission line can be written as

$$V_p = \frac{1}{\sqrt{LC}} = \frac{1}{\sqrt{\mu_0 \varepsilon_0 \varepsilon_r}} \tag{3.1}$$

Where

V_P is the phase velocity of EM wave.

L is the series inductance per unit length.

C is the shunt capacitance per unit length.

ε_r is the dielectric constant of the medium surrounding the conductor.

ε_0 and μ_0 are free-space values of the permittivity and permeability respectively.

From equation (3.1) it is seen that with the value of the dielectric constant (ε_r), the phase velocity of EM waves reduces. One problem arises on this simplest way of reducing the phase velocity. If the value of dielectric constant is increased then the higher-order mode of wave propagates. To avoid this propagation, the cross sectional dimensions of the line must be reduced accordingly. This is the limitation of increasing the value of dielectric constant to get the reduced value of the phase velocity of EM waves.

We know $LC = \mu_0\varepsilon$ for dielectric media. So any attempt of increasing the value of C to reduce the phase velocity is restricted here. Because if the value of C is increased the value of L will be automatically reduced to maintain the relation, $LC = \mu_0\varepsilon$ in a physically smooth transmission line. Under this circumstance, the restriction of a physically smooth transmission line can be relaxed instead of an electrical smooth line. An effective increase in the shunt capacitance per unit length (C) can be achieved without disturbing the value of inductance per unit length (L) by loading lumped shunt capacitance at periodic intervals where the spacing between the loaded shunt capacitance are small compared with the wavelength. At this stage, though the line is not physically smooth but it will be an electrically smooth line. Under this condition the capacitance will be increased which can be observed from the following equation of the phase velocity.

$$V_p = \frac{1}{\sqrt{(C + C_0/d)L}} = \frac{\omega}{\beta} \tag{3.2}$$

Where C_0/d is the loaded lumped capacitance per unit length and C_0 is the capacitance loaded per interval d.

There are many ways of obtaining periodic structures. One of the simplest ways is to load a thin diaphragm at regular intervals in a coaxial transmission line. The diaphragm may be machined as the integral part of the center conductor. The fringing electric field in the vicinity of the diaphragm increases the local storage of the electric energy and hence giving more extra shunt capacitance.

3.2.2 Circuit Analysis of a Periodic Structure

A transmission line can be considered as the combination of finite unit cell of the structure. Fig. 3.1(a) is the equivalent circuit of a basic unit cell of a capacitively

loaded coaxial line and Fig. 3.1(b) is the complete transmission line composed of basic unit cell.

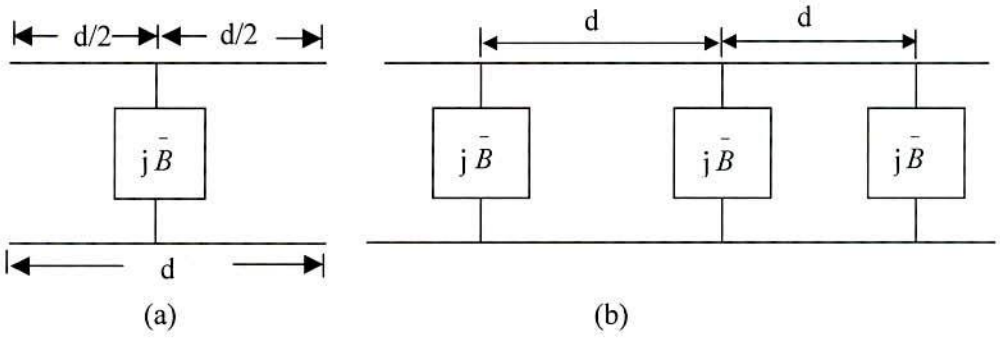

Fig. 3.1: (a) Equivalent circuit model of a unit cell, (b) a transmission line cascaded by unit cells. The unit cell may be divided into three parts as a transmission line of length d/2 on either side of normalized succeptance B.

- **Relationship between input and output variables:**

Let V_n and I_n are the input voltage and current variables respectively.

V_{n+1} and I_{n+1} are the output voltage and current variables respectively.

The relationship can be found by using ABCD transmission matrix. Overall ABCD parameters of a unit cell

$$\begin{bmatrix} A & B \\ C & D \end{bmatrix} = \begin{bmatrix} \cos\theta/2 & j\sin\theta/2 \\ j\sin\theta/2 & \cos\theta/2 \end{bmatrix} \begin{bmatrix} 1 & 0 \\ j\bar{B}1 & \end{bmatrix} \begin{bmatrix} \cos\theta/2 & j\sin\theta/2 \\ j\sin\theta/2 & \cos\theta/2 \end{bmatrix} \quad (3.3)$$

Where $\theta = k_0 d$

Unit cell is symmetrical where A = D

When EM wave propagates through periodic structures, the voltage and current at (n+1)th terminal are equal to the value of voltage and current of the n^{th} terminal except the phase delay. It is noted that voltage and current is valid only for lossless lines.

The relation of V and I are assumed as follows.

$$V_{n+1} = e^{-\gamma d} V_n \quad (3.4)$$

$$I_{n+1} = e^{-\gamma d} I_n \tag{3.5}$$

It can be written

$$\begin{bmatrix} V_n \\ I_n \end{bmatrix} = \begin{bmatrix} A & B \\ C & D \end{bmatrix} \begin{bmatrix} V_{n+1} \\ I_{n+1} \end{bmatrix} = e^{\gamma d} \begin{bmatrix} V_{n+1} \\ I_{n+1} \end{bmatrix} . \tag{3.6}$$

Using equation (3.4) and (3.5), equation (3.6) generates a matrix Eigen value equation for the solution of V_{n+1} and I_{n+1}. The determinant is put to be zero.

$$\begin{bmatrix} A - e^{\gamma l} & B \\ C & D - e^{\gamma l} \end{bmatrix} = 0$$

$AD - BC - e^{\gamma d}(A+D) + e^{2\gamma d} = 0$

Assuming reciprocal circuit, letting AD-BC = 1 we have

$1 + e^{2\gamma d} - e^{\gamma d}(A+D) = 0$

$$\cosh \gamma d = \frac{A+D}{2} \tag{3.7}$$

Expansion of (3.3) shows $A = D = \cos\theta - \frac{\bar{B}}{2} \sin\theta$. Putting these values in equation (3.7), we have

$$\cosh\gamma d = \cos\theta - \frac{\bar{B}}{2} \sin\theta \tag{3.8}$$

Equation (3.8) is very vital equation to understand passband and stopband phenomena created by periodic structure.

- **Explanation**

The phenomena can be explained by the following cases:

***Case 1*:** $\alpha = 0, \beta \neq 0$. This case corresponds to non-attenuating propagating wave on the periodic structure. This case defines the passband of the structure. Then equation (3.8) reduces to

$$\text{Cos}\beta d = \cos\theta - \frac{\bar{B}}{2}\sin\theta \qquad (3.9),$$

which can be solved for β if the magnitude of the right hand side is less than or equal to unity. ***Case 1*** is limited to <1 AND >-1.

Case2: $\alpha \neq 0$, $\beta = 0$. In this case the wave does not propagate, but is attenuated along the line. This case defines the stopband of the structure. As the line is assumed to be lossless, power is not dissipated, rather is reflected back to the input of the line. Under this condition the equation (3.9) reduces to

$$\cosh\alpha d = \cos\theta - \frac{\bar{B}}{2}\sin\theta \qquad (3.10)$$

The magnitude of equation (3.10) reduces to

$$\cosh\alpha d = \left| \cos\theta - \frac{\bar{B}}{2}\sin\theta \right| \geq 1,$$

Equations (3.9)-(3.10) are very important to understand the propagation of EM waves through periodic structures. It is apparent that there will be frequency bands for which unattenuated wave propagation is possible separated by frequency bands in which the wave is attenuated. Fully attenuated wave stems stopband and unattenuated wave generates passband. Thus these equations help understand of stopband and passband phenomena of PBGS.

Let us consider $d \leq \lambda_0$ in a case. So the electrical length $\theta = k_0 d$ will be small and

βd is also small. Under this condition

$$\cos\theta = 1 - \theta^2/2 \qquad (3.12)$$

$$\cos\beta d = 1 - \frac{\beta^2 d^2}{2} \qquad (3.13)$$

Equation (3.9) comes into the following form

$$\Rightarrow 1- \frac{\beta^2 d^2}{2} = 1- \frac{k_0^2 d^2}{2} - \frac{B k_0 d}{2} \qquad (3.14)$$

We have the relations

$$k_0^2 = \omega^2 \mu_0 \varepsilon_0 = \omega^2 LC \qquad (3.15)$$

$$\bar{B} = \frac{B}{Y_c} = \omega C_0 \sqrt{L/C} \qquad [Z_c = \sqrt{L/C}] \qquad (3.16)$$

So $1- \frac{B^2 d^2}{2} = 1- \frac{k_0^2 d^2}{2} - \frac{\bar{B} k_0 d}{2}$

$$\Rightarrow \beta^2 d^2 = k_0^2 d^2 + \bar{B} k_0 d$$

$$\Rightarrow \beta^2 = k_0^2 + \frac{\bar{B} k_0}{d}$$

Substituting k_0 and $\bar{B}$ from (3.15) and (3.16) in the above equation we have

$$\beta^2 = \omega^2 LC + \omega^2 \frac{LC_0}{d}$$

$$\Rightarrow \beta = \omega \sqrt{L(C + C_0 / d)} \qquad (3.17)$$

Equation (3.17) is very important to understand the slow-wave effect of periodic structures. The new value of capacitance $C+C_0/d$ is observed. So capacitance has been increased by C_0/d. Therefore it is found that at low frequencies where d $<<\lambda_0$, the load line behaves as a shunt capacitance $C+C_0/d$ per unit length. The increase in β reduces of the phase velocity.

For periodic structure the characteristic impedance (CI) becomes,

$$Z_B = \sqrt{\frac{L}{C + \frac{C_0}{d}}}$$

It is seen that capacitance has increased by $\frac{C_0}{d}$.

The characteristic impedance of a periodic structure depends on the terminal plane. Lets say if the normalized characteristic impedance in the reference plane is $\overline{Z_B}$ and if the terminal planes are shifted a distance l in the –z direction, the new normalized CI becomes

$$\overline{Z}'_{B'} = \frac{\overline{Z_B} + j \tan k_0 l}{1 + j\overline{Z_B} \tan k_0 l} \tag{3.18}$$

3.4 Transmission Line Model of PBG Structures

This section presents analytical approach of bandgap performance of UC-PBGS. The mathematical formulation of UC-PBG structures has been developed using transmission line model [65].

Basically a unit UC-PBG consists of a square metallic patch with four connecting branches. The period of each cell is approximately half wavelength of the central frequency of the attenuation pole. The slow wave effect of the periodic structures contracts the wavelength of the transmission lines; the period is no longer half wavelength of the same center frequency. Hence, the slow wave effect gives rise to a unique compact device structure. R.F. Yang and T. Itoh [50] design a periodic UC-PBG using complex finite difference time domain (FDTD) method. The method requires writing numeric codes for the analysis of the specific frequency characteristic of a LPF response. The applications of the proposed UC-PBG lattice structure on BPF and CB-CPW for wide rejection band of more than 20 dB at attenuation pole located at 11.5 GHz and cutoff frequency of 10 GHz have been demonstrated. The slow-wave factor (SWF) of the UC-PBG structure is approximately 1.2 to 2.4 times higher than that for the unperturbed line at passband. M. Rahman and M. A. Stuchly [65] have proposed a transmission line

model to calculate the impedance of each section followed by the analysis of the whole structure. The following section presents the transmission line model of a unit UC-PBG cell, the dispersion diagrams and the phase of the reflection coefficient of a wave incident on the structure.

3.4.1 UC-PBG Theory

The analytic models of two high impedance surfaces UC-PBGS are shown on Fig. 3.2(a) and (b). The lattice in Fig. 3.2(a) consist of a distribution of square metal patches, each patch is shorted to the ground plane by a thin pin and the lattice in Fig. 3.2(b) consists of square patches, each indented with four narrow connecting branches placed over a ground plane. The circuits can be considered as arrays of reactively loaded resonators coupled by gap capacitors. If the shorting pins or the connecting branches were disregarded, the period of each cell would be half-wavelength of the resonator frequency. However, the additional shorting pins or connecting branches increase the reactive loading of the cell and consequently caused a lower resonance frequency. This agrees with the slow wave effect of the PBG structure. Thus, the 2-D UC-PBGS arrays shown in Figs. 3.2(a) and (b) can be considered as structures periodically loaded with gap capacitances and inductances provided by either the shorting pins or the connecting branches. Both the TE and TM modes with respect to the normal to the surface exist in these structures and they are coupled.

The equivalent circuit of the reactive loading part for Figs. 3.2 (a) and (b) can be represented in Fig. 3.2(c), where Z_p is the reactance of the resonator. The coupling gap capacitance between the neighboring resonators and the reactance of

the resonator are the two contributions to the total impedance between the two nodes of the periodic circuits. As shown in Fig. 3.3 the capacitive reactance X_c represents the gap capacitance between the resonators.

With reference to Fig. 3.2(c), the impedance Z_p of each resonator section is calculated in two steps using the transmission line formula,

$$Z_{in} = Z_0 \frac{Z_l + jZ_0 \tan(\beta_u l)}{Z_0 + jZ_l \tan(\beta_u l)} \tag{3.19}$$

Step 1: Taking $Z_l = \infty$ at $l = 0$ and calculate Z_m at $l = w/2$ using equation (3.19), that is

$$Z_m = -jZ_0 \cot(\beta_u w/2) \tag{3.20}$$

Step 2: Taking $Z_l = X_L // Z_m$ at $l = w/2$, including the reactance X_L represented by a coil and Z_p can be calculated using equation (3.19) as follows:

$$Z_p = Z_0 \frac{Z_l + jZ_0 \tan(\beta_u w/2)}{Z_0 + jZ_l \tan(\beta_u w/2)} \tag{3.21}$$

For each cell in Figure 3.2 (a), using the numerical method given, the inductive loading X_l of the central shorting pin, with inductance equal to [66]:

$$L = 2\times10^{-7} t\left[\ln\left(\frac{4t}{d}\right) + 0.5\left(\frac{d}{t}\right) - 0.75\right] \tag{3.22}$$

where t and d are the length and diameter of the pin.

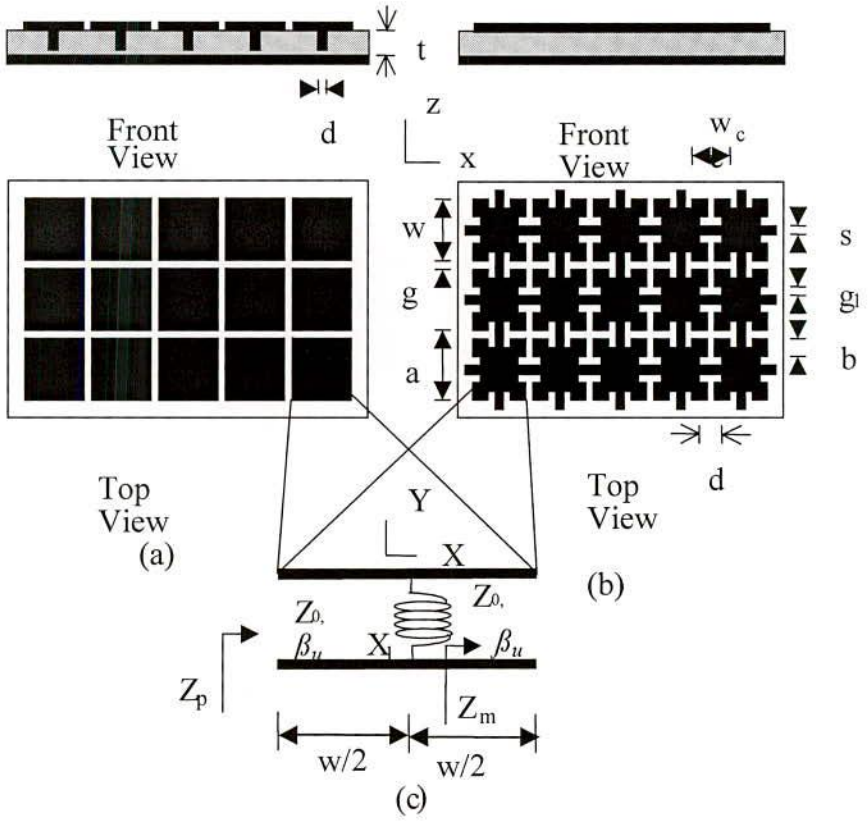

Fig. 3.2:(a) array of square metal plates with shorting pins, (b) array of square metal plates with connecting branches, (c) Equivalent circuit of each resonator section.

The coupling capacitance between resonators can be written as [66]:

$$C = \frac{w\varepsilon_0(1+\varepsilon_r)}{\pi}\cosh^{-1}\left(\frac{a}{g}\right) \tag{3.22}$$

where a, w, g denote the dimensions as shown in Fig. 3.2. In the above figure Z_0 is the characteristic impedance of the line and B_u is the phase constant of a lossless line.

Similarly, considering each cell in Figure 3.2(b), using the numerical method given, the total inductance provided by the four connecting branches, can be calculated as [66]:

$$L = 0.25\times10^{-7}d\left[\ln\left(\frac{d}{s}\right)+0.2235\left(\frac{s}{d}\right)+1.193\right]k_g \tag{3.23}$$

where k_g is a correction factor for the ground plane, which is given as [66]:

$$k_g = 0.57 - 0.145 \ln\left(\frac{s}{t}\right) \tag{3.24}$$

and the coupling capacitance between resonators is [66]:

$$C = \frac{2b\varepsilon_0(1+\varepsilon_r)}{\pi}\cosh^{-1}\left(\frac{w_c}{g}\right) \tag{3.25}$$

Once the impedance of the resonator and the coupling capacitor are known the impedance of the structures shown in Fig. 3.2 is known. Hence, the UC-PBG array in Figure 3.2(a) and (b) can be treated as a transmission line periodically loaded with lumped impedance Z consisting of Z_p in parallel with X_c with a period of a as shown in Fig. 3.3.

$$Z = \frac{Z_p X_c}{Z_p + X_c} \tag{3.26}$$

The equivalent circuit for the wave propagation in the x-direction that is shown in Fig. 3.3 is also an analogous circuit corresponding to the propagation in the y-direction. With reference to [51], the ABCD matrix of a cascade of unit UC-PBG cell, consisting of a transmission line section of length $a/2$, series impedance Z as defined in equation (3.26) and another transmission line section of length $a/2$ is:

$$\begin{bmatrix} A & B \\ C & D \end{bmatrix} = \begin{bmatrix} \cos\frac{\beta_u a}{2} & jZ_0 \sin\frac{\beta_u a}{2} \\ jY_0 \sin\frac{\beta_u a}{2} & \cos\frac{\beta_u a}{2} \end{bmatrix} \begin{bmatrix} 1 & Z \\ 0 & 1 \end{bmatrix} \begin{bmatrix} \cos\frac{\beta_u a}{2} & jZ_0 \sin\frac{\beta_u a}{2} \\ jY_0 \sin\frac{\beta_u a}{2} & \cos\frac{\beta_u a}{2} \end{bmatrix}$$

$$= \begin{bmatrix} \cos\beta_u a + j\frac{Z}{2Z_0}\sin\beta_u a & \frac{Z_0}{2}\cos\beta_u a + jZ_0\sin\beta_u a + \frac{Z}{2} \\ \frac{Z}{2Z_0}\cos\beta_u a + \frac{j}{Z_0}\sin\beta_u a - \frac{Z}{2Z_0^2} & \cos\beta_u a + j\frac{Z}{2Z_0}\sin\beta_u a \end{bmatrix} \tag{3.27}$$

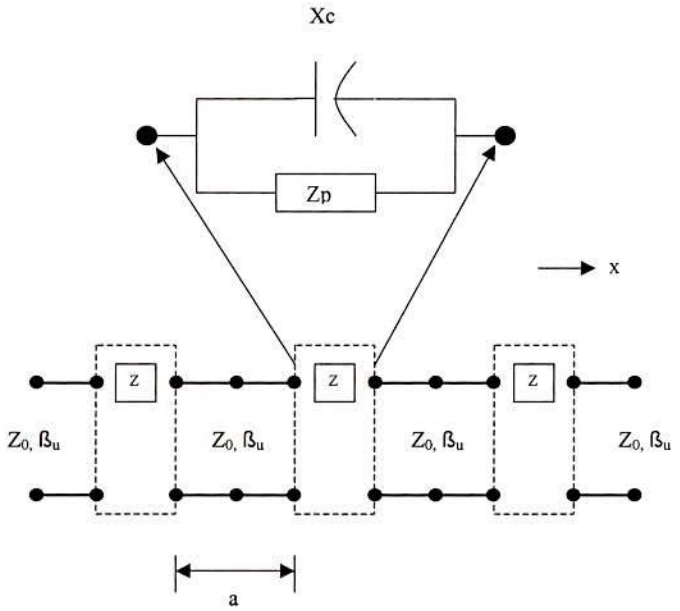

Fig. 3.3: Equivalent circuit of the periodic structure

For the conditions of a reciprocal network, $AD - BC = 1$ and nontrivial solution, the determinant of the matrix must be vanished. The following equation of propagation constant γ is derived along the infinite periodic UC-PBG structure as:

$$\cosh(\gamma a) = \cos(\beta_u a) + j\frac{Z}{2Z_0}\sin(\beta_u a) \tag{3.28}$$

where Z_0 is the characteristic impedance and β_u is the phase constant of the unloaded line, they are the same as those of the resonators.

With $\gamma = \alpha + j\beta$, equation (3. 28) can be rearranged as:

$$\cosh(\alpha a)\cos(\beta a) + j\sinh(\alpha a)\sin(\beta a) = \cos(\beta_u a) + j\frac{Z}{2Z_0}\sin(\beta_u a) \tag{3.29}$$

where α is the attenuation of the wave propagation.

Since Z is purely reactive for lossless (ideal case) resonators, thus making the right hand side of equation (3.29) a real value and this in turn produced a purely real value for the left hand side of equation at the condition which either $\alpha = 0$ or $\beta = 0, n\pi/a$. This corresponds to passband and stopband conditions, which are considered below for the wave propagation in PBG structure.

1. The passband condition of the periodic structure:

   $\alpha = 0$ and $\beta \neq 0, n\pi/a$, equation (3.29) is reduced to

$$\cos(\beta a) = \cos(\beta_u a) + j\frac{Z}{2Z_0}\sin(\beta_u a) \tag{3.30}$$

2. The stopband condition of the periodic structure:

   $\alpha \neq 0$ and $\beta = 0$, $n\pi/a$, equation (3.29) is reduced to

$$\cosh(\alpha a) = \cos(\beta_u a) + j\frac{Z}{2Z_0}\sin(\beta_u a) \tag{3.31}$$

The UC-PBG structure is designed and simulated using MATLAB to show the plot of stopband and passband region of the following UC-PBG structure. The dimensions of the UC-PBG structure presented here are:

Dimensions: w = 15.0 mm, a = 15.13 mm, g = 0.13 mm, g1 = 2.615 mm, b = 1.885 mm, d = 3.8 mm, s = 6.0 mm, w_c = 9.1 mm

The geometry of a modified UC-PBG structure that provides stopband at lower frequency is shown in Fig. 3.4. This type of UC-PBG structure can find applications in harmonic suppression of hairpin filter [67]-[74].

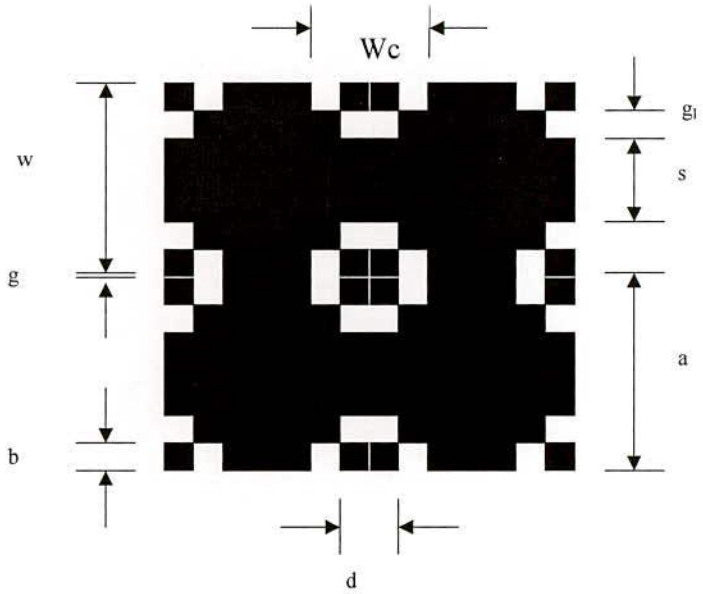

Fig. 3.4: Geometry of a modified UC-PBG structure to yield stopband at lower frequency. Dimensions: w =15.0 mm, a = 15.13 mm, g = 0.13 mm, g1 = 2.615 mm b = 1.885 mm, d = 3.8 mm, s = 6.0 mm, Wc = 9.1 mm

The bandgap performance generated from the simulation of MATLAB is shown in Fig. 3.5. As can be seen in the dispersion diagram in Fig. 3.5, the stopbands are created in 2 ~ 2.8 GHz, followed by a passband.

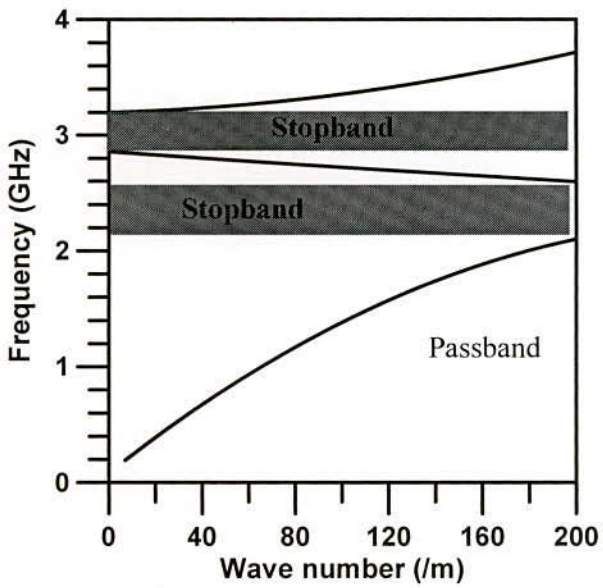

Fig. 3.5: Plot of propagation wave number, passband and stopband frequency range of the 2-D UC-PBG array.

Conventional PBGSs follow Bragg's condition to calculate the center of the stopband frequency. The period will be larger at the stopband frequencies that range from 2 to 2.8 GHz. The unit cell of the PBG lattice consists of a square metal pad with four connecting branches as shown in Fig. 3.4. The narrow branches including connecting insets provide additional inductance. On the other hand gaps between adjacent pads enhance capacitance. The series reactive element along with shunt capacitances provides much larger propagation constant than that of conventional microstrip line. This is the unique property of UC-PBGS to be very compact design. By this scheme both inductance and capacitance are enhanced. Therefore the center frequency of the stopband shifts to lower frequency.

3.7 Uniform PBG (UPBG) Configurations Applied To Microstrip Lines

In the preceding sections the theory and analysis of periodic structures followed by UC-PBG configurations are presented. In modern microwave devices, microstrip transmission lines are commonplace. Therefore, in the following sections, the investigation is concentrated into only on PBG assisted microstrip transmission line. To derive the characteristic performance of PBG assisted lines it is more logical to use scattering parameters (S-parameters) instead of showing K-β diagram. S-parameters are universally accepted format of device characterizations. Moreover, commercially available software tool IE3D will be used to design and to extract S-parameters for all designs due to the flexibility of IE3D. IE3D is a method of moment (MOM) based full-wave analysis tool, hence very accurate.

The perturbation in the ground plane of any microstrip transmission line in the form of PBGS creates stopband that is useful for suppression of surface waves, leakage, and spurious transmission and to improve the performance of antennas, filter and other microwave devices and components. The stopband characteristic is highly influenced by the shape, size and the period of the PBGSs located on the ground plane. Therefore it is useful to see the performance of the standard 50-ohm microstrip transmission line on PBGSs. The lines will be investigated to see the performance of three rows of uniform PBG structure as [34]. In this section uniform circular and square patterned PBGS will be investigated. It is well known that the EM field is highly concentrated under the microstrip line. Under this consideration, one dimensional (1-D) uniform PBGS (one line) will be investigated and compared the result with 2-D structure (three lines). Finally 1-D PBGS will be used as two structures yield similar performances.

3.7.1 Design of Microstrip Transmission Line over Uniform PBGS (uniform circular PBGS)

With the inclusion of PBGSs the dispersion characteristics of a transmission line change. At first a microstrip transmission line with unperturbed ground plane is designed that does not provide any stopband characteristics. Then the effect is observed on the dispersion characteristics in the form of scattering parameters matrices versus frequency by perturbing the ground plane with uniform circular PBGSs.

- **Designing equation**

In the PBG engineering it is a conventional rule to use Bragg's condition [20] to calculate the central stopband frequency provided by PBGSs. Under this condition, inter-cell separation (known as period) is approximately equal to half wavelength of the stopband central frequency. From the inter-cell separation, the size of the PBG element is calculated on the basis of FF.

The center frequency of the stopband is calculated approximately with the following expression:

$$\beta a=\pi \tag{3.32}$$

Where, a is the period of the PBG pattern, and β is the wave number in the dielectric slab and is defined by expression:

$$\beta =\frac{2\pi f_0}{c}\sqrt{\varepsilon_e} \tag{3.33}$$

Where,

f_0 = the center frequency of the stopband

ε_e = the effective relative permittivity of the dielectric slab

c = the speed of light in free space

- **Designs of Uniform Circular PBGSs**

The following different microstrip transmission lines are designed. All the PBGSs are designed at the stopband central frequency of 10 GHz.

1. **Standard 50-ohm transmission line:** In this case the ground plane is fully unperturbed. The configuration of the microstrip transmission line is shown in Fig.

3.6. A standard 50-ohm line is realized on RT/Duroid substrate having dielectric constant of 10.5 and height of 25 mils.

2. **2-D uniform circular elements in the ground plane:** Here three PBG structures under 50-ohm transmission lines with FF of 0.125, 0.25 and 0.45 are designed to produce the same result of [34]. This design gives the idea of optimum value of FF to be 0.25. The geometry of a three rows (2-D) uniform hole patterned PBGSs in the ground plane of a 50-ohm transmission line is shown in Fig. 3.7.

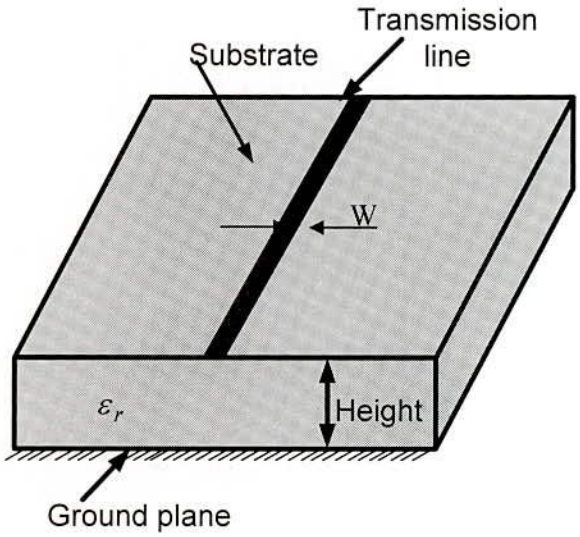

Fig. 3.6: Geometry of a standard 50-ohm microstrip transmission line on RT/Duroid substrate. Substrates: ε_r = 10.5 and height (h) = 25 mils, tanδ = 0.00015 and W = 24 mils.

3. **1-D uniform circular PBGSs with FF of 0.25:** This design will yield the performance to consider 1-D PBGSs that replace 2-D PBGSs.

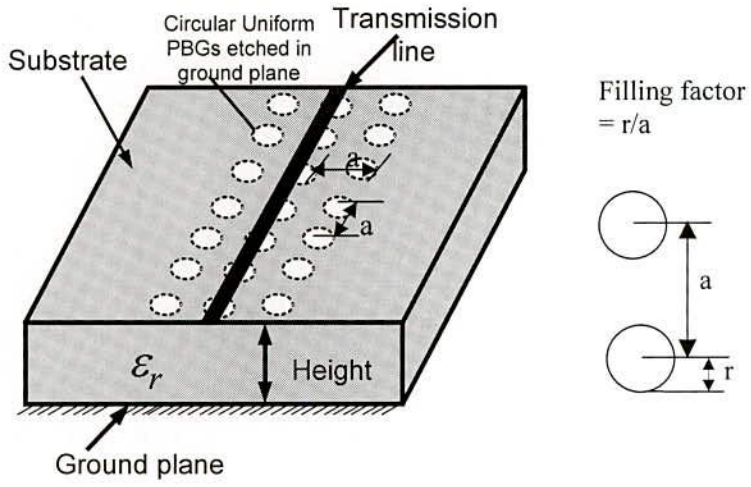

(a) (b)

Fig. 3.7: Geometry of a 50-ohm microstrip transmission line where 2-D (three lines) uniform circular PBGSs are etched in the ground plane. (b) The filling factor (FF) explanation.

The geometry of 1-D uniform hole patterned PBGSs is shown in Fig. 3.8. In this design only one row of PBG elements are etched in the ground plane just under 50-ohm transmission line.

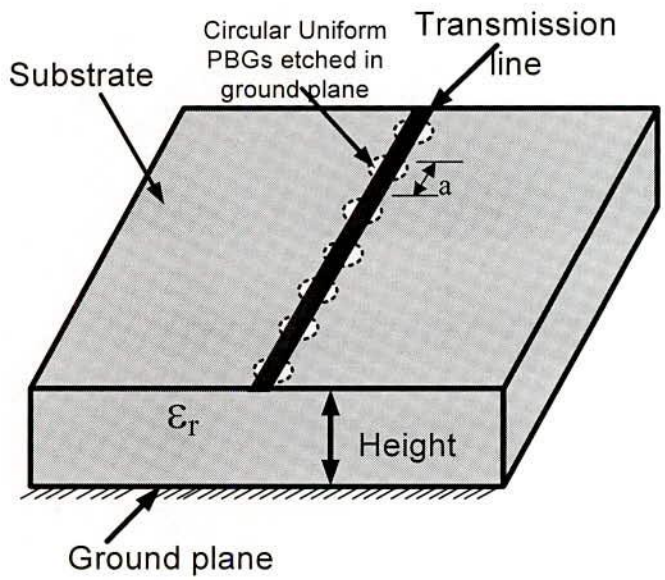

Fig. 3.8: Geometry of a standard 50-ohm transmission line with 1-D uniform circular PBGSs etched in the ground plane.

- **Designs of Uniform Square Patterned PBGSs**

Uniform square patterned PBGSs will also be designed. Here three rows and one row PBGSs will be designed and their performances will be compared. It will be useful to replace three rows PBGSs by 1-D PBGSs. On the basis of the availability of the materials for the fabrications Taconic substrate with $\varepsilon_r = 10$ and height (h) = 25 mils is used in the simulation.

- **2-D Uniform Square Patterned PBGSs**

The conventional uniform square patterned PBGSs are shown in Fig. 3.9. Three lines of total 27 PBG elements are etched under the standard 50-ohm transmission line. The FF is taken to be 0.46.

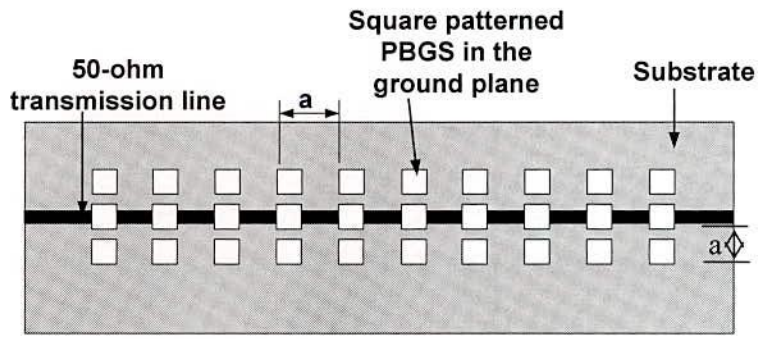

Fig. 3.9: 2-D (three lines) of square patterned PBGSs under standard 50-ohm transmission line. Substrates: $\varepsilon_r = 10$ and height (h) = 25 mils, $\tan\delta = 0.00015$ and W = 24 mils. The inter-element spacing (period) a = 226 mils.

- **1-D square patterned PBGSs**

The geometry of 1-D (one line) circular patterned PBGSs is shown in Fig. 3.10. Here only 9 PBG elements are etched in the ground plane.

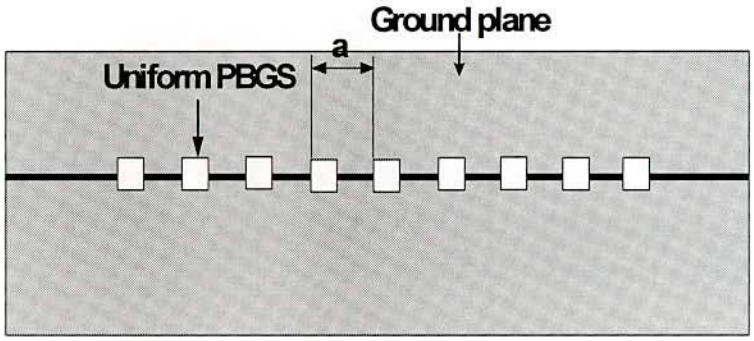

Fig. 3.10: 1-D square patterned periodic structures under standard 50-ohm transmission line. The substrate is Taconic having dielectric constant of 10 and height of 25 mils. The inter-element spacing (period) a = 226 mils.

3.7.2 Results

An ideal transmission line as well as transmission lines having circular and square patterned uniform PBGSs in the ground plane have been investigated. The performances have been analyzed of the lines in terms of 10 dB return loss bandwidth, 20 dB rejection bands, ripple heights in passband, depth of the stopband and maximum value of return loss. The S-parameters of the designs have been investigated to conceive the idea of 1-D PBGSs in lieu of 2-D PBGSs, optimized FF and the influence of number of PBGSs on the dispersion characteristics of the microstrip transmission line. The same substrate as [34] is used in the simulation for the ideal and uniform circular patterned PBGSs. The aim is to validate the results of uniform circular PBGSS simulated by EM software Zeland IE3D with published results of [34]. The simulated S-parameters performances of an ideal transmission line are shown in Fig. 3.11. The insertion loss is approximately zero dB throughout the whole frequency range from 0 to 16 GHz.

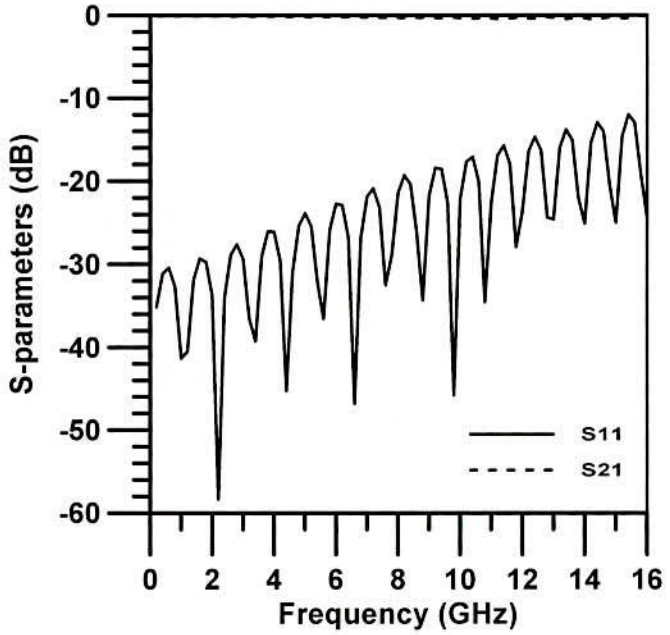

Fig. 3.11: IE3D simulated S-parameters versus frequency of an ideal 50-ohm transmission line. The substrate is RT/Duroid having height of 25 mils and the dielectric constant is 10.5.

It can be seen from the graph that the signal is transmitting between two ports of transmission line with negligible loss. Therefore within the whole range of frequencies (0-16 GHz) there is no stopband. The return loss performance of the ideal microstrip line over the whole frequency range is also excellent and > 10 dB. Obviously the S-parameters performance shown in Fig. 3.11 characterizes an ideal transmission line.

- **The Transmission Line with 2-D (three lines) Uniform Circular PBGS with Different FFs**

At first, small uniform and circular holes have been introduced in the ground plane to observe their effects on the performance of a standard 50-ohm transmission line. The uniform circular PBGSs are of 25 mils and the period is 200 mils. The S-parameters performance is shown in Fig. 3.12.

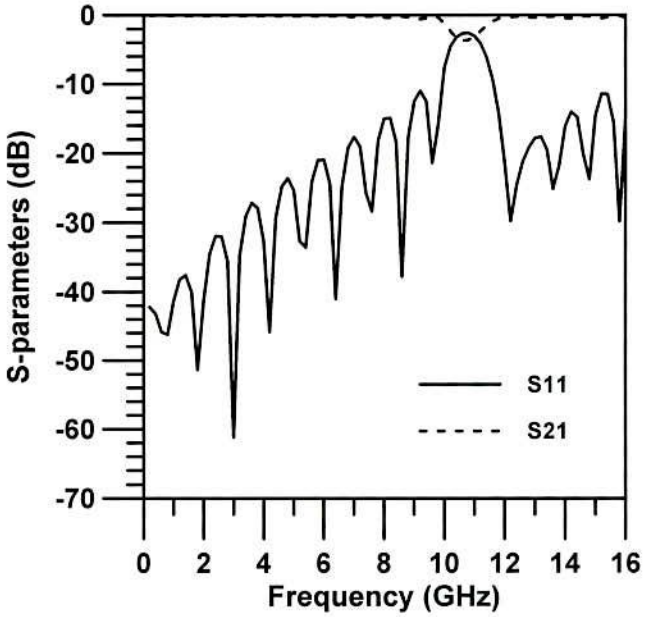

Fig. 3.12: Simulated S-parameter performances of a standard 50- ohm transmission line perturbed by 2-D (three lines) uniform circular PBGSs in the ground plane. The substrate is RT/Duroid having height of 25 mils and dielectric constant of 10.5. The uniform circular PBGSs are of 25 mils and the period is 200 mils (FF=0.125).

It can be seen from Fig. 3.12 that the 10 dB return loss bandwidth is very large (10 GHz). But the stopband is very negligible around the central frequency of 10 GHz. The passband ripple height is very negligible. From this figure it can be concluded that small sizes of PBGSs (smaller FF) cannot generate wider stopband.

Secondly the same line with larger UPBG elements is investigated. In this case, the radius of the PBGSs is 50 mils corresponding to 0.25 FF. The performance of the microstrip transmission line perturbed by uniform circular PBGSs having FF of 0.25 is shown in Fig. 3.13.

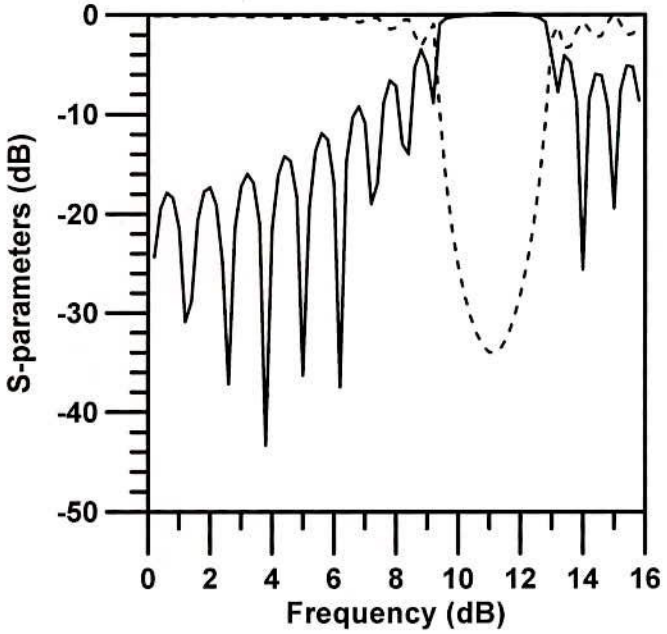

Fig. 3.13: Simulated S-parameter performances of a standard 50- ohm transmission line perturbed by 2-D (three lines) uniform circular PBGSs in the ground plane. The substrate is RT/Duroid having height of 25 mils and dielectric constant of 10.5. The uniform circular PBGSs are of 50 mils and the period is 200 mils (FF=0.25).

It can be seen from the figure that this design provides wider passband and deeper stopband. The 10 dB return loss bandwidth is found to be 6.59 GHz; the 20 dB rejection bandwidth is 2.73 GHz. The ripple height along the passband is negligible. But around cut-off frequencies ripples are observed. The center frequency is found to be shifted around 11.07 GHz resulting in 10.7% frequency deviations from the design frequency. The maximum value of isolation is found to be 35 dB.

Finally the sizes of circular UPBG elements are varied to be 90 mils corresponding to FF of 0.45 to investigate the performance of the same microstrip line. The S-parameter performances are shown in Fig. 3.14. It can be seen that huge amount of ripples are present all along the passband. The stop bandwidth has improved significantly but the passband ripples and return loss are very poor. No 10 dB

return loss bandwidth is found. The stopband is wider (more than 6 GHz) and maximum isolation is 47 dB. Huge ripples appear in the passband. Therefore considering all these factors, FF of 0.25 may be considered as the optimum value of FF that well agrees with [34]. This is one of the very crucial limitations of uniform circular PBGSs.

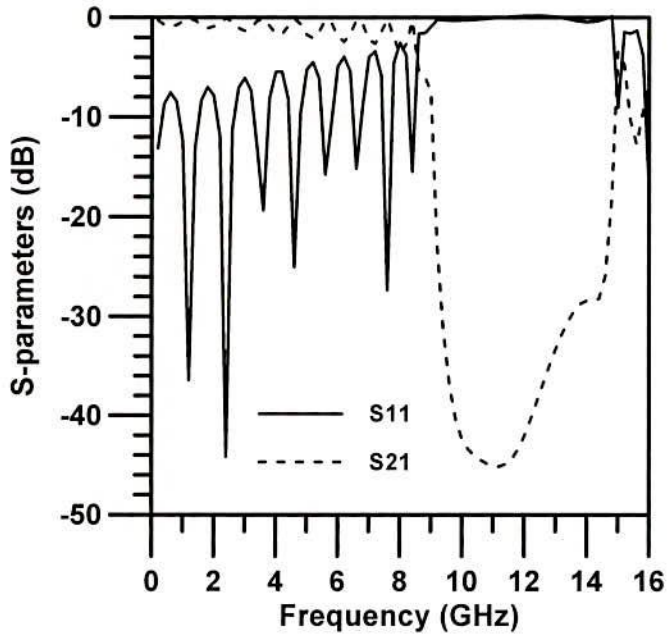

Fig. 3.14: S-parameter performances of a standard 50- ohm transmission line perturbed by 2-D (three lines) uniform circular PBGSs in the ground plane. The substrate is RT/Duroid having height of 25 mils and dielectric constant of 10.5. The uniform circular PBGSs are of 90 mils and the period is 200 mils (FF=0.45).

The simulated performance of uniform circular PBGSs with published result [34] having FF of 0.25 has been compared in Fig. 3.15. It can be seen that there exists an impressive agreement between the simulated and published performances. Besides the simulated performances are compared with the experimental investigations are shown for the case of uniform square patterned PBGSs. The one line (1-D) and three lines (2-D) of uniform square patterned PBGSs are studied there.

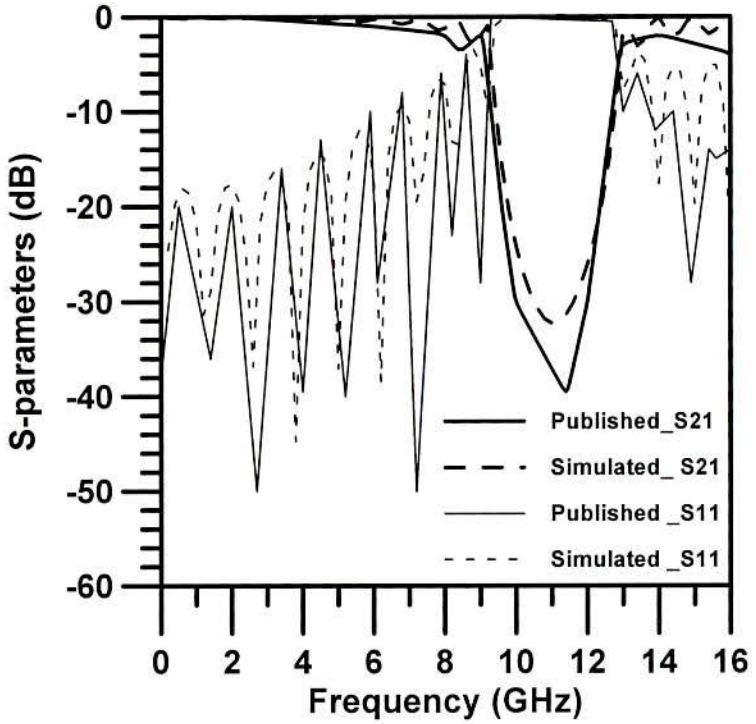

Fig. 3.15: S-parameter performances of a standard 50- ohm transmission line perturbed by uniform circular PBGSs of three columns in the ground plane. The substrate is RT/Duroid having height of 25 mils and dielectric constant of 10.5. The uniform circular PBGSs are of 50 mils and the period is 200 mils (FF=0.25) as [34].

- **The Transmission Line with 1-D Uniform Circular PBGSs**

It is mentioned that 0.25 is the optimum FF for RT/Duroid with dielectric constant of 10.5 and height of 25 mils. Based on this value a microstrip transmission line with 1-D uniform circular PBGSs has also been investigated. The simulation result is shown in Fig. 3.16. From this figures (Fig. 3.13 and Fig. 3.16) it is very clear that 1-D PBGSs and 2-D PBGSs provide very similar performances. From the Fig. 3.16, it can be seen that return loss performance, stopband characteristics and ripple height for two designs are similar. A little difference in the value of maximum isolation (2 dB) is observed. In the case of three rows of uniform circular PBGSs the maximum isolation is found to be approximately 35 dB. On the other hand, one row of uniform circular PBGS provides approximately 33 dB

maximum isolation. Therefore it can be considered that they provide similar results.

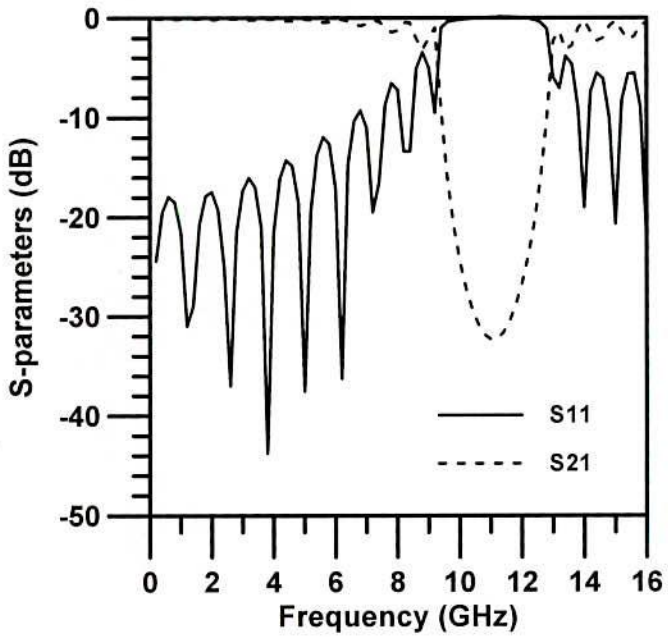

Fig. 3.16: Simulated S-parameter performances of a standard 50-ohm transmission line perturbed by 1-D (one line) uniform circular PBGSs in the ground plane. The substrate is RT/Duroid having height of 25 mils and dielectric constant of 10.5. The uniform circular PBGSs are of 50 mils and the period is 200 mils (FF = 0.25).

As 2-D and 1-D PBG elements provide very similar performances, therefore the investigations are confined into the microstrip transmission line with 1- D PBGSs.

- **Square Patterned Uniform PBGSs**

The S-parameters performances of uniform square patterned PBGSs have also been analyzed. The simulated and measured S-parameters performances of three lines (2-D) uniform square patterned PBGSs are shown in Fig. 3.17. Insignificant discrepancies are there between the simulated and measured performances.

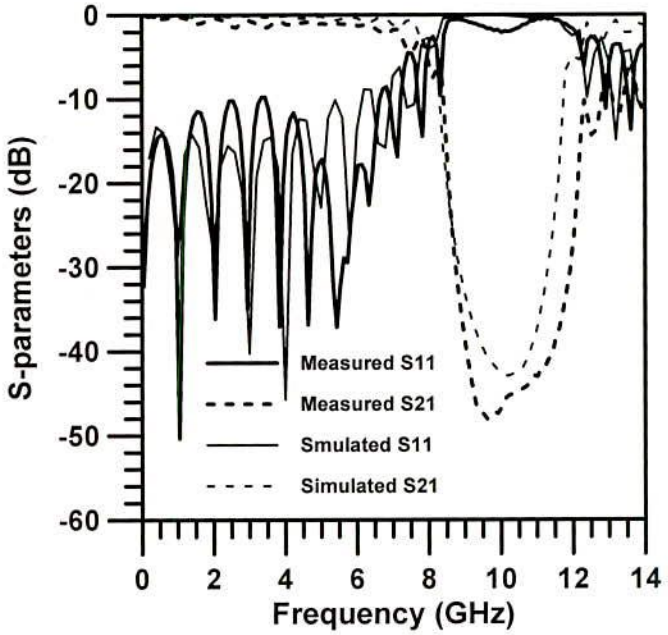

Fig. 3.17: S-parameters performances of three lines uniform square-patterned PBG structures. The substrate is Taconic having dielectric constant of 10 and height of 25 mils. The inter-element spacing is 226 mils and FF is 0.46.

The simulated performances of 1-D and 2-D uniform square patterned PBGSs are shown in Fig. 3.18.

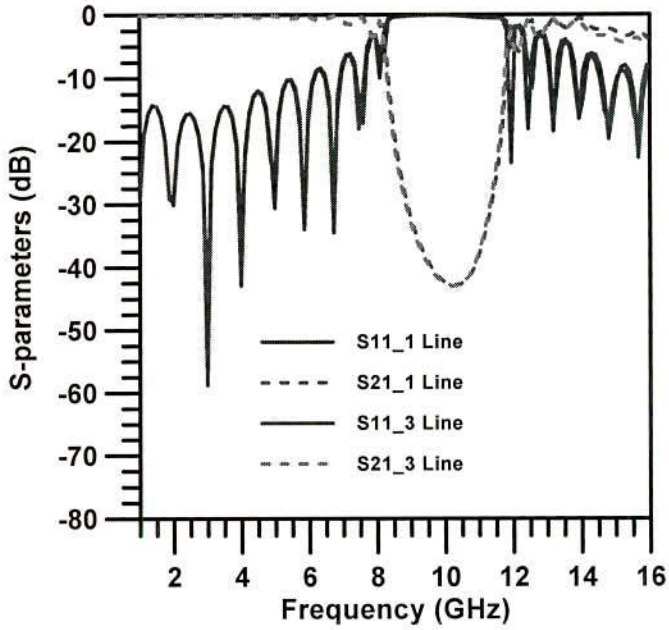

Fig. 3.18: Simulated S-parameters performances of 1-D and 2-D uniform square-patterned PBG structures. The substrate is Taconic having dielectric constant of 10 and height of 25 mils. The inter-element spacing is 226 mils and FF is 0.46.

The investigation of the replacement of 2-D PBGSs by 1-D PBGSs simplifies the PBGSs design used for beam steering of phased array antenna as can be seen in chapter seven. The simulated performances shown in Fig. 3.18 are very identical. The measured results for these same designs are shown in Fig. 3.19. Measured results are also identical.

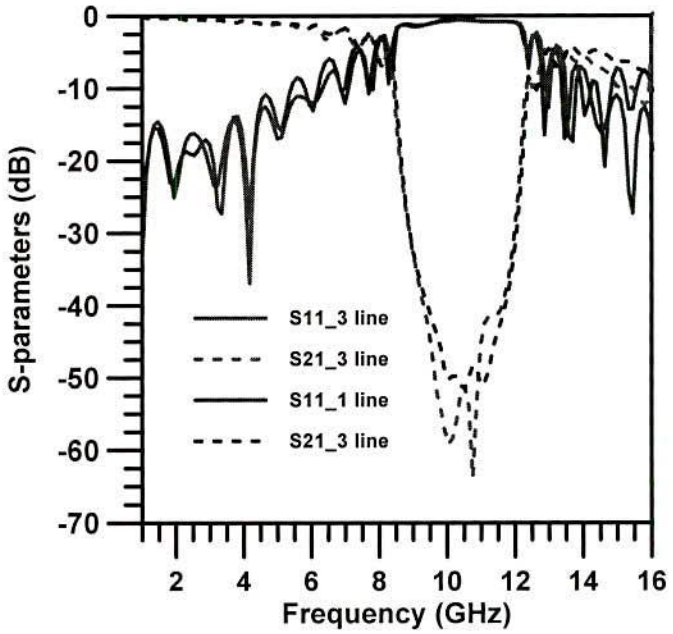

Fig. 3.19: Measured S-parameters performances of 1-D and 2-D uniform square-patterned PBG structures. The substrate is Taconic having dielectric constant of 10 and height of 25 mils. The inter-element spacing is 226 mils and FF is 0.46.

To validate the performances generated by the software the simulated and measured performances of 1-D uniform square patterned PBGSs are shown in Fig. 3.20. The small discrepancies between simulated and measured performances cannot be avoided as the center of the stopband frequency is approximately calculated by equation (3.32). The value of the effective permittivity is also approximated to unperturbed ground plane for the calculation of the inter-element spacing of PBG elements. The ground plane is always considered to be infinity in the simulations. The conductor losses are not included in the simulations.

Moreover there are always some fabrication errors. Measured results ensure the replacement of 2-D PBGSs by 1-D PBGSs and show sufficient accuracy of the commercial software IE3D.

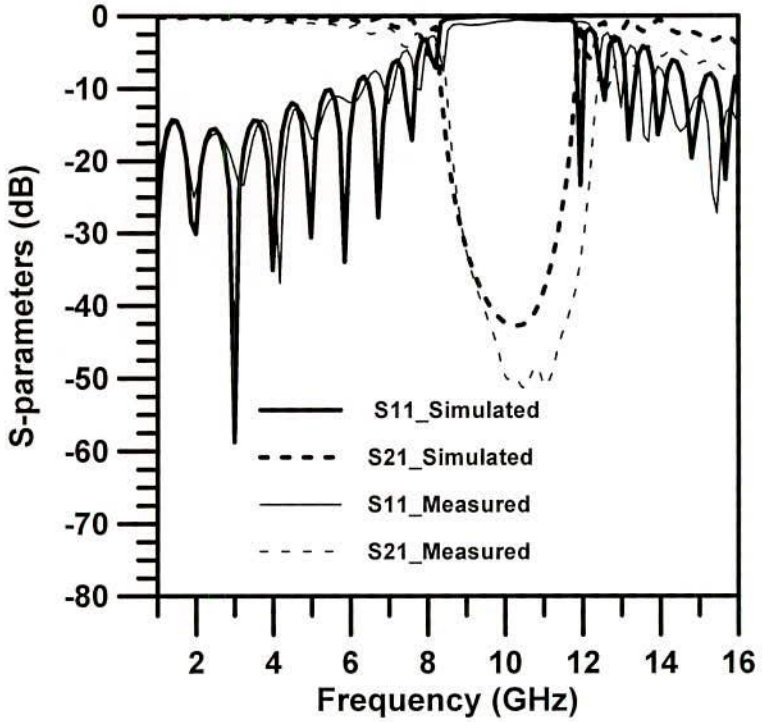

Fig. 3.20: Measured and simulated S-parameters performances of 1-D uniform square-patterned PBG structures. The substrate is Taconic having dielectric constant of 10 and height of 25 mils. The inter-element spacing is 226 mils and FF is 0.46.

In practical design the uniform circular PBGSs use FF of 0.25. In circular PBGSs the FF is r/a where r is the radius of circular PBGS. On the other hand in case of square patterned PBGSs the FF is defined to be ratio of b/a where b is the arm length. The radius is half of the diameter that is used in defining the FF. But for the square patterned PBGS uses the total arm length to calculate the FF. During the design the author always keeps in mind the FF so that it does not go beyond the limit of the optimum value. Let's say for square patterned PBGS, FF is used 0.46, which is still below the optimized value as it is square patterned PBGS. The physical explanation of FF can be explained as the enhancement of the etching area

of PBG unit. It can be understood from Figs. 3.12-3.14. The FF of any PBG element increases means its physical dimension increases. Figs.3.12-3.14 explain how the FF (Physical dimension) controls S-parameter performances.

3.8 Number of Uniform Circular PBGS on Performance of Line

Here a PBG engineered 50-ohm microstrip line with the variable numbers of circular uniform circular PBGSs has been analyzed. The effect of FF on the performance of PBG structured line has already been analyzed. Here FF is kept constant and that equals to 0.25.

- **Results**

The theoretical results are shown in Figs. 3.21-3.26 for a standard 50-ohm line along with other design perturbed by number of uniform circular PBG elements to be 2, 4, 6, 8 and 10 respectively. The purpose of inclusion of the theoretical results of a 50-ohm transmission line is to see how the performances are changing gradually under the loading conditions by the number of uniform circular PBG elements in the ground plane of the same 50-ohm line. The simulated results for 4, 6, 8 and 10 PBG elements are shown in the form of return loss and insertion loss performances. The return loss and insertion loss performances are shown in Figs. 3.21 and 3.22 respectively.

For 2 PBG a tendency is observed to generate the stopband is observed but it is not significant. The maximum isolation is 4 dB and 10 dB passband return loss bandwidth is 5.17 GHz. The result is not shown here.

It can be seen from Fig. 3.22 that the isolation and widths of the stopband are increasing with the number of PBG elements. For 4 PBG elements the maximum isolation is found to be 12 dB. From the return loss performances as shown in Fig. 3.21 it is seen that the 10 dB passband return loss bandwidth is 5.96 GHz.

It can be seen from Fig. 3.22 that 6 PBG elements provide maximum isolation of 21 dB and the approximate value of 20 dB rejection band of 1 GHz. Fig. 3.21 provides 10 dB passband return loss BW to be 6.85 GHz for 6 PBG elements. Near the cut-off frequency very small amount of ripples are observed.

For 8 PBG elements maximum isolation is 30 dB and the 20 dB rejection band is 2.31 GHz. The 10 dB return loss BW is 6.487 GHz. Now significant improvement in rejection band is obtained. It can be seen that ripple height in the passband is becoming larger with the PBG elements. In this case ripple is found to be 2.2 dB.

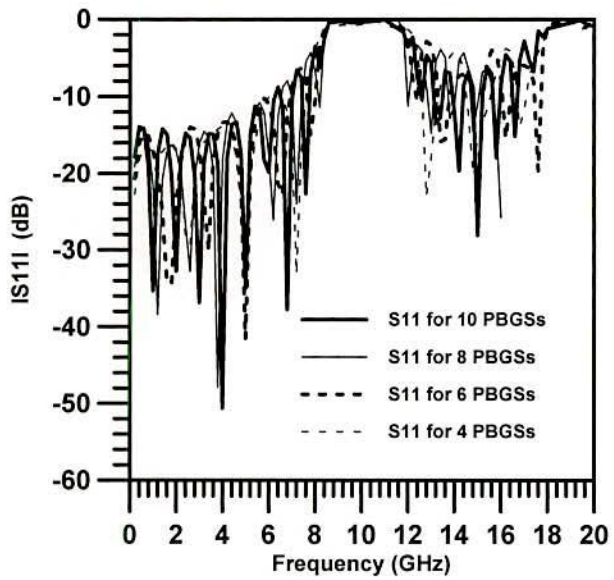

Fig. 3.21: Simulated return loss performances of a standard 50- ohm transmission line perturbed by 4, 6, 8 and 10 uniform circular PBGSs of one column in the ground plane. The substrate is RT/Duroid having height of 25 mils and dielectric constant of 10.5. The uniform circular PBGSs are of 25 mils and the period is 200 mils (FF = 0.25)

Finally the line is investigated with the number of uniform circular PBGSs to be 10. From Fig. 3.22 it can be seen that maximum stopband is 2.78 GHz and the maximum isolation is 36 dB. Fig. 3.21 shows that the 10 dB return loss BW is 7.10 GHz. In the present design the passband ripple height is found to be 3 dB.

The passband ripples are found to be 0, 1, 1.5, 2.2 and 3 dB for the numbers of circular uniform circular PBG elements to be 2, 4, 6, 8 and 10 respectively. Controlling FF it is easy to control the passband ripple height. This will be demonstrated in Chapter 4.

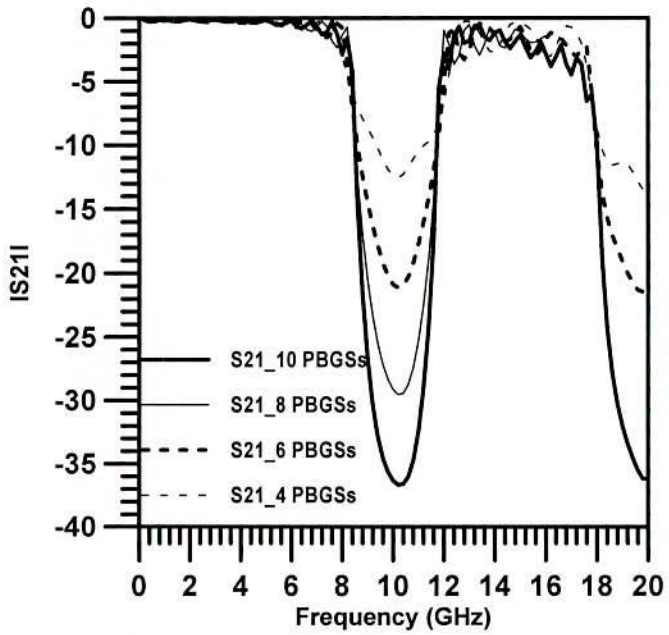

Fig. 3.22: Simulated insertion loss performances of a standard 50- ohm transmission line perturbed by 4, 6, 8 and 10 uniform circular PBGSs of one column in the ground plane. The substrate is RT/Duroid having height of 25 mils and dielectric constant of 10.5. The uniform circular PBGSs are of 25 mils and the period is 200 mils (FF=0.25).

The relationship of number of PBG elements with the maximum isolation is shown in Fig. 3.23. It can be seen that an excellent linear relationship exists between the number of PBG elements and the maximum isolation.

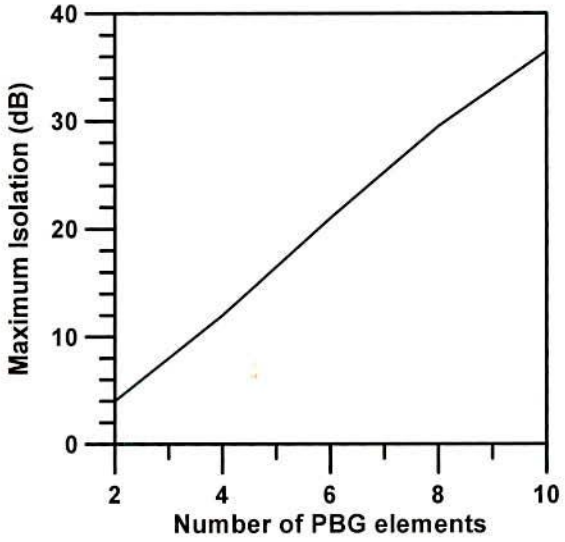

Fig. 3.23: Relationship between number of PBG elements and maximum isolation.

The relationship of number of PBG elements and 10 dB return loss BW is shown in Fig. 3.24. It can be seen that the relationship is non-linear. Maximum passband return loss BW is achieved for 6 PBGSs.

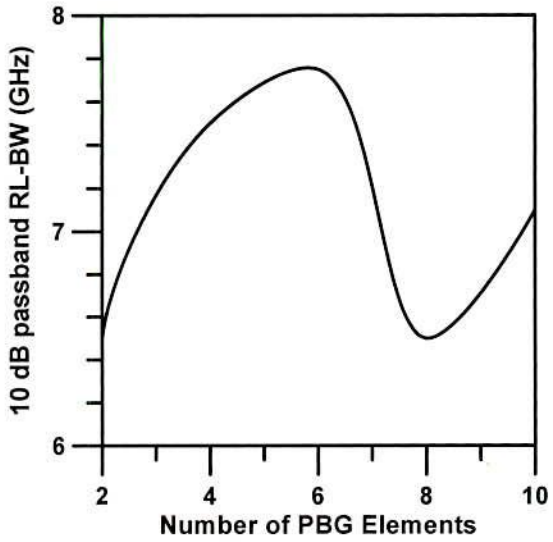

Fig. 3.24: Relationship between number of PBG elements and 10 dB passband return loss BW.

Fig. 3.25 provides the relationship of 20 dB rejection bands and the number of PBG elements. It can be seen that the stop bandwidth increases with the number of PBG elements. For PBGSs = 2, no 20 dB stopband is achieved.

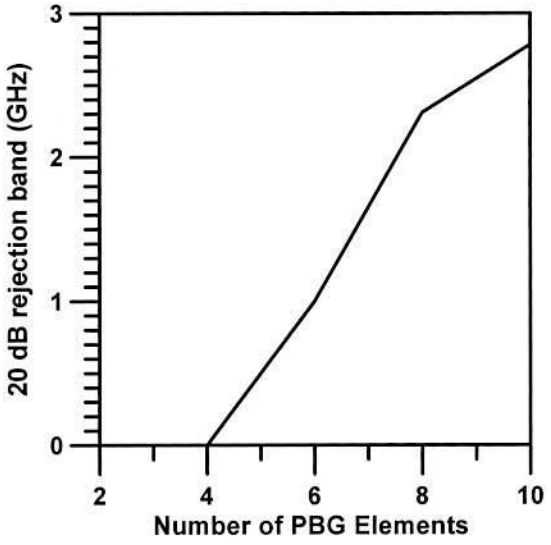

Fig. 3.25: Relationship of 20 dB rejection bands and the number of PBG elements.

The relationship of passband ripple height and the number of PBG elements is shown in Fig. 3.26.

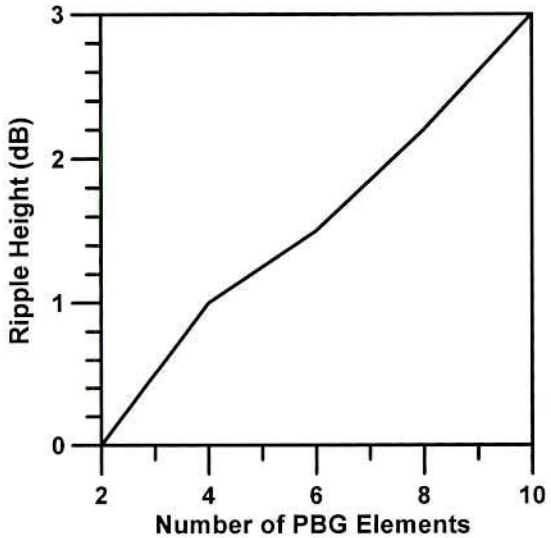

Fig. 3.26: Relationship between passband ripple height and the number of PBG elements.

The performances of the different number of PBGSs are mentioned in Table 3.1.

TABLE 3.1 PERFORMANCES OF A MICROSTRIP TRANSMISSION LINE LOADED BY DIFFERENT NUMBER OF UNIFORM CIRCULAR PATTERNED PBGSS

No. of uniform circular PBGSs	Maximum Isolation (dB)	10 dB passband return loss bandwidth (GHz)	20 dB rejection bandwidth (GHz)	Passband ripples (dB)
2	4	6.5	0	0
4	12	7.5	0	1
6	21	7.75	1	1.5
8	29.5	6.5	2.308	2.2
10	36.5	7.10	2.78	3.0

Conclusions

To understand the properties of PBGSs the theory of PBG structures has been reviewed in short extent. Since they are also periodic in nature all theories for periodic structures hold true for PBGSs. Then transmission line model of UC-PBG structures has been presented. Writing MATLAB code has generated the bandgap effect of UC-PBG structure.

Uniform circular and square shaped PBGSs have been analyzed. Three designs have been investigated with circular uniform circular PBGSs with FFs of 0.125, 0.25 and 0.45. It is found that 0.25 is considered to be the optimum value of FF. Three rows and one row uniform PBGSs are studied to replace 2-D PBG elements by 1-D PBG elements for both the shapes. Both the designs provide very similar performances. Throughout whole investigations it is preferred to use 1-D PBGSs rather than 2-D PBGSs.

Next the effect of variation of PBG elements under the microstrip transmission line has been investigated. The numbers are varied to be 2, 4, 6, 8, and 10. From all the designs and simulated results of the PBG engineered 50-ohm transmission lines with 0.25 FF, it has been observed that the depth and width of the rejection band increase with the number of PBG elements. In the present study the maximum rejection bandwidth is achieved for uniform circular PBG elements. It is also seen that the passband ripple height is also maximum for this configuration. But without changing the number of PBG elements, the ripple height can be controlled with the FF. It is noted that the return loss BW does not scale with the number of PBG elements. The investigations of course have elucidated the role of the number of PBG elements responsible for generating significant return loss bandwidth, rejection band and the depth of the stopband.

Chapter 4 Non-Uniform PBGSs

4.1 Introduction

In chapter 3, uniform circular patterned PBGSs with different FFs and the number of PBG elements have been addressed. High passband ripples and poor passband matching are the two serious problems of conventional uniform PBGSs. In this chapter non-uniform PBGSs with Binomial and *Chebyshev* distributions are investigated. How proposed PBGS improves these two problems and simplifies the filter synthesis are demonstrated. The chirping technique is also discussed that makes the PBGSs to be aperiodic. The aperiodicity of non-uniform structure is realized by standard chirping technique and *Chebyshev* distribution. The non-uniformities of the chirped PBG elements are realized by implementing *Chebyshev* distribution in calculating the amplitudes of PBG elements.

In this chapter, novel PBG structures in the form of non-uniform distributions of circular patterns are proposed to investigate the improvement in S-parameters performance and it will be seen if they can be used as an ideal LPF. Two distributions–Binomial [35] and *Chebyshev* [36] polynomials as applied to antenna array synthesis, are used to taper the dimensions of the etched circular patterned PBG units on the ground plane of a standard microstrip transmission line. While the uniform distribution of the circular patterned PBG [34] is hindered with high passband ripples near the cut-off frequency, the non-uniform distributions in the forms of Binomial and *Chebyshev* polynomials yield superior performances by suppressing passband ripples and producing distinct wide stopbands. The novelty

of the proposition is that Binomial and *Chebyshev* polynomials are exploited to control the LPF response and selectivity. Hence the filter synthesis is substantially relaxed in the present approach. Also the depth of passband return loss, selectivity and the ripples can be controlled with the side-lobe level (SLL) index of *Chebyshev* polynomial. Since the passband ripple height increases with the FF, the uniform circular patterned PBG limits the wideband applications. Using the non-uniform distribution of PBG patterns, both passband ripple and stop bandwidth problems are alleviated and the selectivity of the stopband of planar PBGSs increases.

In the open microwave literature it is seen that the inter-cell separation is also varied, which is known as chirping that has been done using standard chirping technique. In amplitude calculation Laso *et al.* [75] have used Gaussian distribution. *Chebyshev* distribution is proposed for the chirping purpose. On the other hand the amplitudes of the PBG elements have also been varied with *Chebyshev* distribution.

The circular pattern metallic perturbation into the conventional hole patterned PBGSs results in uniform annular ring structure. The ratio of inner and outer radius of uniform ring patterned PBG elements is termed as aspect ratio (AR). The variation in AR controls the stop bandwidth. Non-uniform ring patterned PBGSs with *Chebyshev* distribution is also investigated.

The novel finding can be very useful for wideband surface wave suppression in planar and microstrip antennas, diplexers, filters and amplifiers. In a nutshell the

research results in this chapter can be represented by the following tree structures as shown in Fig. 4.1.

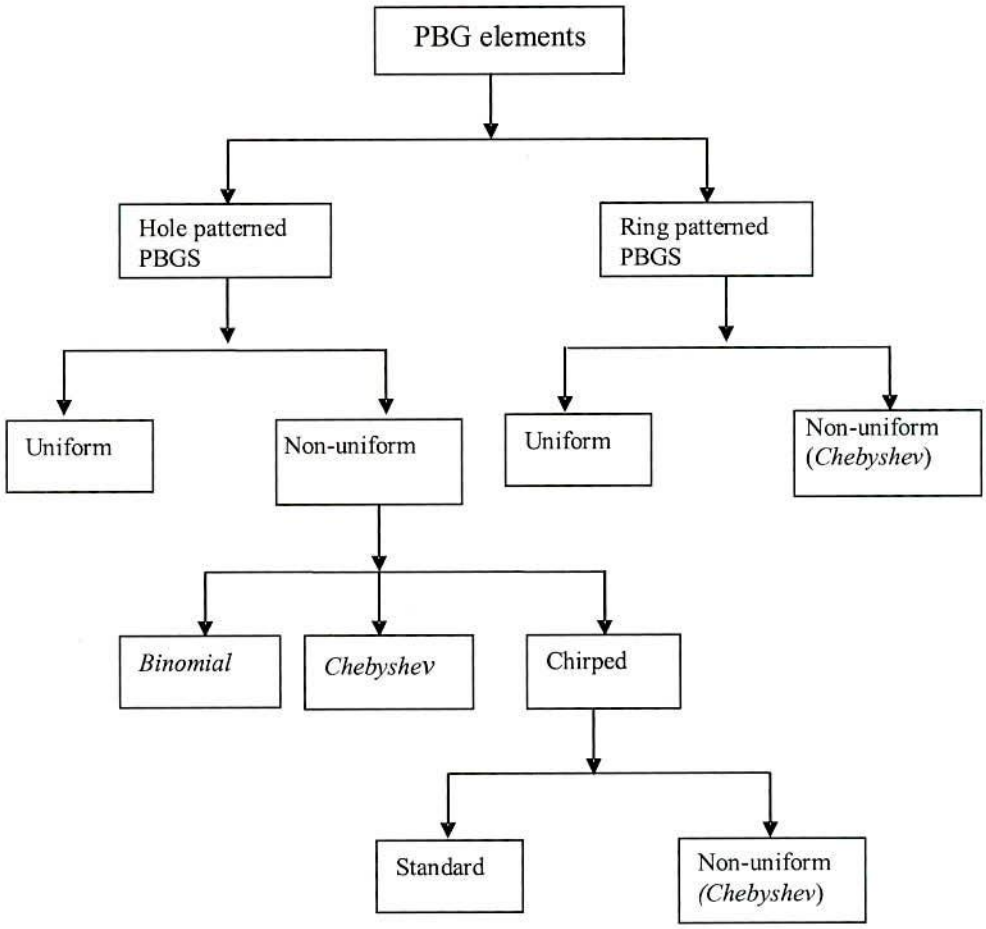

Fig. 4.1: Tree structure of PBGSs

4.2 Theory of Non-uniform 1-D Microstrip PBGSs

- **Binomial Distribution**

A maximally flat passband transmission characteristic is obtained when the coefficients of the polynomial [13, 14] are determined by the following expression:

$$(1+x)^{m-1} = 1 + (m-1)x + \frac{(m-1)(m-2)}{2!}x^2 + \frac{(m-1)(m-2)(m-3)}{3!}x^3 + \ldots \qquad (4.1)$$

The positive coefficients of the series expansion for different values of m are expressed in terms of the Pascal's triangle [76]. If the values of m represent the numbers of elements in an array, the coefficients of the expansion represent the relative amplitudes of the elements. Generally, this type of array suffers from practical limitation of bandwidth and efficiency due to the abrupt change in amplitude tapering between adjacent elements. In this work the dimensions of the circular PBGSs are varied proportionally to the relative amplitudes of the polynomial.

- ***Chebyshev* Polynomial**

Instead of maximally flat passband characteristics, an equally useful characteristic is one that may permit the transmission coefficient to vary with minute ripples over the stopband. This provides a considerable increase in bandwidth with respect to Binomial distribution. This equal-ripple characteristic is obtained by making the distribution according to *Chebyshev* polynomial. The basic properties of the polynomials [76] are expressed as follows:

$$T_m(z) = 2zT_{m-1}(z) - T_{m-2}(z) \tag{4.2}$$

where $T_m(z)$ is expressed as:

$$T_m(z) = \cos[m\cos^{-1}(z)] \quad \text{for } |z| \leq 1 \tag{4.3}$$

The coefficients of the polynomial are determined for any prescribed side lobe level (SLL). In the design example, a 10-element PBG array with a tapered distribution according to *Chebyshev* coefficients is taken. For a prescribed voltage ratio between the peak and the SLL, for instance for 25 dB, the amplitudes are determined as follows:

0.36	0.49	0.71	0.78	1	1	0.78	0.71	0.49	0.36

The amplitude 1 is for the two center elements of the 10-element array and the rest elements follow suit. For PBG design the radii (Type-A) and area (Type-B) of the circles and annular rings are varied proportionally to the relative amplitudes, respectively.

- **Selectivity of the Lowpass Filters**

One important parameter of the filter is the selectivity at 3-dB cut-off frequencies. The selectivity of the LPF is defined as:

$$\xi = \frac{\alpha_{min} - \alpha_{max}}{f_s - f_p} (dB / GHz) \tag{4.4}$$

Where, ξ = selectivity in dB/GHz, α_{max} = the 3 dB attenuation point, α_{min} = 20 dB attenuation point, f_s = 20 dB stopband frequency in GHz, f_p= 3 dB cut-off frequency in GHz. In the work, how the selectivity of the PBG engineered LPF will improve will be shown with Binomial and *Chebyshev* distributions.

4.3 Design of LPF Using 1-D Microstrip PBGSs

Fig. 4.2 and Fig. 4.3 show different varieties–a *uniform* circular and *non-uniform* circular patterned planar PBGSs on microstrip substrates respectively. As can be seen in the figures, the uniform and the non-uniform circular patterns are etched with a period '*a*' on the ground plane of standard microstrip transmission lines. The important design parameters to achieve a stopband characteristic are the period '*a*' and the filling factor *'r/a'*. For the uniform circular patterned PBG, the circles are of the same radius 'r_0' and period '*a*'. For non-uniform patterned PBGSs, the

central elements have the largest radii of 'r_0' and the radii of the adjacent circles decrease proportionally to the amplitude coefficients of the polynomials. For *Chebyshev* distribution, the area of the PBG patterns will vary proportionally to the coefficients of the polynomial for a particular SLL (voltage ratio). Here two distinct relationships are proposed between amplitudes of the coefficients of the polynomials and the physical dimensions of the PBG circles. They are: (1) polynomial coefficient's amplitude $\propto$ the radius of the PBG circle (r), called Type-A, and (2) polynomial coefficient's amplitude $\propto$ the area of the PBG circle (πr^2); called Type-B. The investigations are carried out with the two types of PBG configurations with circular patterns and the respective results are produced in this section. For all the designs the center frequency of the stopband is calculated approximately with the equation of Bragg's condition.

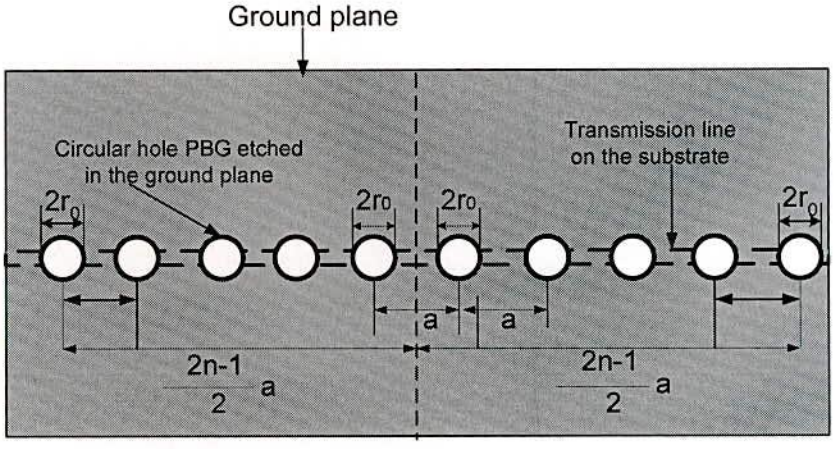

Fig. 4.2: Geometry of circular uniform PBGS. The PBG elements are having radius of r_0 etched in the ground plane.

For an N-element PBG patterns, the n-th element's location from the center of the PBG period can be derived from the following equation:

$$d_n = \begin{cases} \dfrac{2n-1}{2}a & for\ even\ N \\ (n-1)a & for\ odd\ N \end{cases} \qquad (4.5)$$

Fig. 4.2 and Fig. 4.3 show such distribution for even *N*.

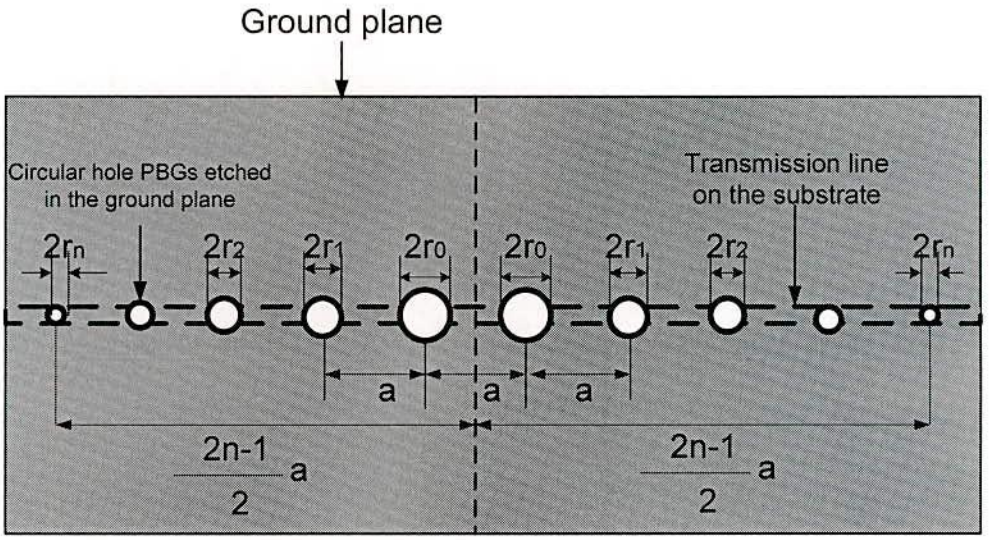

Fig. 4.3: Geometry of circular non-uniform PBGSs etched in the ground plane. The central two elements have largest value and the remaining PBGS follow *Chebyshev* distribution.

4.4 Results

In present work RT/Duroid 6010 with ε_r = 10.2 and thickness h = 25 mils is used. The center frequency is selected at 10 GHz and the period a = 224 mils. Based on the design parameters, two different distributions–the Binomial and *Chebyshev* distributions of PBG patterns have been designed and analyzed. Following sections present the results of the dispersion characteristics in terms of S-parameters vs frequency for (i) uniform, (ii) Binomial, and (iii) *Chebyshev* distributions.

4.4.1 Uniform 1-D Microstrip PBG

Fig. 4.4 shows the S-parameters vs frequency for two different filling factors 'r/a' = 0.25 (r = 56 mils) and 'r/a' = 0.375 (r = 84 mils) for the uniform distribution of

circular patterns with a period of 224 mils. As can be seen from this figure, the filling factor plays important role in determining the rejection bandwidth. For r = 56 mils (solid lines), the 20 dB (S_{21}) rejection bandwidth is 1.89 GHz while for r = 84 mils (dotted lines) the 20 dB rejection bandwidth is 4.95 GHz. As shown in Fig. 4.5 the ripples in measured S-parameters near the cut-off frequencies and in the lowpass region are significantly high and no distinct lowpass response is observed for both cases. As can be seen, near (3-dB S_{21}) cut-off frequencies the return loss is less than 5 dB for r = 56 mils and close to 0 dB for r = 84 mil. Over the low-pass region both the return loss and insertion loss performances are very poor for both cases. It is also worthwhile to note that with the filling factor, the center frequency of the rejection band increases slightly.

Comparing the measured and simulated results it can be concluded that the measured lowpass ripples are significantly high. Therefore, it is not a lowpass filter at all. The measured frequency shifts a little in higher frequency region and the stop bandwidth is larger than that for the simulated results. The discrepancies can be attributed to the dielectric and conductor losses in the microstrip lines, and fabrication tolerance and errors, which are not considered in the simulation. In general, the agreement is quite well.

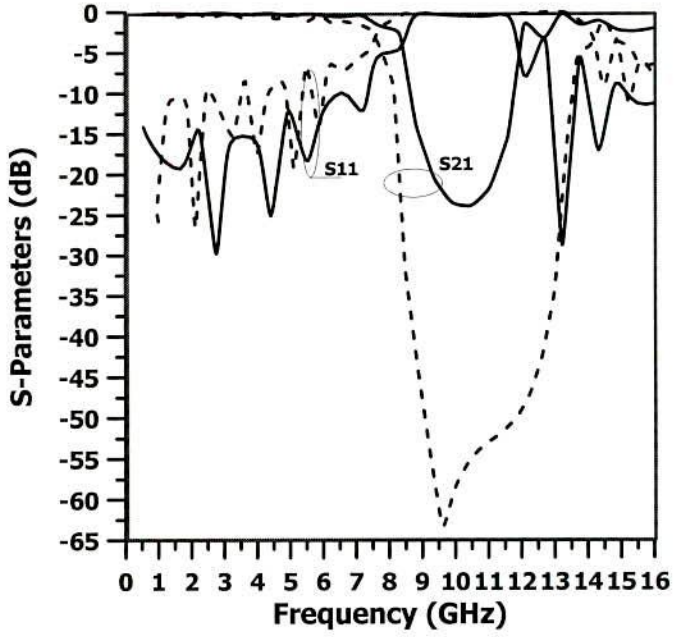

Fig. 4.4: Simulated results of S-parameter vs frequency for different radii of the uniform circular PBG lines. Solid lines: r = 56 mils, dotted lines: r = 84 mils with a period a = 224, line width 24 mils (50 Ω). Dielectric substrate: ε_r = 10.2, h = 25 mils.

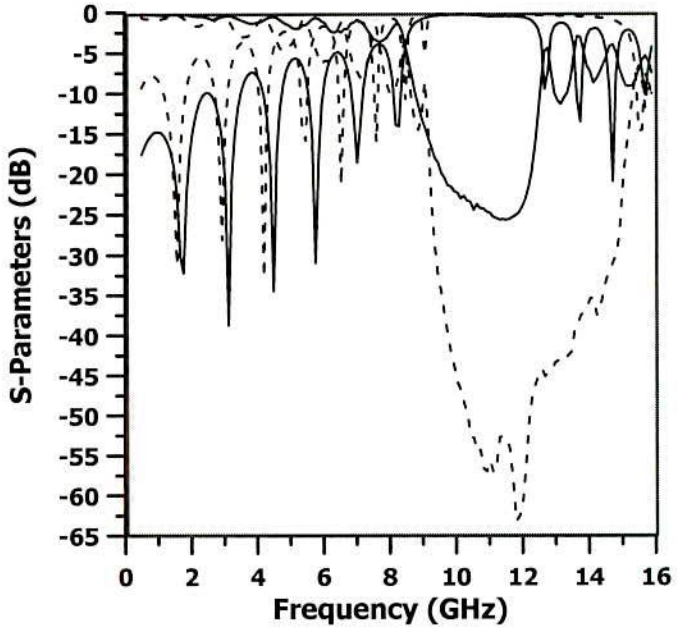

Fig. 4.5: Measured result of S-parameter vs frequency for different radii of the uniform circular PBG lines. Solid lines: r = 56 mils, dotted lines: r = 84 mils with a period a = 224, line width 24 mils (50 Ω). Dielectric substrate: ε_r = 10.2, h = 25 mils.

To improve the performance of the conventional uniform circular patterned PBGSs, two non-uniform distributions–Binomial and *Chebyshev* polynomial distributions for circular patterned PBGSs are proposed. Followings are the results to show how the S-parameter performances have improved.

4.4.2 Binomial Distribution of Circular Patterned PBGSs

Fig. 4.6 shows the simulated S-parameters vs frequency with the FF as a parameter for the Binomial distribution of circular patterned PBG with a period of 224 mils. The radii of the largest circles are 56 mils (solid lines), 84 mils (dashed lines) and 110 mils (dotted-dashed line) for Type-A (where the radii of the circles are proportional to the polynomial coefficients) and 110 mils (double dotted-dashed line) for Type-B (where the area of the circles are proportional to the polynomial coefficients). As can be seen in the figure, the FF plays an important role in determining the rejection bandwidth. Consequently, the ripples at the cut-off frequencies and the lowpass frequencies have improved considerably. Also is noted here, the center frequency of the rejection band has shifted slightly upward with the radius. Table 4.1 summarizes the results. As can be seen, the $S_{21\ (max)}$ in the rejection band increases with the FF and the 20 dB isolation bandwidth also increases.

As can be seen in Table 4.1, the rejection bandwidth and the selectivity have increased considerably in Type-B compared to Type-A. Also in the low pass region the 20 dB return loss bandwidth has improved.

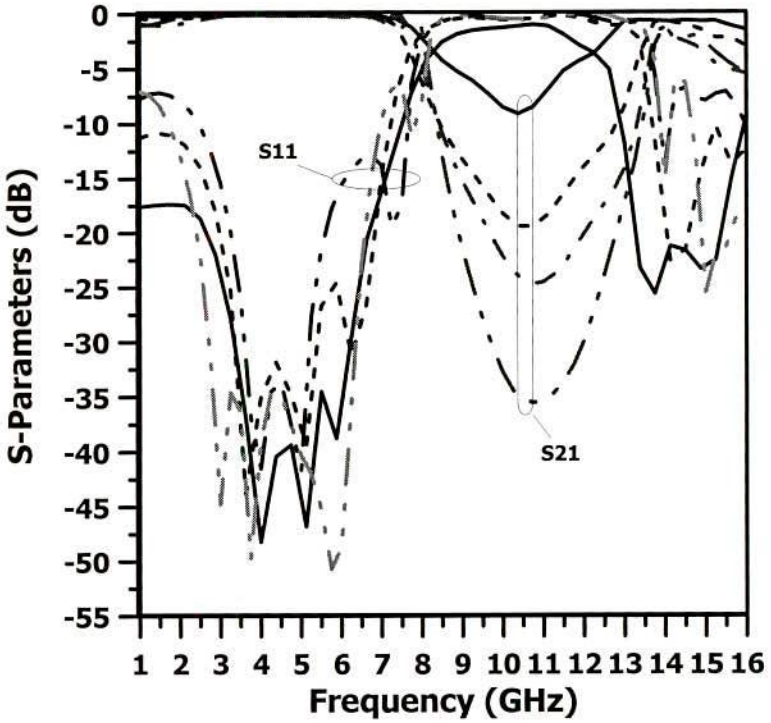

Fig. 4.6: Simulated S-parameter vs frequency for different radii of the circular PBG lines with Binomial tapering. Type-A–Solid lines: r_0 = 56 mils, dotted lines: r_0= 84 mils, dotted-dashed lines: r_0 = 110 mils; Type-B–double dotted-dashed line: r_0 = 110 mils with a period a = 224, line width 24 mils (50 Ω). Dielectric substrate: ε_r = 10.2, h = 25 mils.

TABLE 4.1: COMPARATIVE STUDY OF CIRCULAR PATTERNED PBGS WITH BINOMIAL DISTRIBUTION:

Type	r_0 (mil)	Stopband Isolation		1st null return loss (dB)	20dB Isolation BW (GHz)	Selectivity: dB/($f_s - f_p$) (dB/GHz)	20dB Pass-band Return loss BW (GHz)
		S_{21max} (dB)	f_0 (GHz)				
Type-A: x ∝ r	56	8	10.2	38	0	0	4.125
	84	20	10.4	32	0	5.66	3.875
	110	25	10.6	20	2.5	11.33	2.375
Type: B x ∝ area	110	35	10.6	11	4	21.25	4.25

The etching area of Type-B is always more than Type-A. As the width of the stopband increases with the etching area, so it is confirmed that it holds true for

every case. For this reason only one type of structures has been considered to compare the performance of Type-A and Type-B.

Followings are the analyses of different important findings in the above investigations.

- **Selectivity**

As can be seen in Fig. 4.7, the selectivity of the LPF as well as the depth of the transfer function (S21max) in the rejection band increases with the FF. With the FF of 0.25 the selectivity is zero and at 0.49 filling factor the selectivity has increased to 21.25 dB/GHz. Also the S21max in the rejection band increases from 8 dB for a FF of 0.25 to 25 dB for a FF of 0.49.

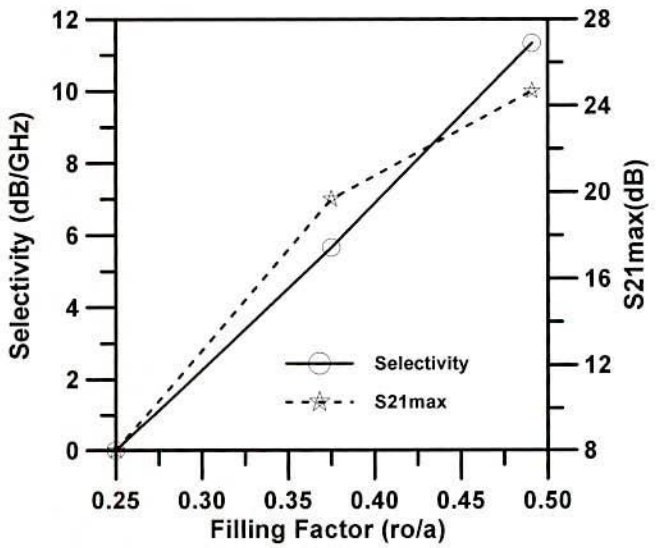

Fig. 4.7 Selectivity and maximum isolation vs filling factor for the circular patterned PBGSs with the Binomial distribution with a period a = 224, line width 24 mils (50 Ω). Dielectric substrate: ε_r = 10.2, h = 25 mils.

- **Passband return loss characteristics**

Fig. 4.8 shows the lowpass characteristics of the Binomially distributed PBGSs. The 10 dB passband return loss bandwidth and the first null of return loss near the cutoff frequency increase with the FF.

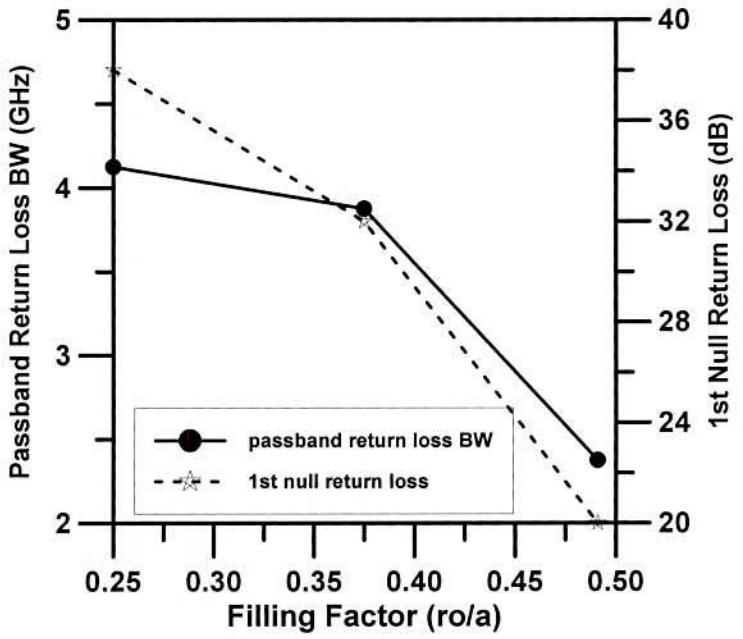

Fig. 4.8: Lower passband return loss bandwidth and 1st null return loss vs filling factor for the circular patterned PBGS with Binomial distributions with a period a = 224, line width 24 mils (50 Ω). Dielectric substrate: ε_r = 10.2, h = 25 mils.

This means that while the FF for conventional uniform circular patterned PBGSs generates ripples, the problem can be alleviated significantly with the Binomial distribution of the PBG patterns.

4.5 Optimum FF for Binomial distribution at X-band

Most often open literature provides the information of the performance of the PBGSs with optimized FF [34]. Their performances may vary with FFs at different frequencies. In this section Binomial distribution of circular PBGSs are investigated. The present research conveys the message of frequency dependency for transmission line perturbed with Binomial distribution designed at X-band. The optimum value of FF will be found. The transmission lines are investigated at X-band namely at 9, 10.5 and 12 GHz respectively. The theoretical results have been reported [77]-[78] here for different PBG structures at these frequencies with

Binomial distribution (Type-B) designed at 9 GHz, 10.5GHz and 12 GHz with FFs of 0.3, 0.4 and 0.5 respectively. From the investigations, the optimized value of FF in case of Binomial distribution has been reported. Measured results have also been produced to compare the investigations.

As it is clear that the size of the PBG elements are very small in case of Type-A except the central element due to abrupt transition among the co-efficient values, so Type-B configuration is used at 9 and 10.5 GHz. In the investigation, RT/Duroid substrate with thickness of 25 mill (0.635 mm) and dielectric constant of 10.2 has been used. The transmission lines are simulated on Binomially distributed PBG structures. There are abrupt transitions in amplitudes among the PBG structures for Binomial *distribution*; so central two elements are mostly responsible to produce stopband due to very insignificant size of remaining PBG units especially for Type-A distribution. The performances at 9, 10.5 and 12 GHz with FFs of 0.3, 0.4 and 0.5 are shown in Table 4.2.

- **Performances at 12 GHz**

Though Type-A distribution yields fair ripple free passband but it does not generate wider and deeper stopband. From the Table 4.2 it can be seen that the PBGSs designed at 12 GHz (Type-A) provides ripple free transmission with distinct and wider return loss passband of 7.55 GHz for FFs of 0.3 and 0.4. The FF of 0.5 provides 20 dB rejection bandwidth of 1.43 GHz and 10 dB return loss bandwidth of 5.75 GHz. Maximum isolation is found to be 22.5 dB. It can be concluded that there is no distinct stopband for FFs of 0.3, 0.4 and 0.5 that are beyond the optimized value of 0.25. On the otherhand Type-B designs improve the

performances. It can be seen from the Table 4.2 that 0.4 and 0.5 provide 20 dB rejection BWs of 2.74 and 3.77 GHz respectively. The corresponding 10 dB return loss bandwidth are 8.06 and 6.29 GHz respectively. The FF of 0.3 does not yield any significant stopband. For FFs of 0.3, 0.4 and 0.5 the maximum isolations are 17.5, 25 and 29 dB respectively.

- **Performance at 10.5 GHz**

The 20 dB rejection BWs for the FFs 0.4 and 0.5 are 3.27 and 3.94 respectively. The corresponding 10 dB return loss bandwidths are 7.16 and 4.37 GHz respectively. The FF of 0.5 provides highest passband ripple that is found to be 2.5 dB. The FF of 0.3 does not provide significant stop bandwidth. The FF of 0.4 provides optimized performances with passband ripple height of only 0.5 dB.

- **Performance at 9 GHz**

Finally the same structures at 9 GHz are investigated. It can be seen from the Table 4.2 that the FF of 0.3 provides 20 dB rejection bandwidth of 1.46 GHz and the 10 dB return loss bandwidth of 5.84 GHz. The corresponding values for the FFs of 0.4 and 0.5 are 3.65 and 3.90 GHz and 6.5 and 4.5 GHz respectively.

It can be seen that the FF of 0.5 provides maximum passband ripple heights at all frequencies. So for optimum design this filling factor can be avoided. On the other hand FF= 0.3 does not provide distinct and wider stopband for all these frequencies. The FF of 0.4 provides a fair transmission of signal with moderate ripple for all these frequencies. Therefore the FF of 0.4 is considered to be optimum value of FF for Binomially distributed PBG configuration. It is observed From Table 4.2 that the FF of 0.4 yields maximum isolation at 9 GHz, maximum

10 dB passband return loss bandwidth at 12 GHz and maximum stop bandwidth at 10.5 GHz. Still it is believed that this value is the approximate value as there is a scope to find the value between 0.4 and 0.5 taking more precision value of FF.

TABLE 4.2: PERFORMANCE OF A 50-OHM TRANSMISSION LINE ON BINOMIALLY DISTRIBUTED PBGSS HAVING FF=0.3, 0.4 AND 0.5 AT 9, 10.5 AND12 GHZ. THE SUBSTRATE IS RT/DUROID HAVING DIELECTRIC CONSTANT =10.2 AND HEIGHT =25 MIL.

Frequency (GHz)	FF	20 dB rejection bandwidth (GHz)	10 dB passband return loss bandwidth (GHz)	Ripples (dB)	S21 (max) (dB)
Binomial (Type-A) at 12 GHz	0.3	0	7.55	0	-12.5
	0.4	0	7.55	0	-17.5
	0.5	1.43	5.75	0	-22.5
Binomial (Type-B) at 12 GHz	0.3	0	8.06	0	-17.5
	0.4	2.74	8.06	0.3	-25
	0.5	3.77	6.29	1	-29
Binomial (Type-B) at 10.5 GHz	0.3	0	7.16	0	-20
	0.4	3.27	7.16	0.5	-30
	0.5	3.95	4.37	2.5	-35
Binomial (Type-B) at 9 GHz	0.3	1.46	5.84	0	-25
	0.4	3.65	6.5	1	-37.5
	0.5	3.90	4.5	2.5	-45

- **Measured Results of Binomially Distributed PBG Structures**

From the simulation results, it can be seen that the filling factor 0.4 yields a distinct rejection bandwidth with minimum passband ripple. So one PBG assisted transmission line designed at 9 GHz with FF of 0.4 is fabricated. Taconic substrate having ε_r =10 and h = 0.635 mm is used in fabrication. Prototype PBG structured transmission line is tested using vector network analyzer (VNA). The measured results along with the simulated results are shown in Fig. 4.9. It can be seen that the measured 10 dB return loss passband is 6.5 GHz and 20 dB rejection BW is 3.84 GHz with maximum isolation of 32 dB. On the otherhand the simulated return loss passband is 6.5 GHz and 20 dB rejection BW is 3.65 GHz. The simulated and measured S-parameter performances are impressive. The minor descrepancies of

measured and simulated performances may be due to descrepencies of effective permittivittis in simulation and in practical investigation. Besides the frequency dependence of the effective permittyvitty specially at higher frequencies is not taken into account.

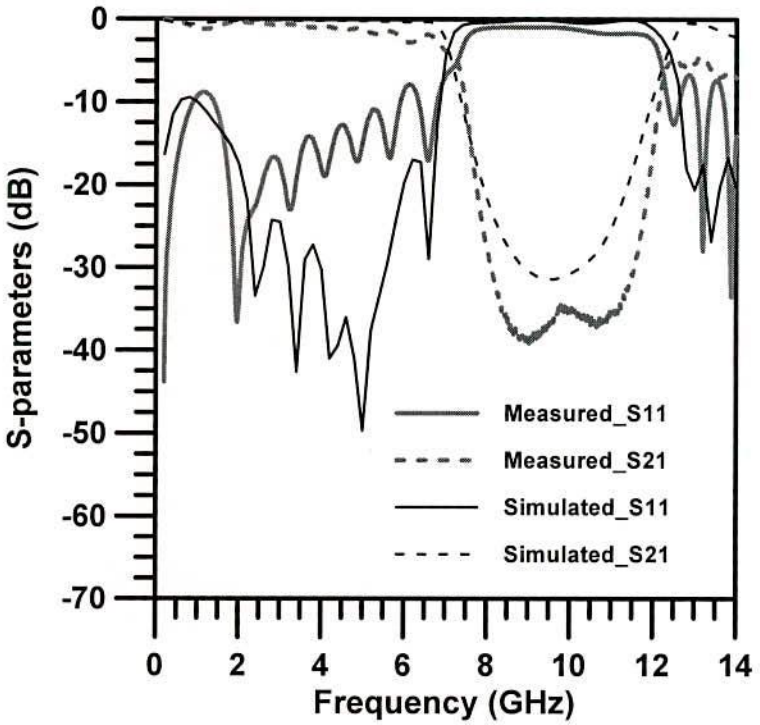

Fig. 4.9: S-parameters of a 50-ohm transmission line on Binomially distributed PBG structure with filling factor 0.4 at 9 GHz. Substrate is Taconic.ε_r=10 and h = 0.635 mm.

The measured and simulated performances of the Binomially distributed PBG assisted transmission line with FF of 0.4 is also shown in Table 4.3.

TABLE 4.3: PERFORMANCE OF A 50-OHM TRANSMISSION LINE ON BINOMIALLY DISTRIBUTED PBGSS HAVING FF = 0.4 AT 9 GHZ. THE SUBSTRATE IS RT/DUROID HAVING DIELECTRIC CONSTANT =10 AND HEIGHT =25 MIL

Performance	10 dB return loss BW (GHz)	20 dB rejection BW (GHz)	Passband ripple (dB)	Maximum isolation (dB)
Simulated	6.5	3.65	1	37
Measured	6.5	3.84	1.25	39

- **Tandem of 2 Binomially Distributed PBG lines**

Finally, two 10-element circular PBGSs are connected in tandem. The total length of the line is double than that for a single 10-element circular PBG line. Fig. 4.10 shows the S-parameters vs frequency for the tandem Binomially distributed (Type-A) 20-element circular PBG line. The filling factor of 0.375 (r = 84 mils) with the period of 224 mils is used. Comparing Fig. 4.6 and Fig. 4.10 it can be concluded that the tandem PBG line has improved the stopband and lowpass performances significantly.

While the 10-element Binomial line has no stopband, in the 20-element tandem line, the stopband bandwidth is 4.86 GHz and 20 dB passband return loss bandwidth is 3.87 GHz. Therefore, by cascading two Binomially distributed lines, the stopband and passband performances of the PBG structures can be improved.

The length of the transmission lines used for Figs. 4.6 and 4.10 are not same. It is well known that the length of the line does not affect the S-parameters performance. Rather it changes the phase properties.

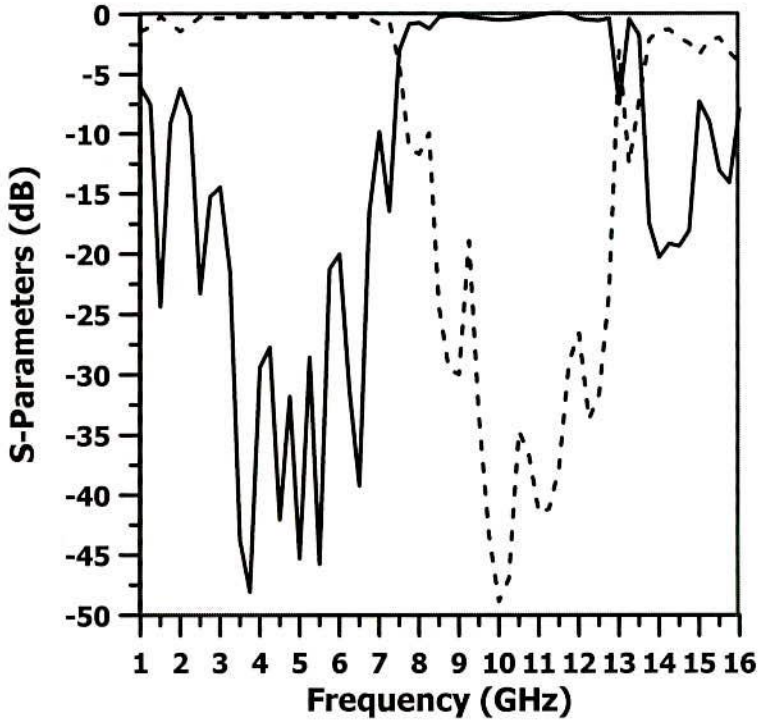

Fig. 4.10: Simulated S-parameter vs frequency for a cascade of two 10-element circular patterned PBG lines with Binomial distribution (Type-A) with r_0 = 56 mils, a period a = 224, and line width 24 mils (50 Ω). Dielectric substrate: ε_r = 10.2, h = 25 mils. Solid line - S_{11} and Dotted line-S_{21}

Once the characteristics of Binomially distributed circular PBGSs, are investigated next the performances for *Chebyshev* distributions of circular PBGSs are presented.

4.6 PBGSs with *Chebyshev* Distribution

While Binomial distribution suffers from narrowband performance and restricted lowpass selectivity, the performance can be improved significantly with the *Chebyshev* distribution. Fig. 4.11 shows the measured and simulated S-parameters vs frequency for a 10-element circular patterned PBG line (Type-A) with 25 dB SLL *Chebyshev* polynomial distribution with r_0 = 84 mils, a period a = 224, and line width 24 mils (50 Ω). As can be seen, the measured passband ripples have reduced significantly similar to that for an ideal transmission line; whereas in

uniform distribution the ripples were very high in the passband region. This is a significant improvement over the uniform circular patterned PBG transmission lines as shown in Fig. 4.4-Fig. 4.5. However, in this case the stop bandwidth has reduced with respect to the uniform circular patterned PBG with r = 84 mils. As usual, it can be seen that there is a stopband resonant frequency shift, which may be due to the fabrication errors of the PBG, engineered line.

Comparing the measured results alone in Fig. 4.4, Fig. 4.5 and Fig. 4.11, it can be concluded that the improvement of *Chebyshev* distributed circular patterned PBG is very significant as a lowpass filter design where filter synthesis has been greatly reduced due to the implementation of simple *Chebyshev* polynomial.

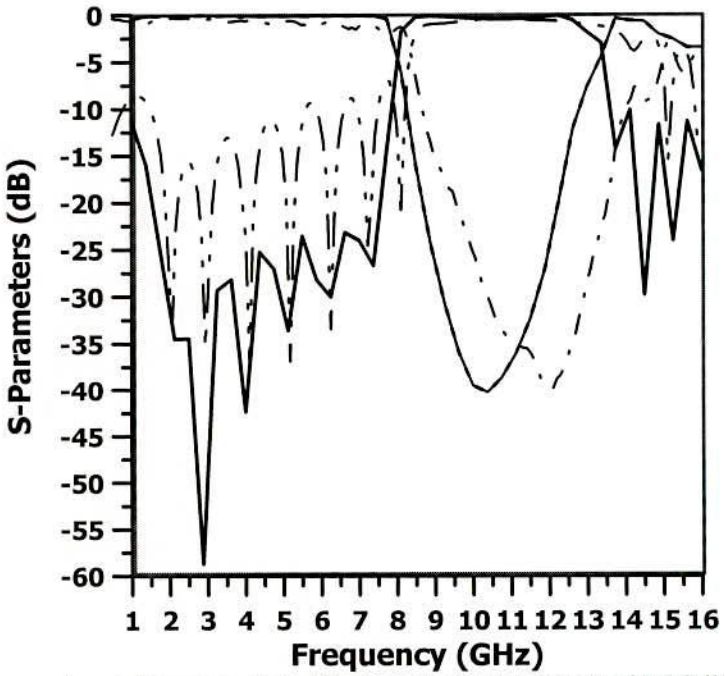

Fig. 4.11: S-parameter vs frequency for a 10-element circular patterned PBG line (Type A) with 25 dB side lobe level *Chebyshev* polynomial distribution. Dielectric substrate: ε_r = 10.2, h = 25 mils. Solid line–simulated and dashed double dotted lines–measured results for –25 dB SLL.

- **Prescribed SLL (25 dB and 35 dB)**

Fig. 4.12 shows the S-parameters vs frequency response for 10-element circular patterned PBG line (Type-A) with *Chebyshev* polynomial distributions with two prescribed SLL of 25 dB (solid line) and 35 dB (dotted lines), respectively. As can be seen in the figure, both distributions yield very sharp cut-off performance and the lowpass return loss performance has improved significantly. S-parameters vs frequency for a 10-element circular patterned PBG line with 25 dB side lobe level *Chebyshev* polynomial distribution (Type-A) with r_0 = 84 mils, a period a = 224, and line width 24 mils (50 Ω) is shown in Fig. 4.12.

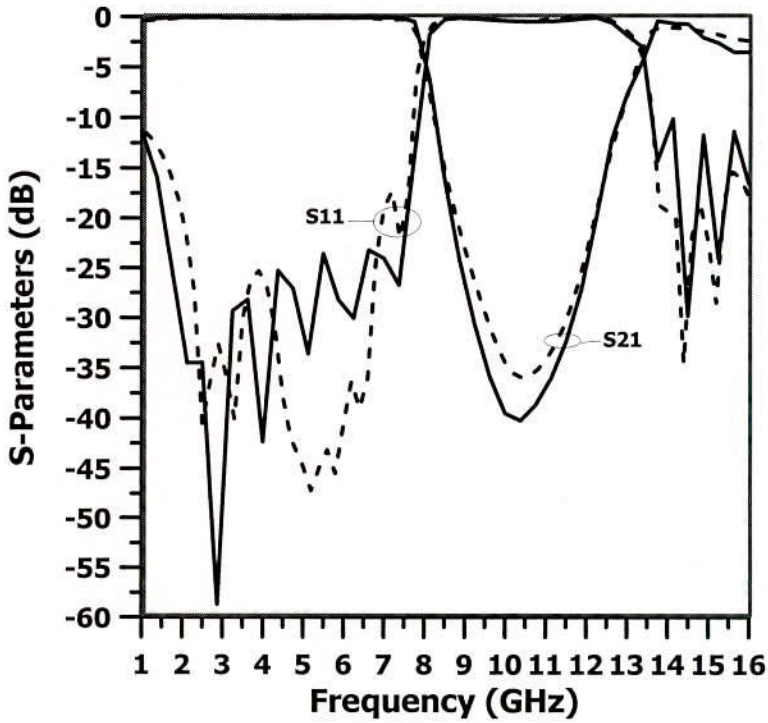

Fig. 4.12: Simulated S-parameter vs frequency for a 10-element circular patterned PBG line with 25 dB side lobe level *Chebyshev* polynomial distribution (Type-A). Dielectric substrate: ε_r = 10.2, h = 25 mils. Solid line–25 dB; dotted line–35 dB.

For both cases the rejection bandwidth is 4.5 GHz, the first null in return loss near cutoff is 27 dB and the selectivity is 27 dB/GHz. The two performances are very

similar except the deep in S_{21max} and first return loss nulls. For 35 dB distributions, the first return loss null is 17 dB and the S_{21max} is 36 dB.

- **Comparison with Uniform Distribution**

Fig. 4.13 shows the comparison of S-parameters performances with different frequencies for uniform and *Chebyshev* Type-A and Type-B distributions for 25 dB side lobe level voltage ratio. The radii are: $r = r_0 = 84$ mils.

The results are summarized in Table 4.4. From the figure and the table it can be concluded that *Chebyshev* Type-B yields similar bandwidth performance to that for the uniform distribution, but the selectivity (20.92 dB/GHz) of Type-A is poorer than that for Type-B (56.6 dB/GHz).

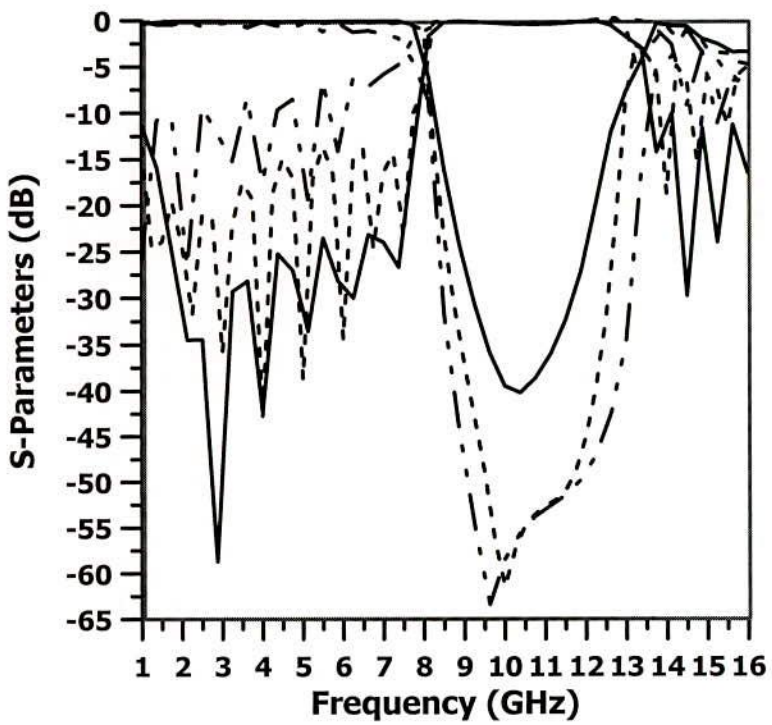

Fig. 4.13: Simulated S-parameters vs frequency for a 10-element circular patterned PBG line with 25 dB side lobe level *Chebyshev* distribution with $r_0 = 84$ mils, a period $a = 224$, and line width 24 mils (50 Ω). Dielectric substrate: $\varepsilon_r = 10.2$, h = 25 mils. Solid line– *Chebyshev* (Type-A); dotted line– *Chebyshev* (Type-B), double dotted-dashed line– uniform distribution

For Type-B the selectivity of the filter is much more improved than that for the uniform distribution (21.7 dB/GHz). The characteristic of the filter response near the cut-off also improves significantly for both *Chebyshev* types. The 1st null of return loss is 27 dB for Type-A and 23 dB for Type-B compared to 7.2 dB for uniform distribution of circular PBGSs.

TABLE 4.4: COMPARATIVE STUDY OF CIRCULAR PATTERNED PBGS WITH UNIFORM AND *CHEBYSHEV* DISTRIBUTIONS: $\varepsilon_R = 10.2$, H = 25 MILS, R = 84 MILS, PERIOD $a = 224$ MILS.

Type	Stopband Isolation		20 dB Isolation bandwidth (GHz)	Selectivity: dB/($f_s - f_p$) (Lower cutoff) (dB/GHz)	1st null and peak Return loss (dB)	
	$S_{21(max)}$ (dB)	f_0 (GHz)			Null	Peak
Uniform	**63.4**	**9.6**	**5.68**	**21.7**	**7.2**	**6.14**
Type-A	**61.5**	**10**	**5.04**	**20.92**	**27**	**24**
Type-B	**40.3**	**10.2**	**4**	**56.6**	**23**	**15**

- **Analysis of cutoff performances**

Fig. 4.14 and Fig. 4.15 show the close-up view of the cutoff performances of the S-parameters for uniform and the *Chebyshev* Type-B distribution for $r = r_0 = 84$ mils. As can be seen form Fig. 4.14, the chart for S-parameters near lower cut-off region, the selectivity for the uniform distribution is 21.7 dB/GHz while for the *Chebyshev* Type-B the selectivity is 56.6 dB/GHz.

Fig. 4.15 shows the similar performance at the upper cutoff region where the selectivity is 18.06 dB/GHz and 43.35 dB/GHz for uniform and *Chebyshev* Type-B distributions, respectively. In both lower and upper cut-off (3 dB) regions, the return loss for the uniform distribution is merely 3 dB, while for *Chebyshev* Type-B the return loss shows distinct nulls of about 20 dB.

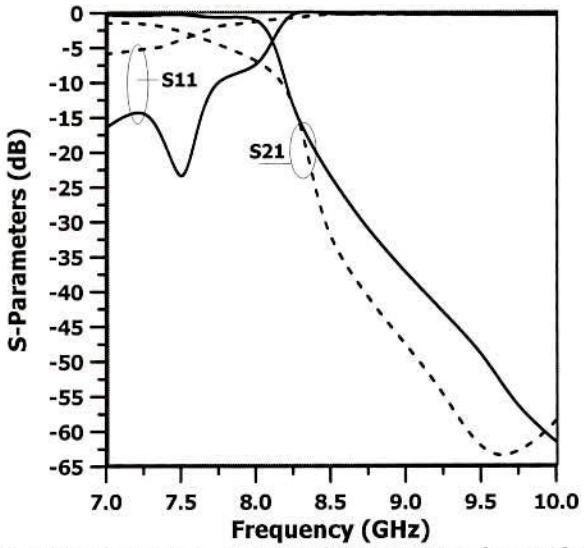

Fig. 4.14: Analysis of S-parameters at cut-off frequencies for uniform and *Chebyshev* distribution of 10-element circular patterned PBG lines at lower cut-off region. r_0 = 84 mils, a period a = 224, and line width 24 mils (50 Ω). Dielectric substrate: ε_r = 10.2, h = 25 mils. Solid line–*Chebyshev* (Type-B); dotted line–uniform.

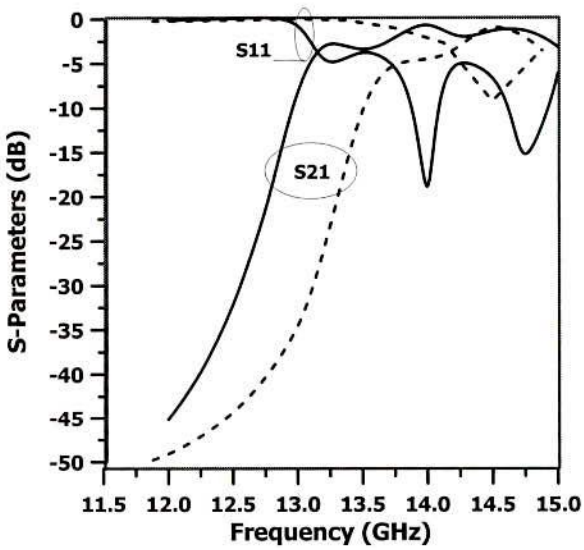

Fig. 4.15: Analysis of S-parameters at cut-off frequencies for uniform and *Chebyshev* distribution of 10-element circular patterned PBG lines at upper cut-off region. r_0 = 84 mils, a period a = 224, and line width 24 mils (50 Ω). Dielectric substrate: ε_r = 10.2, h = 25 mils. Solid line–*Chebyshev* (Type-B); dotted line–uniform

4.7 Optimum FF for *Chebyshev* distribution at X-band

In the present research, the sensitiveness of the performance to the designed frequencies of a non-uniform distribution PBG structured line based on *Chebyshev*

distribution is proposed. Here the element size is proportional to the co-efficient of *Chebyshev* polynomial. The investigation that is carried out in this section is very similar to previous section 4.5. The corresponding period of the lattice structures are calculated to be 248, 213 and 186 mils respectively for the center frequencies of the stop bandwidths of 9, 10.5 and 12 GHz respectively. The simulation results present the dispersion characteristics in terms of S-parameters vs frequency for *Chebyshev* engineered structure at 9, 10.5 and 12 GHz with FF of 0.3, 0.4 and 0.5 respectively.

- **Performance at 12 GHz**

The simulated performances of the PBG assisted lines with FFs of 0.3, 0.4 and 0.5 at 9, 10.5 and 12 GHz are summarized in Table 4.5. As can be seen from the table, that the 10 dB passband return loss BWs are 8.782, 8.813 and 7.7603 GHz for FF of 0.3, 0.4 and 0.5 respectively. Corresponding to these FFs the 20 dB rejection BWs are found to be 0, 3.84 and 4.573 GHz, the maximum isolations are 20, 29.79 and 36.67 dB respectively. The pass band ripple height is 3.14 dB for FF = 0.5. The maximum isolations are 20, 29.79 and 36.67 dB for the FFs of 0.3, 0.4 and 0.5 respectively. It is seen that the optimum performance in terms of ripple height, isolation, passband return loss bandwidth and 20 dB rejection BWs are achieved for FF of 0.4.

- **Performance at 10.5 GHz**

At 10.5 GHz, the maximum 10 dB return loss bandwidth is found to be 8.375 GHz for FF = 0.3 with minimum 20 dB rejection BW of 1.88 GHz. Maximum stop bandwidth of 4.53 GHz is achieved for the FF of 0.5 with maximum passband

ripple height of 2.25 dB. From Table 4.5 it is clear that the FF of 0.4 is considered to be the optimum FF.

- **Performance at 9 GHz**

Lastly the same designs at 9 GHz are investigated. From the Table 4.5 it is observed that the maximum 10 dB passband return loss BW of 7.073 GHz with minimum stop bandwidth of 2.219 GHz is achieved for FF of 0.3. A reasonable stopband of 4.105 GHz is obtained with zero passband ripple at FF = 0.4. Though 4.21 GHz stopband is obtained in case of FF = 0.5, it yields passband ripple to be 4.25 dB.

Considering performances in all these frequencies 0.4 may be considered as the approximate value of optimum FF for PBGS design with *Chebyshev* distribution. It is observed from the Table 4.5 that the performances are sensitive to the frequencies. From Table 4.5 it can be seen that the maximum stopband width is found to be 4.105 GHz at 9 GHz. Maximum passband return loss BW of 8.81 GHz is achieved at 12 GHz. It can also be seen that the maximum isolation is obtained at 9 GHz and the minimum return loss is found to be at 10.5 GHz.

TABLE 4.5: PERFORMANCE OF A 50-OHM TRANSMISSION LINE PERTURBED WITH *CHEBYSHEV DISTRIBUTION* HAVING FF = 0.3, 0.4 AND 0.5 AT 12, 10.5 AND 9 GHZ. THE SUBSTRATE IS RT/DUROID HAVING DIELECTRIC CONSTANT =10.2 AND HEIGHT =25 MIL.

Frequency (GHz)	FF	20 dB rejection BW (GHz)	10 dB passband return loss BW (GHz)	Ripples (dB)	S21 (max) (dB)	Max. return loss (dB)
12 GHz	0.3	0	8.78	0	-20	61
	0.4	3.84	8.81	0	-29.79	47
	0.5	4.57	7.76	3.14	-36.67	45
10.5 GHz	0.3	1.88	8.38	0	-25.5	47
	0.4	4.05	7.8	0	-44	44
	0.5	4.53	7.58	2.25	-52	35
9 GHz	0.3	2.219	7.07	0	-30	48
	0.4	4.105	6.8	0	-56.5	38
	0.5	4.215	6.48	4.25	-58	37

4.8 Chirped PBGSs with *Chebyshev* Distribution

In this section chirped PBG elements with *Chebyshev* distribution is presented. The period is not equidistant rather chirped as [75]. The results stemmed from this type of novel structure show their superiority over the conventional uniform hole patterned PBGSs. In [75] the amplitudes are tapered with the Gaussian distribution. Uniform PBGSs provide poor performance when the FF exceeds the optimized value of 0.25. The results with conventional PBGSs have not been compared. Rather, more attention has been given to investigate the performance of a chirped PBGS to compare the performance with that author's works [35], which possesses the superior performance over the conventional design. The performances are presented in terms of 10 dB passband return loss BW and 20 dB rejection BW.

4.8.1 Theory

Primarily the Bragg's condition is chosen to calculate the period of the uniform structure with respect to central stopband frequency.

- **Variations in amplitudes**

Here *Chebyshev* polynomial has been used to determine the amplitudes of the PBG elements. Equations (4.2) and (4.3) define *Chebyshev* polynomials.

- **Chirping Technique**

For the calculation of all the chirped periods the following equation [75] is used.

$$a_i = a_0 (1 + i\delta) \tag{4.7}$$

where a_0 is the conventional period (equidistant period), δ is the chirp parameter that controls the variation of distance between PBG elements. Here δ is chosen to be 4.18×10^{-2} as this value is considered to be moderate value of the chirp parameter [75] and i = 0, ±1, ±2, ±3… etc depending on the location of PBG elements with respect to central elements. Here a new design is investigated, assisted by chirped PBGSs having *Chebyshev* distributions.

4.8.2 Designs

The following structures are designed to show the improved performances of Chirped design. The amplitudes of all the PBG elements are calculated as per Type-B properties of *Chebyshev* distribution.

- **Non-Chirped PBGSs with *Chebyshev* Distributions**

PBGSs with constant inter-cell separation are designed. The amplitudes are varied with the coefficients of *Chebyshev* distribution. The geometry has not been shown here, as the geometry is similar to Fig. 4.3.

- **Non-uniform Chirped PBGSs**

The inter-cell separations are calculated in accordance with equation (4.7) that is well known equation for chirping technique. The dimensions of PBG elements are calculated with the *Chebyshev* distribution. Both Types-A and B circular PBGSs with medium value of chirping parameter [75] have been investigated. One photograph of ground plane perturbed by chirped PBGSs (Type-B) is shown in Fig. 4.16.

- ***Chebyshev* distributed Chirped PBGSs**

A new chirping technique is applied in this design that replaces the conventional approach of chirping. Here the inter-cell separation is also calculated as per the co-efficient of *Chebyshev* distribution. Type-A distribution is used in this case owing to the fact that if the period is varied as per *Chebyshev* distribution Type-B then overlapping takes place between elements. No geometry is shown here.

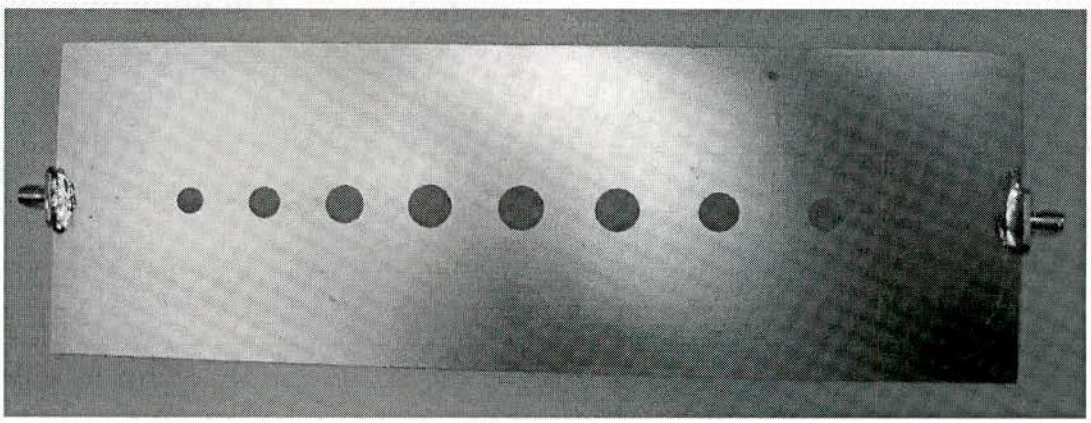

Fig. 4.16: Photograph of the non-uniform chirped PBGS assisted ground plane of a microstrip transmission line.

4.8.3 Results

The microstrip transmission lines to be investigated are: (a) non-chirped PBG elements with *Chebyshev* distributions (in amplitudes) and (b) chirped PBG

elements with *Chebyshev* distributions (Type-B). The performances of all the designs are investigated in terms 10 dB passband return loss BW and stopband and the depth of the stopband under the consideration of negligible ripples in the passband. To validate the theoretical performances two prototypes are fabricated. The simulated performances are compared with the measured performances.

- **Non-Chirped PBGS with *Chebyshev* Distributions**

The S-parameter performances of PBGSs with non-chirped periods having the amplitudes with Type-B configuration are shown in Fig. 4.17. It can be seen that this model yields a significantly wide passband with minimum ripple height. The approximate 10 dB passband return loss BW is found to be 1.407 GHz and the 20 dB rejection bandwidth is 1.65 GHz with maximum isolation of 69 dB. The frequency shifting is found to be 5.16%.

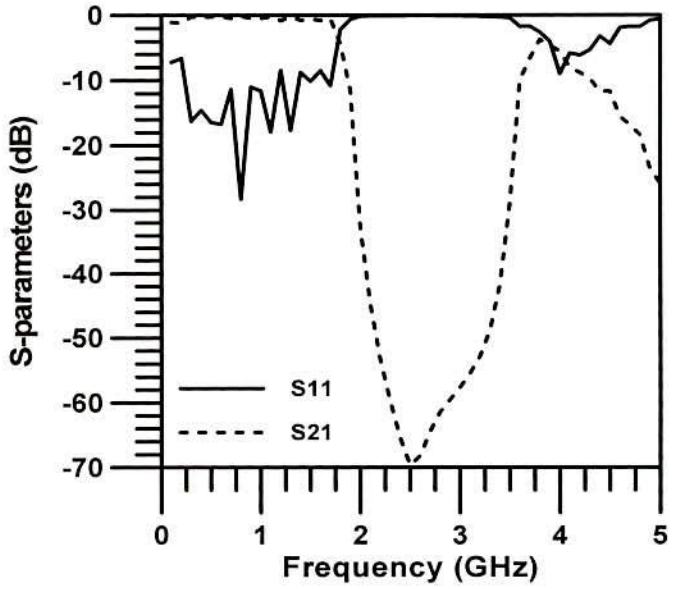

Fig. 4.17: Simulated S-parameters of a 50 ohm microstrip transmission line perturbed by non-chirped PBGSs with *Chebyshev* distribution (Type-B) at 2.5 GHz having FF = 0.4. The substrate is Rogers RO3010^{TM} with dielectric constant of 10.2 and height of 1.27 mm.

- **Non-uniform Chirped PBGSs**

The S-parameters performance of PBGSs with chirped periods that are varied in accordance with the standard equation as shown in equation (4.7) and the amplitudes are varied as per *Chebyshev* distribution (Type-B) is shown in Figs. 4.18. It can be seen that the transmission of signal in the passband is uniform ensuring minimum ripple height. The 10 dB passband return loss BW is found to be 1.276 GHz and the 20 dB rejection bandwidth is found to be 1.75 GHz with maximum isolation of 52 dB. The frequency shifting is found to be 13.79%.

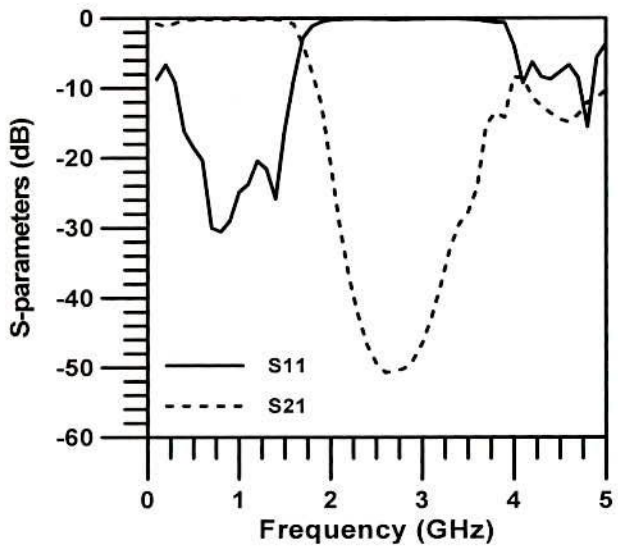

Fig. 4.18: Simulated S-parameters of a 50 ohm microstrip transmission line perturbed by chirped PBGSs with *Chebyshev* distribution (Type-B) at 2.5 GHz having FF = 0.4. The substrate is Rogers RO3010^{TM} with dielectric constant of 10.2 and height of 1.27 mm.

It is interesting to note that the chirped PBGSs provide little bit less return loss passband than the non-chirped PBGSs. However, the important parameter namely stopband is enhanced for chirped PBGSs. In the case of return loss performance it is seen that the return loss always remains below 20 dB corresponding to passband indicating very good matching throughout the entire passband. The shifting in 20

dB central stopband is obvious due to inclusion of chirping technique for calculating all the periods of PBG elements at both sides with respect to central elements.

- ***Chebyshev* Distributed Chirped PBGSs**

From Fig. 4.19 it can be seen that the approximate 10 dB passband return loss BW is 1.481 GHz and the 20 dB stopband is 2.2 GHz. The controlling parameter of central stopband frequency is the period of PBGS. Since the period is not equidistant in the chirped PBGS, significant stopband central frequency shift is natural. It is seen that if the period is chirped with *Chebyshev* distributions instead of conventional chirping technique, rejection bandwidth improves very significantly.

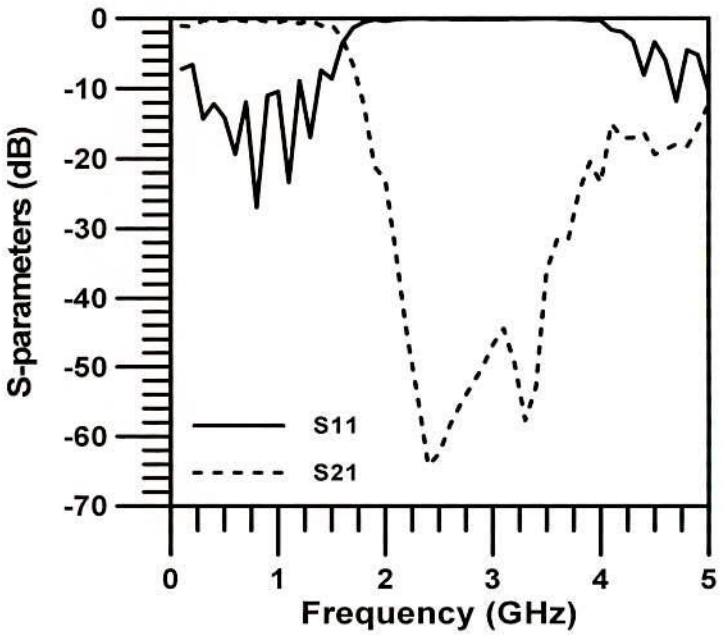

Fig. 4.19: Simulated S-parameters of a 50 ohm microstrip transmission line perturbed by chirped PBGSs with *Chebyshev* distribution (Type-B) at 2.5 GHz having FF=0.4. The substrate is Rogers RO3010^{TM} with dielectric constant of 10.2 and height of 1.27 mm.

The return loss and rejection bandwidth performances of the three designs are tabulated in Table 4.6. As can be seen from the Table 4.6, the chirping improves the stopband and passband performances. Comparing the two chirping techniques, it can be concluded that the passband and stopband performances can be trade off by selecting chirped design. For normal chirped PBGS, the passband frequencies improve significantly with average 25 dB return loss, which is an excellent LPF. On the other hand *Chebyshev* distributed chirping yields wider stopband (450 MHz more BW compared to standard chirped non-uniform PBGS).

TABLE 4.6: COMPARISON OF RETURN LOSS BW AND REJECTION BW AMONG NON-UNIFORM PBGSS, PBGSS WITH STANDARD CHIRPING AND PBGSS CHIRPED WITH *CHEBYSHEV* DISTRIBUTION.

Designs	10 dB return loss BW (GHz)	20 dB rejection BW (GHz)
Non-chirped non-uniform PBGSs *(Chebyshev* Type-B)	1.407	1.655
Non-uniform PBGSs (*Chebyshev* Type-B) with standard chirping	1.276	1.750
Non-uniform PBGSs (*Chebyshev* Type-B) chirped with *Chebyshev* (Type-A)	1.2	2.2

- **Experimental Verifications**

The theoretical and experimental performances of chirped PBGSs (Types-A and B) are shown in Figs. 4.20 and 4.21. The designs are fabricated on Taconic substrate with dielectric constant of 10 and height of 25 mils. Both figures provide similar theoretical and experimental performances.

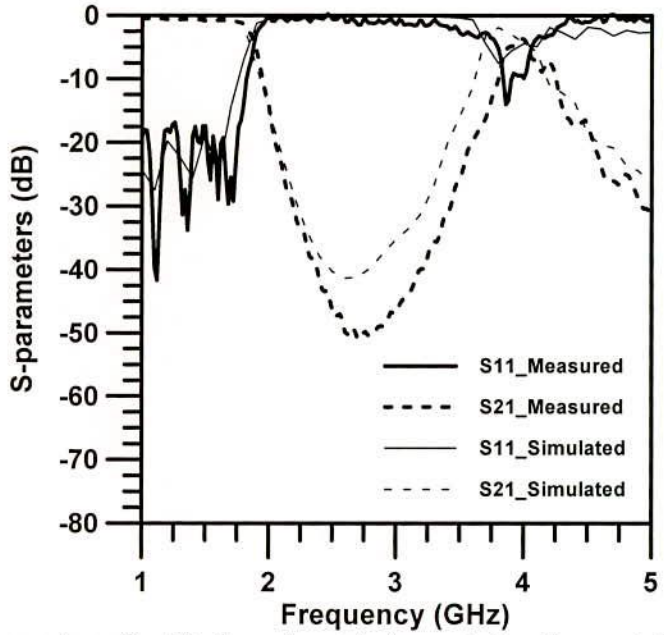

Fig. 4.20: S-parameters of a 50 ohm microstrip transmission line perturbed by chirped PBGSs with *Chebyshev* distribution (Type-A) at 2.5 GHz having FF = 0.25 (Central two elements). The substrate is Taconic with dielectric constant of 10 and height of 25 mils.

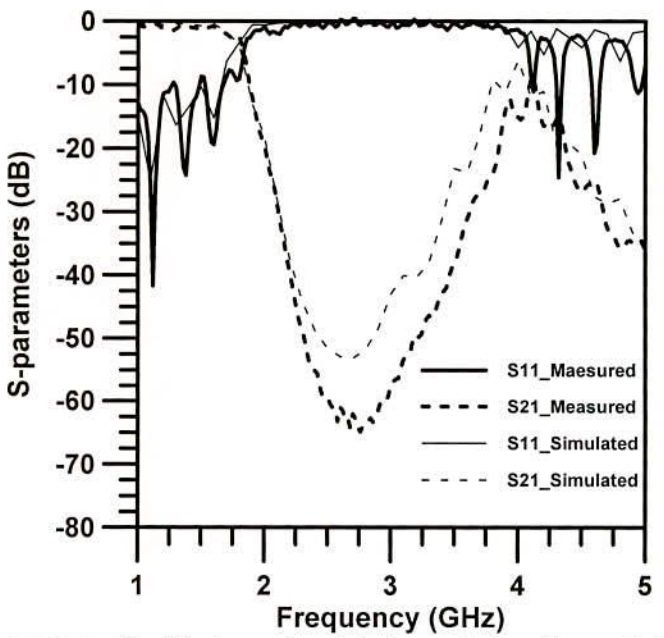

Fig. 4.21: S-parameters of a 50 ohm microstrip transmission line perturbed by chirped PBGSs with *Chebyshev* distribution (Type-B) at 2.5 GHz having FF=0.25 (Central two elements). The substrate is Taconic with dielectric constant of 10 and height of 25 mils.

Very small amount of return loss is seen in the stopband region that may originate from the reflection of SMA connector. The small discrepancies in depth of width

of the rejection band may arise due to different assumptions and factors during total process that is already mentioned in chapter three.

From the Figs. 4.20-4.21 it can be seen that Type-B non-uniform PBGSs being chirped with the standard technique provides wider stopband that is also already mentioned in previous sections. It is worthwhile to mention that FF is 0.25 is used in these designs. It could be stretched up to 0.4. Yet this smaller value of FF for non-uniform distribution yields good performance as a whole. FF of 0.4 will surely generate wider and depth stopband.

4.9 Metallic Perturbation into the Conventional PBGS

So far conventional non-uniform circular patterned PBGSs have been discussed. In this section perturbed circular patterned PBGSs will be investigated. The metallic perturbation into the conventional circular PBGSs provides more flexibility to control the dispersion characteristic of the PBG structures. Ring structure is achieved when a small amount of circular metallic pad is introduced in the center of the conventional hole patterned PBG structure. A typical microstrip transmission line over non-uniform ring patterned PBG elements is shown in Fig. 4.22.

In this section the performance of uniform [79] and non-uniform annular ring PBG assisted microstrip lines are demonstrated. Ring PBG structures provide easier control of aspect ratios to optimize the performances. The annular ring PBGSs are studied with respect to its aspect ratio, rejection bandwidth and passband ripple heights.

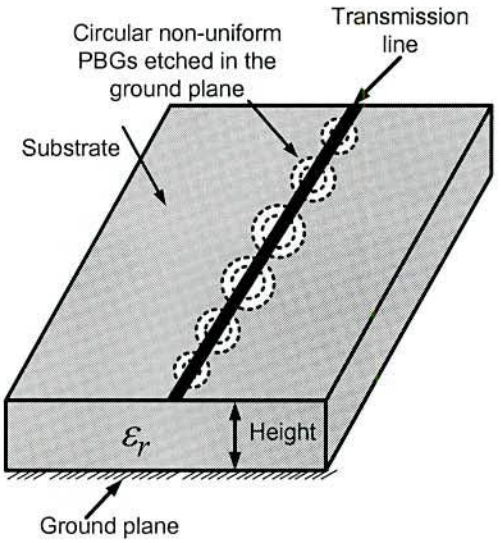

Fig. 4.22: Isometric view of a non-uniform ring patterned PBG elements in the ground plane of a standard 50-ohm transmission line.

For the aspect ratio study, the same FF, which is the ratio of the outer radius and the period of the annular ring, is used. Total number of PBG elements is ten. The inner ring radius (aspect ratio) is varied and the S-parameter performance is recorded. Microwave material: RT/Duroid 6010 with ε_r = 10.2 and thickness h = 25 mil is used in the investigation. The period a = 224 mil is used in all investigations. Different uniform and non-uniform annular ring PBG structures are designed and simulated. The measured results are compared with the simulated results.

4.9.1 Uniform 1-D Ring PBGSs

In an annular ring PBGS the outer dimension has been kept constant while the inner dimensions have been changed to vary the aspect ratio of the ring PBG unit. Simulation results for aspect ratio (AR) = 0.1785 and 0.892 are shown in Fig. 4.23. From the simulation results it is seen that the rejection bandwidth reduces with the aspect ratio. The uniform ring PBG assisted transmission line yields ripple in the

passband. This ripple can be suppressed with non-uniform distribution of the ring PBG units under the transmission line.

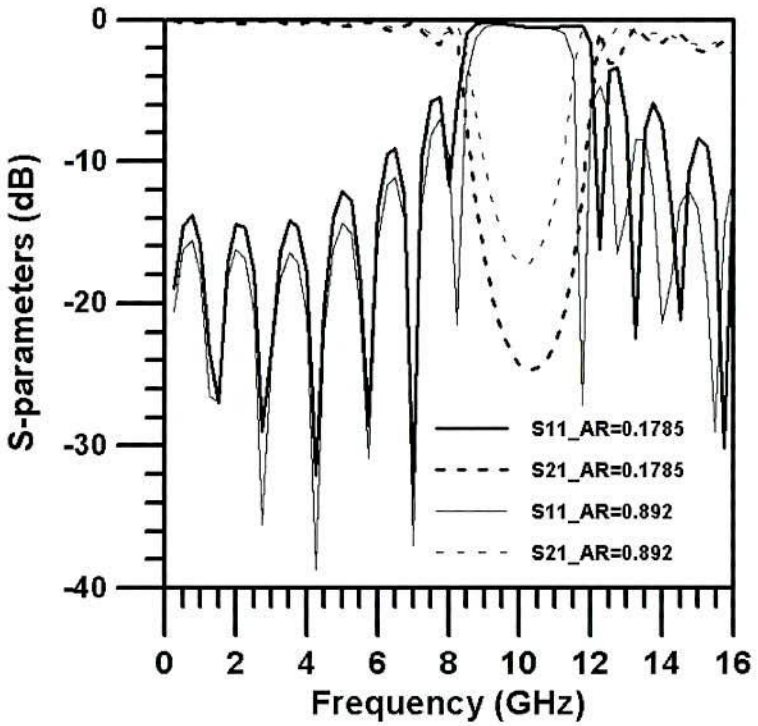

Fig. 4.23: Simulated S-parameters vs frequency for annular ring PBG with different aspect ratios. R_{out} = 56 mil, period 224 mil, substrate: ε_r = 10.2, h = 25mil.

The experimental investigation is also carried out for uniform circular ring patterned PBGSs. The comparison of the theoretical and measured S-parameters performances of uniform ring patterned PBGSs with aspect ratio of 0.1785 are shown in Fig. 4.24. It can be seen that there is an acceptable agreement between simulated and measured performances.

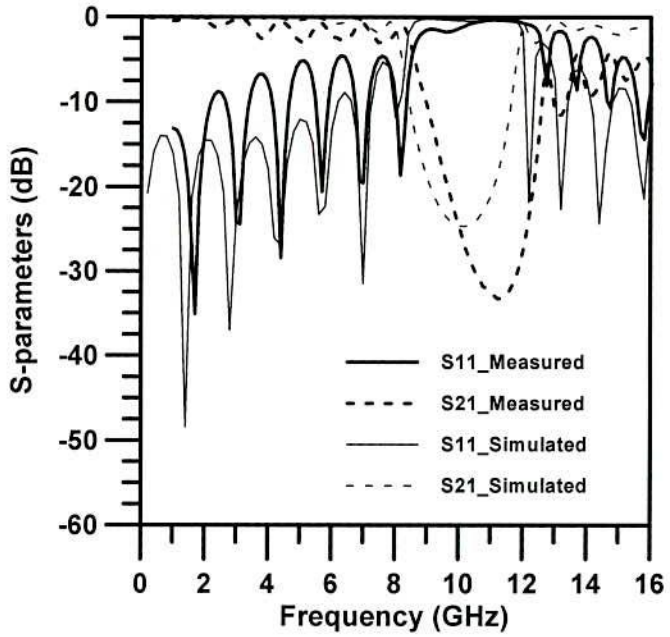

Fig. 4.24: Measured and simulated S-parameters vs frequency for 7-elements annular ring PBGSs with aspect ratio of 0.1785. R_{out} = 56.5 mil, period 226 mil, substrate: ε_r = 10, h = 25 mils.

4.9.2 Non-uniform Ring PBG Structure with *Chebyshev* Distribution

Both Type-A and Type-B non-uniform ring PBG structures with different ARs were investigated. For different ARs, smoother passband at low and high frequencies are obtained. For the optimum FF of 0.25, the outer dimension of the central rings was 56 mils, but the outer dimension of the central two elements for non-uniform distribution has been stretched to 62.5 mils. The simulated results for the aspect ratio of 0.15 are shown in Fig. 4.25. As can be seen in Fig. 4.25, significant improvement in passband ripples at both low and high frequencies is achieved. For different aspect ratios such as 0.15, 0.35, 0.55, 0.75 and 0.95, all 20 dB rejection bandwidth are calculated. The variation of 20 dB rejection bandwidth with AR is shown in Fig. 4.26.

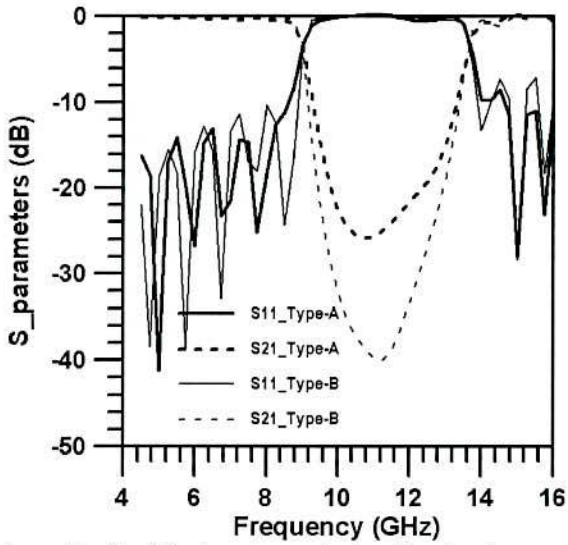

Fig. 4.25: Simulated result of a 50-ohm transmission line having w = 24 mils on a ring patterned PBG ground plane. Aspect ratio = 0.15 (For both *Chebyshev* Type-A and Type-B), a = 224 mils, substrate: ε_r = 10.2, h=25 mils.

It is observed in Fig. 4.26 that the 20 dB rejection BW reduces with AR. From this figure it is clear that Type-B is certainly superior to Type-A PBGS.

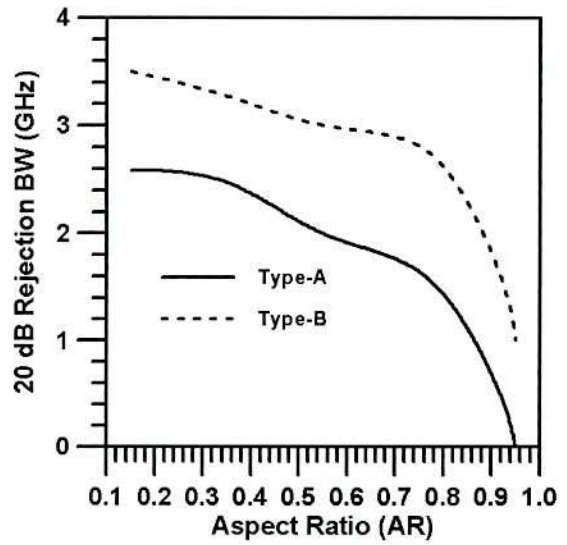

Fig. 4.26: The variation of bandwidth versus aspect ratio for both Type-A and Type-B with *Chebyshev* distribution of ring patterned PBG structure.

Finally the prototype of *Chebyshev* ring patterned PBG assisted microstrip transmission lines is fabricated and the S-parameters are measured on HP 8510C

VNA. Fig. 4.27 shows the measured and simulated S-parameters vs frequency plot. Significant improvements of passband ripples and return loss are achieved for both the cases. Comparing all the results mentioned above, it can be concluded that the S-parameter performances are much superior in non-uniform annular ring patterned PBG assisted line.

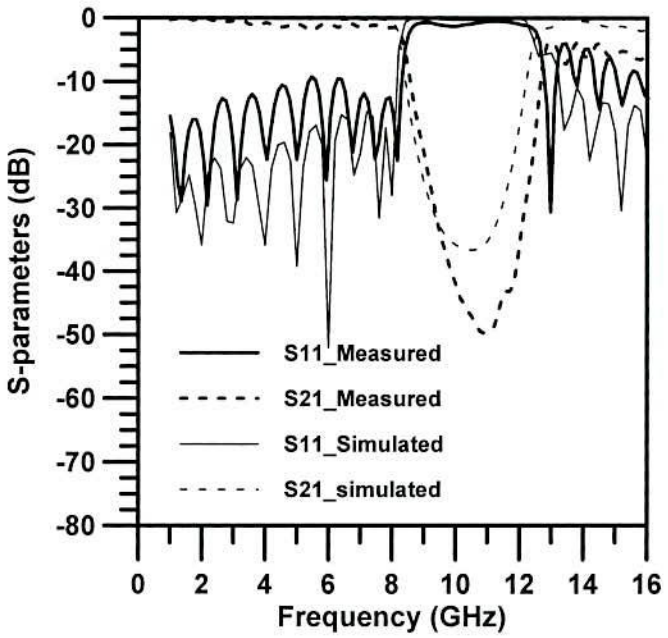

Fig. 4.27: The S-parameters of one line non-uniform (*Chebyshev* distribution Type-B) ring patterned PBGSs with FF of 0.2765 and aspect ratio 0.15. Substrate is Taconic having dielectric constant of 10 and height of 25 mils. The inter-element spacing is 226 mils.

The center frequency is little bit shifted and there exists small discrepancies in rejection band as shown in Figs 4.24 and 4.27. The center frequency is approximately calculated and the size of the PBG element is related with the period by FF. So any change in period in turn affects the perturbation of the ground plane, which controls the stopband performances.

Conclusions

In this chapter non-uniform PBGSs with Binomial and *Chebyshev* distribution have been described. They have been analyzed in the light of LPF performances.

Due to the limitation of optimum FF of uniform PBGS they are investigated. Non-uniform distribution of PBGSs has been proposed where the FF can be stretched beyond the optimized FF 0.25. To get the idea of optimum FF 50-ohm transmission lines on a Binomially distributed PBG structure having FF = 0.3, 0.4 and 0.5 at 9, 10.5 and 12 GHz respectively have been simulated. Doing all these simulations it is seen that the Binomially distributed PBGSs provide better results than those for uniform PBGSs. Better performance with Binomial distribution with Type-B are found. The optimum value of FF for Binomial distribution has been found. It is observed that 0.4 may be considered as the approximate value of optimized FF. It is better to note that there is still some scope to investigate the value of optimum FF within the intermediate value ranging from 0.4 to 0.5. This is the first time, it is reported about the approximate value of optimum FF for Binomially distributed PBGSs. The potential finding of this present research is also to see the frequency dependence of the performance. Considering the improved performance in terms of passband return loss, ripples, return loss BW and rejection BW, it can be seen that at 9, 10.5 and 12 GHz (X-band), the FF 0.4 can be considered as the optimum value of FF in case of Binomial (Type-B) distribution. In this investigation, the substrate has the dielectric constant of 10.2 and the height of the substrate is 25 mils. The depth of the stopband, the rejection bandwidth and the ripples are different at different frequencies. So they provide wider scope to designer for specific design purpose of stopband filter. It is important to note that frequency shifting is common feature of PBG structures. The center frequency is controlled by the period of the PBG lattice structure that is determined from the Bragg's condition. So shifting can be minimized by optimization of the designs. In the simulation results, conductor loss, substrate loss and the loss due to connectors

are not included. Above all, all the simulations have been done on infinite ground plane. All the structures are fabricated using milling machine. So fabrication errors are there. This type of error may cause variations in size and period of the lattice structures resulting in the variation in S-parameters and frequency of interests.

Microstrip lines perturbed by PBG structures with *Chebyshev distribution* have also been designed and analyzed at 9, 10.5 and 12 GHz for FF of 0.3, 0.4 and 0.5 respectively. In this case 0.4 may also be considered as the optimum value of FF.

Again a novel PBG engineered microstrip transmission line is designed and investigated theoretically by tapering and chirping the PBGSs. In first design the amplitude has been tapered with the *Chebyshev* distribution. The over all performance of the proposed model (non-uniform PBGSs with standard chirping) is always superior to conventional hole patterned PBG structured transmission line. Even this model stems the superiority over the author's recent work [35] on hole patterned PBGSs with *Chebyshev* distributions. In the second design the chirping has been done on the basis of the *Chebyshev* distribution (Type-A) and the amplitudes are varied as per *Chebyshev* distribution (Type-B). This design provides wider stopband performance and proves its superiority to uniform, non-chirped non-uniform PBGSs and non-uniform PBGSs with standard chirping. As a whole it can be concluded that the new model (non-uniform PBGSs that is chirped with *Chebyshev* distribution) is more attractive and more useful where the wider stopband is crucial need than other parameters.

The influence of metallic perturbation into the conventional hole patterned PBGSs has been investigated. The AR in case of ring patterned PBGSs can be varied. It is

observed that ring patterned PBGSs with *Chebyshev* distribution (Type-B) having AR = 0.15 provides very smoother passband transmission as well as wider stopband.

Chapter 5 Defected Ground Structures

5.1 Introduction

The uniplanar compact PBG (UC-PBG) structure has been used for few applications [32]. UC-PBG structure has been applied to conventional LPF that improves the filter performance [32]. Low and high impedance transmission line sections have realized the LPF. The UC-PBG structure has been used in the ground plane of the filter. This structure is complex in nature. Next the researcher appeared with DGS [19] where regular PBGS are connected with narrower slots in the ground plane. The frequency of operation can be changed with the DGS dimensions. The DGS can also be used to realize LPF [33]. Two designs for LPF having T-junction stub as well as cross-junction opened stub in conjunction with DGS is used in the ground plane. DGS has been modeled with the lumped parameters. L. Garde *et al* [62] proposed non-uniform ring patterned dumbbell shaped DGS to design LPF as PBGS with non-uniform distribution is proposed [35]. They have used DGS in the ground plane of a conventional LPF. The conventional LPF is implemented with transmission line obtained by the Richard's transformation that yields different transmission with different impedances (High-Low impedance sections). H-W Liu *et al.* [80] proposed a LPF with multilayer fractal PBGS. A two-level fractal PBG plane has replaced the ground plane. In the intermediate plate PBGS have different shapes as the top layer is made of 3rd-order Sierpinski gaskets and the bottom layer is made of 1st-order Sierpinski carpets. Significant ripples appear in the passband. Although the LPF performance reported in [63] and [80] produces wide stopband yet the designs need to take care of both the bottom and top layouts that may be contrast to high-level applications.

The new model of DGS provides a perturbed surface as ground plane of standard 50-ohm transmission line that yields the performance of LPF. It provides smoother passband and wider stopband. Only the perturbed ground plane needs to be taken care of.

In this chapter the evolution of DGS from conventional square patterned PBGS are reported. The frequency characteristics of dumbbell shaped DGS unit are presented. The influences of the dimension of larger slots and the gap distance of the narrow slot on cutoff frequencies and attenuation pole-location have been explained. Chronological development of (i) a double row square PBGS (ii) a conventional dumbbell shaped DGS, (iii) an interleaved uniform PBGS, (iv) an inter-leaved non-uniform PBGS and (v) finally *Chebyshev* distribution applied to both the conventional DGS and inter-leaved PBGS are presented in this chapter. To understand the usefulness of non-uniform distribution a standard 50-ohm microstrip transmission line on 1-D uniformly distributed square patterned PBGS and a microstrip line on 1-D non-uniform PBG configuration with *Chebyshev* distribution have been designed. *Chebyshev* distribution has been applied on conventional circular patterned PBG design to achieve better performance than that for the conventional circular patterned PBGS.

A simple design of dual stopband filter by modified DGS is also reported. In a conventional DGS normally two larger square/rectangular patterned PBG elements are vertically connected by narrow slot in the ground plane as shown in Fig. 5.1. The standard microstrip line is centrally placed on the thin slot in the conductor layer. In the modified DGS three larger square patterned PBG elements that are

connected vertically by two narrow slots are proposed. The standard 50-ohm transmission line is placed centrally on the middle larger PBG elements. The chapter is arranged as follows. Firstly theory of DGS with parametric studies of the DGS unit has been presented. Novel designs are presented followed by results and conclusions.

5.2 Theory

The center frequency of the stopband of a PBG is approximately calculated by well-known formula of Bragg's condition. Using this formula, the period for any stopband frequency can be determined. The theory of DGS is different from PBGS. In DGS, the dimensions of the dumbbell shaped slot (DGS unit cell) control the current paths on the ground plane hence the equivalent inductance and capacitance of the ground. Fig. 5.1 shows the unit cell of a dumbbell shaped DGS. It is composed of two larger slots connected by a narrow vertical slot. The larger slot is a square patterned PBG element. On the other hand narrower vertical slot is a rectangular patterned PBG element.

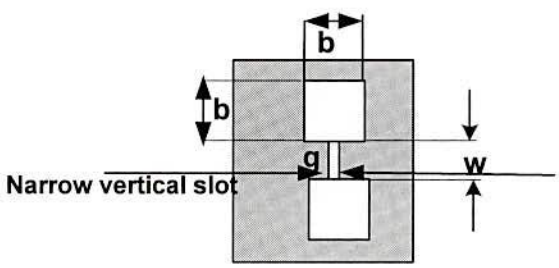

Fig. 5.1: Geometry of a unit cell of a dumbbell shape DGS. The arm length of a larger square patterned slot is 'b'. The vertical slot is a rectangular patterned slot with w×g dimension; w is known as width and g is known as gap in the open literature.

The unit cell is etched in the ground plane of a standard 50-ohm transmission line. In order to investigate the frequency characteristics of the unit DGS cell, few

structures having different 'b' and 'g' are simulated. All simulation results in one-pole LPF characteristics, which is obvious. There are two frequency properties; one is pole location, another is existence of cut-off frequencies. Employing DGS section increases the effective permittivity and hence effective inductance. Cut-off frequency is mainly dependent on the etched larger square patterned slot that depends on the value of 'b'. The pole location mainly depends on the gap distance 'g'. Two parameters 'b' and 'g' are studied to observe the frequency characteristics.

The lumped LC equivalent model can be expressed as [33]:

$$C = \frac{\omega_c}{Z_0 g_1}\left[\frac{1}{\omega_0^2 - \omega_c^2}\right] \quad \text{..... .....} \tag{5.1}$$

$$L = \frac{1}{4\pi^2 f_0 C} \quad \text{.....} \tag{5.2}$$

where f_0 is the frequency of the attenuation pole, ω_c is the angular cutoff frequency, Z_0 is the characteristic impedance of the line, and g_1 is the admittance value of the Butterworth low pass filter response.

The equivalent circuit of DGS unit cell is shown in Fig. 5.2.

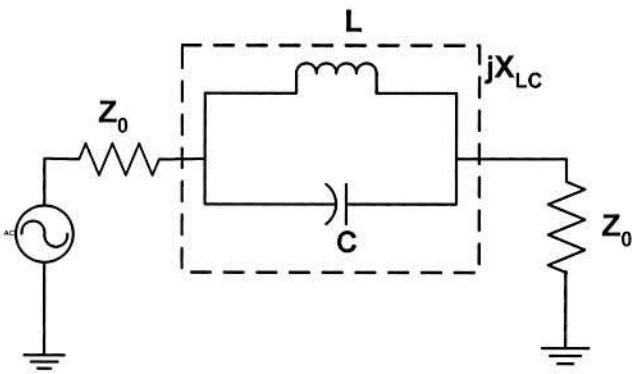

Fig. 5.2: The equivalent circuit of dumbbell shaped DGS unit.

Chebyshev distribution has been applied to vary the amplitudes of PBG elements in few designs that will help provide better filter performances. In the design the coefficients of the polynomial are determined for 25 dB SLL. The closed form expression of the equivalent circuit and the dimension can be extracted from the standard microstrip line filter synthesis.

- **Parametric Studies**

The influences of different dimensions of unit cell are presented bellow.

(1) Influence of Dimension of Larger Slot (b): The dimensions of larger square slot have been varied by making b = 113, 135.6, 158.2 and 180.8 mils. The gap and width are maintained constant for all designs having g = 15 mils and w = 20 mils. The insertion loss performances of these four designs are shown in Fig. 5.3.

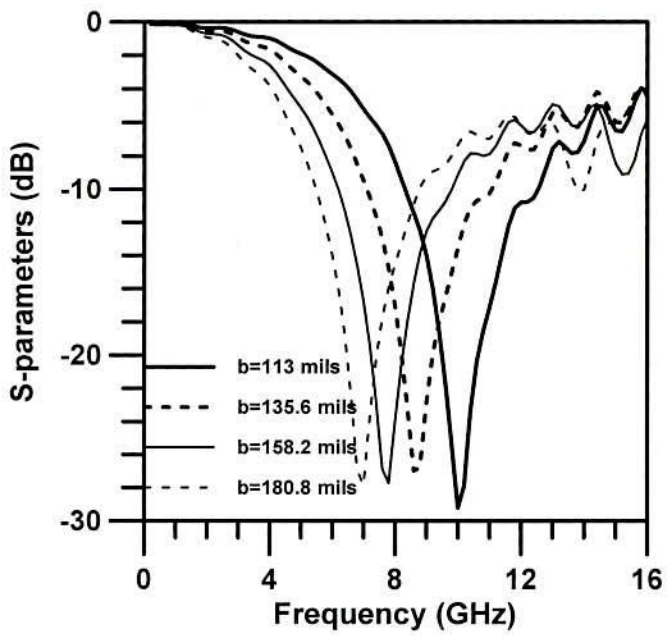

Fig. 5.3: Insertion loss performances of different dimensions of square patterned slots of a dumbbell shape unit cells.

The cut-off frequencies are different for different dimensions. When the dimension is larger, the series inductance increases and the cut-off frequency decreases as expected. The gap capacitance remains constant for the fixed dimension of the narrower slot. It is seen that the attenuation pole locations are also changed. This arises from the fact that the parallel combination of variable series inductance and constant shunt capacitance are always different due to change in dimension of larger slot. The location of the attenuation pole is the resonant frequency of LC circuit.

(2) Influence of the Gap Distance of Narrow Slot (g): The term 'g' that is known as gap distance in the open literature is varied. Gap distances are varied by making g = 20, 30, 40 and 50 mils. The dimension of the larger slot, b = 104 mils and the width of the narrow slot, w = 50 in all four designs. The Insertion loss performances are shown in Fig. 5.4.

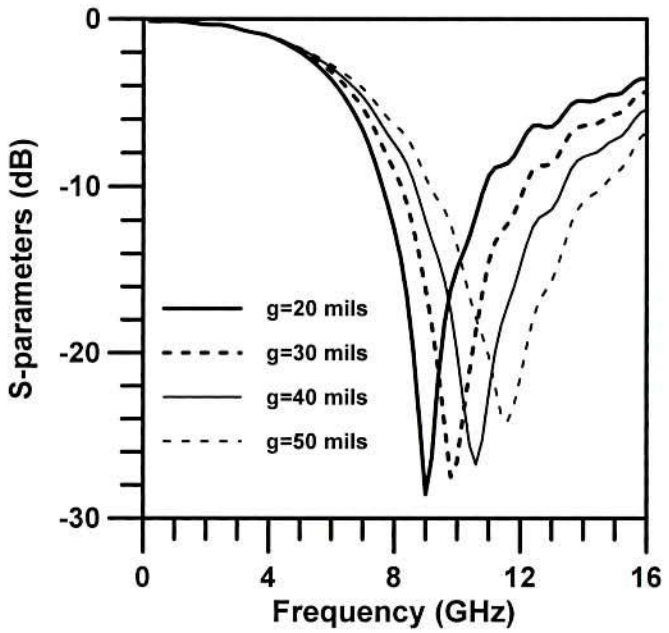

Fig. 5.4: Insertion loss performance of a unit cell of dumbbell shaped DGS with variable gap distances of 20, 30, 40 and 50 mils respectively.

It can be seen that the cut-off frequencies are approximately same. That means the gap distance has no significant influence on the series inductance. Rather it controls the pole location. As the gap distances increases the gap capacitance decreases and hence the pole location moves up to higher frequency.

(3): Influence of width (w): Here the width of the narrow slot is varied. It is already seen that the increase in gap distance results in movement of location of pole at higher frequencies. The effect of increasing the width is supposed to provide more capacitance as the increase in dimension of the slot is perpendicular to the microstrip line. On the other hand the inductive effect will also be significant. The insertion loss performances with different widths of a unit DGS cell are shown in Fig. 5.5.

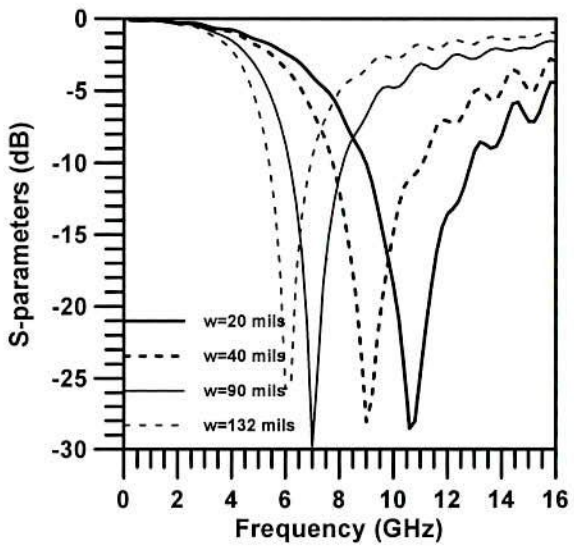

Fig. 5.5: Insertion loss performances of a unit DGS cell with the variations in widths having w = 20, 40, 90 and 132 mils.

It can be seen that both the pole location and the cut-off frequencies are influenced by the width of the narrow slot as expected. Increasing width enhances the inductive and capacitive effect.

5.3 Novel Hybrid DGS

It is started from a conventional 2-D square patterned periodic PBG structure designed at 10 GHz based on Bragg's condition [20]. The original design is modified to achieve the performance of a LPF. The following designs are investigated.

- **Design 1**

It is a conventional 2-D square patterned PBGS. But they are offset from the center of transmission line. No PBG elements are just under the transmission line in the ground plane. The arm length of PBG elements is 104 mils. Inter cell separation is 226 mils. The FF (b/a) is taken to be 0.46. The design is shown in Fig. 5.6.

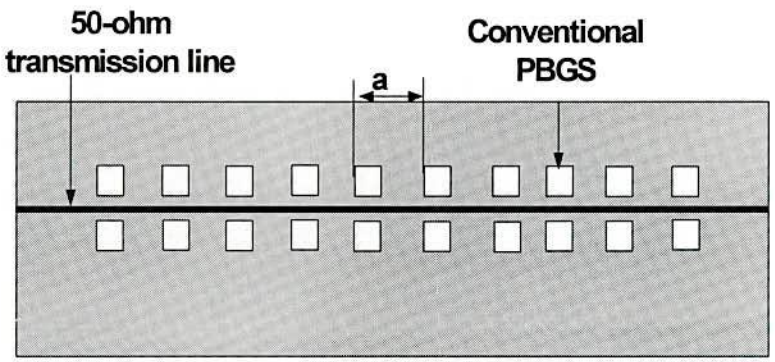

Fig. 5.6: Geometry of a conventional square patterned PBGSs that are offset from the center of the transmission line.

- **Design 2**

The conventional PBGSs are connected by narrow vertical slots to form dumbbell shape periodic structures. This is known as DGS in the literature [19]. The narrow slot's location is centrally below the microstrip transmission line. The dimension

of the narrow slot is 15 × 50 square mils. The conventional DGS is shown in Fig. 5.7.

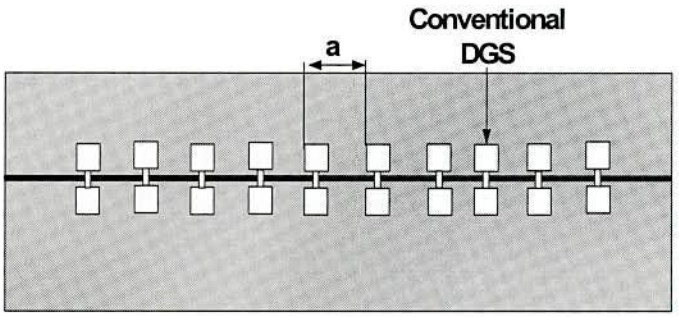

Fig. 5.7: Geometry of (a) conventional DGSs resulting from the vertical connection of narrow slots and larger square patterned EBGS

- **Design 3**

Then the uniform EBGS has been interleaved that is 1-D in nature and the individual elements are similar to Design 1. With a view to generating another stopband around 10 GHz, this interleaved EBGS will be useful. The combined design of PBGS-DGS is shown in Fig. 5.8.

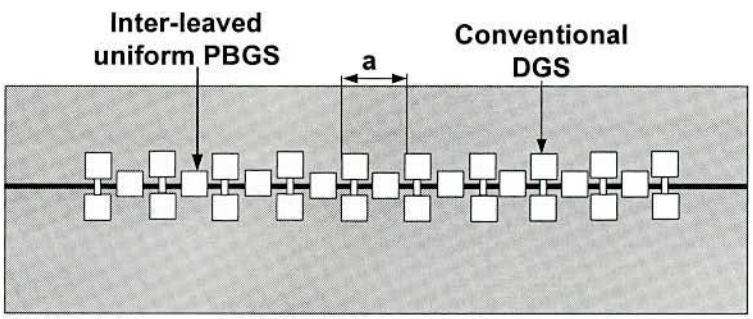

Fig. 5.8: Geometry of conventional DGS with inter-leaved uniform PBGS

- **Design 4**

To see the usefulness of EBGS with *Chebyshev* distribution an 1-D uniform EBGS is designed. The geometry of uniform square patterned EBGS having FF of 0.46 is

same as shown in Fig. 3.10. It is attempted to show the usefulness of using *Chebyshev* distribution in later design. The results of uniform EBGS and EBGS with *Chebyshev* distribution will be compared.

- **Design 5**

Design 5 provides 1-D non-uniform PBGS with *Chebyshev* distribution. The square patterned non-uniform PBGS with *Chebyshev* distribution is shown in Fig. 5.9. The FF of the central element is 0.53.

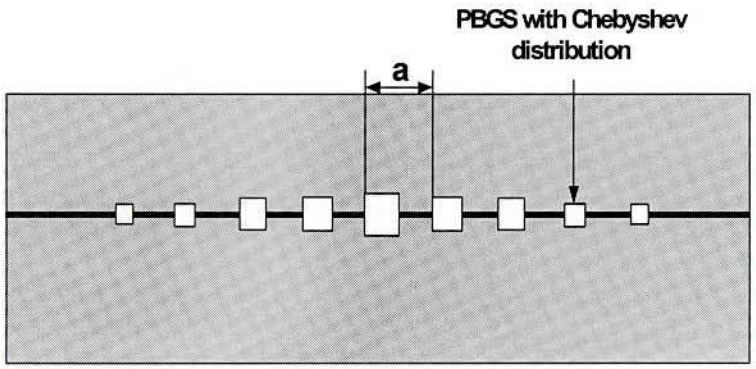

Fig. 5.9: Geometry of 1-D non-uniform EBGS with *Chebyshev* distribution.

- **Design 6**

Another set of regular inter-leaved non-uniform PBGS with *Chebyshev* distribution designed at 10 GHz is used as shown in Fig. 5.10.

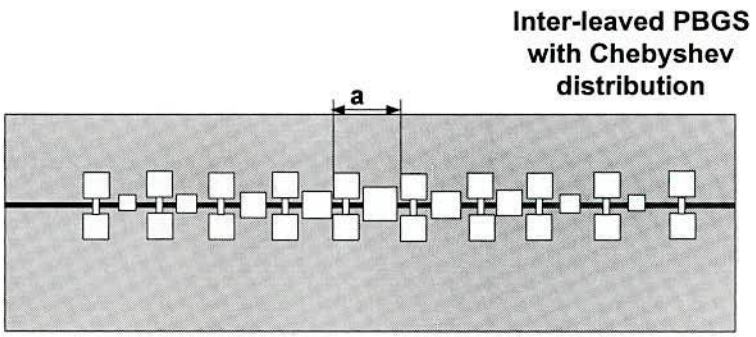

Fig. 5.10: Geometry of conventional DGS with inter-leaved PBGS having *Chebyshev* distribution.

- **Design 7**

This is the final design. The amplitudes of both the conventional DGS and PBGS have been tapered as per the co-efficient of *Chebyshev* distribution for further improvement. The geometry is shown in Fig. 5.11.

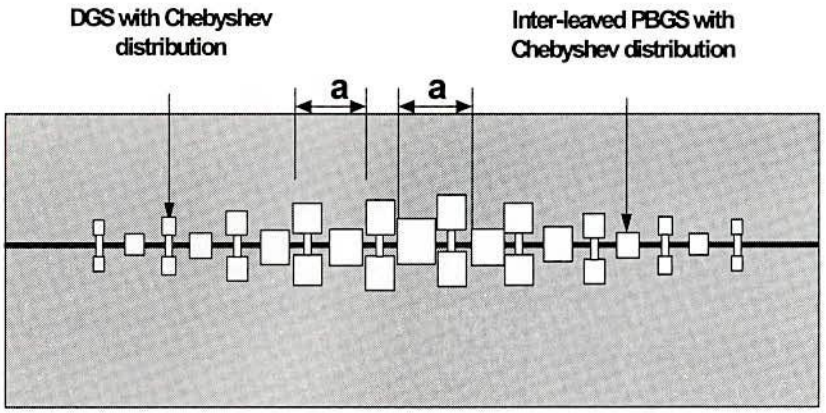

Fig. 5.11: Geometry of LPF realized by novel DGS configuration where the amplitudes of both the DGSs and PBGSs are varied with *Chebyshev* distribution

5.3.1 Results

S-parameter performances of different novel designs have been investigated. The DGS elements are 10 in number and square patterned PBGSs are 9 in number. Taconic substrate with dielectric constant of 10 and thickness of 25 mils are used in all designs. The return loss and insertion loss performances have been investigated.

- **Design 1**

The S-parameters performances vs frequencies of Design 1 are shown in Fig. 5.12. It can be seen from the insertion loss performance as shown in Fig. 5.12(b) that there is very small stopband throughout performance as expected for this type of structure. This is because there are no PBG elements exactly under the

transmission line in the ground plane. The return loss performances are shown in Fig. 5.12(a).

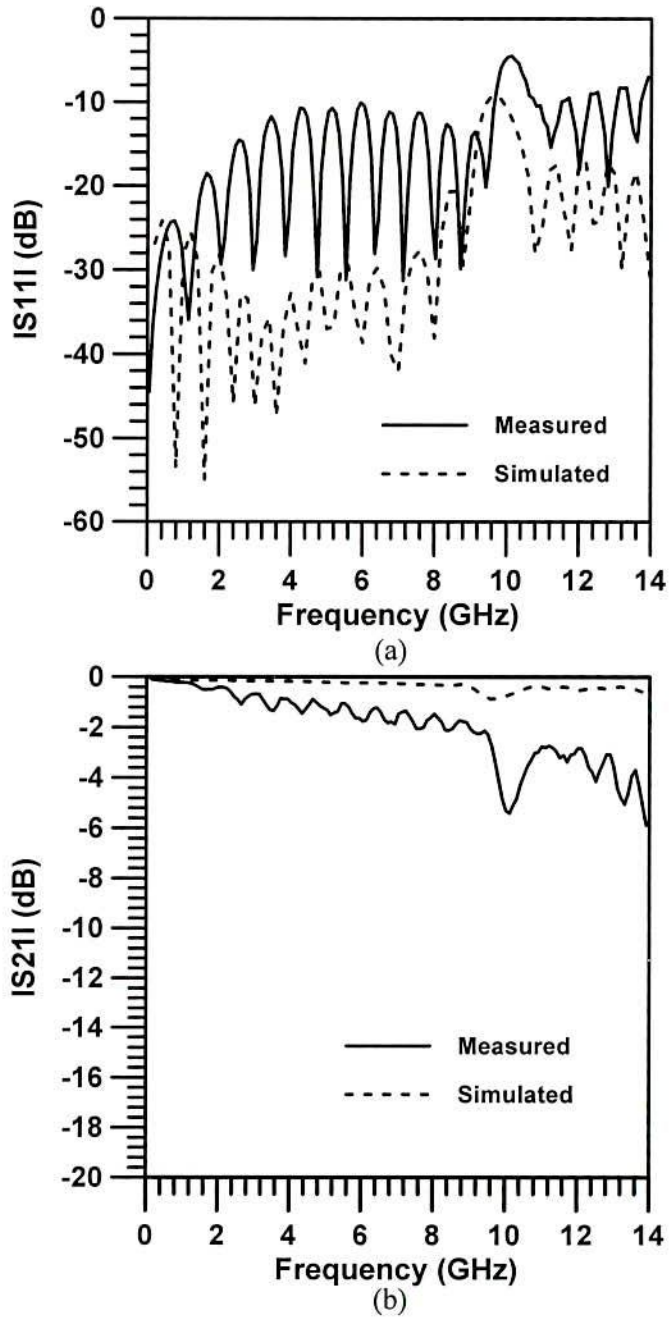

Fig. 5.12: The performances of Design 1 (a) return loss, (b) insertion loss; where the two rows PBGSs are offset from the center of the microstrip transmission line. The square patterned PBGS is of 104 × 104 square mills with inter cell separation of 226 mils.

- **Design 2**

The simulation result along with the experimental result of Design 2 is shown in Fig. 5.13.

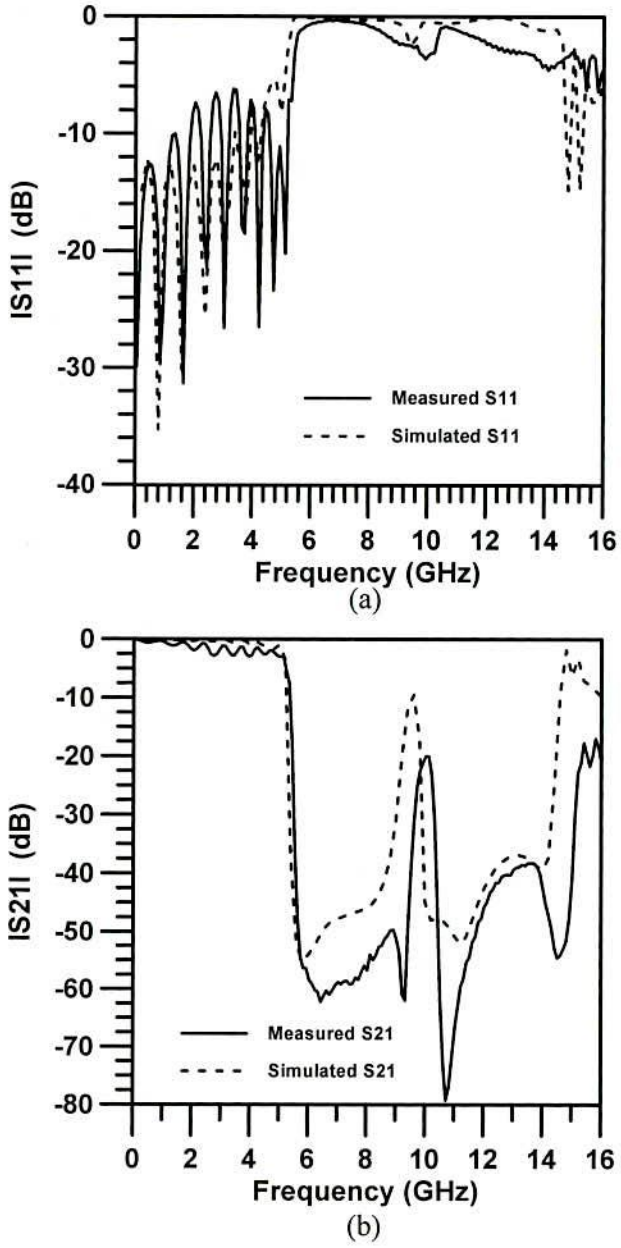

Fig. 5.13: S-parameter performances of conventional DGSs (a) return loss, (b) insertion loss. The larger square patterned PBGS is of 104 × 104 square mills and with vertical slot is of 15 × 50 sq mils. The inter cell separation is 226 mils.

The passband input matching is poorer (-5 dB) as can be seen from the return loss performance. Insertion loss performances show that around 10 GHz the stopband is not so deeper. The simulation result provides less than 10 dB isolation and the measured result provides approximately 21 dB isolation around 10 GHz. 4 dB ripples appear in the measured passband. To improve the performance, inter-leaved PBGS in Design 2 is applied to yield deeper stopband around 10 GHz.

- **Design 3 and 6**

The S-parameters performance of a dumbbell shape DGS with inter-leaved PBGS has been shown in Fig. 5.14. The simulation results include the S-parameters performances of two designs, where square patterned PBGSs are with and without *Chebyshev* distribution. The theoretical results for Design 3 and 6 have been shown together to compare their performances.

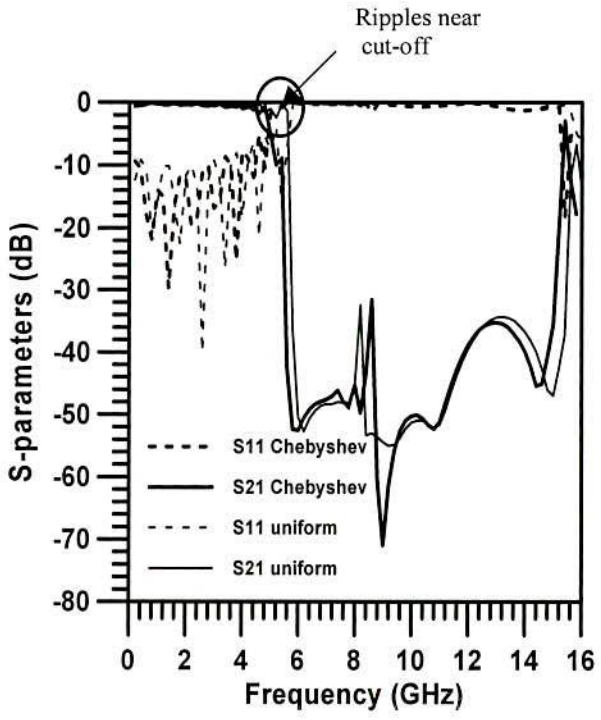

Fig. 5.14: Simulated S-parameters performances of a conventional dumbbell shape DGS with inter-leaved PBGS with and without *Chebyshev* distribution.

It can be seen that the design with inter-leaved EBGS having uniform distribution contains ripple near the cut-off. On the other hand the design with interleaved EBGS having *Chebyshev* distribution yields better performance in the pass band.

- **Design 4 and 5**

To observe the effect of PBGS with *Chebyshev* distribution clearly the performance of a standard transmission line on 1-D square patterned uniform PBGS is investigated and compared with the result of non-uniform PBGS. The performance is shown in Fig. 5.15. It is worthwhile to mention that the uniform square patterned EBGS has FF of 0.46. To compensate the windowing effect the FF of central element of non- uniform EBGS has FF of 0.53.

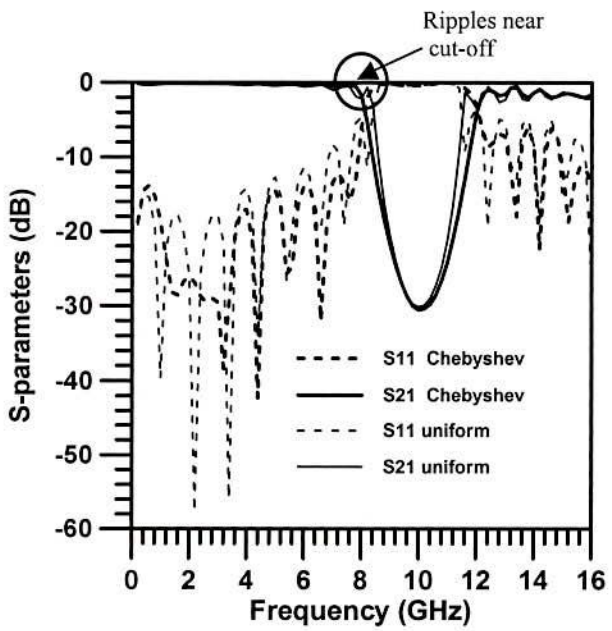

Fig. 5.15: Simulated S-parameters performances of a 1-D square patterned PBGS with and without *Chebyshev* distribution.

From the Fig. 5.14 and 5.15, it can be seen that ripples appear near cut-off frequency for the uniform distribution of PBGS. The application of *Chebyshev* distribution in amplitudes provides better performances. It is observed that the

improvement is marginal in Figs. 5.14-5.15 compared to the improvement described in chapter four. The hole patterned PBGSs differ from the square patterned PBGSs by the etching area though their filling factor is defined to be same. The etching area of hole patterned PBGSs described in chapter four is larger than square patterned PBGS described in chapter 5. If the etching area would be same their performance should be same as can be seen in [19].

- **Design 6**

The performances of Design 6 are shown in Fig. 5.16. Here measured and simulated results have been compared. The return loss performances are less than 5 dB in the passband. The insertion loss performance provides small ripples (approximately 2 dB) in the passband. It can be seen from the insertion loss performances that the stopband is wider than that for Design 2. The passband performances are yet to be improved.

Hence Design 7, where both DGS and PBG cells are non-uniform, is envisaged. In Design 6 though wider stopband is obtained yet it is required to improve ripples near the cutoff frequency and the stop bandwidth can further be enhanced.

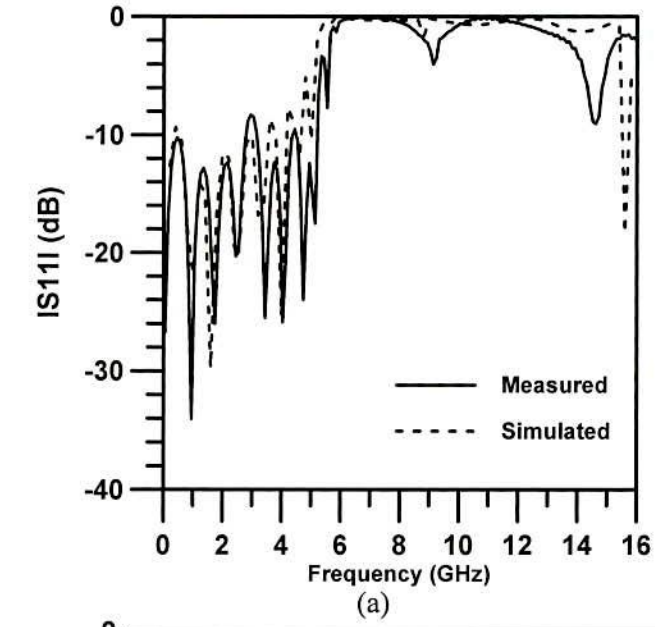

(a)

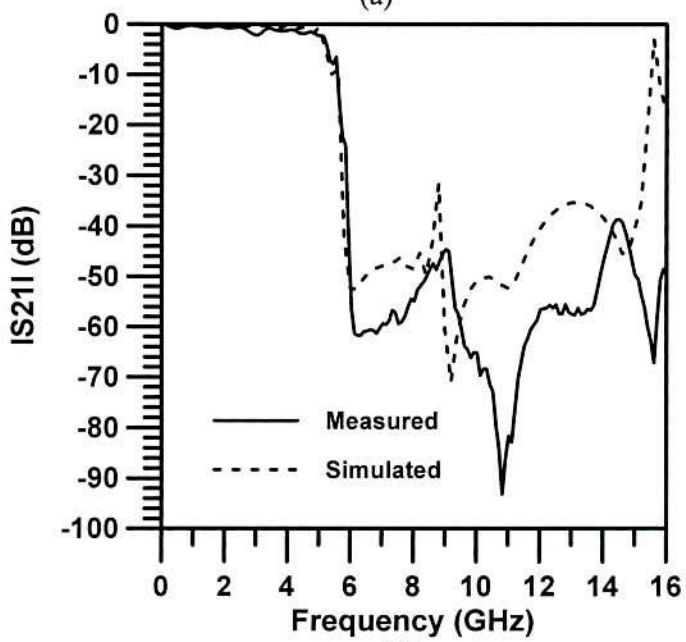

(b)

Fig. 5.16: S-parameters performances of a conventional DGS combined with inter-leaved PBGSs with *Chebyshev* distribution (a) return loss, (b) insertion loss

- **Design 7**

The theoretical and experimental S-parameters versus frequencies are shown in Fig. 5.17. The insertion loss performance as shown in Fig. 5.17(b) provides smoother passband transmission. The passband ripple is less than 1 dB. The stop

bandwidth is enormously large that are always less than 40 dB in measurement. The average passband return loss is 20 dB, with maximum reflection > 10 dB. As can be seen from the return loss performance this design yields very good return loss BW.

The 10 dB return loss BW is wider and is about 5.5 GHz. The application of *Chebyshev* distribution in both inter-leaved PBGS and DGS improves the over all performances. To the best of author's knowledge, this is the best performance so far achieved for PBGS under 50-ohm transmission line. This performance is considered as the response of LPF that is realized by the surface perturbed by the non-uniform PBGS and DGS.

It can be seen from the return loss performances as shown in Fig. 5.17 that there are spurious reflections in the stopband region. The discrepancies in result can be attributed to the radiation from PBGS and DGS, which can be suppressed by shielding. There is also fabrication errors resulting from the limitation of etching process especially in between of DGS and inter-leaved PBGS as the conducting surface between the DGS and PBGS is very narrow. This limiting factor may be one of the issues regarding the insignificant discrepancies between simulated and measured results.

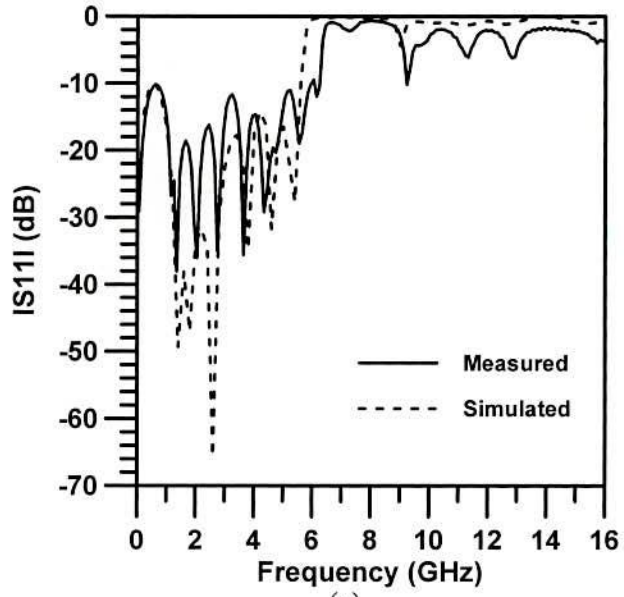

(a)

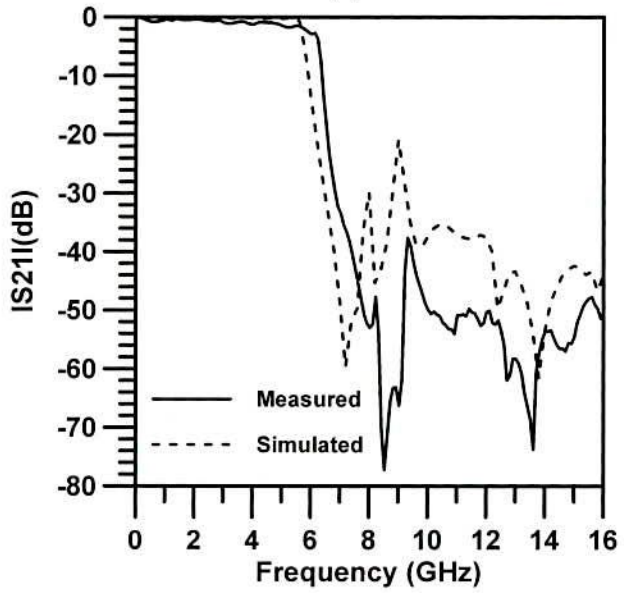

(b)

Fig. 5.17: S-parameters performances of DGSs combined with PBGSs where *Chebyshev* distribution has been applied in both the designs of inter-leaved PBGS and DGS (a) return loss, (b) insertion loss.

5.4 Modified DGS as a Dual Stopband Filter

In this section a novel defected ground plane is proposed, which yields distinct multi-stopband at half the frequency of a conventional PBGS of the similar size. Hence a compact PBG design is achieved. Conventional PBGSs can yield dual-

band performance with two sets of PBG elements designed at two separate frequencies. This concept makes the design length to be larger. The present motivation is to develop dual-band stopband filter within the space of one set of PBGSs. For this purpose three rows of square patterned PBGSs are proposed, which are vertically connected with two thin slots. This configuration resembles the DGS reported in [19] with the exception that another larger slot is included with the conventional DGS. For this reason it is called modified DGS. To obtain the second distinct stopband, a PBGS is interleaved in the 3-rows vertical DGS and very distinct second stopband similar to that for the first one is achieved. To improve the passband and second stopband performance (both S_{11} and S_{21}) the *Chebyshev* distribution is applied to the interleaved square PBGS. This hybrid design yields two distinct stopbands with smoother passband. All the designs are fabricated and measured with vector network analyzer and the results are compared with the simulation results.

5.4.1 Designs

Four designs will be discussed in this subsection. Dual stopband filter will be developed starting from the three rows conventional PBGSs.

- **Design 1**

The conventional uniform square patterned three rows under the standard 50-ohm transmission line are shown in Fig. 5.18. This is conventional concept of PBG elements to be etched in the ground plane of a 50 ohms microstrip transmission line. The approximate center frequency of the stopband is 10 GHz. The period is 226 mils. The FF is 0.46. The arm length of square EBG elements is 104 mils.

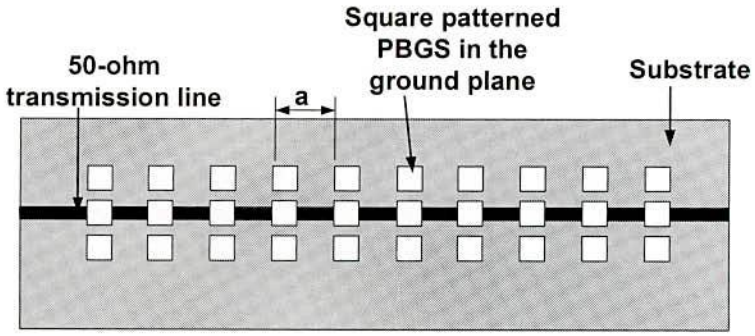

Fig. 5.18: Three Rows Square patterned periodic structures under standard 50-ohm transmission line. The substrate is Taconic having dielectric constant of 10 and height of 25 mils. The inter-element spacing (period) a = 226 mils.

- **Design 2**

Simple modification is made in Design 1. A narrow rectangular slot has done vertical connection. The design is shown in Fig. 5.19 (a). This design provides stopband at approximately half the frequency of Design 1. To get better understanding about the geometry a single cell has been shown in Fig. 5.19 (b).

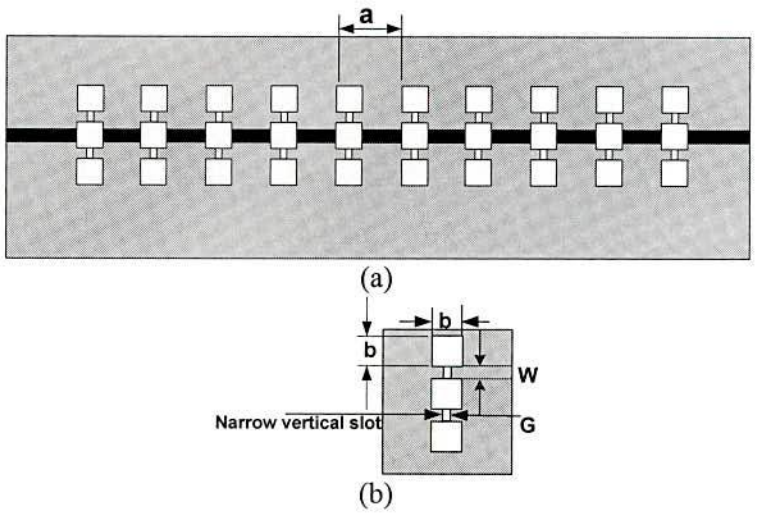

Fig. 5.19: (a) Modification of design 1(a) by vertical connection with narrows slots. (b) Single PBG element with dimensions; b= 104 mils, w =50 mils, G=15 mils

In a conventional DGS, narrow thin slots connect two larger square patterned PBG elements. In the proposed modified DGS the larger slots are 3 and the vertically connected narrow slots 2 for one cell.

- **Design 3**

In this design there are two sets of periodic structures that result from the hybrid combination of Design 1 (middle row only) and Design 2. It is noted that the number of cascaded slots are 10 and nominal PBG are 9, respectively. The objective of this design is to get the distinct dual stopbands. The geometry of this design is shown in Fig. 5.20.

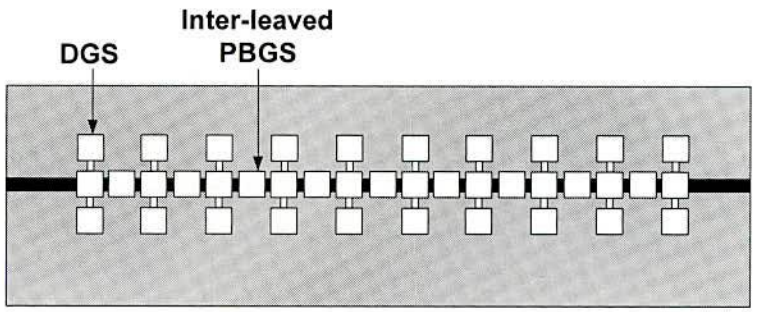

Fig. 5.20: Insertion of second set of periodic structures in the gap of Design 2 to produce dual stopband.

- **Design 4**

The dimensions of 9 EBG elements and the middle row elements of modified DGS are varied as per *Chebyshev* distribution shown in Fig. 5.21. The filling factor of the central element of nominal EBG elements is 0.53. The DGSs are 10 in number and PBGSs are 9 in number.

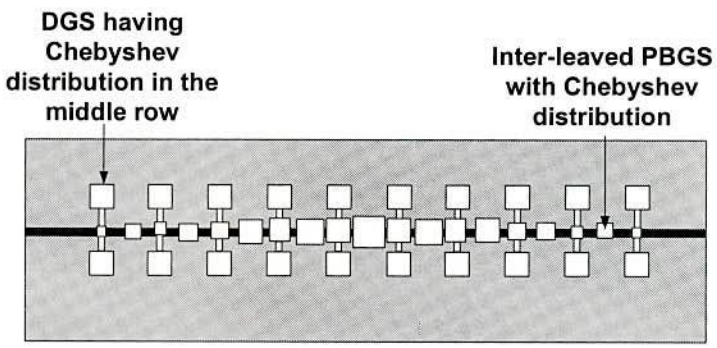

Fig. 5.21: Implementation of *Chebyshev* distribution in the middle rows of Design 3 to yield deeper and wider second stopband

5.4.2 Results

The performances of fabricated items are measured by VNA and the simulated results are compared with the measured results.

- **Design 1**

The measured and theoretical S-parameters performances are shown in Fig. 5.22. It can be seen that the stopband is centered at approximately 10 GHz. The 20 dB rejection bandwidth is approximately 3 GHz with maximum attenuation of 45 dB. Observing the passband ripples, there are 9 poles from the 10 elements.

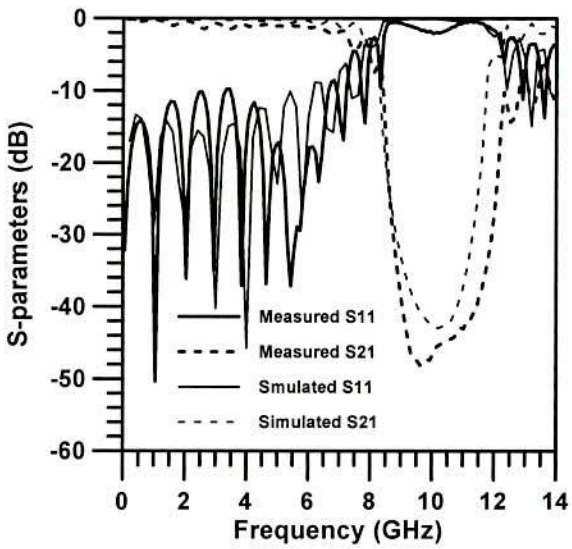

Fig. 5.22: S-parameter performance of a 3 rows square-patterned PBG structures.

- **Design 2**

As in Fig. 5.23, the stopband is centered at approximately 5 GHz. The maximum isolation is 48 dB and the 20 dB rejection bandwidth is 2.65 GHz. The second stopband is at approximately 11 GHz and is not distinct. The objective is to make it distinct. The passband poles are divided into two: 5 poles in the first passband and 5 poles in the second passband. The results represent a dual stopband filter circuit

with two distinct passbands with an in-between distinct stopband at 2.65 GHz. Therefore, this circuit can be used as a dual stopband filter circuit.

On the other hand if the first stopband is designed with the same for Design 1, a reduction of ~200% in frequency is achieved with the same dimension. Therefore, the design yields a compact PBG design with half the period of the original one.

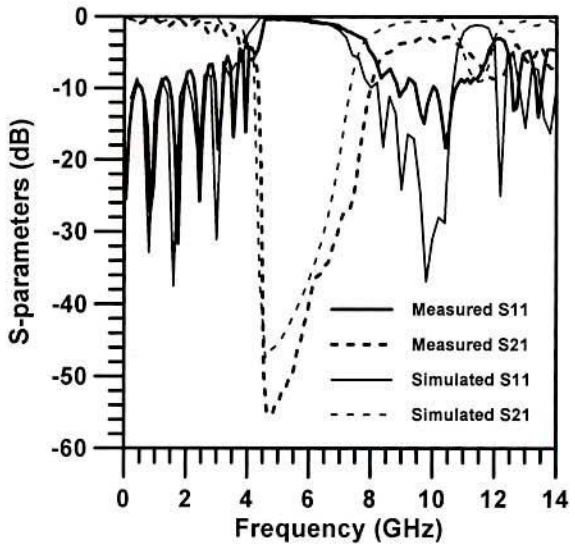

Fig. 5.23: S-parameters performances of a 3 rows of square patterned PBG structures with vertical slot connection.

- **Design 3**

This design yields distinct 2nd stopband with the interleaved PBG of original period. It can be seen from Fig. 5.24 that two stopbands are generated around 5.6 and 10.5 GHz, respectively. The 1st stopband provides maximum isolation of 46 dB and 20 dB rejection bandwidth of 2.08 GHz. The 2nd stopband yields maximum isolation of 30 dB and 20 dB rejection bandwidth of 1.50 GHz.

- **Design 4**

Further improved is made with *Chebyshev* distribution in this design and is shown in Fig. 5.25. It can be seen that the 1st passband return loss has improved

significantly with the expense of 2nd passband performance, but the 2nd stopband has improved significantly.

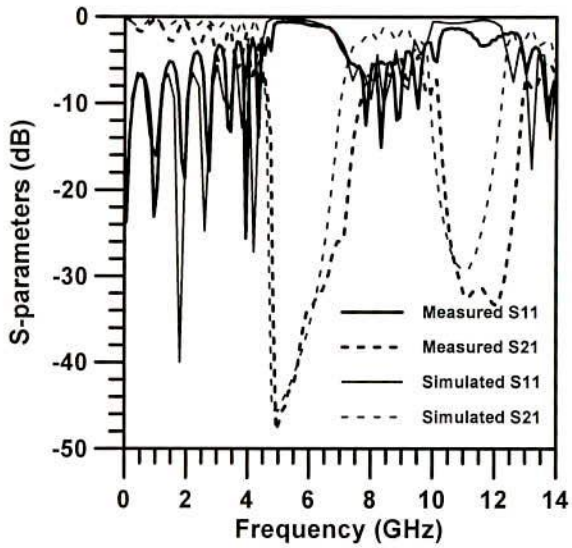

Fig. 5.24: S-parameters performances of design 3; hybrid structures of conventional DGSs and PBGSs.

The 1st stopband is at 5.6 GHz and the second stopband is at 11 GHz. Both stopbands are deeper, wider and distinct at these frequencies. The maximum isolations are 46 and 44.5 dB for first and second stopbands, respectively. The corresponding 20 dB rejection bandwidths are 2.26 and 2.503 GHz, respectively. This circuit can be used for multi-mode harmonic suppression in filters.

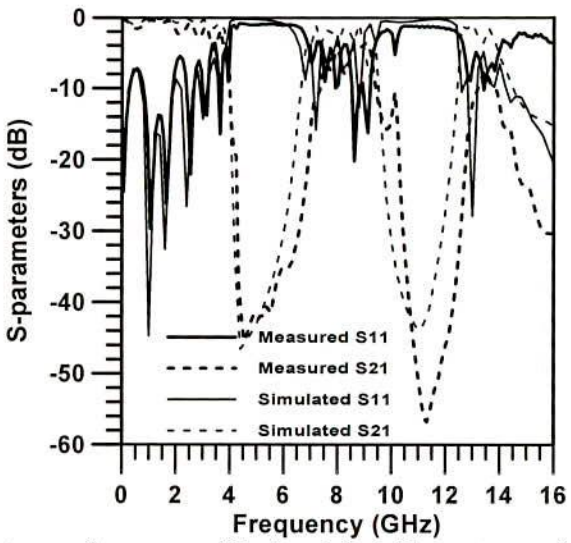

Fig. 5.25: S-parameters performances of design 4; hybrid structures of conventional DGSs and PBGSs with *Chebyshev* distribution

How the gap distance, the width of the narrow slot and the dimensions of the bigger slot influence the S-parameter performances that are explained in Figs. 5.3-5.5. The conventional PBGS is designed based on the Bragg's condition. Two types of DGSs have been discussed. Conventional dumbbell shaped DGS where the non-uniform distribution is realized by using *Chebyshev* distribution in order to achieve improved performance. In case of conventional dumbbell shape DGS Figs.5.3-5.5 help choose the location of attenuation pole and cut-off frequency. Mainly narrow slot controls capacitance and bigger slot controls inductance. Varying the various dimensions can control the performance. Secondly in lieu of conventional dumbbell shaped DGS, a modified dumbbell shaped has been proposed to yield the performances at lower frequencies. In the conventional PBGS design it is observed that the etching area is increased if the design frequency is low. The dimension of the PBG unit cell decreases with the increase of design frequency. The modified dumbbell shaped DGS makes the etching area larger that in turns increases the inductance. Finally the increased inductance causes them to resonate at lower frequency. It can be seen that the different performances agree well with this concept. Incorporation of *Chebyshev* distribution improves the performance that also agrees well with the published result [35].

Conclusion

In this chapter the frequency properties of the unit cell of a dumbbell shaped DGS has been investigated. In DGS the dimension of larger square patterned slots controls the cutoff frequencies and the gap distance controls the location of attenuation pole. The standard 50-ohm transmission line on conventional and modified DGS has been investigated. Another set of regular PBGSs have been

inserted in between conventional DGS and modified DGS. Various hybrid PBG-DGS designs have been etched in the ground plane of a standard 50-ohm transmission line to develop LPF and dual stopband filter. At first few structures are investigated to yield better LPF performance in terms of passband return loss BW, ripple free transmission and wider stopband. 2-D uniform square patterned PBGSs are firstly investigated that are offset from the central position of the microstrip line. Under this condition no PBG elements are under the microstrip line in the ground plane. Hence no significant stopband is found. Then the conventional dumbbell shaped DGS has been investigated that produces wider stopband. Insertion loss performances show that around 10 GHz the stopband is not so deeper. The simulation result provides less than 10 dB isolation and the measured result provides approximately 21 dB isolation around 10 GHz. A combination of DGS and interleaved uniform square patterned PBGS suppresses the middle passband hence very wider stopband is achieved. *Chebyshev* distribution is applied to square patterned EBGS designed at 10 GHz that enhances the performance. Finally, *Chebyshev* distribution is applied to both DGS and interleaved PBGS. In the final design, the transmission band is smoother (passband ripple is less than 1 dB) and the average input matching is more than 20 dB. The stopband is extremely wide. This novel design provides an impressive LPF. The wider stopband can be used to mitigate the surface wave problem and suppression of spurious and leakage transmission. This structure can also find potential application in RF front-ends to isolate transmitters from receiver modules.

Secondly effort has been made to realize dual stopband filter with the help of modified DGS having hybrid combination of regular PBGSs. Thus a novel DGS

has been proposed, which can be used either a dual stopband filter or a multimode harmonics suppressor in a BPF. The interleaved PBGS and DGS hybrid structure is a promising candidate for broadband device applications. *Chebyshev* distribution of the interleaved PBGS further improves the passband and stopband performance significantly. All the theoretical results agree well with the measured results.

Chapter 6 PBG Engineered Antennas and Filters

6.1 Introduction

In recent years a lot of research has been carried out in favor of beneficial effects of PBGS in microwave engineering. In the literature many advantageous features on antennas, filters, mixers, oscillators, amplifiers, and phased arrays have been reported. In antennas, PBGS improves return loss BW, gain, radiation patterns, front to back ratio (FBR), directivity, polarization and mode control etc. [81]-[96]. In filters PBGS suppresses higher order harmonics [32], [97]. In amplifiers PBGS performs harmonic tuning [98]. PBGS has also been used in beam steering for phased arrays [18].

In this chapter an overview of a microstrip patch antenna is given. Primarily focus has been given on feeding technique of microstrip patch antennas. Aperture coupled patch antennas (ACPAs) are discussed with their advantageous features. The improvement in the performance of ACPA due to PBGS inclusion will be reported. As an ACPA is a multi-layered structure, therefore there are scopes to use PBGSs in different layers. In such a way ACPAs with single and double-layered PBGSs will be investigated.

In this chapter UPBG assisted dual-band antenna is investigated that may be used for fundamental block of very small aperture terminal (VSAT) antennas [45], as VSAT technology is very demanding now a days.

Harmonic suppression is very important in filter design. It has already been mentioned that UC-PBGSs suppress the harmonics. PBGSs not only suppress the harmonics but also improve the return loss and insertion loss performances at desired fundamental frequency. The BPFs loaded by uniform circular PBGSs will be investigated to suppress the harmonics. The Binomially distributed PBGSs (B-PBGSs) will then be investigated for harmonic suppression to see if there is any improvement in the performance of BPF. Additionally to these, the DGS will also be used for the same purposes.

6.2 Microstrip Patch Antenna

Microstrip antennas received considerable attention starting in the 1970s due to many exciting features such as low profile, lightweight, simple and inexpensive to manufacture, conformable to planar and nonplanar surfaces, mechanically robust etc. But they suffer from narrow bandwidth, low gain, poor scan performance and spurious feed radiation. Microstrip antennas consist of a very thin metallic strip known as patch placed on the top layer of the substrate. The bottom layer is ground plane. The height of the substrate is small fraction of the wavelength. The microstrip patch is designed to achieve the pattern maximum normal to the patch. For a rectangular patch, the length L of the element is usually $\lambda_g/3< L<\lambda_g/2$, where λ_g is the guided wavelength.

Different types of substrates are available on which the patch can be designed. The dielectric constants of commercially available substrates vary ranging from $2.2 \leq \varepsilon_r \leq 12$. Thick substrates with low dielectric constants are good for enhancing the bandwidth and efficiency. The size of the patch becomes very large with lower

value of dielectric constant. Thin substrate with higher value of dielectric constant provides compact design but they are less efficient and have relatively smaller bandwidth. Inclusion of PBGSs in the ground plane of microstrip patch antenna can improve the performance. The patch can be integrated with other microwave circuitry easily.

The radiating patch may be square, rectangular, thin strip (dipole) circular, elliptical, triangular or any other configurations. A rectangular microstrip patch antenna is shown in Fig. 6.1.

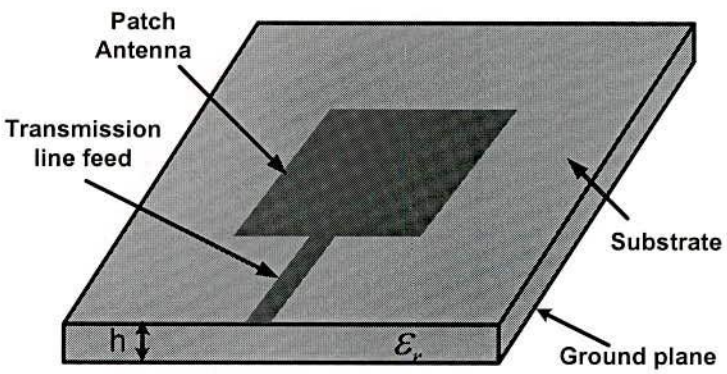

Fig. 6.1: Geometry of a microstrip patch antenna. The substrate is having the height of h and dielectric constant of ε_r.

6.3 Feeding Methods

The patch radiates the space wave but it needs feeding energy from source. Normally a 50-ohm line is used to feed the patch. There are different techniques to feed the patch that includes mainly microstrip line feed, coaxial probe feed, aperture coupling feed and proximity feed [99]-[102]. Following is a detailed discussion of the different feeding techniques of microstrip patch antennas.

- **The Microstrip line feed**

The microstrip line feed is of two types, namely (1) direct microstrip line feed and (2) inset feed. Both of them are easy to fabricate, simple to match by controlling the inset position of the feed and rather simple to model. Direct microstrip line feed is realized by connecting a 50-ohm conducting strip directly with the patch radiator. The conducting strip has much smaller width compared to patch. Such geometry is shown in Fig. 6.1. The edge impedance of the patch radiator is normally high that ranges from 150-ohm to 300-ohm. For matching extra quarter-wave length line may easily be added. The inset feed gives exactly the 50-ohm point, which is recessed from the edge of the microstrip patch antenna. A microstrip patch antenna with inset feed is shown in Fig. 6.2.

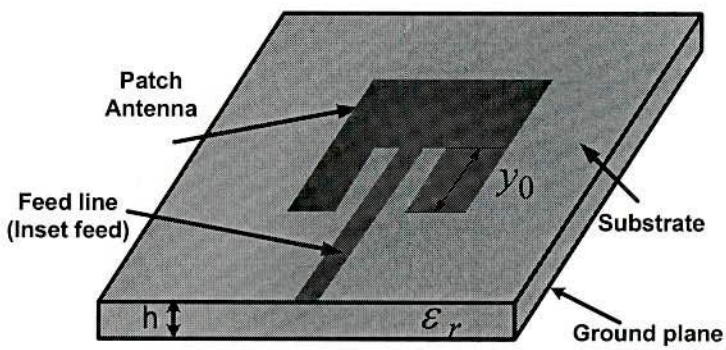

Fig. 6.2: Geometry of an inset feed microstrip patch antenna. The substrate height is h and dielectric constant is ε_r. The 50-ohm point is at the recessed distance y_0 from the edge of the patch radiator.

- **The Co-axial probe feed**

In the co-axial probe feed the inner conductor of the co-axial connector is connected with the radiating patch and the outer conductor is connected with the ground. In many practical applications this type of feed technique is also used widely. Matching can be achieved by the proper choice of the location of the

coaxial feed probes. However it has narrow bandwidth and it is more difficult to fabricate.

- **Proximity feed**

In this type of feed technique the ground plane is situated on the bottom layer of the lower substrate and the feed line is fabricated on the top layer of the lower substrate or bottom layer of the upper substrate. There is no slot in the ground plane in this feed technique. The feed line is also not connected with the patch radiator directly. By aperture coupling and proximity coupled feeding technique, good polarization purity and the radiation without cross-polarization can be achieved. Among four types of feeding technique proximity coupled feed technique provides largest bandwidth and easy to model than aperture coupling and has low spurious radiation. The length of the feeding stub and the width-to-line ratio of the patch can be used to control the matching [103].

- **Aperture Coupling**

In the microstrip line feed and co-axial probe feed the patch radiator is connected with the feed line. They support higher order modes that results cross-polarized radiation. To overcome this problem aperture coupling is an excellent option of feeding technique. In this technique the patch radiator is not fed directly rather fed coupling through aperture etched in the ground plane. They are multi-layer structure. The geometry of a microstrip patch antenna with the aperture feed is shown in Fig. 6.3. The patch radiator is fabricated on the top layer of upper substrate. The ground plane is the top-layer of the lower substrate. In the bottom layer of the lower substrate the feed line is fabricated.

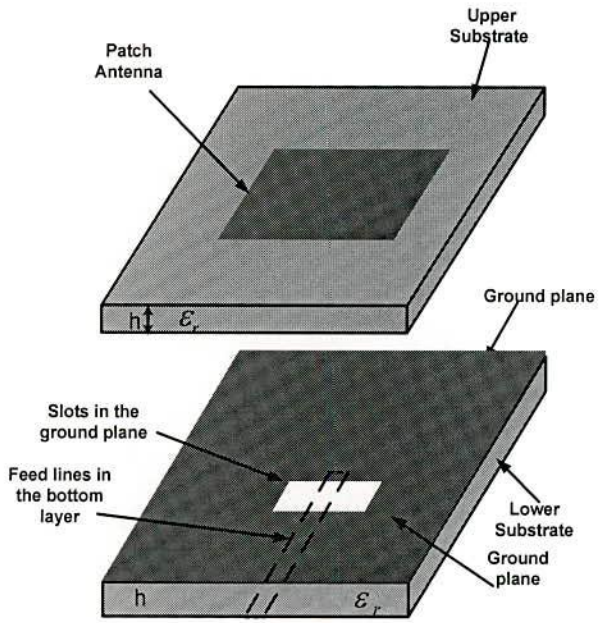

Fig. 6.3: Geometry of a microstrip patch antenna with aperture coupling. The slot is on the ground plane; the feed line is on the bottom layer of a lower substrate. The patch is on the top layer of upper substrate.

The radiating patch element located on the top layer of the upper substrate receives energy from the feed line via the aperture etched in the ground plane that is located on the top layer of the lower substrate. Two substrates may have same height and dielectric constants. But the normal trend is to use thinner substrate (higher dielectric constant) for the feed layer and thicker substrate (lower dielectric constant) for the patch-radiating element. The ground plane isolates the feed from the radiating element and minimizes interference of spurious radiation for pattern formation and polarization purity. The aperture coupling arrangements provide independent optimization. The substrate electrical parameters, feed line width, slot size and position can be used to optimize the design [104].

Since the introduction of aperture coupled patch antenna (ACPA) in 1985, the advantageous features provided by the ACPA have shown its varieties of

applications and the versatility of the basic design has drawn the attention of the researchers throughout the world. Some of the useful features of ACPA are mentioned below:

- Demonstrated impedance bandwidths ranging from 5% to 50%
- Two-layer construction shields radiating aperture from feed network
- Theoretically zero cross-polarization in principal planes
- Convenient integration for active arrays
- Increased substrate space for antenna elements and feed lines
- Independent selection of antenna and feed substrate materials
- Many possible variations in patch shape, aperture shape, feed line type, radomes etc
- Extension to aperture coupled microstrip line couplers, waveguide transitions, dielectric resonators etc

6.4 PBG Engineered ACPA

The emerging technology is demanded for versatile applications of ACPAs ranging from military to commercial sectors. The shape, size, profile and expenditure have made microstrip ACPA more attractive in WLAN, cellular phone, DBS installation, RF identification systems (RFID), and mobile data systems. Worldwide satellite communication systems such as MSAT, GLOBALSTAR, AMSC, and IRIDIUM are making effort to replace their bulky and expensive antennas by microstrip ACPA arrays. It is already mentioned that the microstrip patch antenna is enriched with many advantageous features yet they suffer from narrow bandwidth and lower gain. Enlarging the thickness of the substrate can

enhance the bandwidth but it is contrary to compact design. In this context, researchers used PBG engineered microstrip antennas to enhance their performances.

PBGSs may be used in the slot layer or in the patch layer. Even PBGSs can be used in a separate layer as back shield to reduce backward radiation of ACPAs. The typical geometries of PBG assisted ACPAs are shown in Fig. 6.4 and Fig. 6.5. As can be seen in Fig. 6.4, the circular PBGSs are etched in the ground plane. In Fig. 6.5 it can be seen that PBGSs can be realized in both patch and slot layers. In the patch layer PBGSs are the metallic perturbation. On the other hand they are the slots in the ground plane. The substrates height is 'h'. The substrates may differ in patch and feed layers.

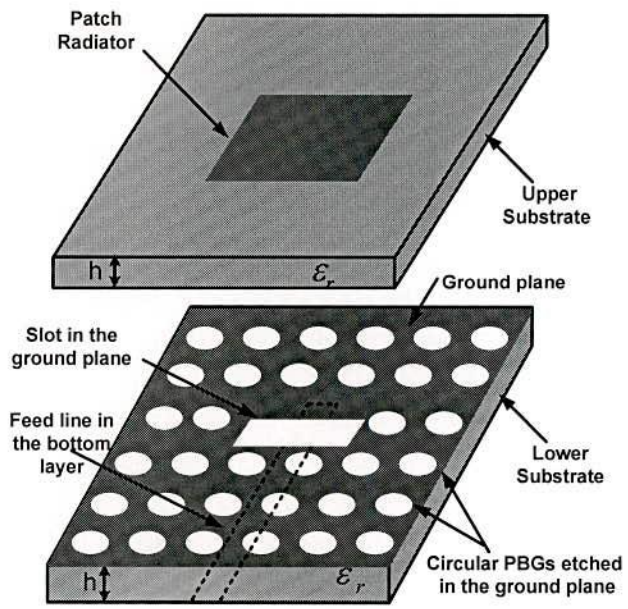

Fig. 6.4: Typical geometry of an ACPA where the ground plane is perturbed by uniform circular uniform PBGSs.

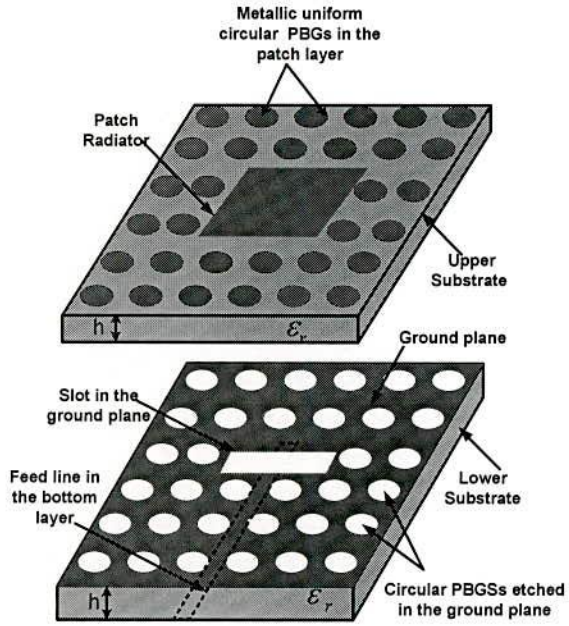

Fig. 6.5: Typical geometry of an ACPA with double layered PBGSs. In the upper substrate PBGSs are metallic perturbation and in the ground plane they are slots.

6.5 Designs of PBG Engineered ACPAs

Different PBG engineered ACPAs will be investigated to improve antenna performance. The return loss performance, BW, front to back ratio (FBR) and gain will be reported. Dual-band dual polarized ACPAs suitable for VSAT applications will be investigated to see the improved performances in terms of matching, bandwidth and gain. Both the uniform and non-uniform PBGSs are used to improve the input matching. The conventional ACPA on uniform ring patterned PBGSs has also been investigated.

6.5.1 Improvement of Matching in dual-band dual polarized antennas

In this sub-section the reference dual-band antenna is the same as mentioned in [45]. Here the improvement of input matching by using circular patterned uniform and non-uniform circular PBGSs. One design having double layered (ground plane and upper patch layer) uniform circular PBGSs will also be investigated to see if

there any change in return loss performances. During the investigation careful attention will be taken not to sacrifice BW and isolation required for VSAT applications.

- **Antenna Design**

In case of dual-band dual polarized reference antenna design, three substrates layers have been used. On the top of the upper substrate, a patch antenna is realized. In the second substrate second patch antenna is realized. The stacked patch configuration is useful to achieve larger BW. On the top of the third substrate two slots are etched corresponding to two feed lines realized in the bottom layer of third substrates. The longer side (Lx) of the microstrip patch antenna is for lower frequency resonance (in the present case 3.8 GHz), the shorter side (Ly) is for higher frequency resonance (6.28 GHz). The substrates parameters are: Dielectric constant is 2.45 and the height is 0.787 mm for all the substrates. The geometry of a reference dual band dual polarized antenna is Fig. 6.6.

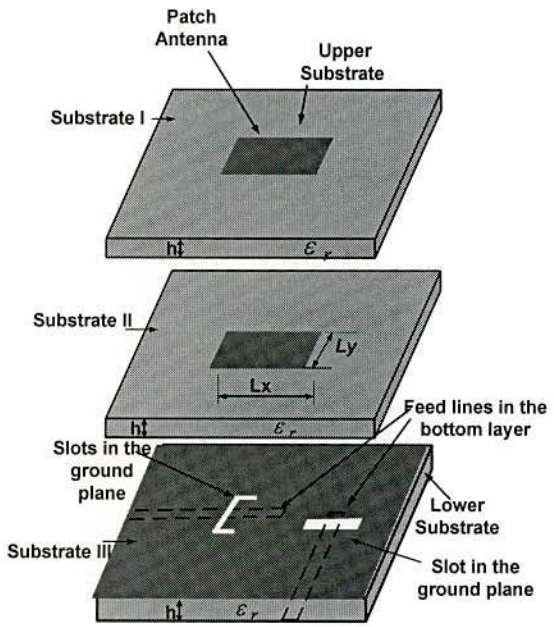

Fig. 6.6: The geometry of a reference aperture coupled patch antenna. Upper and lower substrates have the same dimension and electrical properties.

Foam of 4 mm thickness having dielectric constant of 1.07 is placed between bottom and middle layer and foam of 2 mm thickness is placed between upper and middle layer having same dielectric constant. This arrangement will ensure 21% impedance BW to meet the specification required for VSAT application.

- **Uniform Circular PBGS Design**

Using the optimized FF of 0.25, uniform circular PBGS is designed. It is mentioned that the lattice structure is rectangular as their stopband frequencies are concerned to dual-band operations. So their periods are not same in horizontal and vertical direction. Along the longer side of the patch the period is found to be 27.45 mm and along the shorter side it was 16.6 mm. The geometry of an ACPA with double-layered PBGSs is similar to Fig. 6.5 in PBGS concern.

- **Non-uniform PBGSs Design**

Binomially and *Chebyshev* distributed PBGSs are designed with FF of 0.4 (for central two elements). The non-uniform PBGSs are mainly Binomially and *Chebyshev* distributed PBGSs (Type-B). PBGSs are located in the ground plane. Number of non-uniform circular PBG elements is same as uniform circular PBG elements. So the geometries are not shown.

6.5.2 Improvement of Bandwidth and Gain

- **Antenna Design**

The rectangular patch antenna is fabricated on the top substrate and the orthogonal feed lines are etched on the bottom side of the bottom layer. The orthogonal

coupling apertures are made on the top of the bottom layer. The design principle is similar to design shown in Fig. 6.5. In that design extra patch is fabricated in an additional layer located in between the top and bottom layers of conventional ACPAs. Here no extra patch layer is used. The feed line along the longer patch length is dog-bone shape instead of C-shape. To increase the bandwidth foam is placed between the top and bottom layers. The designed parameters as follows:

Patch substrate: $\varepsilon_{r1} = 2.54$, $\tan\delta_1 = 0.0015$, $h_1 = 0.78$ mm, foam insert: $\varepsilon_{r2} = 1.06$, $\tan\delta_2 = 0.001$, $h_2 = 4.0$ mm, feed substrate: $\varepsilon_{r3} = 2.54$, $\tan\delta_3 = 0.0015$, $h_3 = 0.78$ mm. Design frequencies are 3.8 and 6.28 GHz. To increase the isolation and impedance matching the slots are pushed off-center of the rectangular patch.

- **PBGS Design**

Uniform circular patterned PBGS has been etched in the ground plane only. The periods are same as the periods of PBGS used for improved matching in sub-section 6.5.1. As the periods are different so the FF are different to maintain the same size of PBG structures in both orthogonal directions. The geometry of a PBG assisted dual band ACPA with dog bone slot is shown in Fig. 6.7.

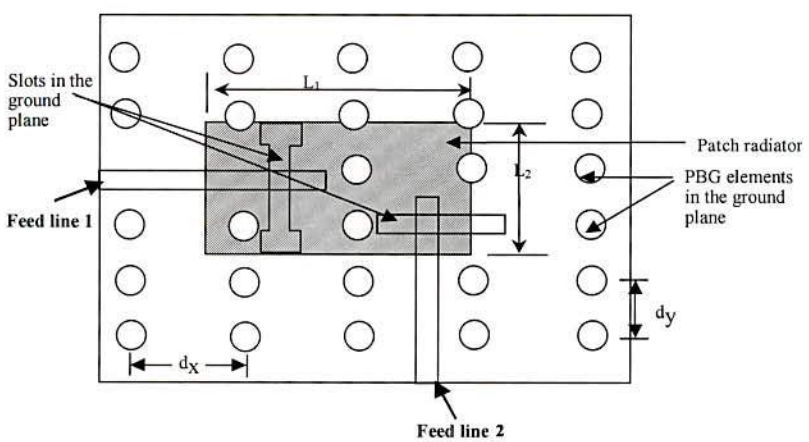

Fig. 6.7: Geometry of a VSAT antenna with orthogonal feeds.PBGS are 2-D with different periods designed at two frequencies of operations.

6.5.3 Number of Ring PBGSs in ACPAs.

An ACPA is designed with ring PBG structure in the ground plane. The number of ring PBG units is varied in 4 by 5, 6 by 7 and 8 by 9 arrays in the ground plane of the antenna. The designed frequency is 10.4 GHz. The length and width of the patch were 6 mm and 5.52 mm respectively. The aperture length was 8 mm and width was 1.56 mm. The stub length was 7.2 mm.

6.6 Results

The S-parameters performances of all the designs have been investigated.

6.6.1 Improved Input Matching of Dual-band Antenna

- **Reference dual band antenna**

From Fig. 6.8 it can be seen that the reference VSAT antenna yields 10 dB return loss BW at terminal 1 of 23 % (average) and at port 2 of 21%.

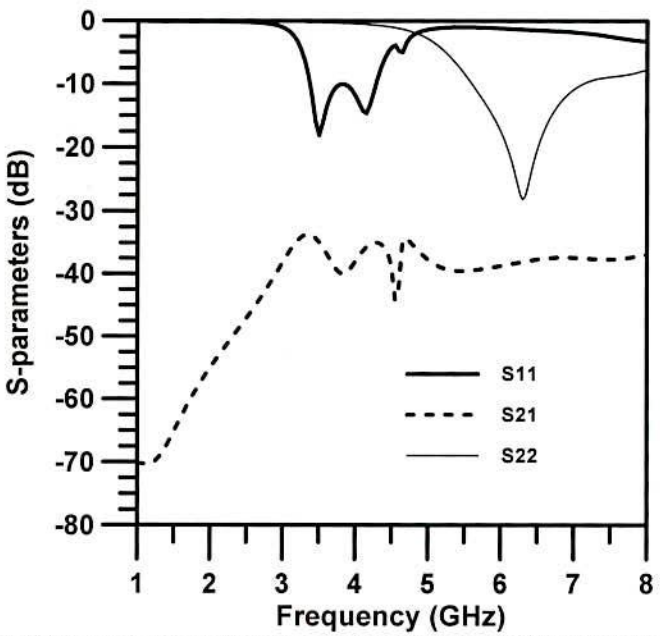

Fig. 6.8: Simulated S-parameter performance of a reference VSAT antenna. The substrate is having height of 0.787 mm and dielectric constant of 2.45

The center frequency of operation at port 1 is found to be 3.79 GHz. On the other hand the center frequency of operation at port 2 is found to be 6.26 GHz. The isolation between two ports is of around 35 dB. Port 2 is well matched. But the input matching at port 1 is not good. It is seen that the return loss is less than 10 dB within a significant portion of impedance BW. The VSAT ACPA is a broadband design with 21% BW in S-band. Effort will be made to improve the input matching at port 1 by the inclusion of PBGSs.

- **Uniform Circular PBGS in upper patch layer**

In this case the uniform circular PBG elements are in the form of metallic perturbation in the upper patch layer. In the upper patch layer the periodicities are not maintained exactly same along horizontal direction to avoid the overlapping of PBG elements with radiating patch. It can be seen from Fig. 6.9 that the 10 dB BW in port 1 is approximately 23 % and the return loss is improved within a lower portion of the BW.

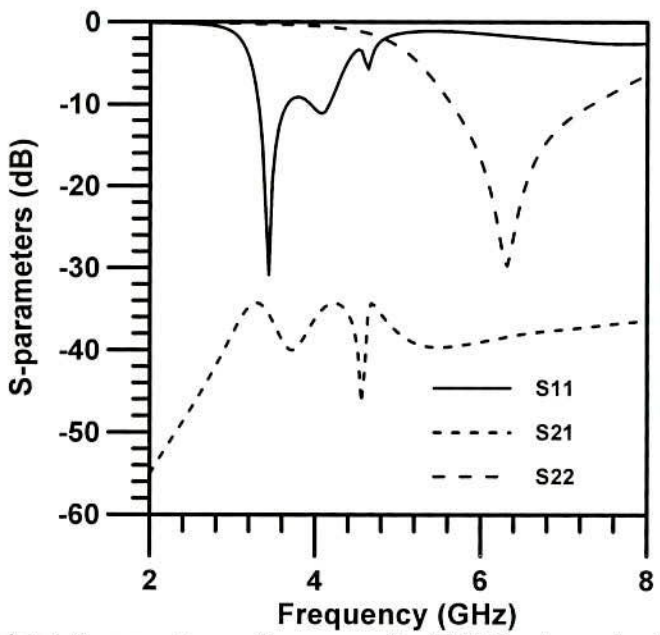

Fig. 6.9: Simulated S-parameter performance of a VSAT antenna loaded by uniform circular PBGSs in the patch layer.

Still there is a scope to improve the matching. Port 2 is well matched and the isolation between two ports is enough.

- **Double layer uniform circular PBGS**

In this design, the PBG elements in the upper patch layer are in the form of metallic perturbation and the PBG elements in the slot layer are slots. In the slot layer, the periodicity is also somewhat disturbed along horizontal direction to avoid overlapping of PBG elements with the slot. The PBG elements of upper patch layer and slot are little bit asymmetric. From the Fig. 6.10 it can bee seen that the port 1 yields 10 dB return loss BW of 23 %. In this case input matching is better than single layer PBGSs. Further attention is given to improve the input matching at port 1. Port 2 is also well matched.

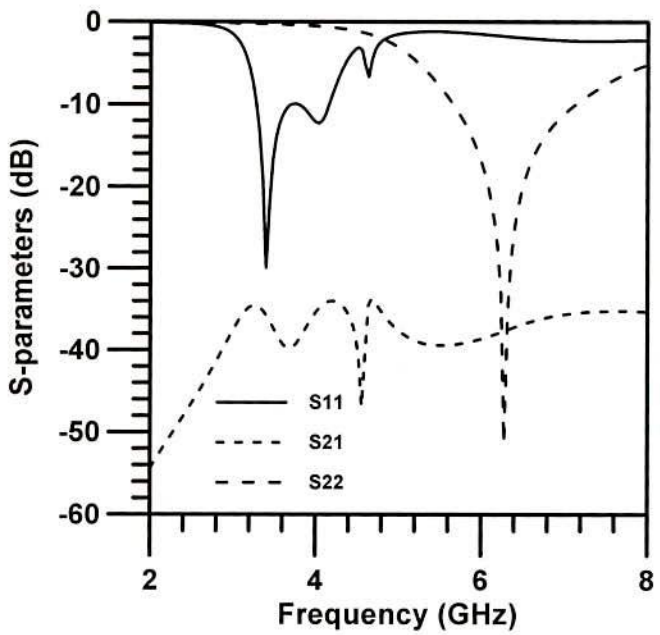

Fig. 6.10: Simulated S-parameter performance of a VSAT antenna with double-layer uniform circular PBGS.

It can be seen from the performances of uniform circular PBGS assisted VSAT dual-band ACPAs that the input matching at lower band is improved but the matching is not over the whole BW. In chapters 4-5 it has been mentioned that Binomial and *Chebyshev* distributed PBGS improves the performance. So the same antennas assisted by Binomial and *Chebyshev* distributed PBGSs are investigated to see if there is any improvement at lower band.

- **Binomially Distributed PBGSs**

The performance of VSAT antenna with Binomially distributed PBGSs in the ground plane is shown in Fig. 6.11. The filling factor of the central elements is 0.4 as it is found to be optimum FF in chapter four. It can be seen that the 10 dB return loss bandwidth is 23% and the input matching at port 1 is significantly improved throughout the bandwidth. The satisfactory matching at port 2 and the isolation are also achieved.

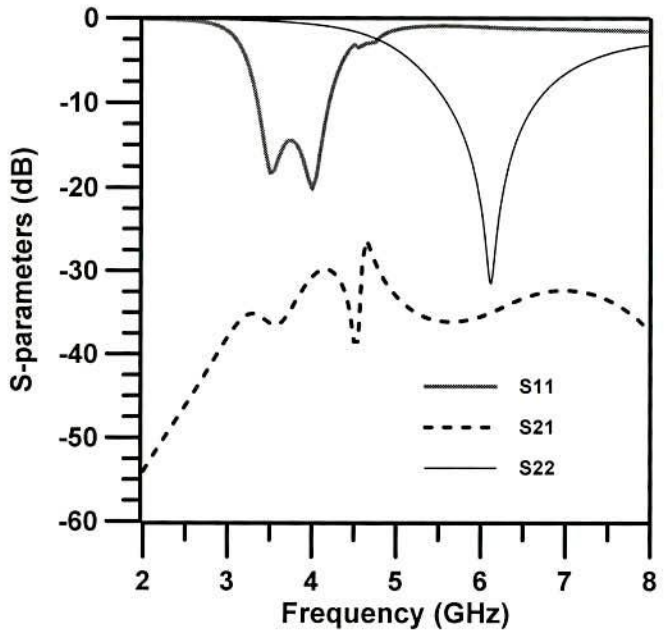

Fig. 6.11: Simulated S-parameter performance of a VSAT antenna with Binomially distributed PBG elements in the ground plane.

- ***Chebyshev* Distributed PBGSs**

The performance of a VSAT antenna with *Chebyshev* distributed PBG element in the ground plane is shown in Fig. 6.12. It can be seen that the input matching at port 1 is significantly improved over the whole bandwidth. The input impedance BW is 23 %.

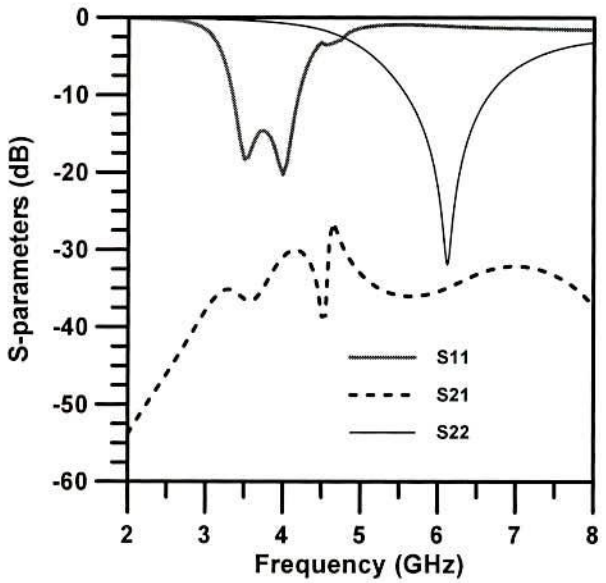

Fig. 6.12: Simulated S-parameter performance of a VSAT antenna with *Chebyshev* distributed PBG elements in the ground plane.

6.6.2 Improvement of Bandwidth and Gain in Dual-band Antenna

The dual-band antenna was fabricated and measured the S-parameter performances by vector network analyzer (VNA) and spectrum analyzer calculated the gain.

- **Measured Results**

The S-parameters of the proposed antenna and for the reference antennas were measured. Ports 1 and 2 of the antenna system correspond to lower and higher frequencies respectively. The performances of a reference and PBG assisted dual

band antennas are shown Fig. 6.13 and 6.14. The input impedance BWs of the reference antenna are 18.62% and 28.3% corresponding to port 1 and port 2 respectively. The isolation is more than 30 dB, which satisfies the VSAT specifications. For PBG assisted dual band antenna the BWs are 22 % and 29% respectively. The isolation is also more than 30 dB.

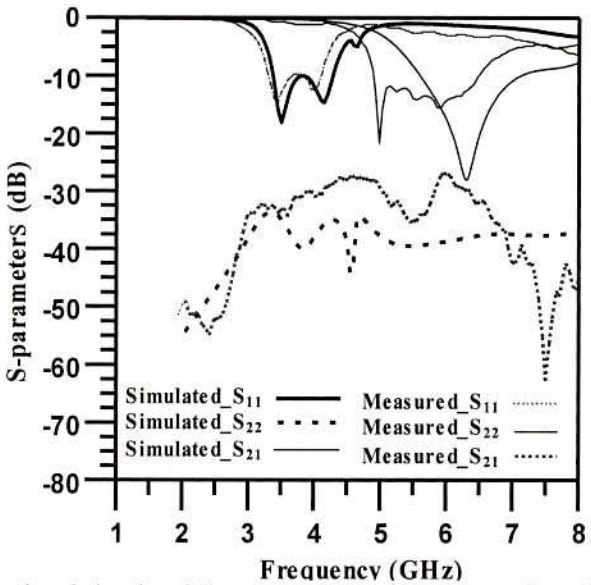

Fig. 6.13: Measured and simulated S-parameters performances of a reference dual band antenna

Therefore the enhancement of the BW due to inclusion of PBGSs in the ground plane of VSAT antenna is observed.

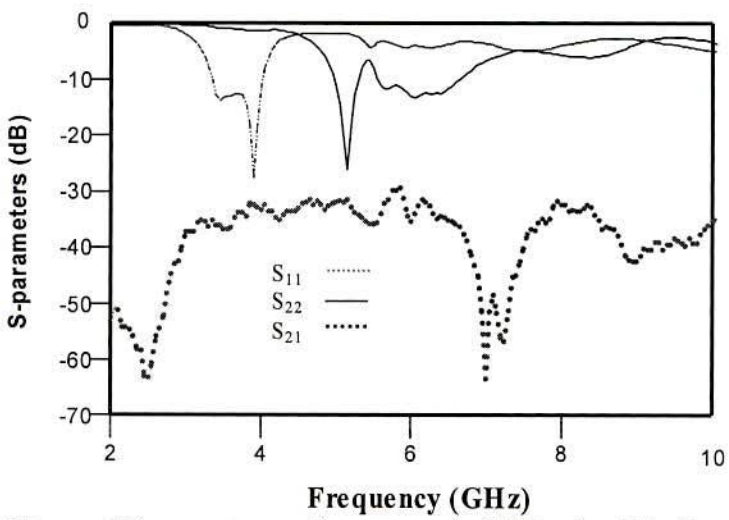

Fig. 6.14: Measured S-parameters performances of a PBG assisted dual band antenna

In Fig. 6.13, both the simulated and measured return loss performances of the reference dual-band antennas are shown. It can be seen that they agree well. The performances of uniform circular PBGS assisted dual-band antennas as shown in Fig. 6.9 and 6.14 are not shown in the same graph, as the designs are different. The performance shown in Fig. 6.9 corresponds to dual-band antenna having uniform circular PBGSs in the upper patch layer but the performance shown in Fig. 6.14 correspond to dual-band antenna having uniform circular PBGSs in the ground plane.

The VSAT ACPA is a broadband design with 21% BW in S-band. The coupling aperture dimension is comparable to the patch radiator. Due to the large aperture size for broadband coupling, back radiation is the natural consequence of such ACPA. To achieve 21% BW at S-band, the matching becomes poor due to the over-coupling of the aperture but it is still greater than 10 dB return loss over the required frequency band. Though the slot radiation can be controlled by a phase matched back-shield under the feed line but in this work PBG structure is proposed.

The effect of PBG structures on gain over the 10-dB bandwidth frequencies is also observed. Gain is calculated over the bandwidth by the spectrum analyzer. Fig. 6.15 elucidates the increase of gain due to the inclusion of PBG structures for lower frequency operation.

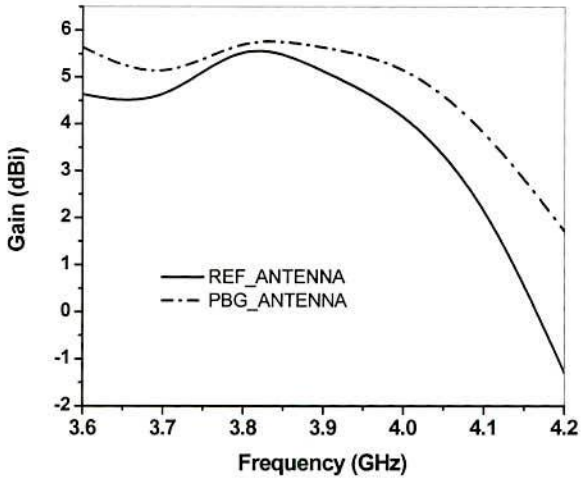

Fig. 6.15: Gain versus frequency curves of a dual band antenna at lower frequencies.

At higher frequencies no improvement is achieved. Further investigations with some modifications may improve the performance. The gain performance at higher frequency is shown in Fig. 6.16.

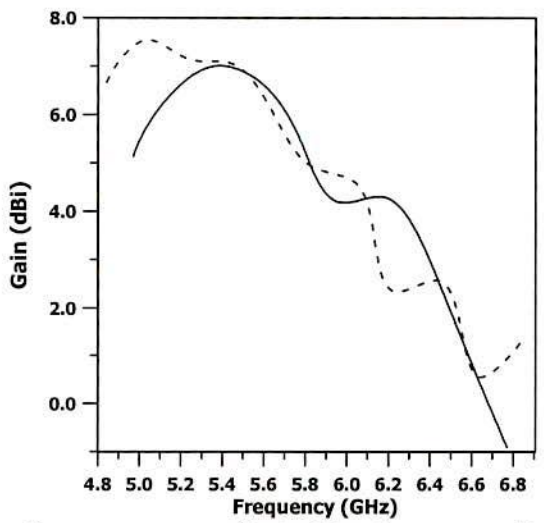

Fig. 6.16: Gain versus frequency curves of a dual band antenna at higher frequency. Solid and dotted line represent reference and PBG assisted antenna respectively.

6.6.3 Number of Ring PBGSs in ACPAs for Gain and Bandwidth Enhancement

PBG engineered ACPA with uniform annular ring PBGSs is simulated. It is seen that PBG assisted ACPAs enhance the BW and gain. Here the influence of number

of PBG element on ACPAs performances was investigated. The numbers of rings were varied. The two-dimensional PBG structures were 4 by 5, 6 by 7, and 8 by 9 arrays of rings. The BW, gain, and FBR of ACPAs with ring patterned PBG structure were investigated and compared with a reference antenna. The 10-dB return loss BWs were found to be 4.5%, 5.62%, and 4.3% for 4 by 5, 6 by 7, and 8 by 9 arrays of rings respectively. The relationship of 10 dB return loss BW and the number of rings is shown in Fig. 6.17. The BW, gain and front-to-back ratio of a reference ACPA are 4.08%, 6 dB and 13 dB, respectively. In the simulation, maximum BW is achieved with 6 by 7 rings array.

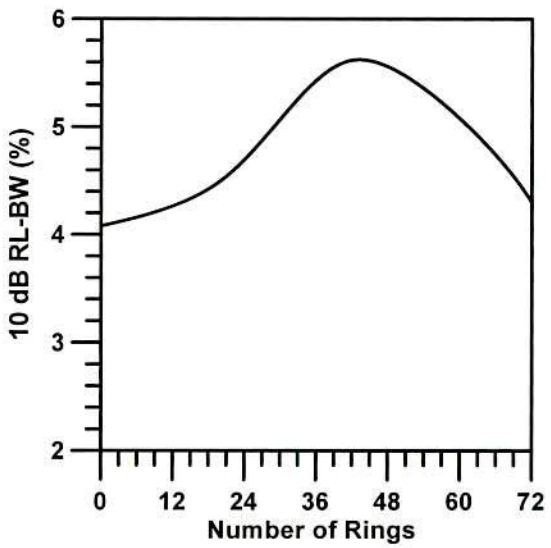

Fig. 6.17: 10-dB return loss bandwidth versus number of ring patterned PBG in ACPA.

For these same arrays, the corresponding gain was found to be 7.64, 7.08 and 7.59 dB respectively. The relationship between number of rings and the gain is shown in Fig. 6.18. It can be seen that the ACPA with 4 by 5 rings yields maximum gain of 7.64 dB.

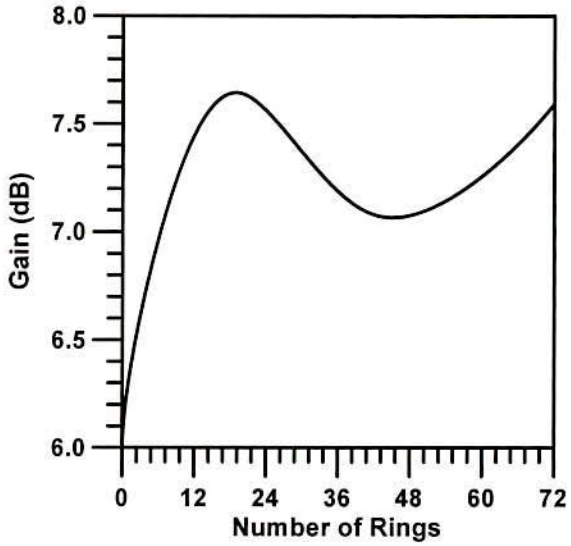

Fig. 6.18: Gain versus number of rings patterned PBG structure in an ACPA.

Maximum front-to-back ratio was 20 dB for 4 by 5 arrays of rings. The relationship of front-to-back ratio with number of ring is shown in Fig. 6.19.

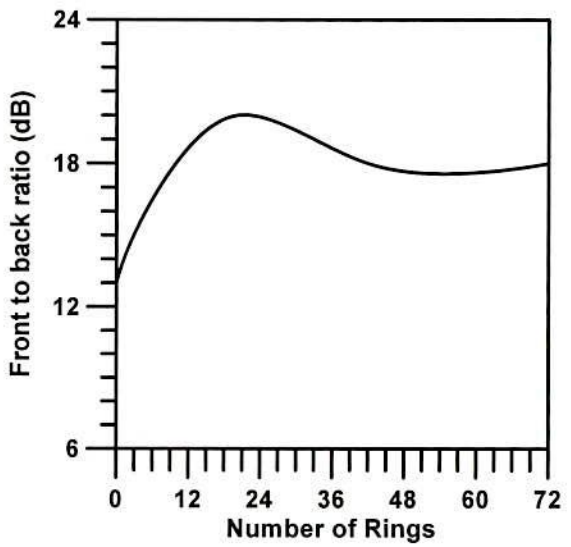

Fig. 6.19: Front-to-back ratio versus number of ring PBG structures in ACPA.

From the analyses it is found that the ring patterned PBG structures improve BW, gain and FBR. But all these parameters do not increase with the number of ring

PBG structures. The improvement in BW, gain and FBR is not achieved simultaneously.

6.7 PBGSs in Harmonic Suppression of BPF

Now-a-days microstrip BPFs are extensively used in modern microwave integrated circuits. But the performance of the overall RF system is affected by the spurious transmission of a conventional parallel-coupled BPF. T. Itoh *et al.* [47] proposed uniplanar compact PBG (UC-PBG) to suppress the spurious transmission. The UC-PBG is a complex design on a 2-D plane and occupies more space in a circuit. On the other hand, classical circular patterned PBGSs are simple in design and can be made 1-D that need less space and create fewer problems in electronic packaging. It is seen that 1-D uniform circular PBGS provides stopband performance similar to 2-D uniform circular PBGS. So there is a scope to use 1-D uniform circular PBGS to use in a filter to suppress 2^{nd} harmonics. It is already seen that the number of PBG elements has significant influence on S-parameter performances. The effect of variation of the number of PBG elements in harmonic suppression will also be investigated.

It is reported in Chapter 4 that non-uniform PBGSs realized by the implementation of Binomial and *Chebyshev* distribution yield better S-parameter performances. It will be reported that if the configuration of non-uniform PBGSs can improve the harmonic suppression. Only Binomially distributed PBG elements will be used. Additionally to this, the effect of variation of PBG elements in this distribution will also be observed.

In general the harmonics are the multiplication of fundamental frequency. So it is very difficult to achieve simultaneous and significant harmonic suppression by 1-D/2-D PBGSs. It is seen in Chapter 4 that DGS can yield wider stopband. This unique property will be used to suppress 2nd and 3rd harmonics of a filter simultaneously.

6.7.1 Design of uniform circular PBGSs for Harmonic Suppression

Uniform circular PBGSs are implemented to form different designs. PBG assisted BPF with different lattices and PBG elements have been investigated that include (i) BPF on 2-D array of uniform circular PBGSs which forms square lattice, (ii) BPF on dense 2-D uniform circular PBGSs that forms rectangular lattice, (iii) BPF on 1-D uniform circular PBGSs that exactly located under the two extreme 50-ohm lines and the central coupled line, (iv) BPF on uniform circular PBGSs that are located under two extreme line only and finally (v) BPF on uniform circular PBGSs that are located under all the lines of a BPF. All these designs are shown in Fig. 6.20. These investigations are very useful to understand the behavior of poles of BPFs in the presence of PBGSs.

- **Standard BPF**

A 4-section asymmetric coupled line BPF is shown in Fig. 6.20(a). The dimensions of the coupled lines are: W1 = 0.425 mm, W2 = 0.525 mm, G1 = 0.2 mm, G2 = 0.7 mm, L1 = L2 = 3.625 mm and W50 = 0.6 mm. The dimensions of the reference BPF are same as [32].

- **BPF on 2-D array of uniform circular PBGSs**

In this design the uniform circular PBGSs are etched in the ground plane having their periodicities in X-and Y-directions that forms square patterned lattice

structure. Here PBG elements form square lattice. The geometry is shown in Fig. 6.20 (b) that consists of 3 rows of 9 PBG elements.

- **BPF with dense 2-D uniform circular PBGSs**

2-D array of uniform circular PBGSs are situated beneath all the lines of BPF including outside of the line having rectangular lattice structures. The Bragg's condition is applied in X-direction. The geometry is shown in Fig. 6.20 (c).

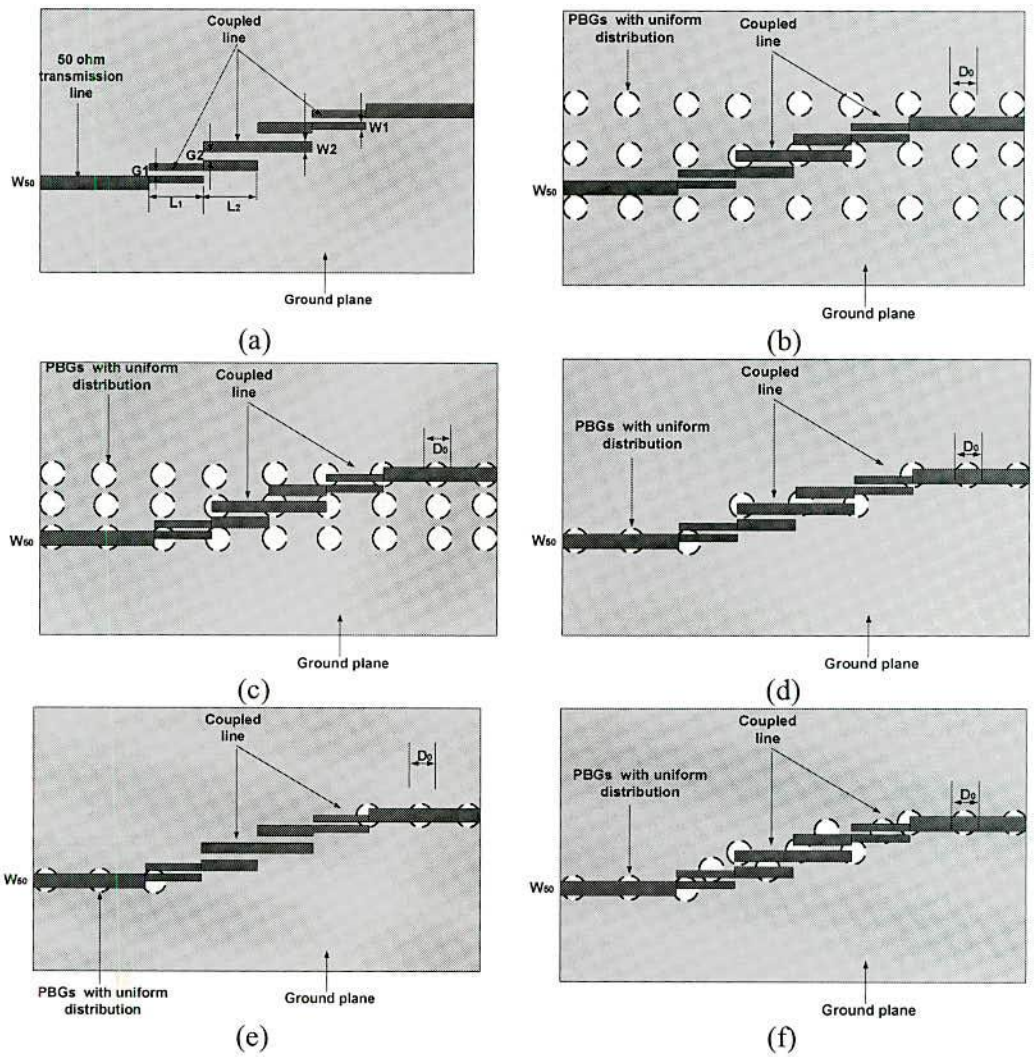

Fig. 6.20: Various designs of BPFs assisted by uniform circular PBGSs, (a) standard 4-section asymmetric coupled line BPF (b) BPF on 2-D square lattice PBGSs, (c) BPF with dense 2-D PBGSs (rectangular lattice), (d) BPF with PBGSs under 50-ohm and central coupled lines, (e) BPF with PBGSs under 50-ohm lines only and (f) BPF with PBGSs under all lines only.

- **BPF with PBGSs under 50-ohm and central coupled lines**

Here PBG elements are located under 50-ohm and central coupled lines. This design consists of total 9 PBG elements. The geometry of this design is shown in Fig. 6.20(d).

- **BPF with PBGSs under 50-ohm lines only**

In this design, PBG elements are located under 50-ohm lines only. There are 6 PBG elements in this design as shown in Fig. 6.20(e).

- **BPF with uniform circular PBGSs under all lines only**

Uniform circular PBGSs are under all the microstrip line of BPF thinking over the idea that the field is confined below the lines. Beyond the lines there are no PBG elements. The geometry is shown in Fig. 6.20(f).

6.7.2 Performance of uniform circular PBGS Assisted BPF

Theoretical results are produced for different geometries of uniform circular PBGS assisted BPF. To see the effect of uniform circular PBGS in harmonic suppression the performance of reference BPF is shown. Finally the insertion loss performances of a standard BPF and uniform circular PBGS assisted BPF are shown to compare the results.

- **Performance of reference BPF**

The performance of standard asymmetric coupled line BPF is reproduced. The performance as obtained from the simulation result is shown in Fig. 6.21. The presence of spurious transmission around 15 GHz is obvious in case of a reference

BPF. At this frequency maximum value of return loss is found to be 9 dB and insertion loss is found to be 2.5 dB. At 7.5 GHz, which is the frequency of interest, the maximum value of return loss is 22.5 dB and insertion loss is 0.5 dB. For harmonic suppression 2-D array of uniform circular PBGS are used in the ground plane of a reference BPF.

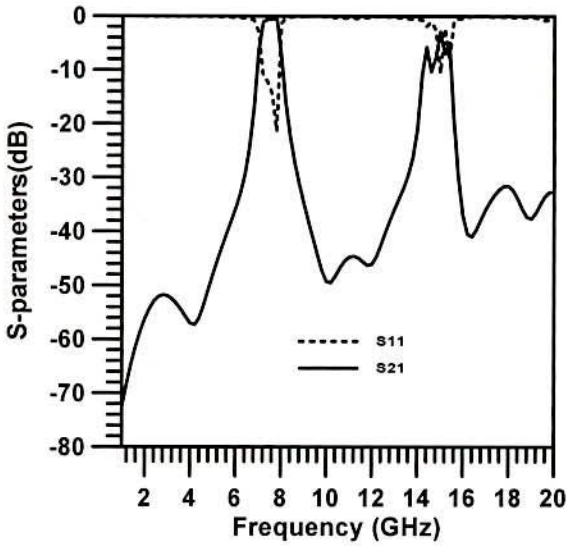

Fig. 6.21: IE3D simulated S-parameters performances of a standard coupled line BPF. Substrate is RT/Duroid having dielectric constant of 10.2 and height of 0.635 mm.

- **Performance of BPF on 2-D array of uniform circular PBGSs**

The harmonic is suppressed due to application of 2-D array of uniform circular PBGSs as shown in Fig. 6.22.

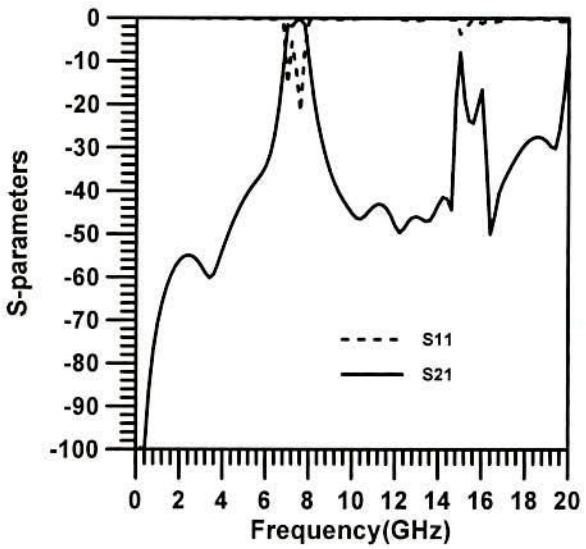

Fig. 6.22: Theoretical S-parameters performances of a BPF with 2-D uniform circular PBGSs. Substrate is RT/Duroid having dielectric constant of 10.2 and height of 0.635 mm.

The return loss performance at second harmonic should ideally be zero for proper harmonic suppression. But the maximum value of return loss is here 2 dB and the value of insertion loss 9.5 dB. It is clear that the uniform circular PBGSs are not exact under the lines. So they are not strong enough to suppress the transmission at second harmonic frequency.

- **Performance of BPF on dense 2-D array of uniform circular PBGSs**

Fig. 6.23 shows the simulation result of a BPF with 2-D PBGSs that are denser than conventional 2-D square lattice structure. In this case they are rectangular lattice structure. It is seen that at 7.5 GHz the maximum return loss is 25 dB and the maximum return loss at 15 GHz is about to zero dB. The insertion loss is more than 30 dB. Significant suppression is achieved here.

- **Performance of BPF with three line uniform circular PBGSs**

The BPF is simulated where the PBGSs are under two 50-ohm line and the central coupled lines. The performance is shown in Fig. 6.24. In this structure, the uniform circular PBGSs are situated under two 50-ohm lines and the central coupled line. From the simulation results it can seen that at 15 GHz the maximum value of return loss is about 1 dB only and the insertion loss is found to be 11 dB.

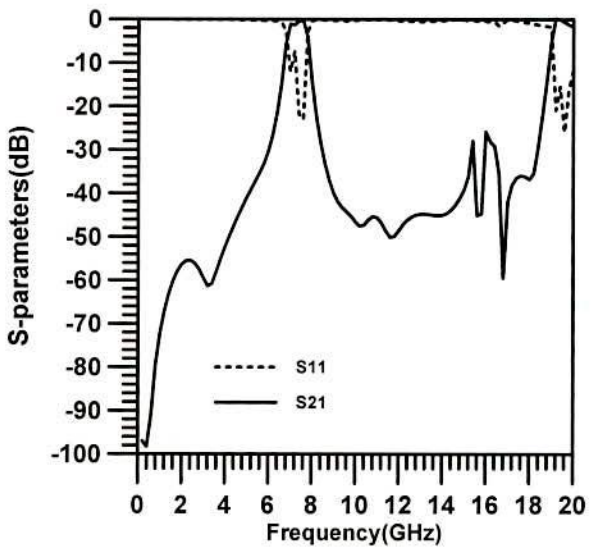

Fig. 6.23: Simulated S-parameters performance of BPF when it is loaded by dense 2-D uniform circular PBGSs. Substrate is RT/Duroid having dielectric constant of 10.2 and height of 0.635 mm.

Harmonic suppression is not satisfactory. In addition to this, the return loss performance at fundamental frequency is poor.

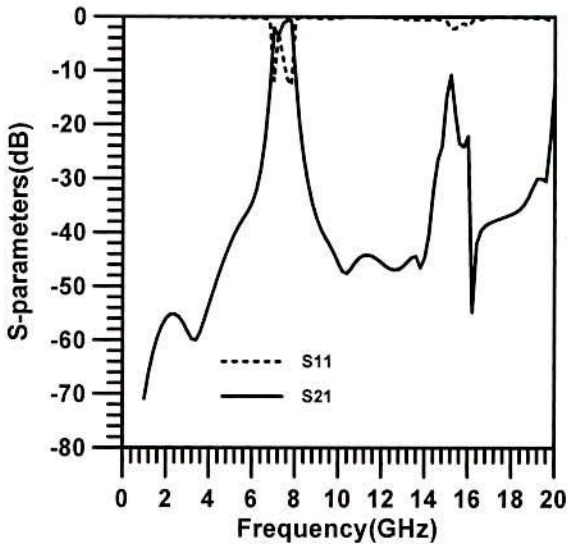

Fig. 6.24: Simulated S-parameters performances of a BPF with three line uniform circular PBGSs. Substrate is RT/Duroid having dielectric constant of 10.2 and height of 0.635 mm.

- **Performance of BPF with uniform circular PBGSs under two extreme 50 ohm lines**

Thinking over the philosophy that the EM propagation takes place through the 50-ohm line first, uniform circular PBGSs are used under two 50-ohm lines only to see their effect in harmonic suppression. The simulation result is shown in Fig. 6.25.

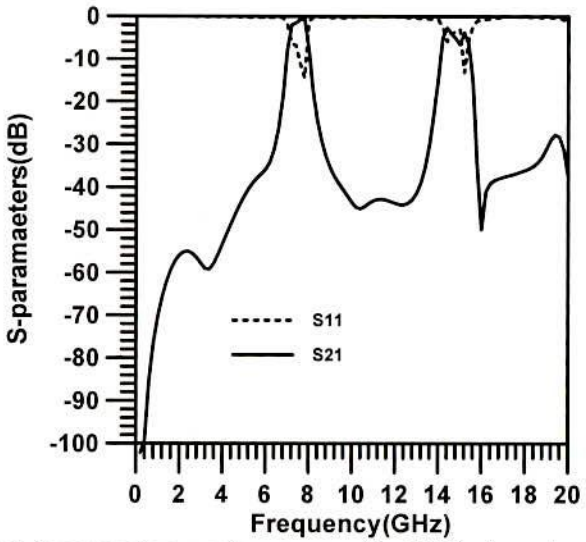

Fig. 6.25: Simulated S-parameters performances of a BPF where two 50-ohm lines are only perturbed with uniform circular PBGSs. Substrate is RT/Duroid having dielectric constant of 10.2 and height of 0.635 mm.

It can be seen that the result is not promising at all. Rather the performance at fundamental and second harmonic frequencies the performances are worse.

- **Performance of BPF with uniform circular PBGSs under all the lines**

Finally PBGS is used just under all the lines. The design provides S-parameters performances as shown in Fig. 6.26. It can be seen that at 7.5 GHz the maximum return loss is more than 30 dB. At 15 GHz the maximum return loss is zero dB and the insertion loss 30 dB. In this case significant improvements in fundamental and second harmonic frequencies are achieved. Only small ripple in transmission band is noticed that can be controlled with resizing the uniform circular PBG elements.

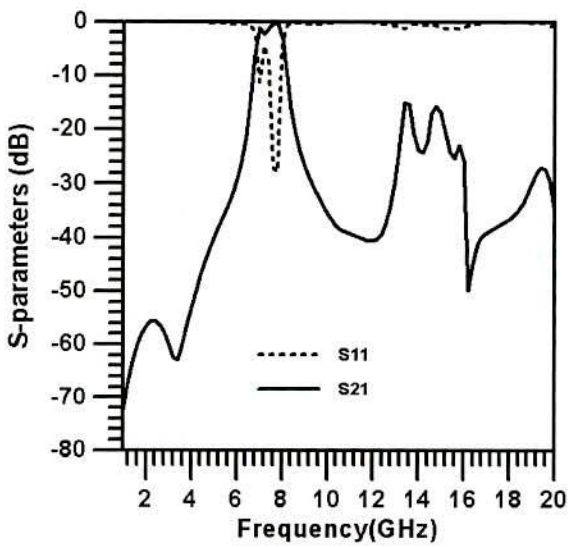

Fig. 6.26: Theoretical S-parameters performances of a BPF when uniform circular PBGSs are situated under all the lines. Substrate is RT/Duroid having dielectric constant of 10.2 and height of 0.635 mm.

- **Comparison of S_{21} Performances**

Finally optimized reference and uniform circular PBGS assisted BPF are fabricated. The measured insertion loss performances are shown in Fig. 6.27.

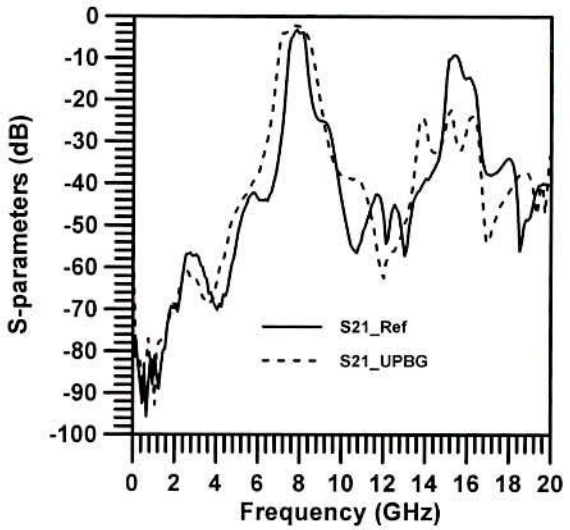

Fig. 6.27: Measured insertion loss performances of an optimized BPF. Substrate is Taconic having dielectric constant of 10 and height of 0.635 mm.

From the measured result it can be seen that the fundamental frequency is little bit shifted and the second harmonic also. For the reference BPF the average 3 dB insertion loss and 10 dB return loss bandwidths are 7.18% and 5.96% respectively. On the other hand uniform circular PBGS assisted BPF provides maximum 26 dB return loss at fundamental frequency. Average insertion loss at second harmonic is found to be 26 dB. 3 dB insertion loss and 10 dB return loss bandwidths are found to be 16.02% and 15.2% respectively. So uniform circular PBGS assisted BPF improves the performances in terms of return loss, insertion loss and BW.

6.7.3 Designs of B-PBGSs for harmonic suppression

BPFs are designed with Binomially distributed PBGSs (B-PBGSs). Harmonic suppression is investigated due to the variation of number of PBG elements in B-PBGS assisted BPF (B-BPF). Various designs of B-BPFs are shown in Fig. 6.28. In Fig. 6.28, B-PBGSs have FF of 0.4 (0.4 is the optimum FF for Binomially distributed PBGSs as mentioned earlier). The insertion loss performances of B-

BPF are investigated for different cases where the number of PBG elements are varied. The variation is done by using conducting copper tape to close or open the PBG elements. Thus fabrications of many prototypes for the investigations are avoided.

(1) Design 1: The ground plane of the reference BPF is perturbed by PBGSs with Binomial distribution. In this design three lines (consists of two extremes 50-ohm lines and central coupled line) are perturbed by B-PBGSs having FF of 0.4. The rests are loaded with uniform PBGSs having FF of 0.25. Total number of PBG elements are 13 in B-BPF.The geometry is shown in Fig. 6.28 (a).

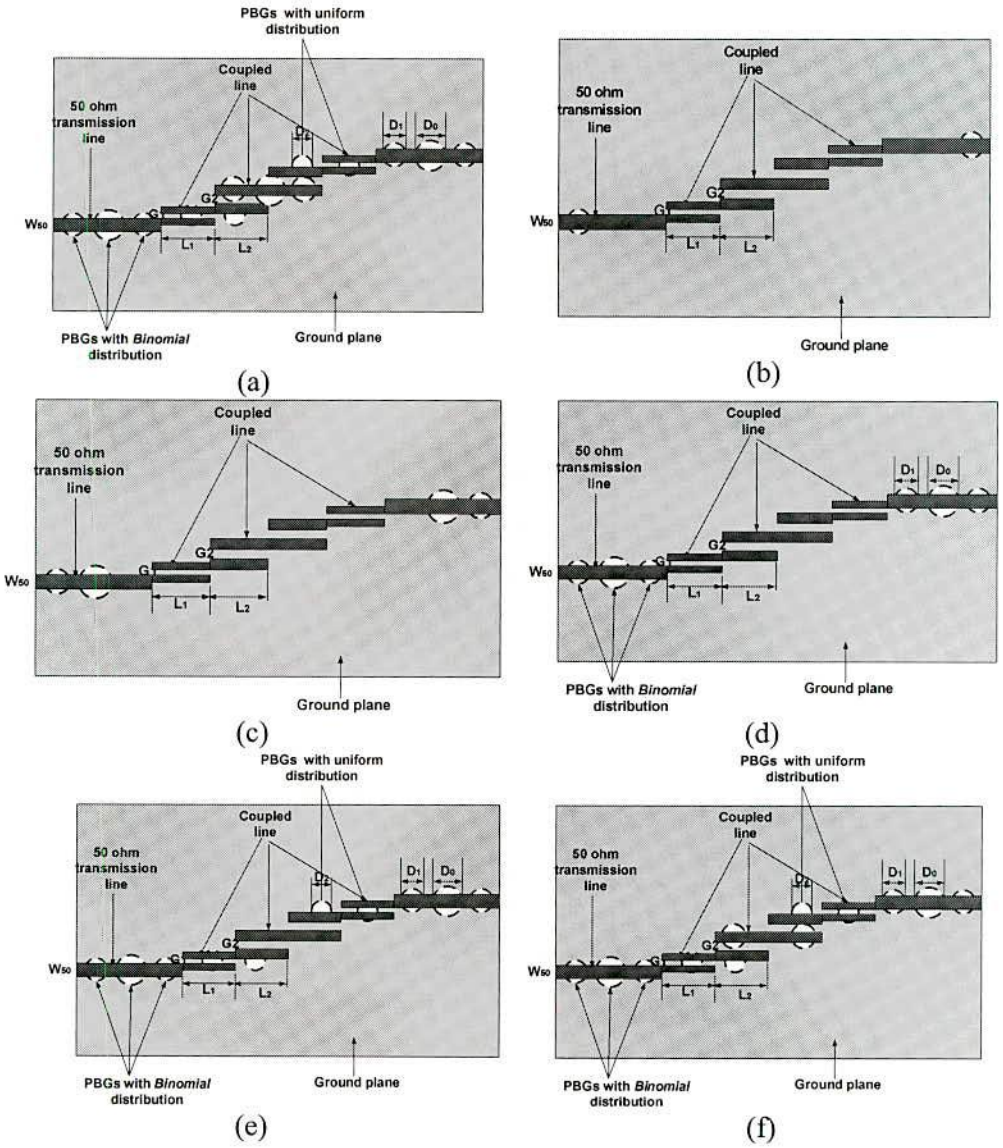

Fig. 6.28: Various designs of B-BPFs with B-PBGSs, (a) elements are under all lines (b) 2 elements under 50-ohm lines only, (c) 4 elements are under 50-ohm lines, (d) 6 elements are under 50-ohm lines, (e) elements are under all lines except central coupled lines and (f) elements are under all lines except the central larger PBG elements in the central coupled line.

(2) Design 2: In this design only 2 PBG elements are used from the two extremes and rest PBG elements of B-BPF are closed as shown in Fig. 6.28(b).

(3) Design 3: In this case BPF is loaded by 4 PBG elements from the two extremes. Rests PBG elements are closed as shown in Fig. 6.28(c).

(4) Design 4: In this design the BPF is loaded by 6 PBG elements from the two extremes. PBG elements are under 50-ohm lines only as shown in Fig. 6.28(d).

(5) Design 5: In this design total 10 PBG elements of B-BPF are used. The design is shown in Fig. 6.28(e). No PBG elements are situated under the central coupled line.

(6) Design 6: This design consists of 12 PBG elements in the ground plane of a BPF. Here the central PBG element of the central coupled line is omitted. The design is shown in Fig. 6.28(f).

6.7.4 Performance of B-BPF

All the designs are fabricated and measured by VNA. The measured results are mentioned as follows. The insertion loss and return loss performances are shown for reference BPF. The return loss performances are not shown for the rest designs. Only insertion loss performances are shown to indicate harmonic suppression.

- **Reference optimized BPF**

The experimental S-parameter performance of a standard BPF is shown in Fig. 6.29. The harmonics (2^{nd} and 3^{rd} harmonics) are investigated by varying the number of PBG elements. For standard BPF the measured 2^{nd} and 3^{rd} harmonics are found to be 13 and 8 dB respectively.

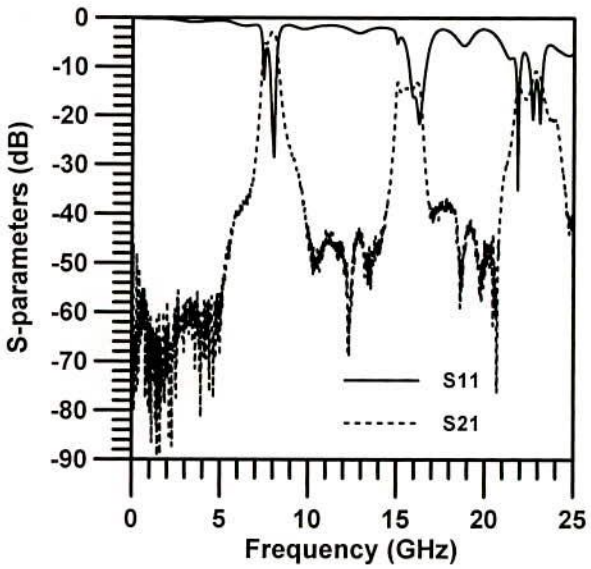

Fig. 6.29: Measured S-parameters performance of a standard BPF. Substrate is Taconic having dielectric constant of 10 and height of 0.635 mm.

(1) Design 1: Insertion loss Performance of B-BPF

The insertion loss performance of the B-BPF is shown in Fig. 6.30. In this design total 13 PBG elements are used to suppress the harmonics. B-BPF provides 2nd and 3rd harmonics to be 32 and 20 dB. The harmonics are suppressed by 19 and 12 dB respectively. But the insertion loss performance in the transmission band is seen to be poor. Under this circumstance the influence of different numbers on the performance of BPF will be investigated.

(2) Design 2: The BPF is investigated with 2 PBG elements. During the measurement the insertion loss performances show 2nd and 3rd harmonics to be 30 and 17.5 dB respectively (The graph is not shown here).

(3) Design 3: It is seen that 4 PBG elements etched in the ground plane of a BPF stems the insertion loss performance which provides 2nd and 3rd harmonics to be 37 and 16 dB respectively (The graph is not shown here).

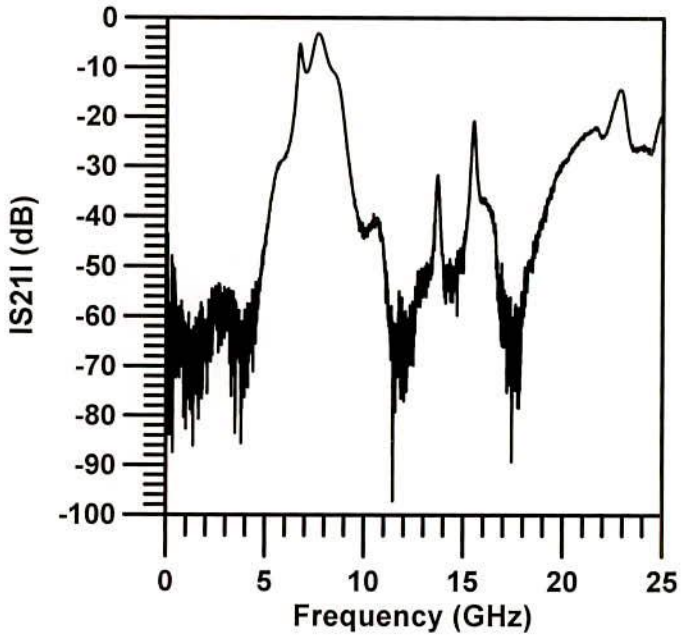

Fig. 6.30: Measured insertion loss performance of a B-BPF where PBG elements are periodically loading under all the lines. Substrate is Taconic having dielectric constant of 10 and height of 0.635 mm.

(4) Design 4: It is seen during measurement that the insertion loss performance of a BPF loaded by 6 PBG elements provides 2^{nd} and 3^{rd} harmonics are found to be 34 and 14 dB respectively. It is worthwhile to mention that this configuration hold completely Binomially distributed PBGS under two 50-ohm lines of a BPF (The graph is not shown here).

(5) Design 5: This design provides 40 and 22 dB insertion loss as 2^{nd} and 3^{rd} harmonics. The transmission band at fundamental frequency is also seen to be improved. The insertion loss performance for 10 PBG elements is shown in Fig. 6.31.

(6) Design 6: As can be seen from Fig. 6.32 that the Design 5 yields ILs of 38 and 21 dB at 2^{nd} and 3^{rd} harmonics. The transmission band at the fundamental frequency is better than the insertion loss performance of B-BPF.

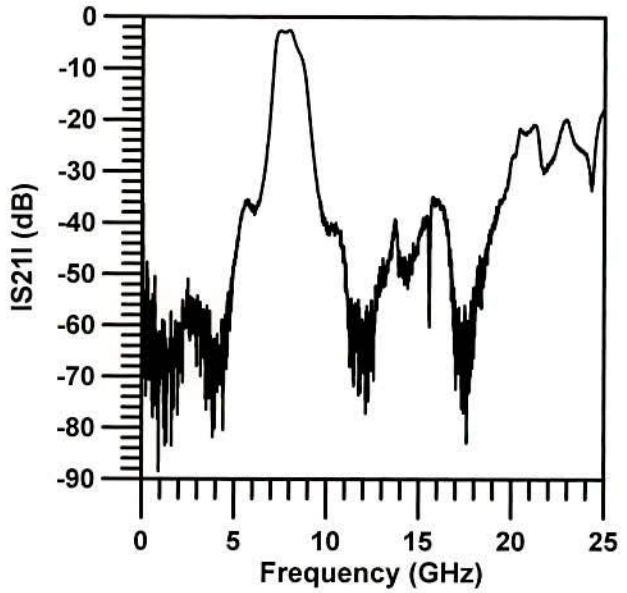

Fig. 6.31: Measured insertion loss performance of BPF when 10 PBG elements are under all the lines except the central coupled line

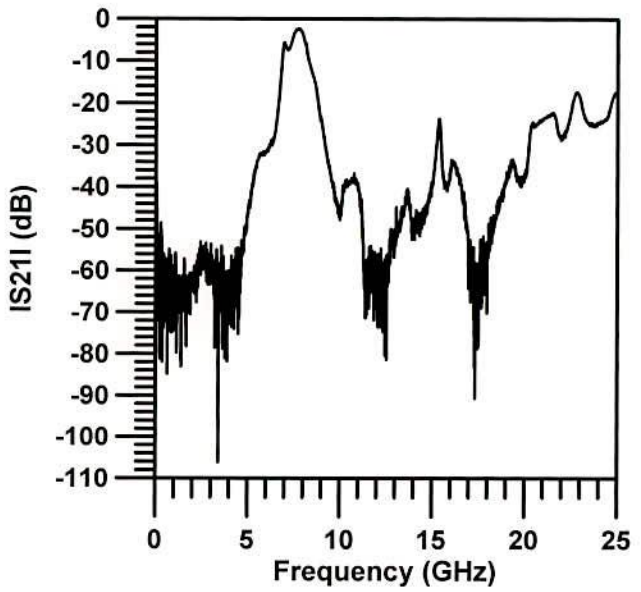

Fig. 6.32: Measured insertion loss performance of a BPF loaded by 12 PBG elements. Only one larger element under the central coupled line is closed.

The insertion loss performances for all the designs are mentioned in Table 6.1. It can be seen from the Table 6.2 that the 10 PBG elements provides best performance. 12 elements provide also better performance. It is also clear that 2nd and 3rd harmonics do not scale with number of PBG elements. The important

finding is the role of larger PBG elements of the central coupled line. It can be concluded that the middle larger element under the central coupled line degrades the performance.

TABLE 6.1: PERFORMANCE OF A COUPLED LINE BPF WITH BINOMIALLY DISTRIBUTED PBGS ALONG WITH DIFFERENT NUMBER OF PBG ELEMENTS.

Number of PBG elements	Insertion loss (dB)	
	2^{nd} harmonics	3^{rd} harmonics
0 (Reference BPF)	13	8
2	30	17.5
4	37	16
6	34	14
10	42.5	22
12	38	21
13	20	17.5

- **Comparison**

In order to investigate the improved performance of B-BPF over the UBPG assisted BPF, the combined insertion loss performances are shown in Fig. 6.33.

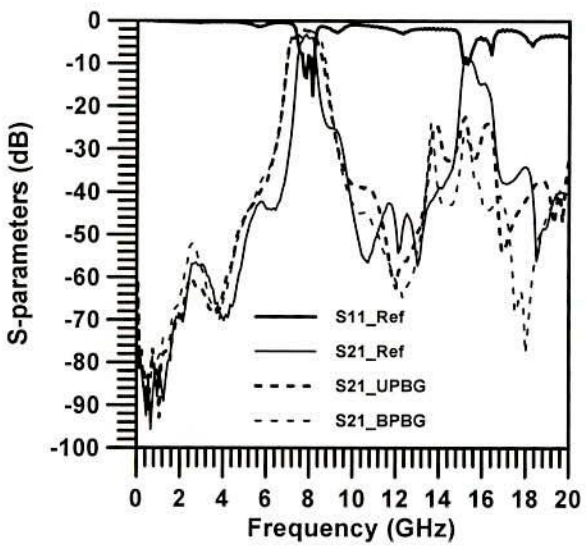

Fig. 6.33: Measured S-parameters performance of an optimized BPF along with the insertion loss performances of B-BPF and uniform circular PBGS assisted BPF.

It can be seen that the average 10 dB return loss BW at fundamental frequency is 16.2 %. The 3 dB insertion loss BW is found to be 19.56%. The average insertion loss value at second harmonic is 29 dB.

The performances of an optimized BPF, uniform circular PBGS assisted BPF and B-BPF is shown in Table 6.2.

TABLE 6.2: PERFORMANCE OF AN OPTIMIZED BPF WITH UNIFORM CIRCULAR PBGSS AND B-PBGSS.

Types	Average 3 dB insertion loss BW (%)	Average 10 dB return loss BW (%)	Average 2^{nd} harmonics (dB)
Standard BPF	7.18%	5.96%	6
Uniform circular PBGS assisted BPF	16.02	15.2	26
B-BPF (with omission of central PBG elements)	19.56	16.2	29

6.7.5 DGS for Harmonic Suppression

In this sub-section the novel idea is reported for simultaneous harmonic suppression of 2^{nd} and 3^{rd} order harmonics generated in a conventional BPF. It is already reported that the dumbbell shaped DGS can stem wider stopband [61], [105]. Now this unique property is implemented into an asymmetric 4-section coupled line BPF to suppress the 2^{nd} and 3^{rd} order harmonics. 1-D EBGSs (dumbbell shaped DGS) are proposed that are located just under standard 50-ohm lines. No DGS will be used under the coupled lines. A novel idea is also given that the dumbbell shaped DGSs are designed at two different frequencies to be located under two end 50-ohm lines. This design is sufficient to suppress the 2^{nd} and 3^{rd} order harmonics. Few designs are investigated.

(1) Design 1: Here total 4 DGSs are used under two 50-ohm lines. Two DGSs will be located under each 50-ohm line. The larger square slot of DGS unit has the dimension of 52×52 square mils and the vertical narrow slot has the dimension of 50×15 square mils. The geometry of a BPF with 4 DGSs in the ground plane is shown in Fig. 6.34.

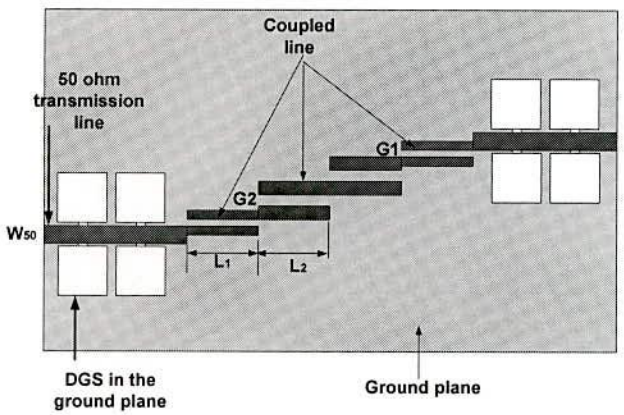

Fig. 6.34: Geometry of a DGS assisted BPF. 4 DGSs are located under two 50-ohm lines

(2) Design 2: In this case 4 DGSs are used under only left-sided 50-ohm line. There is no DGS under right-sided 50-ohm line.

(3) Design 3: 4 DGSs are located under left sided 50-ohm line designed for 2^{nd} harmonic suppression. Another set of 4 DGSs is located under right-sided 50-ohm line that is suitable for 3^{rd} harmonic suppression.

(4) Design 4: DGSs are located under left-sided 50-ohm line and 8 DGSs are placed under right-sided 50-ohm line. 8 DGS elements are designed for significant suppression of third harmonics.

6.7.6 Performance of DGS assisted BPF

The theoretical investigations have been carried out to DGS assisted BPF to see the effective suppression of 2nd (at 15 GHz) and 3rd (at 22.5 GHz) harmonics. The S-parameters performances for the various designs are given below.

- **Theoretical Performances**

The theoretical performances of the standard optimized BPF that has been used in all designs of DGS has been shown in Fig. 6.35. The insertion loss at 2nd and 3rd harmonics are 6 and 0 dB respectively.

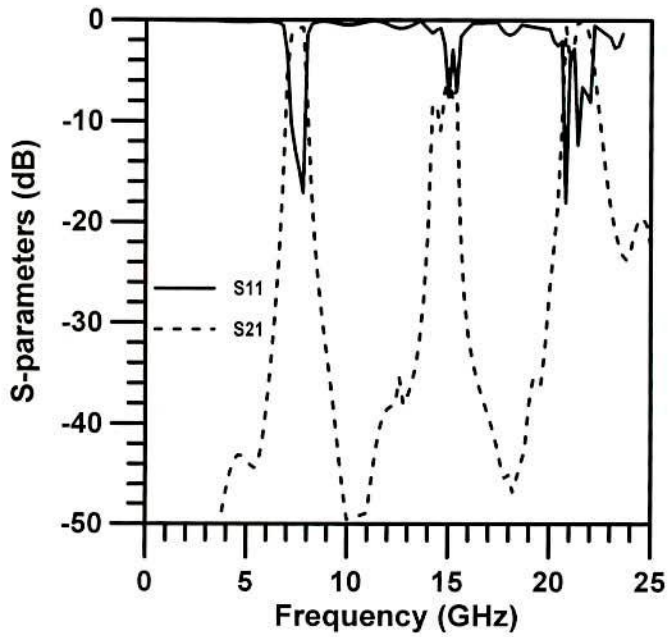

Fig. 6.35: Simulated S-parameters performances of an optimized reference BPF.

(1) Design 1: The S-parameters performances for total 4 DGS (2+2) located under two 50-ohm lines are shown in Fig. 6.36. From the insertion loss performance it can be seen that the 2nd and 3rd harmonics are 28 dB and 6 dB respectively. Input matching is seen to be improved.

(3) Design 2: The S-parameters performances of a BPF assisted by 4 DGSs under left-sided 50-ohm line are shown in Fig. 6.37. It can be seen that this design provides 2nd and 3rd harmonics of 38 and 20 dB, respectively.

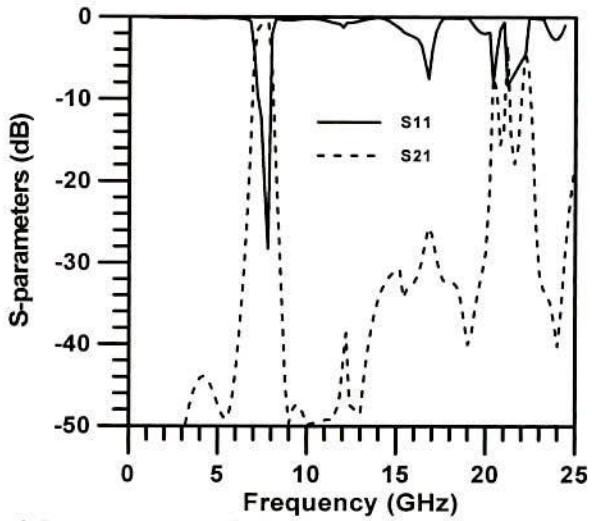

Fig. 6.36: Simulated S-parameters performances of a DGS assisted BPF having total 4 DGS (2+2) lying under two 50-ohm lines.

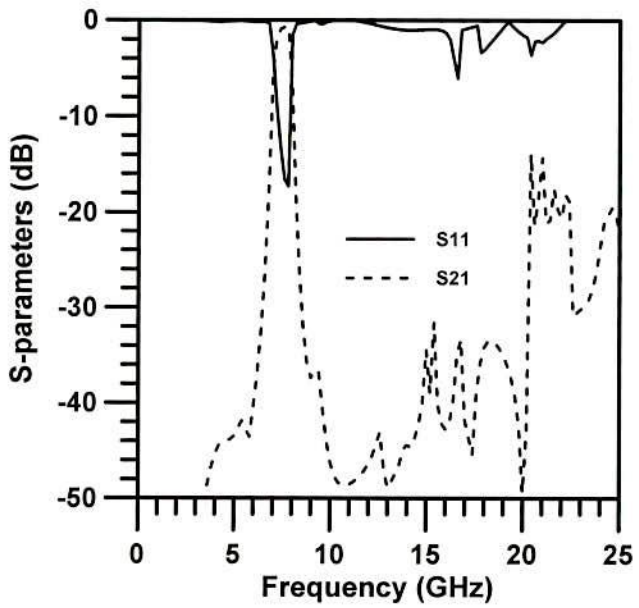

Fig.6.37: Simulated S-parameters performances of a BPF assisted by 4 DGS lying under the left-sided 50-ohm transmission line.

(3) Design 3: In this design 4 DGSs have been placed under left-sided 50-ohm line to be useful for 2nd harmonic suppression and 4 DGSs are placed under right-sided 50-ohm line designed to be useful for 3rd harmonic suppression. This is a new technique that DGSs have been designed at two frequencies for effective harmonic suppression. The S-parameters performances of this design are shown in Fig. 6.38. It can be seen that this design provides 2nd and 3rd harmonics to be 40 and 20 dB respectively.

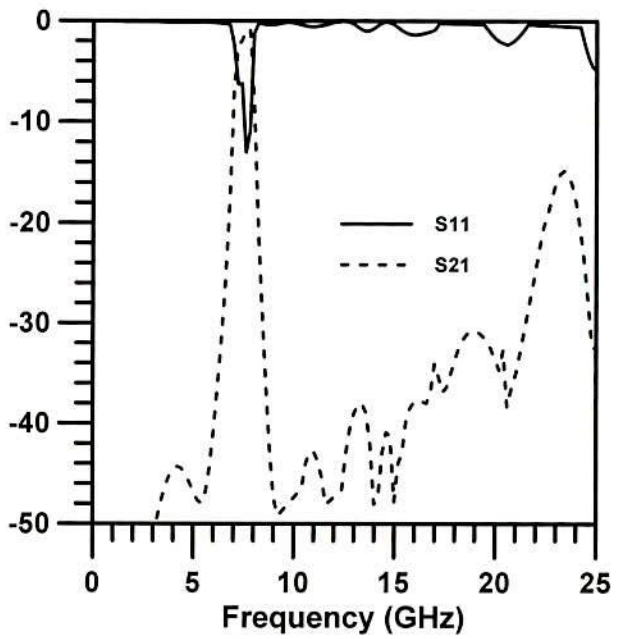

Fig. 6.38: Simulated S-parameters performances of DGS assisted BPF where two sets of 4 DGSs have been placed under two 50-ohm lines.

(4) Design 4: In this case an attempt has been taken to suppress the 3rd harmonic significantly. For this purpose 8 DGSs are used under the right-sided 50-ohm lines to generate deep and wider stopband to suppress the 3rd harmonics. The S-parameters performances of this design are shown in Fig. 6.39. It can be seen that the performance at 3rd harmonic has improved significantly showing 30 dB harmonic suppression.

- **Experimental Performances**

Finally one prototype of DGS assisted BPF having four bigger dumbbell shaped DGS elements located under the 50-ohm line at left side and 8 smaller DGS elements located under the 50-ohm line at right side is developed. Taconic substrate having dielectric constant of 10 and height of 25 mils is used.

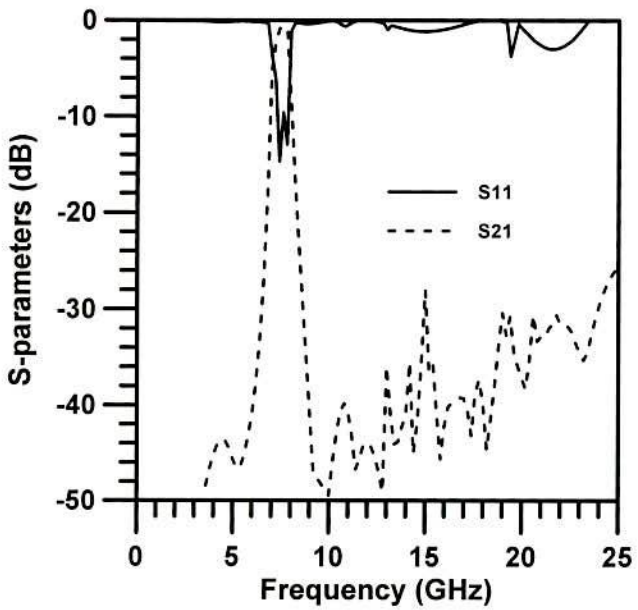

Fig. 6.39: Simulated S-parameters performances of DGS assisted BPF where 4DGSs are used under left-sided 50-ohm line and 8 DGSs are designed for 3rd harmonic suppression and placed under right-sided 50-ohm line.

The measured and simulated performance of this design is shown in Fig. 6.40. It can be seen that both the simulated and measured performances of the design is very impressive. Very insignificant discrepancies are found between the theoretical and experimental investigations. This experimental investigation ensures the validity of the performances as shown in Figs. 6.35-6.39.

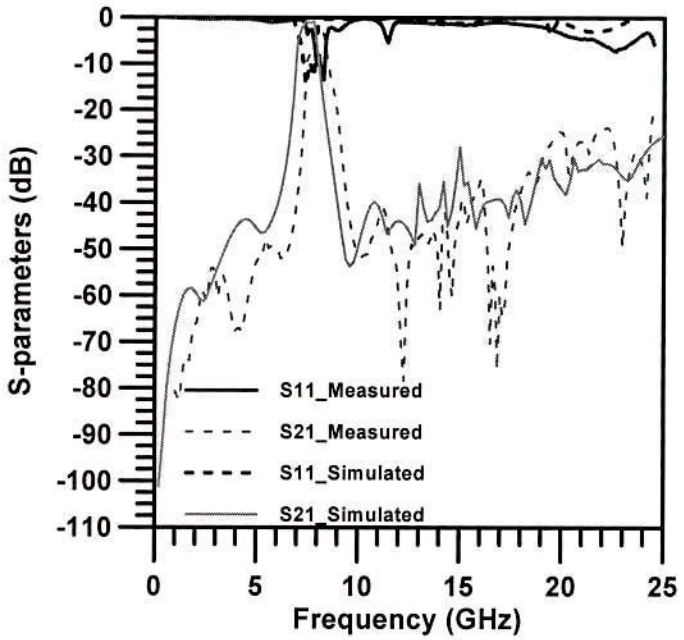

Fig. 6.40: Measured and simulated S-parameters performances of DGS assisted BPF where 4 DGSs are used under left-sided 50-ohm line and 8 DGSs are placed under right-sided 50-ohm line. The substrate is Taconic with dielectric constant of 10 and height of 25 mils.

Conclusions

In the beginning of this chapter the microstrip patch antennas and their feed techniques have been reviewed. PBG assisted antennas have been investigated to see the improved performance in terms of input matching, return loss BW, gain etc. For this purpose, a shared aperture dual-polarized dual-band ACPA has been designed and investigated theoretically. Uniform circular patterned PBGSs on single layer (in ground plane only) and on double layer (in ground plane and in patch layer) have been used. Both designs improve input matching. Double-layered uniform circular PBGSs provide best matching. In this design, two slots are used in the ground plane for feeding purpose. These slots correspond to two feeding lines that ensure dual band operation. One slot is C-shaped and other is a rectangular slot.

Another dual band antenna having one dog-bone slot in the ground plane for feeding purpose was investigated. Uniform circular PBGS assisted dual band ACPAs were fabricated and tested to see their S-parameters performances and gain. From the measured results, it is seen that the proposed PBG assisted ACPA improves the return loss performances and high isolation between two ports. The input impedance bandwidths enhance for both frequencies of operation and they are more than 21% for both frequencies of operation. The isolation between the receiving and transmitting terminal is more than 30 dB. In the lower frequency of operation the gain enhancement over the 10-dB bandwidth is found.

The ground plane of conventional ACPAs has been perturbed. It is seen that the variation in number of PBG elements influences the S-parameters performances significantly. The number of annular ring PBGSs has been varied in the ground plane of ACPAs. The return loss BW, FBR and gain are different for different combinations. Antenna performances can be controlled with the variation in numbers of PBG elements. Double-layered hole patterned PBGSs provide 4 dB more gain compared to a conventional ACPA.

In the previous chapter it is reported that uniform circular PBGS generates stopband as per the designed frequency. It is also mentioned that non-uniform PBGSs having Binomial and *Chebyshev* distribution improve performances. These properties have been used in harmonic suppression of BPFs.

BPF with uniform circular PBGSs has been investigated theoretically with different conditions. From all the results it can be seen that the performance

improves if the PBG elements are situated just under the lines. Optimized reference BPF and a BPF with uniform circular PBGS have also been fabricated. It can be seen that due to inclusion of PBG elements in a conventional BPF the insertion loss performance improves significantly in terms of bandwidth and harmonic suppression as well.

Binomially distributed PBGSs (It is named as B-PBGSs) are designed for the suppression of spurious transmission in a BPF. A compact microstrip BPF with intrinsic spurious suppression is reported [47] where 2-D UCPBGSs are used. 2-D UC-PBG structures are complex and takes more space. So B-PBGSs are proposed that yield ripple free transmission with wider stopband in case of microstrip line. Insertion loss performances of a BPF with variable number of PBG elements have been investigated. It can be seen that B-PBGSs suppress 2^{nd} harmonic significantly. It also suppresses 3^{rd} harmonics. It is very interesting to note that in microstrip transmission line the stopband scales with the number of PBG elements. But the present study reveals that it does not hold true for harmonic suppression of a BPF. It can be explained as the coupling phenomena of BPF and PBG elements. The PBG elements situated under the central coupled line may provide significant coupling with the coupled line. Both the designs with 10 and 12 PBG elements provide better insertion loss performances.

Finally DGS assisted BPF is investigated. Few designs are investigated. All designs suppress both 2^{nd} and 3^{rd} harmonics significantly. A new idea of using two sets of DGSs designed at two different frequencies work well in 2^{nd} and 3^{rd} harmonics suppression. One design is fabricated and measured to compare the

theoretical performances with measured performances. Impressive agreement between the two validates the investigations.

In the next chapter PBG assisted phased array antenna is presented.

Chapter 7 PBG Assisted Phased Array Antennas

7.1 Introduction

Recently, beam steering in microstrip antennas finds potential applications in many modern devices that include automobiles and airplane radars, satellite communication networks and reconfigurable wireless network etc. Beam steering is performed with digital phase shifters. Conventional electronic phase shifters are expensive and the number of phase shifters also increases with the number of antennas in an array. Under this circumstance reconfigurable PBG ground plane is highly preferred for beam steering purpose. B. Elamaran *et al.* [18] proposed a beam-steerer using reconfigurable ground plane. They mentioned only the influence of number of PBG elements on the phase properties. The delay of the line is proportional to the number of PBG elements. Detailed investigations of the relative phase of a PBG assisted transmission line are missing there.

In this chapter the relative phase of PBG assisted transmission lines with different parameters is investigated. The phase properties of PBG engineered microstrip transmission lines with (i) different FFs, (ii) different numbers of PBG elements and (iii) different offset distances of PBG elements from the center of the lines are investigated in details. This investigation is done in the passband of the PBG assisted transmission lines such the insertion losses of the lines are minimum. After satisfactory transmission amplitudes and phases, the lines are incorporated into the feed network of microstrip phased array antenna. Hence the phase properties are

implemented in beam steering. PBGS and DGS assisted feed networks are designed and investigated their phase properties. The feed networks are composed of 4 feed lines to be used for a 4 elements microstrip antenna array. The feed networks are assisted by PBG elements as follows.

(1) Feed lines are on different number of square patterned PBGSs

(2) Feed lines are on PBG elements with different FFs

(3) Feed lines are on PBG elements having different offset distances

Different combinations of the above three designs can be used for required beam squinting. All these combinations are possible on a reconfigurable ground plane. The reconfigurability of the ground plane can be achieved by MEMS switching of PBGSs [106]-[109] or by rolling PBG assisted ground plane as shown in Fig. 7.1. Stepper motors could be used to roll different combinations of PBG assisted GND planes under the microstrip patch antenna array. Hence beam steering is possible without expensive phase shifter.

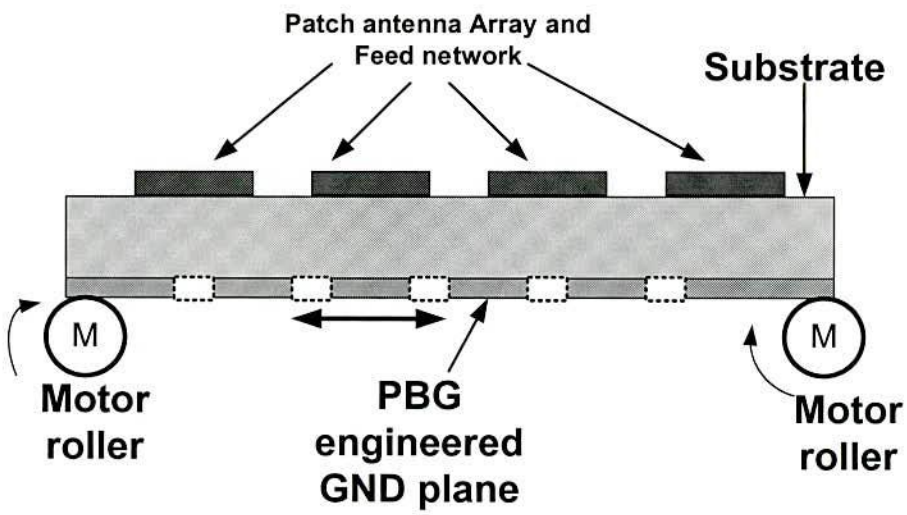

Fig. 7.1: A simple approach to develop a reconfigurable ground plane to realize a PBG assisted phased array antenna.

The proposed technique could be economical solutions for agile phased array antennas.

The possible PBG combinations may have the following combinations:

- Different numbers and different FFs of PBG elements.
- Different numbers and different offset distances.
- Different FFs and different offset distances.
- Different number of PBG elements, different FFs and different offset distances. Triple actions will take place under this scheme.

Fig. 7.2 shows three transmission lines with uniform square patterned PBGSs. As can be seen, N number of square patterned PBGSs are offset a distance 'd' from the center of 50-ohm microstrip transmission line. The FF is b/a, where 'b' is the arm length of the PBG unit and 'a' is the period. Figs. 7.2 (a) and (b) are helpful to understand the variation of FF. The arm length of square patterned PBGSs of Fig. 7.2(b) is larger than that of Fig. 7.2(a). That means the FF of PBGSs of Fig. 7.2(b) is larger than that of Fig. 7.2(a).

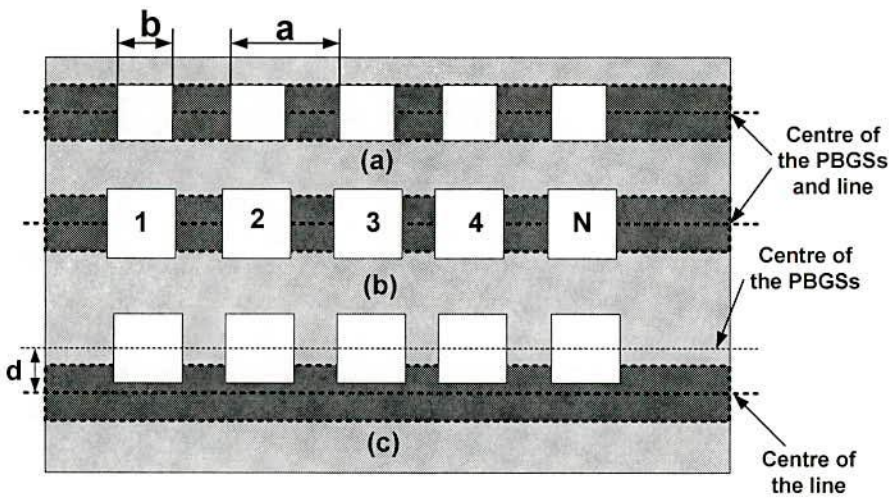

Fig.7.2: Geometries of square patterned PBGSs to understand the variations of FF and offset distance of PBGSs under the microstrip line, (a) and (b) show the variation of FF, (c) shows the offset distance.

In Fig. 7.2(c) PBG elements are offset by distance 'd'. This is the distance between the center of PBGSs and microstrip transmission line. The FF, N and the offset distance d are varied to investigate the relative phase property of the microstrip line. Once satisfactory phase shift is obtained from the PBG assisted lines, the lines will be incorporated in the feed network of the microstrip antenna array for beam steering.

In this chapter a reconfigurable phased array antenna has also been addressed where the antennas resonate at two frequencies. For this purpose 4 dummy patches are connected via 4 PIN diodes with the 4 active patches of the array. The connections of the active and dummy patches are associated with biasing network for proper functioning.

7.2 Phase Properties of PBG Assisted Microstrip Line

When PBGSs are realized under the microstrip transmission lines both transmission amplitude and phase change. Firstly the relative phase properties of EBG engineered microstrip transmission lines are investigated thoroughly to understand its suitability for beam steering purposes of microstrip patch antenna arrays. One row of square patterned PBGSs is used under the transmission line. Numbers of PBG elements, FFs and offset distances (the distance from the center of the line to the center of PBG elements) are varied in the investigation.

The sizes of the square patterned PBG elements are changed to vary FF. FFs are varied in steps of 0.3, 0.4, .0.5, 0.6 and 0.7. Phase properties of PBG engineered microstrip line at 5.6 and 6 GHz are investigated. These frequencies are chosen, as

they are within the passband of the designed PBG engineered transmission lines. Two frequencies are selected to investigate the phase and frequency dependence of PBGSs. Higher frequencies are expected to yield more phase lag, as they are closer to the edge of the bandgap.

7.3 PBG Assisted Feed Networks for Phased Arrays

In this section PBG assisted feed networks will be investigated. The array is a uniform array having identical elements and each with progressive phase. All the lines of feed networks are terminated with matched ports. The array factor is defined as [76].

$$\mathrm{AF} = \sum_{n=1}^{N} e^{j(n-1)\psi} \tag{7.1}$$

Where $\psi = kd_n\cos\theta + \beta$, k is the wave number, θ is the elevation angle, and β is the progressive phase shift at any scan angle θ_0.

The maximum array factor occurs when

$$\beta = -kd_n\cos\theta_0$$

$$= -2\pi/\lambda_0\,(2n-1)/2d\cos\theta_0 \tag{7.2}$$

Due to the perturbation in the ground plane progressive phase shift changes significantly. Equation (3.30) is very useful to understand the phase variation in passband.

The different concept of phase variations developed in previous section in a 4 by 1 feed networks will be implemented. The geometries are developed in EM software

IE3D. The phases will be used in EM software PCAAD to see the radiation pattern. Upon the satisfactory performances of PBG assisted feed networks 4 patches will be loaded with the PBG assisted feed networks. The simulation results obtained from IE3D and PCAAD are compared. Finally few designs are fabricated and the measured results are compared with the theoretical results.

7.3.1 Designs of PBG Assisted Feed Networks

Fig. 7.3 shows a feed network for a 4-element array. The design consists of two steps namely the complete reference array and PBG assisted feed networks. The complete feed network comprises 3 sets of transformers, 4 bends and 3 power dividers. The substrate having dielectric constant of 2.46 and height 31 mils has been used. The inter-element spacing is 21 mm, which is approximately 0.6 times the free space wavelength. The input impedance of each element is 50-ohms. So it is needed to transform 50-ohms to 100-ohms. A quarter-wave power transformer having the characteristics impedance of 70-ohms and power combiner are used to yield 50 ohms back from two 100-ohms lines. This is a primary design of a reference feed network. Now on the basis of the design requirements 50-ohms line is enlarged to include PBG elements underneath the feed lines. The array is designed at 8.65 GHz.

- **Feed networks with different FFs**

In this scheme square patterned PBG elements are designed with different FFs that are 0.4, 0.5 and 0.6 respectively. The geometry of a 4 by 1 feed network perturbed with 0-6-12-18 PBG elements distributions with FF of 0.5 is shown in Fig. 7.3. There are 4 feed lines. The first feed line, which constitutes reference phase, is

unperturbed. PBG distribution is designated as 0 PBG elements. On the other hand second, third and fourth lines are perturbed with 6, 12 and 18 PBG elements, respectively. This distribution of PBG elements is designated as 0-6-12-18.

- **Feed Networks with different PBG numbers**

In this scheme the number of PBG elements is changed under the feed lines of the feed network. Different PBGS distributions have been used under the feed lines of the network. The FF is 0.5 for all the designs. The PBGS distributions are 0-3-6-9, 0-5-10-15 and 0-8-16-24 etc. The geometries are similar to Fig. 7.3 except the numbers of PBG elements are changed.

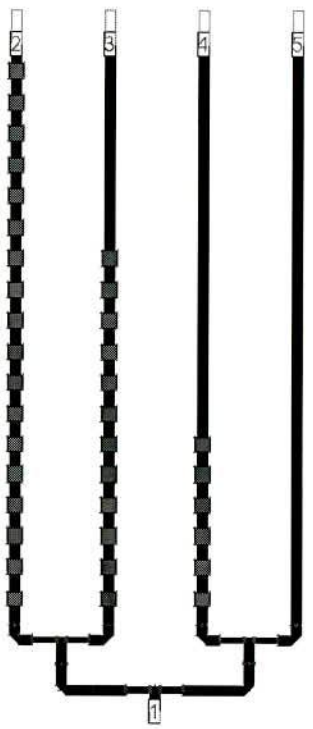

Fig. 7.3: Geometry of a 4 by 1 feed network assisted by 18 square patterned PBG elements with FF of 0.5. The geometry is developed in MGRID of IE 3D on substrate having dielectric constant of 2.46 and height of 31 mils.

- **Feed Network with different PBG elements location (different offset distances)**

Here PBG elements are offset from the center of the microstrip transmission lines. The PBG assisted feed network are investigated with the off distances of 1, 2 and 4 mm. The PBG distributions are 0-6-12-18 with FF of 0.8.

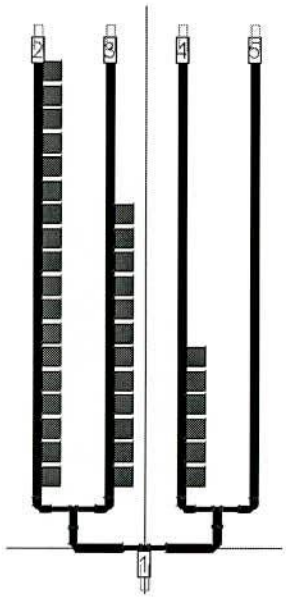

Fig. 7.4: Geometry developed in MGRID of IE3D for PBGS assisted feed network with square patterned PBGSs that are 4 mm offset.

7.3.2 Relative phases of PBG Assisted Feed Networks

All the feed networks are simulated in IE3D. The unperturbed feed line is considered as reference line. The unperturbed reference line provides relative phase shift of 0 degree. Relative to the unperturbed line all relative phases corresponding to second, third and fourth feed lines are calculated.

7.4 Results

7.4.1 PBG assisted Transmission lines

The phase properties at 5.6 and 6 GHz for different FFs are shown in Fig. 7.5. Total 9 square patterned PBG elements are used in this investigation. It can be seen that the phase of the PBG engineered line increases with FFs. The PBG engineered line having PBG elements with FF of 0.7 provides the largest relative phase.

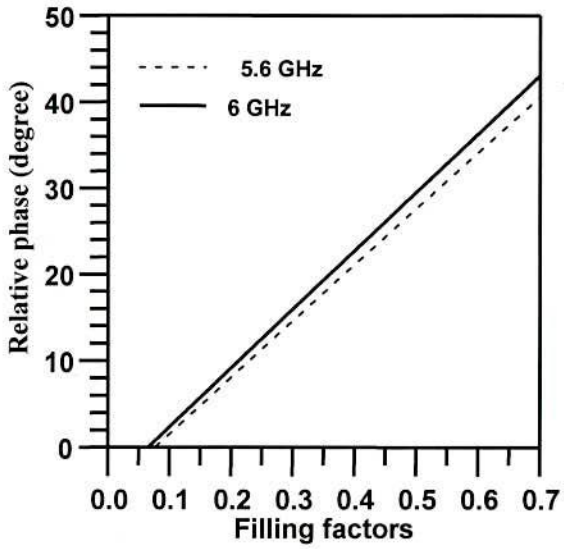

Fig. 7.5: Simulated phase properties of 9 square patterned PBG elements with different FFs. Dimension of PBG unit cells: arm length = 104 mils. Substrate: Taconic having dielectric constant of 2.45 and height of 31 mils.

The number of square patterned PBG elements is varied that ranges from 1 to 8 which means that the distributions are 1 by 1, 2 by 1, and 3 by 1 up to 8 by 1 PBGSs under the standard 50-ohm microstrip transmission line. The FF is 0.5 and the arm length of square patterned PBG elements is 113 mils. The numbers of PBGS play a vital role to change the phase of a transmission line, which can be understood from Fig. 7.6.

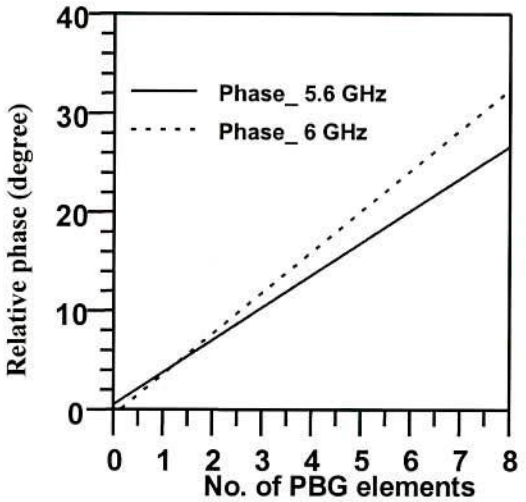

Fig. 7.6: Simulated phase properties of a PBG engineered microstrip line with the variations in number of square patterned PBG elements having FF of 0.46.

From Fig. 7.6 it is clear that the phase increases with the number of PBG elements. The linear relationship reveals that the transmission line with 8 square patterned PBG elements provide the largest relative phase. It is also clear that the phases generated at 6 GHz are more than the phases generated at 5.6 GHz.

Finally the lines with different locations (offsets) of PBG elements are investigated. The EM field is highly concentrated under the microstrip line. For this reason PBG elements are etched in the ground plane of a transmission line that are concentric. Here PBG elements are offset. The influence of offset distances on the phase properties is shown in Fig. 7.7. It can be seen that the relative phases decrease with the increase of offset distance. It is expected, as the offset distance is more, which means the PBG elements are more far away from the center of the line. It can be seen that offset distances ranging from 65 mils to 80 mils provide zero phases that are equal to the standard unperturbed transmission line.

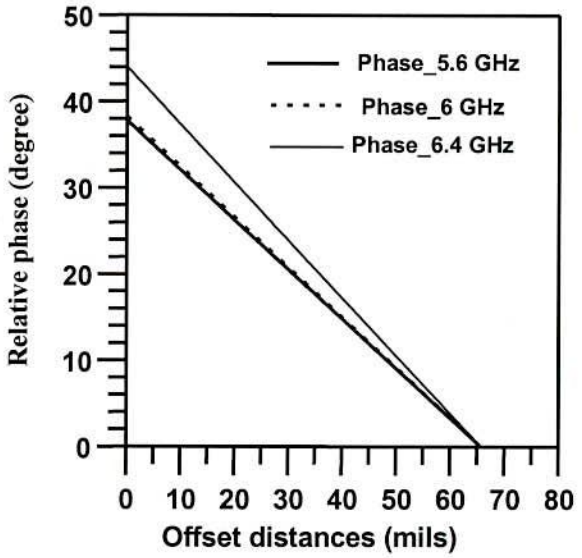

Fig. 7.7: Simulated phase properties of a microstrip line perturbed by square patterned PBG elements with different offset distances.

Beyond these offset distances no effects on phase properties are found. It is noted here that the phase properties at three different frequencies have been investigated. It is because phases at 5.6 and 6 GHz are very similar. To see the significant differences the phase properties at 6. 4 GHz has also been investigated.

7.4.2 PBG Assisted Feed Network

- **Feed Network with Different FFs**

It can be seen from the simulation results that different FFs provide different phases corresponding to different feed lines. PBGSs with 0.4 FF having 0-6-12-18 PBG elements distribution provide 0, 14.9, 46.4 and 72.1 degrees relative phases. The same PBG assisted feed network with PBGSs of 0.5 FF provides 0, 37.2, 101.4 and 162.98 degree relative phases. Finally the performance for FF of 0.6 is investigated. Under this distribution relative phases are seen to be 0, 74.2, 164.53

and 228.876 degrees. The relative phases corresponding to different FFs are shown in Table 7.1.

TABLE 7.1: PHASE PROPERTIES OF A PBG ASSISTED 4 BY 1FEED NETWORK WITH DIFFERENT FFS HAVING 0-6-12-18 PBG ELEMENTS

FFs	Relative phases (degree)			
	Line 1	Line 2	Line 3	Line 4
0.3	0	14.9	46.4	72.1
0.4	0	37.2	101.4	162.98
0.5	0	74.2	164.53	228.78

- **Feed networks with different PBG elements**

PBG assisted feed network is simulated with variable number of PBG elements under the feed lines. From the simulation results it is seen that the relative phases change with the number of PBG elements etched under the feed lines. The relative phases for 0-3-6-9 and 0-5-10-15 distributions are seen to be 0, 23.5, 60.1 76.1 and 0, 41.4, 101.7, 134.87 degrees respectively. For 0-8-16-24 PBG elements distributions the relative phases are seen to be 0, 68.5, 135 and 198 degree. The relative phases for different distributions are shown in Table 7.2.

TABLE 7.2: RELATIVE PHASES OF PBG ASSISTED FEED NETWORKS WITH DIFFERENT PBG NUMBERS

PBGSs distributions	Relative phases (degree)			
	Line 1	Line 2	Line 3	Line 4
0-3-6-9	0	23.5	60.1	76.1
0-5-10-15	0	41.4	101.7	134.87
0-8-16-24	0	68.5	135	198

- **Feed Networks with Different Offset distances**

Finally the phase properties of PBG assisted feed networks are investigated with different offset distances. PBG elements with relatively larger FF are chosen. The PBG elements have the distributions of 0-6-12-18 with FF of 0.8. The relative phases are different for different offset distances. The relative phases corresponding to different offset distances are shown in Table 7.3.

TABLE 7.3: RELATIVE PHASES OF A PBG ASSISTED FEED NETWORK WITH DIFFERENT OFFSET DISTANCES

Offset distances (mm)	Relative phases (degree)			
	Line 1	Line 2	Line 3	Line 4
0	0	112	255	356
1	0	88	180	254
2	0	19	63	112
4	0	6	13	15

It can be seen that relative phases decrease as the location of PBG elements move away from the center of the transmission line. It is obvious that the design provides maximum phases when the center of PBG elements and the center of the transmission line are in the same alignment.

7.4.3 Implementation of Phases in PCAAD

PBG assisted feed networks are simulated to be applied for 4 by 1 phased arrays. The relative phases are tabulated in the previous section. These phases will be implemented in EM software PCAAD. All the 4 by 1 feed networks will be loaded by 4 patches and will be investigated. Patch length =1.1075 cm and patch width = 1.1425 cm are used in PCAAD software. The patch antennas resonate at 8.65 GHz. The relative phases will be used for a particular design.

- **Beam steering with different FFs**

Radiation patterns corresponding to phases obtained from different PBG assisted feed network with different FFs are shown in Fig. 7.8. Different phases are used corresponding to different FFs with same patch antenna dimensions. Here no mutual coupling effect is considered in the calculation

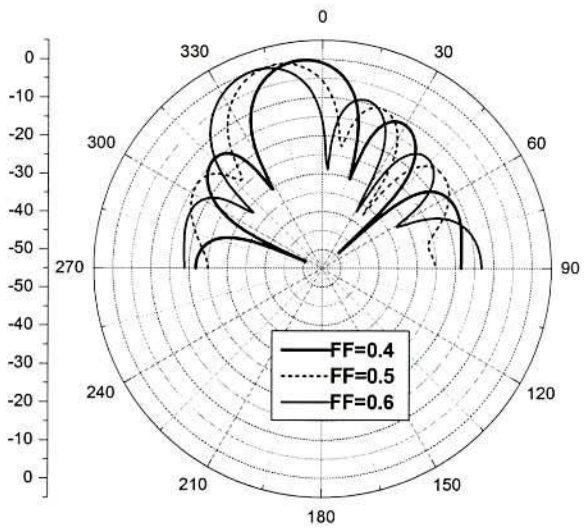

Fig. 7.8: Radiation patterns for different FFs generated in EM software PCAAD 4.0 having the distribution of PBGSs as 0-6-12-18 with zero offset distance.

It can be seen that the beam steering angle increases with FFs. The FF of 0.4 provides beam steering of 6 degree. The FFs of 0.5 and 0.6 provide beam steering of 14 and 20 degrees respectively. The maximum value of FF yields the maximum steering. The relationship of beam steering angle of a PBG assisted 4 by 1 phased array antenna with PBGSs etched in the ground plane with different FFs is shown in Fig. 7.9. It can be seen that almost linear relationship exists between FFs and beam steering angle.

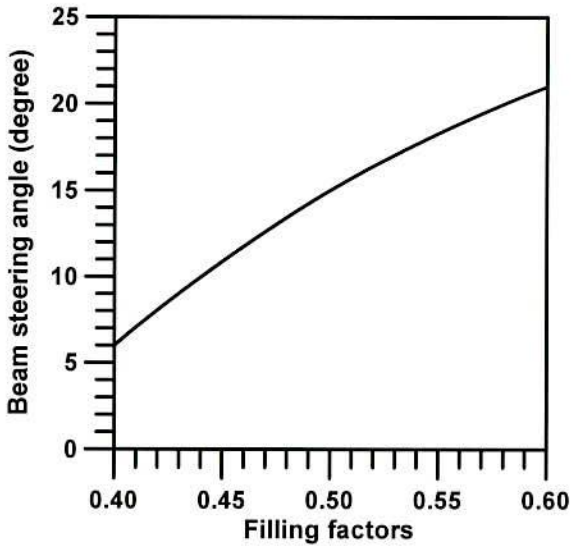

Fig. 7.9: Relationship between FFs and beam steering angle of a 4 by 1 microstrip phased arrays assisted PBGSs with different FFs having distribution of PBGSs as 0-12-18 with zero offset distance.

- **Beam Steering with different number of PBG elements**

Here different phases are used generated by varying the number of PBG elements under feed lines of PBG assisted feed networks. The radiation patterns for different distributions of PBG elements (generated by EM software PCAAD 4.0) are shown in Fig. 7.10. Here the relative phases are obtained with PBG distributions of 0-3-6-9, 0-5-10-15 and 0-8-16-24 under 4 feed networks, respectively. The FF of PBGSs is 0.5. They provide beam steering of 8, 13 and 18 degrees respectively. It can be seen that the beam steering increases with the number of PBG elements.

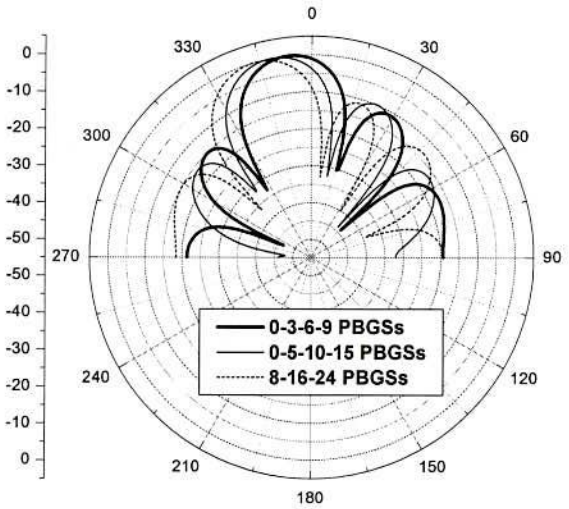

Fig. 7.10: Radiation patterns generated in PCAAD 4.0 of 4 by 1 phased arrays with different number of PBGSs under the feed lines having FF of 0.5 and zero offset distance.

- **Beam steering different offset distances**

The EM field is highly concentrated under the microstrip line. If the PBG elements are concentric then the design provides best stopband performance. Under this condition stopband is deeper and wider.

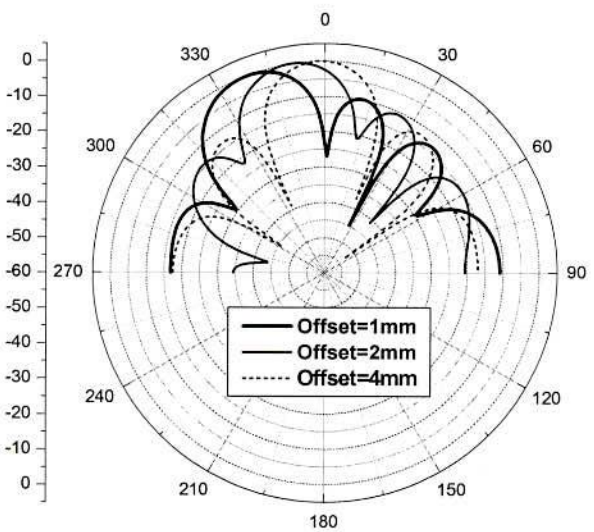

Fig. 7.11: Radiation patterns of PBG assisted phased arrays for different offset distances of PBG elements with respect to the center of microstrip transmission line.

Similarly it is seen that due to change of location of PBG elements the relative phases are changed. When the PBG elements are located exactly under the transmission line, then maximum phase shift is achieved.

PBG elements are offset from the central position. The offset distances are 1, 2 and 4 mm. Relative phases tabulated in Table 7.3 are used in PCAAD to see the radiation patterns. It can be seen that the beam steering angle decreases with offset distances. It is owing to the fact that the relative phases decrease with offset distances. The radiation patterns generated in PCAAD 4.0 is shown in Fig. 7.10. It can be seen that maximum beam steering is achieved when the offset distance is minimum. In present investigation offset distance of 1 mm provides the maximum beam steering angle of 22 degree. Offset distances of 2 and 4 mm yield beam steering angles of 10 and 1 degrees respectively. The relationship of beam steering angle and offset distances is also given in Fig. 7.12.

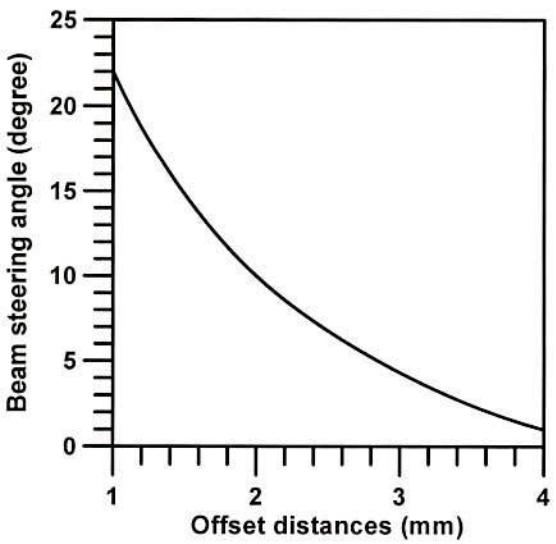

Fig. 7.12: Relationship of beam steering angle and offset distances of PBG elements under feed lines of 4 by 1 phased array antennas.

From the three investigations of FF, different numbers of PBGSs and offset distance, as shown from Fig. 7.8 to Fig. 7.12, it is observed that using large FF, number of PBGSs and offsetting the PBGSs from the center of the feed lines, a wide scan angle is achieved. In the current investigation 0.8 FF is used with the distribution of PBGSs of 0-6-12-18 and offsetting 1 to 4 mm a wide scan angle of 0 to 22 degree are achieved. Later it will be shown that offsetting from 0 to 4 mm can yield scan angle of 0 to 35 degree. This is certainly an important finding for planar phased array antenna. Mechanically offsetting the PBG assisted ground plane is much easier and cost effective compared to an electronic phase shifter. This proposition is illustrated in Fig. 7.1.

7.5 PBG Assisted Phased Array Antennas in IE3D

In the previous section PBG assisted feed networks are simulated and the phases obtained from the simulation results are used in PCAAD to see the radiation patterns of PBG assisted phased arrays. In this section the radiation patterns of different PBG assisted phased array antennas will be shown where all the designs of phased array antennas will be simulated by IE3D. Therefore mutual coupling effects are included in the computation. More realistic results are obtained from IE3D. In this section 4 patches are connected with the PBG assisted feed networks. The effects of FFs, number of PBG elements and the offset distances of PBG elements have been investigated.

- **PBG Assisted Phased Array Antennas with different FFs**

4 elements phased array antennas are investigated where the ground planes under 4 feed lines are perturbed with uniform square patterned PBG elements. Under microstrip patch antennas the ground plane is kept unperturbed. Same PBG assisted feed networks have been used that have been discussed in the previous section. A 4 elements phased array antenna assisted by square patterned PBG elements with FF of 0.8 is shown in Fig. 7.13.

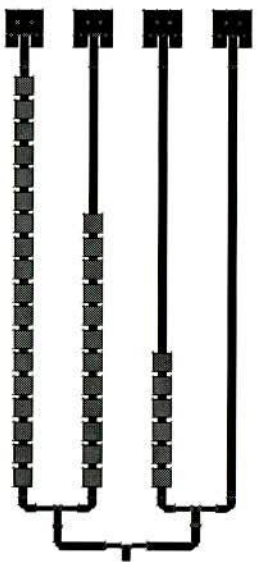

Fig. 7.13: Geometry of a PBG assisted 4 elements phased array antenna. The PBG elements are located under the feed lines having distribution of 0-6-12-18 with FF of 0.8

The distribution of PBG elements is 0-6-12-18. The radiation patterns for different designs with different FFs are shown in Fig. 7.14. It can be seen from Fig. 7.14 that the beam steering angles are 5, 15 and 20 degrees corresponding to FFs of 0.4, 0.5 and 0.6 respectively. FF of 0.8 provides more than 35 degree beam steering. It can be concluded that the beam steering angles increase with FFs.

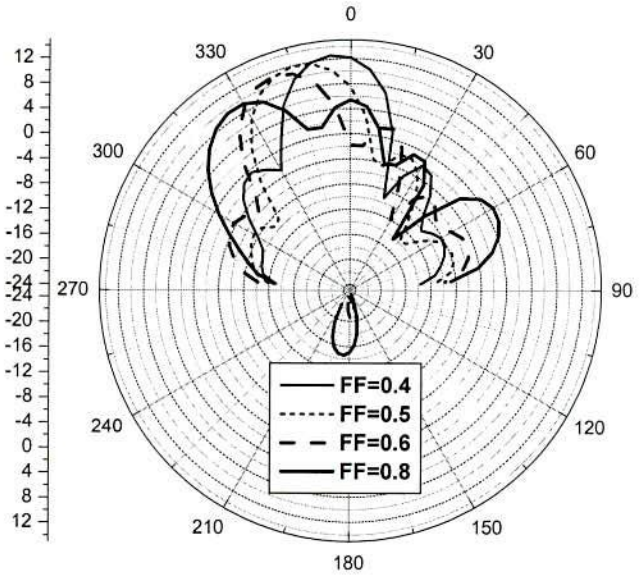

Fig. 7.14: Simulated radiation patterns of PBG assisted phased array antennas with different FFs of 0.4, 0.5, 0.6 and 0.8 respectively.

- **PBG Assisted Phased Array Antennas with Different Numbers of PBG elements**

The number of PBG elements is changed here. The designs with different PBG distributions have been simulated. The radiation patterns for different PBG distributions are shown in Fig. 7.15. PBG assisted phased array antennas have been investigated with PBG element's distribution of 0-3-6-9, 0-5-10-15 and 0-8-16-24. It can be seen that 0-3-6-9, 0-5-10-15 and 0-8-16-24 distributions of PBG elements provide approximately 7, 14 and 20 degrees beam steering respectively. The beam steering angles increase with number of PBG elements etched under the feed lines of PBG assisted phased array antennas.

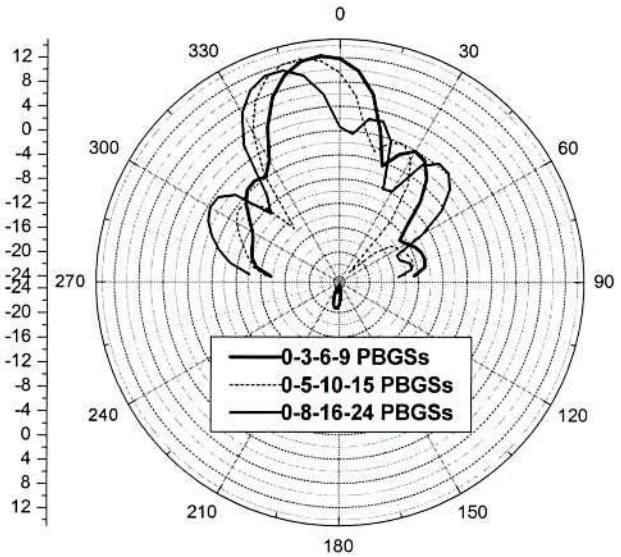

Fig. 7.15: Simulated radiation patterns of PBG assisted phased array antennas with different distribution of PBG elements having FF of 0.5 and zero offset distance.

- **PBG Assisted Phased Array Antennas with Different Offset Distances of PBG Elements**

The radiation patterns for different offset distances of PBG elements are shown in Fig. 7.16.

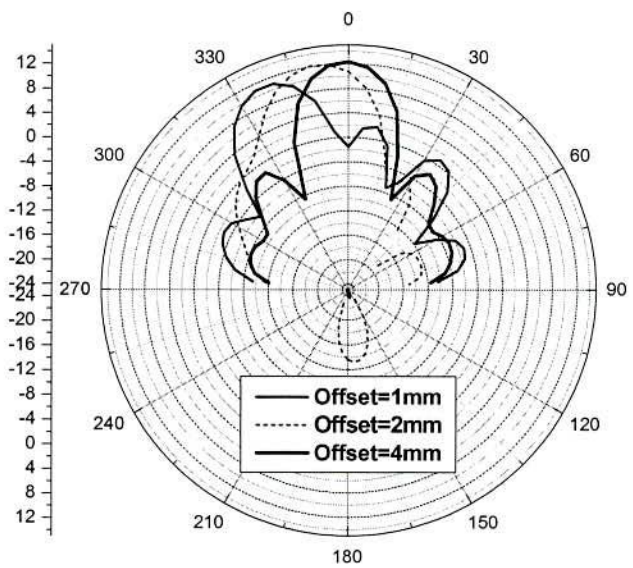

Fig. 7.16: Simulated radiation patterns of PBG assisted phased array antennas with offset distances of 1, 2 and 4 mm respectively. The distribution of PBGSs is 0-6-12-18 with FF of 0.8.

It can be seen that 1mm offset distance provides maximum steering angle of 24 degree. Offset distances of 2 and 4 mm provide 9 and 2 degrees beam steering angle respectively. The EM field is highly concentrated under the microstrip line. When the offset distance is 4 mm then the EM field is weaker within region of PBG elements. PBG elements yield smaller relative phases that in turns provides smaller beam steering angle. It is well agreed with the general concept of PBG assisted phased arrays. The comparison of beam steering performances of PBG assisted phased array antennas are shown in Table 7.4. From the Table 7.4 it is seen that the radiation patterns obtained by EM software IE 3D and PCAAD 4.0 are identical. Minor discrepancies are observed as in PCAAD no mutual coupling is considered. Simulation results in IE 3D consider the mutual coupling among all the elements and lines of the designs.

TABLE 7.4: BEAM STEERING PERFORMANCES OF PBG ASSISTED PHASED ARRAY ANTENNAS WITH DIFFERENT CONTROLLING PARAMETERS INVESTIGATED AT 8.65 GHZ

Controlling parameters		Beam steering angle (degree)	
		IE 3D	PCAAD 4.0
FFs (distributions of 0-6-12-18 PBGSs with FF of 0.5)	0.4	5	6
	0.5	15	14
	0.6	20	20
PBGSs distribution (FF of 0.5 without offset)	0-3-6-9	7	8
	0-5-10-15	14	13
	0-8-16-24	20	18
Offset distances (mm) distribution of 0-6-12-18 PBGSs with FF of 0.8	4	0	1
	2	8	10
	1	24	22

7.6 DGS Assisted Phased Array Antennas

PBG assisted microstrip lines have been investigated with different numbers of PBG elements, different FFs and offset distances. It is seen that all the parameters

have influences on relative phases. These properties have been used to develop PBG assisted phased array antennas. In this section dumbbell shape DGS assisted microstrip line will be investigated to see their relative phases. The number of dumbbell shaped DGSs etched under a standard 50-ohm transmission line will be varied. The relative phases of conventional square patterned PBGSs and dumbbell shape DGSs will be compared.

The phase properties of DGS assisted transmission lines will be implemented into 4 elements array of microstrip antennas to realize DGS assisted phased array antennas. It is already seen that EM software PCAAD and IE3D provide very similar beam steering performances. Any radiation pattern generated by PCAAD will not be produced. Rather DGS assisted phased array antennas will be simulated in IE3D with different number of DGSs and will be monitored the beam steering angles.

7.6.1 DGS Assisted Transmission Line

DGS assisted transmission line has been investigated with different elements that ranges from 1 to 8. The relative phases that are obtained from square patterned PBGSs have been compared. Same square patterned PBGSs are used that have been used in section 7.2. DGSs have same dimensions and geometry as discussed in Chapter 5. Larger square patterned slots of the DGS have the arm length of 113 mils. The narrow slots between two larger slots of dumbbell shape DGS are having dimensions of 15 by 50 square mils that is described earlier. For both PBGSs and DGSs, highest numbers of elements are 8.

7.6.2 DGS Assisted Phased Array Antennas

DGS assisted phased array antennas are investigated with the distributions of DGSs as 0-6-12-18, 0-8-16-24 and 0-12-24-36. A DGS assisted phased array antenna with distribution of DGSs as 0-6-12-18 is shown in Fig. 7.17. DGSs have been used such a way that 8.65 GHz must lie within the passband. The distribution of DGSs has been used as 0-12-24-36 under the same 4 elements array that is used for the distribution of PBGSs as 0-6-12-18. The lengths of all feed lines remain same. The substrate is Taconic having dielectric constant of 2.46 and height of 31 mils. The arm length of the larger square slot is 68.30 mils. The narrow slots between two larger slots of dumbbell shape DGS are having dimensions of 15 by 50 square mils.

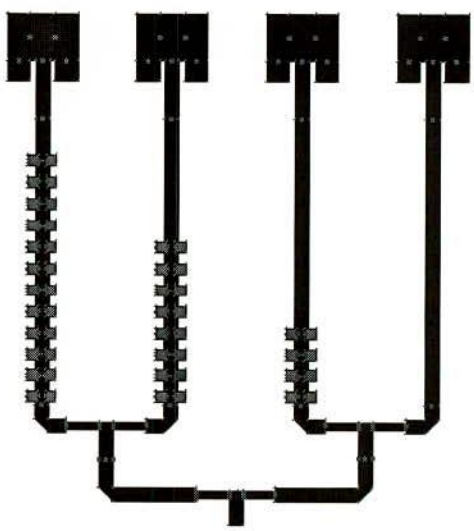

Fig. 7.17: DGS assisted phased antenna with the distribution of DGSs as 0-4-8-12.

7.6.3 Results

The phase properties at lower frequency are investigated to compare the phase properties of both PBGSs and DGSs. It is mentioned in Chapter 5 that DGS

provides compact design. For PBGS 6 GHz was within the passband. But due to compactness of DGSs, 6 GHz will lie within stopband. For this reason phase properties at 4 GHz have been investigated. 4 GHz will be far away from the edge of the stopband for the case of conventional square patterned PBGSs as the center of the stopband is 10 GHz. Under this situation phases at 4 GHz are expected to be smaller than relative phases at 6 GHz. For the case of DGSs 4 GHz will be closer to the edge of the stopband as the center of the stopband will be shifted towards lower frequencies. Thus DGSs will provide more relative phases. Phase properties of both PBGSs and DGSs are shown in Fig. 7.18. It can be seen that regular square patterned PBG elements provide much less relative phases compared to dumbbell shape DGSs. This investigation reveals the impressive agreement with the expectation.

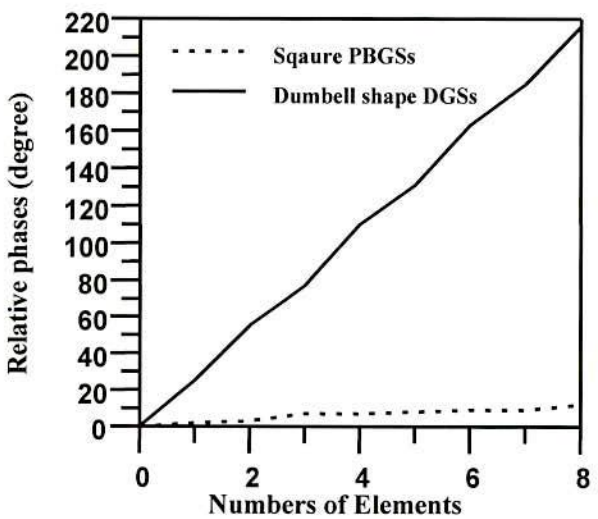

Fig. 7.18: Relative phases at 4 GHz provided by different number of square patterned PBGSs and dumbbell shape DGSs. The arm length of square patterned PBGSs is 113 mils. Larger slot of the DGSs is 113 mils and the narrow vertical connecting slot of DGSs has the dimensions of 15 by 50 square mils.

The radiation patterns for different number of DGSs distributions are shown in Fig. 7.19. It can be seen that the DGSs distribution of 0-4-8-12 provides beam steering

angle of 25 degree. Similarly the DGSs distributions of 0-8-16-24 and 0-12-24-36 yield beam steering angles of 45 and 255 (45 degree in clockwise direction) degrees respectively. The distribution of DGS as 0-12-24-36 provides vary larger relative phase shift. Therefore the beam is squinted at 45 degree in clockwise direction. Fig. 7.19 reveals important findings regarding compact design and beam steering capacity in wider ranges. These two important findings will be discussed.

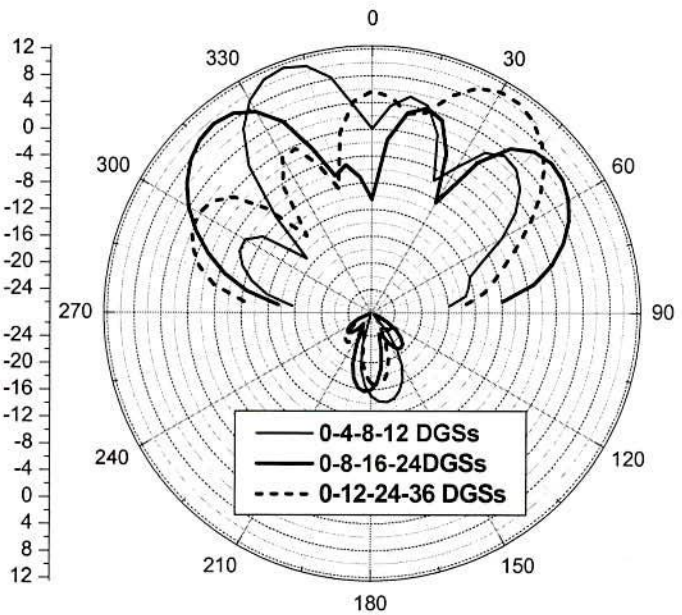

Fig. 7.19: Simulated radiation patterns of DGS assisted phased array antennas with different distributions with variable numbers of DGSs.

- **Justification of Compactness**

If a DGS assisted phased array antenna is developed with a distribution of 0-4-8-12 the feed line lengths are significantly reduced than PBG assisted antenna with same distribution. It is seen that the lengths of the DGS assisted feed networks are about to half of the length of PBG assisted feed network. The compactness is approximately 200%.

- **Beam Steering in Wider Range**

The radiation patterns of two phased array antennas will be compared. First one is PBG assisted and second one is DGS assisted phased array antenna. Both antennas have same distribution of 0-4-8-12. Radiation patterns for these two designs are shown in Fig. 7.20. It can be seen from radiation patterns shown in Fig. 7.20, that the PBG assisted phased array antenna provides beam steering of 6 degree only. On the other hand DGS assisted phased array antenna with same distribution yields about 24 degree beam steering. In this case DGS assisted antenna with same distribution provides 4 times beam steering than that of conventional square patterned PBGSs. This is obvious a noble finding to develop a phased array antenna for beam scanning in wider range.

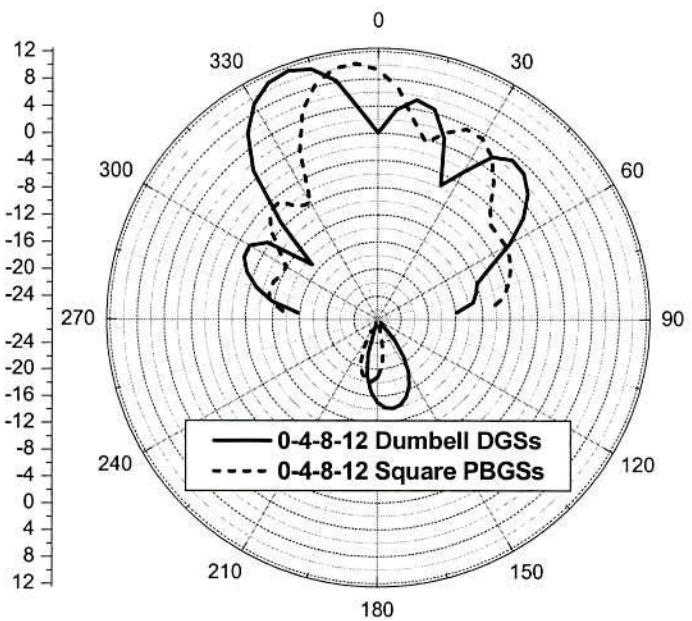

Fig. 7.20: Simulated radiation patterns of DGSs and PBGSs assisted phased array antennas with their distribution of 0-4-8-12.

The performances of DGS assisted phased array antennas with different distributions of DGSs are shown in Table 7.5. The beam steering angles of corresponding PBGS assisted phased array antennas are also given in this Table.

TABLE 7.5: COMPARISON OF BEAM STEERING CAPACITIES OF DGS AND PBGS ASSISTED PHASED ARRAY ANTENNAS WITH DIFFERENT DISTRIBUTIONS (PBGSS HAVE FF OF 0.5; THE LARGER SLOTS OF DGSS HAVE THE SAME DIMENSIONS AS PBGSS.

Distribution of PBGSs/DGSs	Beam steering angle (degree)	
	DGS	PBGS
0-3-6-9	17	7
0-5-10-15	26	14
0-8-16-24	45	20

Mainly beam steering has been focused. Later measured results of different PBG assisted phased array antennas will be shown. The distributions of PBGSs are 0-6-12-18 with FF of 0.8, 0-8-16-24 with FF of 0.8 and 0-6-12-18 PBGSs with FF of 0.8 having offset distance of 1 mm. The beam steering performances of the PBG assisted phased array antennas have mainly be reported. It can be seen from the radiation patterns that FFs, numbers of PBG elements have the effect on Gain, 3dB beamwidth and grating lobes. They will have the effect of return loss performance also. It is already mentioned that PBG assisted antenna improves return loss BW. Details studies on these parameters for the PBG assisted phased array antennas are out of the scope of the present investigations.

7.7 Experimental Investigations

It is seen that the beam steering properties of PBG assisted phased array antennas in EM software PCAAD and IE 3D. To validate their performances few designs are fabricated. Regarding FF, a prototype of PBG assisted phased array antenna is developed having distribution of PBG elements as 0-6-12-18 with FF of 0.8. The photograph of the design (Top and bottom view) is shown in Fig. 7.20. To

investigate the effect of the numbers of PBG elements in beam steering one design is fabricated having the distribution of PBG elements as 0-8-16-24 with FF of 0.5. One design is fabricated where PBG elements are offset by of 1 mm having the distribution of PBG elements as 0-6-12-18 with FF of 0.8. The photograph of the prototype is not seen here, as it is very similar to Fig. 7.21 except that PBG elements are offset by 1 mm. Top views of all the designs are same. The bottom views correspond to the perturbed ground plane. So the bottom views are shown. The bottom view of a PBG assisted phased array antenna with the distribution of PBGSs as 0-8-16-24 is shown in Fig. 7.22. Finally a DGS assisted phased array antenna is fabricated. The photograph of the bottom view of the antenna is shown in Fig. 7.23.

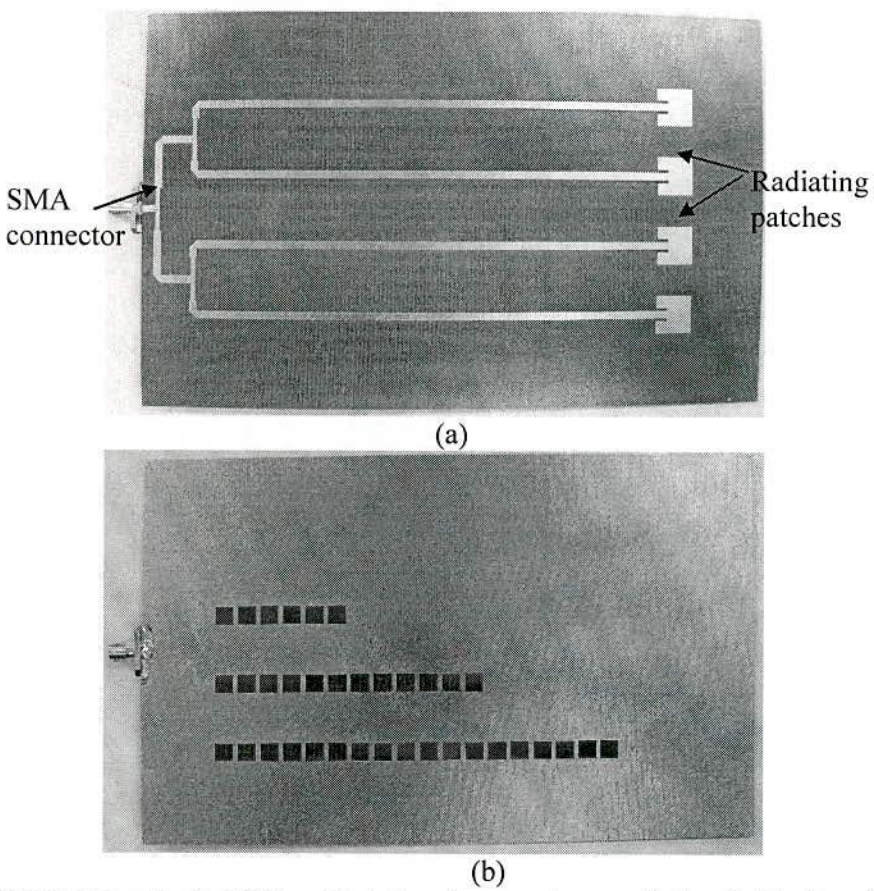

Fig. 7.21: Photograph of a PBG assisted phased array antenna with the distribution of PBG element as 0-6-12-18 with FF of 0.8; (a) top view (b) bottom view.

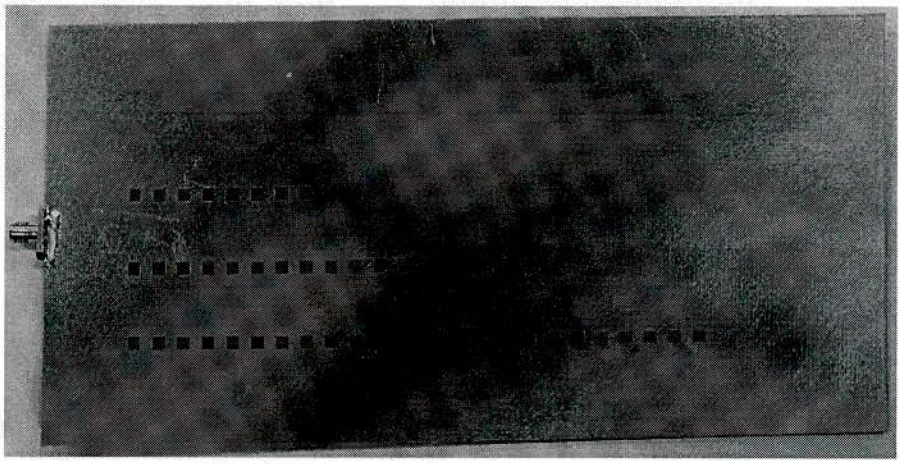

Fig. 7.22: Photograph of the perturbed ground plane of a PBG assisted phased array antenna with the distribution of PBG elements as 0-8-16-24 having FF of 0.5.

The distribution of DGS elements is 0-12-24-36 etched in the ground plane that are located exactly under the feed lines of the feed network. Large number of DGS elements is used without increasing the length of the feed lines. They are the same as PBGS assisted feed lines with the distribution of PBGSs as 0-6-12-18.

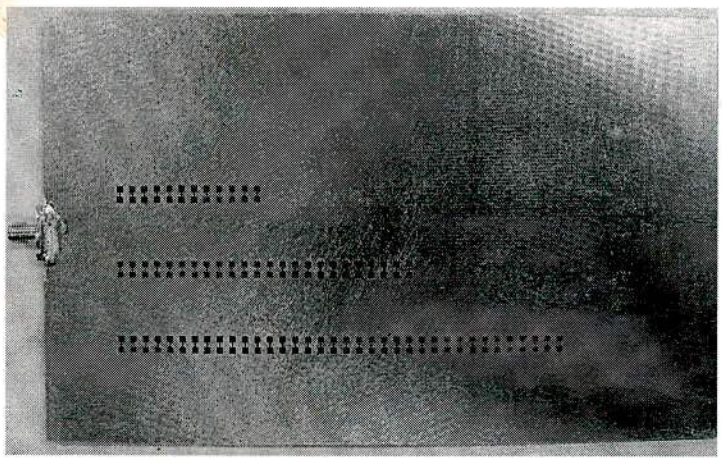

Fig. 7.23: DGS assisted ground plane of a phased array antenna with the distribution of DGS as 0-12-24-36.

7.7.1 Results

The radiation patterns of 4 prototypes of PBG/DGS assisted phased array antennas are measured in the anechoic chamber. The measured radiation patterns for 4

prototypes phased arrays are shown in Fig. 7.24. It can be seen from the Fig. 7.24 that PBG assisted phased array antenna with a distribution of uniform square patterned PBGSs as 0-12-6-18 having FF of 0.8 (without having any offset distance) provides beam steering angle of 26 degree. The same design with offset distance of PBGSs of 1mm provides beam steering of 18 degree. The distribution of PBGSs as 0-8-16-24 having FF of 0.5 without any offset distance contributes beam steering of 18 degree. It is mentioned that these PBG assisted phased array antennas yield beam squinting in anti-clockwise direction. On the other hand DGS assisted phased array antenna with the distribution of DGSs as 0-12-24-36 yields beam squinting of 43 degree in clockwise direction.

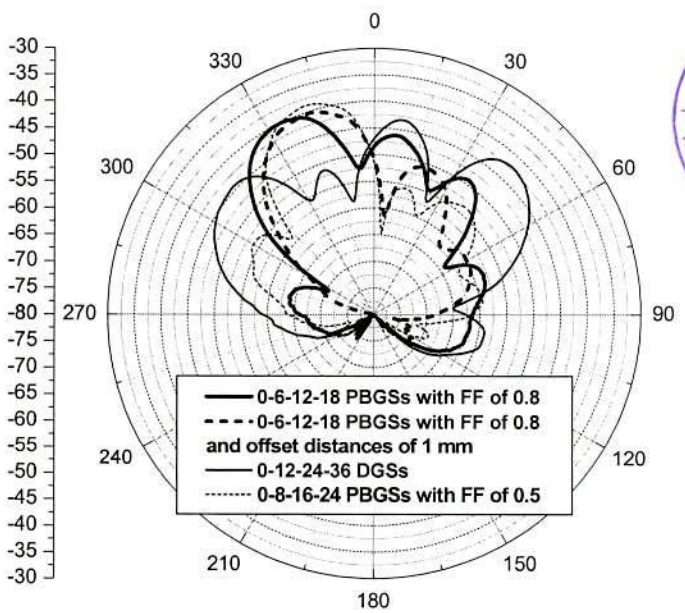

Fig. 7.24: Measured radiation patterns of PBGSs/DGS assisted 4 elements phased array antennas.

- **Comparison of Radiation Patterns**

The measured and simulated radiation patterns of a PBG assisted 4 elements phased array antennas are summarized in Table 7.7.

TABLE 7.7: COMPARISON OF SIMULATED AND MEASURED BEAM SQUINTING OF PBGSS/DGSS ASSISTED PHASED ARRAY ANTENNAS

PBGSs/DGSs distributions	Beam steering angle (degree)		3dB beamwidth (degree)	
	IE3D simulated	Measured	IE 3D simulated	Measured
0-6-12-18 PBGSs with FF of 0.8	35	26	23	20
0-6-12-18 PBGSs with FF of 0.8 having offset distances of 1mm	22	18	22	21
0-8-16-24 PBGSs with FF of 0.5	20	18	19	22
0-12-24-36 DGSs	45	43	25	23

It can be seen that the measured radiation patterns have impressive agreement with simulated beam squinting of PBG/DGS assisted phased array antennas especially for the distribution of PBGSs as 0-8-16-24 and the distribution of DGSs as 0-12-24-36 respectively. For these two cases the measured beam steering differs by 2 degree only. For the distribution of PBGSs as 0-6-12-18 without any offset distance, the difference between measured and simulated beam squinting is 9 degree. The phased array antenna with the distribution of PBGSs as 0-6-12-18 having FF of 0.5 with offset distance of 1 mm provides 4 degree difference between simulated and measured beam steering. The discrepancies may arise due to the following facts.

(1) In IE3D simulation the ground plane is considered to be infinite. But in the realistic environment the ground plane of the antenna is finite. Truncation of the ground plane affects the performances.

(2) During the measurement the orientations of antennas under test (AUT) may not be same.

(3) The cable connectors used for the antenna measurements are not considered in IE3D simulations.

7.8 PBG Assisted Reconfigurable Phased Array Antennas

EBG assisted reconfigurable phased array antenna is investigated applicable for dual-band operations. With a view to achieving dual-band operation another set of 4 antennas is connected with shorter resonant length ($\lambda g/4$ that is $1/4^{th}$ wavelength). 4 patches connected with the feed networks are known as active patches. Shorter 4 patches will be connected by PIN diode and they are known as dummy or parasitic patches. Dummy patches are connected with the active patches with associated biasing networks. During the forward bias condition of PIN diodes, total patch length increases as the patch length of the active and dummy patches are added. Over all patches resonate at lower frequency. During the reverse biased condition the resonant frequency corresponds to the length of active patches. Thus controlling the bias condition of diodes, dual band operations of antennas are achieved. To have a clear idea on the design to reconfigure the frequencies of operations one side connection of a 4 elements array is shown. One dummy patch needs two PIN diodes to be connected with one active patch. One 4 elements array requires total 8 PIN diodes. So there are total 8 biasing networks to control 8 PIN diodes. One sample connection of patches with biasing network is shown in Fig. 7.25.

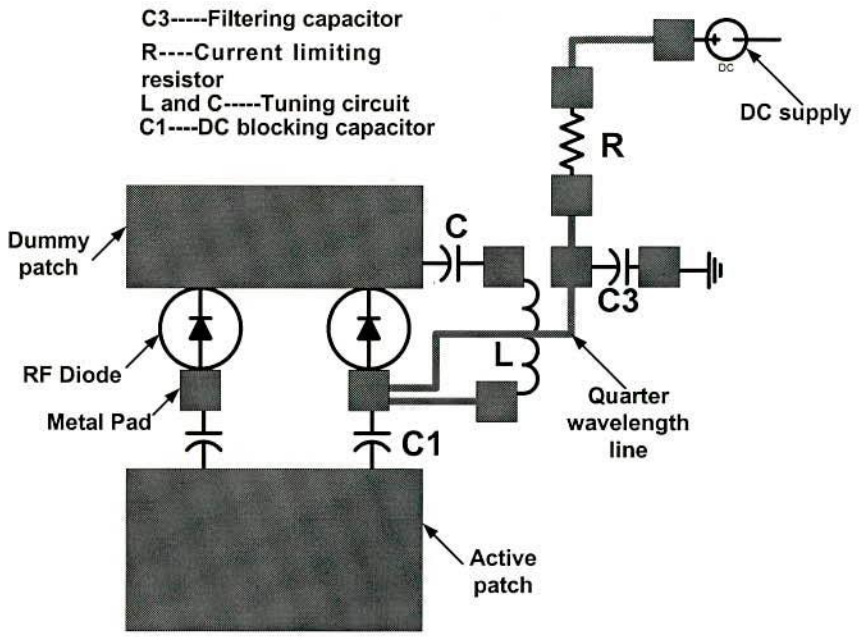

Fig. 7.25: Geometry of reconfigurable patches with associated biasing networks to control PIN diodes (only one connection has been shown).

Biasing networks consist of LC tuning circuit, filtering and DC blocking capacitors. There is also a current limiting resistor. The feed network of a PBG assisted phased array antenna is designed with the distribution of square patterned PBGSs as 0-8-16-24 having FF of 0.5. The length and width of the active patches are 11.075 mm and 11.425 mm respectively. To achieve dual-band operation another set of 4 elements dummy patches is used. The length of the dummy patch is 6.019 mm having same width.

The connections of current limiting resistors and voltage supplies are transferred to the ground plane for the minimum perturbation of the patch layer. It is shown in Fig. 7.25. Due to unavailability of X-band RF diodes conductive copper tape is connected with the active patches. The conducting copper tape has the same dimensions of dummy patches.

7.8.1 Results

The simulated return loss performances of PBG assisted reconfigurable phased array antenna are shown in Fig. 7.26. The return loss performances show two resonant frequencies at 5.6 and 8.65 GHz respectively. The input matching at 8.65 GHz is very good. When the dummy patches are connected to enhance the patch length, the resonant frequency shifts to 5.6 GHz. The input matching is poor at this frequency. The average 10 dB return loss BW at 5.6 and 8.65 GHz are 10.19% and 13.75% respectively. The maximum return loss at 5.6 and 8.65 GHz are 17 and 28 dB respectively.

It is worthwhile to mention that in Fig. 7.26 the simulation of the PBG assisted reconfigurable phased array antenna has been restricted within limited frequencies to avoid large data calculation. Therefore they look discrete rather than continuous.

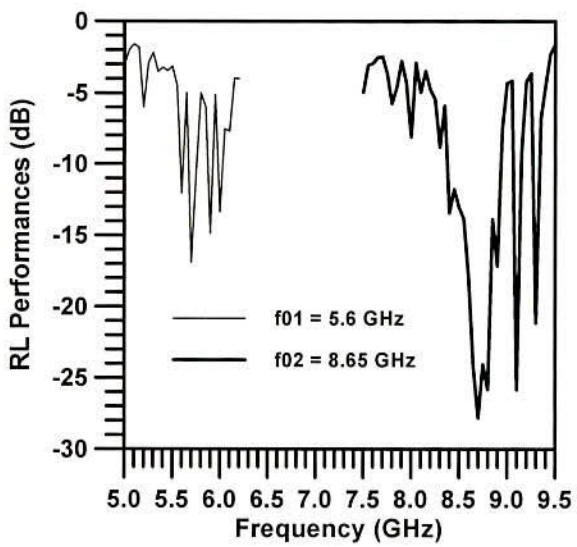

Fig. 7.26: Simulated return loss performances of a PBG assisted reconfigurable phased array antenna. Substrate: Taconic having dielectric constant of 2.45 and height of 31 mils.

The PBG assisted reconfigurable phased array antenna during the OFF period is same as PBG assisted phased array antenna. The measured return loss performances of PBG assisted phased array antenna with the distribution of PBGSs as 0-8-16-24 is shown in Fig. 7.27. It can be seen that this design provides very good matching in simulated and measured performances. So this design is preferred to develop a PBG assisted reconfigurable phased array antenna.

From the simulated radiation patterns as shown in Fig. 7.28 it can be seen that the PBG assisted reconfigurable phased array provides beam squinting at both frequencies.

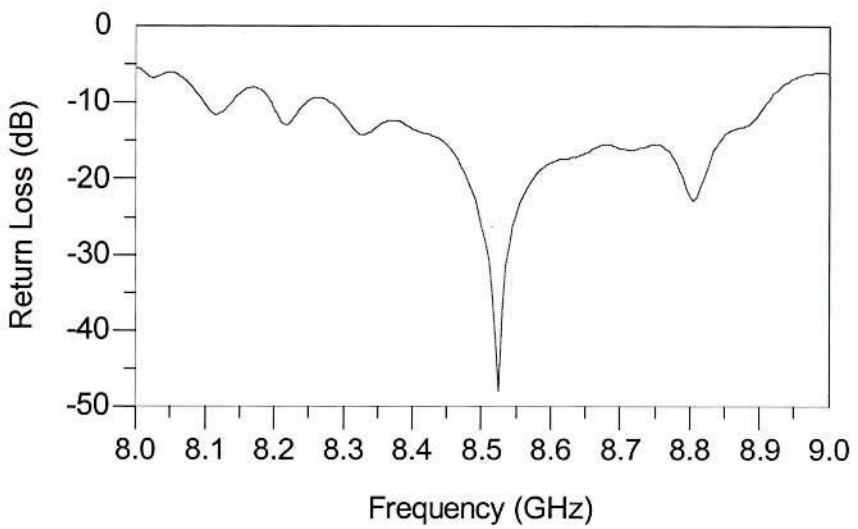

Fig. 7.27: Measured return loss performance of a square patterned PBG assisted reconfigurable phased array antenna during the OFF period of diodes. The PBGSs have distribution of 0-8-16-24 with FF of 0.5

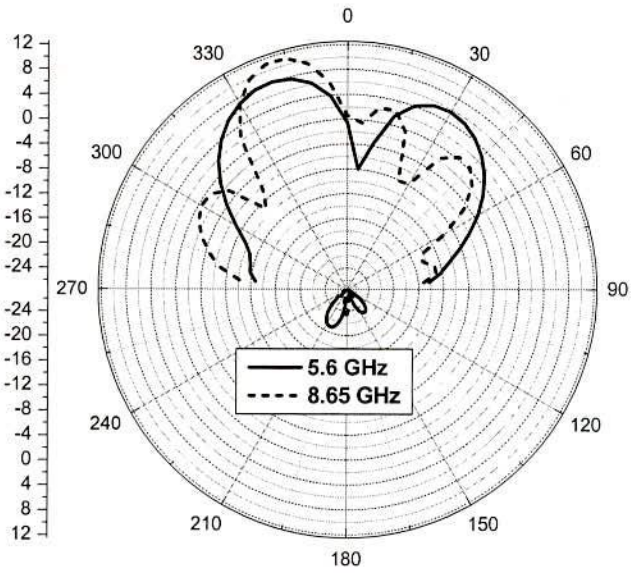

Fig.7.28: Simulated radiation patterns of a PBG assisted reconfigurable phased array antenna at 5.6 and 8.65 GHz respectively.

Conclusions

In this chapter the phase properties of a microstrip transmission line has been investigated to realize a reconfigurable ground plane for the phased array antennas. Different combinations of PBG elements in the ground plane can achieve a reconfigurable ground plane. The phase properties of a microstrip line perturbed by square patterned PBG elements having variable FFs, number of PBG elements and offset distances has been investigated. Observing the relative phase properties, PBG assisted feed networks have been designed where FFs, numbers of PBG elements and offset distances have been varied. Obtained relative phases corresponding to different designs with different parameters are used in EM software PCAAD 4.0 to investigate the beam steering properties of PBG assisted phased array antennas. It can be seen that beam steering angles increase with the FFs and numbers of PBG elements and decrease with the offset distances. The

PBG assisted feed networks have been investigated with FFs of 0.4, 0.5 and 0.6. Maximum beam steering angle of 21 degree in anticlockwise direction is achieved for FF of 0.6. Beam steering will be more if FF is increased. The number of elements is varied having the distributions as 0-3-6-9, 0-5-10-15 and 0-8-16-24. It can be seen that the distribution of PBG elements as 0-8-16-24 provides maximum beam steering of 18 degree. In case of offset distances it is seen that when PBG elements move away from the central position of the microstrip lines, the beam steering angles decrease. It can be seen that when the offset distance is 4 mm, the beam steering is found to be 1 degree only. If the offset distance is 1 mm, then steering angle is about to 22 degree. For zero offset distance beam squinting is found to be approximately 35 degree. This is due to the fact that relative phases are highly sensitive to the position of the PBG elements. If they are exactly under the lines, they provide maximum relative phases.

PBG assisted phased array antennas have also been simulated in IE3D. Similar beam steering properties have been achieved corresponding to different parameters of the designs. FF of 0.6 provides 20 degree beam steering that is same as generated by PCAAD 4.0. In case of 0-8-16-24 distributions they provide 20 degree beam steering that differs by 2 degree only with PCAAD 4.0. For the offset distance of 1 mm, radiation pattern shows 24 degree beam steering that also differs from PCAAD 4.0 by 2 degrees. The SLLs differ very significantly for all the designs. This is obvious as no mutual couplings are encountered in PCAAD 4.0. But in IE 3D mutual couplings are included in all simulations. Finally three designs have been fabricated corresponding to three parameters namely FFs,

numbers of PBG elements and offset distances. All the measured radiation patterns provide impressive agreement with simulated radiation patterns.

DGS assisted phased array antennas have been simulated. The investigation is confined into different numbers of DGS elements. The designs are simulated with the distributions of DGS as 0-3-6-9, 0-5-10-15 and 0-8-16-24. The beam steering angles are found to be 17, 26 and 45 degrees respectively. It is interesting to note down that DGS is a compact design. So the distribution of DGSs could be placed as 0-12-24-36 under the feed lines that correspond to the distribution of PBGSs as 0-6-12-18. It can be seen that 0-12-24-36 DGSs provide beam steering angle of 255 degree (45 degree beam squinting in clockwise direction). This is due to the fact the DGSs provide more relative phase shift than PBGSs. The finding of DGS assisted phased array antenna is novel.

Few designs have been fabricated and measured radiation patterns in the chamber. The measured and simulated radiation patterns have good agreement with minor discrepancies. Impressive agreement between measured and simulated radiation patterns are achieved for the distribution of PBGSs as 0-8-16-24 and the distribution of DGSs as 0-12-24-36. From all the theoretical and experimental investigations it can be concluded that FFs, number of elements and offset distances are very important parameters to develop PBG assisted phased array antennas. DGSs are more compact than PBGSs and have wider beam squinting capabilities.

In the development of reconfigurable phased array antenna the distribution of PBGSs of 0-8-16-24 have been used as this configuration provides better return

loss performance. From the simulation result of the return loss performance, it can be seen that the design yield maximum return loss of 27 dB for the antenna operating frequency of 8.65 GHz. When the antenna length is increased by $\lambda_g/4$ then the resonant frequency is shifted to 5.6 GHz.

Chapter 8 Conclusions and Future Works

8.1 Conclusions

The work presented in this thesis has been concerned with PBG assisted antennas, filters and phased arrays. At present PBG engineering is an especial area in microwave engineering. PBGSs are found to be very attractive in different microwave devices and components. The open literature has been surveyed very thoroughly to find their applications including their limitations [35]. PBGSs are periodic in nature. PBG theories have been reviewed to understand the passband-stopband and SW phenomena of PBGSs. The depth and width of the stopband depends on few factors like FFs, number of elements, periods and substrate properties. Uniform circular and square patterned PBGSs have been investigated with variable number of PBG elements. The stopband-passband properties are reported by S-parameters performances. Different shapes of the PBG elements and different lattice structures have been shown. Three rows of circular uniform circular PBGSs under the standard 50-ohm transmission line have been simulated. Comparing with the result of one row circular uniform circular PBGSs it is found that three rows of uniform circular PBGSs and one row of uniform circular PBGSs yield very identical S-parameters performances. So only 1-D uniform circular PBGSs have been used onward.

8.2 Fulfilling the Goal of the Thesis

In chapter 4 it is seen that the conventional hole patterned PBGSs suffer from constrained optimized value of FF in the application as a low-pass filter. In this

work a lot of efforts are devoted to find a novel configuration of PBG elements to replace the conventional hole patterned PBG elements. Their filtering properties have been mentioned in details to see the improved performance over the conventional hole patterned PBG elements. The conventional hole patterned PBGSs are found to have poor performance mainly in passband and their performances are hindered by the limiting value of FF.

The alternatives in the form of hole and ring patterned PBGSs with non-uniform amplitudes based on Binomial and *Chebyshev distributions* have been proposed. Standard 50-ohm transmission lines are simulated on Binomially distributed PBGSs having FF = 0.3, 0.4 and 0.5 at 9, 10.5 and 12 GHz respectively. From all these simulation it is seen that the Binomially distributed PBGSs provide better results than uniform circular PBGSs. It is observed that 0.4 may be considered as the approximate value of optimized FF. It is better to note down there is still scope to investigate the value of optimum FF within the intermediate values ranging from 0.4 to 0.5. This is the first time report about the approximate value of optimum FF for Binomially distributed PBGSs. The present research has also revealed the frequency dependence of the performance. It is important to note that frequency shifting is common feature of PBG structures. The center frequency is controlled by the period of the PBG lattice structure that is determined from the Bragg's condition. So frequency shifting can be optimized by the proper choice of period of PBGSs. In the simulation results, conductor loss, substrate loss and the loss due to connectors are not included. Above all, all the simulations have been done on infinite ground plane (ignoring truncation). All the structures are fabricated using milling machine. So there are fabrication errors. This type of error may cause

variations in size and period of the lattice structures resulting in the variation in the magnitude of S-parameters and the frequency of interests.

Microstrip lines perturbed by PBG structures with *Chebyshev distribution* have been designed and analyzed at 9, 10.5 and 12 GHz for FF = 0.3, 0.4 and 0.5 respectively. Total nine designs have been investigated from which the approximate value of optimum FF for *Chebyshev distribution* of PBGSs can be obtained. In terms of passband ripple height, isolation, passband return loss BW and stopband it can be concluded that 0.4 is the approximate value of optimum filling factor. The frequency dependence of the performance of *Chebyshev* distributed PBG structured transmission line has been investigated. It is observed that the maximum rejection bandwidth is obtained at 9 GHz and the maximum passband is achieved at 12 GHz. The maximum isolation is seen at 10.5 GHz. The minimum return loss is found at 9 GHz.

A novel PBG engineered microstrip transmission line has been designed and investigated theoretically by tapering and chirping the PBGSs. The amplitude has been tapered with the *Chebyshev* distribution on the other hand the chirping has been applied as per [75]. The over all performance of the proposed model is always superior to conventional hole patterned PBG structured transmission line. Even the new model stems the superiority over the author's recent work [35] on periodic PBGSs with *Chebyshev distributions*. The present work has been extended further where both the tapering of the amplitudes of the PBG elements and the chirping are done on the basis of *Chebyshev* polynomial. The PBGSs with *Chebyshev* distribution (both Type-A and Type-B) have been investigated. It is pleasant to observe that simple change in the design provides enormous rejection bandwidth.

In chapter 5 conventional DGSs have been reported. Very few works on DGSs are found in the open literature. Some parametric studies of DGSs have been accomplished. Among them the effect of the width of the narrow connecting vertical slot of dumbbell shaped DGS is novel investigation. Non-uniform DGSs and hybrid DGSs have been investigated. The hybrid DGSs are realized by placing conventional square patterned PBGSs in between conventional DGSs. The hybrid DGSs with non-uniform distribution provides excellent performance as LPF. *Chebyshev* distribution has been used in calculating the amplitudes of the PBG elements. The depth and width of the stopband of such structures that is reported in [61] [105] are rarely found in the literature. A new concept of generating a compact dual-band filter has been introduced. Extra one larger square patterned slot is connected with the conventional DGSs and the microstrip line is located above middle larger slot having concentric orientation. It has been called as modified DGSs. Again hybrid DGS is developed by placing conventional square PBGSs in between modified dumbbell shape DGSs. Modified dumbbell shape DGSs with *Chebyshev* distribution that are hybrid in nature provide the performance of dual stopband filter.

In chapter 6 the performance of PBG assisted antennas has been mentioned. The return loss BW, directivity, gain are investigated for various number of ring patterned PBG assisted ACPA. It can be seen that all the performances can be optimized with the number of PBG elements. The return loss BW and gain are increased for dual-band ACPA due to the application of circular PBG elements. It is also seen that matching is improved in a PBG assisted antennas. Double-layered PBG elements provide best input matching.

In microwave engineering the harmonic suppression in BPF is an important and demanding task. In chapter 6 PBG assisted BPF with uniform circular PBGSs and B-PBGSs have been investigated. Both configurations provide harmonic suppression. The superior performance is achieved with B-PBGSs. DGSs have been implemented in harmonic suppression. It can be seen that DGSs can suppress both second and third harmonics significantly.

In chapter 7 the phase properties of a PBG engineered microstrip transmission line are described very elaborately. The relative phases are changed with FFs, number of PBG elements and location of the PBG elements. Later this concept is used in case of beam steering of PBG assisted phased array antenna. It can be seen that beam squinting increases with FFs and number of PBG elements and it decreases with the offset distances.

The beam steering properties have been shown by the use of PBG elements under the feed line. DGS assisted phased array antenna provides more beam squinting than that of PBG assisted phased array antenna. On the other hand the frequency agility properties are achieved by changing the patch length with the help of PIN diode. To control the diode's action biasing network has been provided. The simulated results have only been shown. Experimental verification can further be done with the proposed reconfigurable ground plane. Thus dual-band operation of a phased array antenna is achieved by the forward and reverse bias action of PIN diodes.

8.3 Recommendation for Future Work

In the whole research work, attention has been paid to simulate all the structures by commercial EM software **Zeland IE3D. I**nvestigations are justified experimentally. The performances of PBG engineered transmission lines are measured by VNA and compared with simulated results. VNA measured the return loss performance of the antennas. The reconfigurable phased array antenna has not been investigated experimentally during the ON period of diodes due to unavailability of RF diode switches designed at X-band. This has been left as future work. The future work can be mentioned in the following manner.

8.3.1 Results Validated By Theoretical Modeling

The PBGS are actually complex geometries. For such geometries it is a difficult task to calculate the value of propagation constant. However the wise solution to the exact eigenvalue equation for the 1-D PBGS can be obtained through the use of the Fourier series. It is known as analytical techniques of the plane wave expansion method. The formulation can be derived for transverse electric or transverse magnetic case. The electric field/magnetic field of periodic structures can be expressed with the propagation constant and the period of the structure. Applying the required useful vector operator yield the simplified differential equation that can be expanded by Fourier series. Fourier series can also represent the dependence of dielectric constant in a periodic structure. These double representations of Fourier series yield a Kronecker delta function over a unit cell of PBGS. This equation can have a general matrix form. Writing the code in

MATLAB can solve a generalized linear Eigen system. Then correct picture of passband characteristics could be found out, namely the slow wave factor (SWF) that is useful to calculate the value of compactness of the design. The stopband performance can also be explained nicely by calculating the propagation constant. There is another option to calculate the input impedance of the structure, as at stopband the input impedance will be very larger showing the surface to be perfectly magnetic conductor. In this way the numerical results could be compared with the theoretical and measured results that would give more insight of the present research. The mathematical formulation can also be done by immittance approach [104]. The analytical model can also be developed by the procedure mentioned in [106]-[111].

8.3.2 Reconfigurable Ground Plane

The development of a reconfigurable ground plane needs high-speed and low loss switches. In this regards, MEMS switches [112]-[118] are very potential candidates. They may be used in the ground plane of feed network to reconfigure the ground plane. The reconfigurability can be achieved by many ways such as using the parameters of FFs, number of PBG elements and locations of the PBG elements. Even many combinations of these parameters can be utilized to steer the beam in desired directions. Alternatively PBG engineered ground plane may be rotated to set proper PBG elements under all the feed lines. A mechanical arrangement can be set up for this purpose.

8.3.3 Development of Algorithm

The beam squinting of PBGS/DGS assisted phased array antennas have been investigated. It has been observed that FFs, numbers of elements and offset distance can control relative phase properties. So an algorithm can be developed to integrate these three parameters to steer the beam in any required direction. Even the combinations of these three parameters can steer the beam of PBGS/DGS assisted phased array antennas in wider range. A suitable algorithm can accomplish this novel task easily. Regarding reconfigurable phased array antenna the algorithm is more useful for phase compensation. When the RF diodes are ON then the patches resonate at lower frequencies that may cause to yield in sufficient relative phases. The algorithm can help manage the PBGSs to provide sufficient phase.

List of Publications

A. Book Chapter

1. N. C. Karmakar and M. N. Mollah, "Electromagnetic Bandgap (EBG) for Bandpass Filters," *Encyclopedia of RF and Microwave Engineering,* January 2005 by John Wiley, USA

B. Journal Papers

- **Published/ Accepted**

[2] Md. Nurunnabi Mollah and Nemai C Karmakar, "Uniform Circular PBGSs under BPF for Harmonic Suppression," *International Journal of Telecommunication, Elsevier Science, Germany*

[3] Md. Nurunnabi Mollah and Nemai C Karmakar, Jeffrey Shiang Fu, "Investigation into Chirped Chebyshev distributed PBGS, "Accepted to be published in *International Journal of Infrared and Millimeter waves*, 2005, USA

[4] Md. Nurunnabi Mollah and Nemai C Karmakar, "Binomially Distributed PBG Structures in Harmonic Suppression," Accepted to be published in *International Journal of RFMiCAE, 2005, USA*

[5] Md. Nurunnabi Mollah and Nemai C Karmakar, Jeffrey Shiang Fu, " Novel tapered hybrid defected ground structure," Accepted to be published in *International Journal of RFMiCAE*, 2005, USA

[6] Md. Nurunnabi Mollah and Nemai Chandra Karmakar, "Compact hybrid defected ground plane," *Microwave and Optical Tech. Lett.,* vol. 44, no. 3, pp.266-270, Feb. 2005, USA

[7] Md. Nurunnabi Mollah and Nemai Chandra Karmakar, "Pure harmonic suppression of a bandpass filter using Binomially distributed photonic bandgap

structures," *Microwave and Optical Tech. Lett.,* vol. 44, no. 2, pp. 194-196, Jan 2005, USA

[8] Nemai Chandra Karmakar C and Mohammad Nurunnabi Mollah, "Potential applications of PBG engineered structures in microwave engineering – part two," *Microwave Journal,* vol. 47, no. 9, pp. 122-138, September 2004, USA

[9] Nemai Chandra Karmakar and Md. Nurunnabi Mollah, "Potential applications of PBG engineered structures in microwave engineering – part one," *Microwave Journal*, vol. 47, no. 7, pp. 22-44, July 2004, USA

[10] N. C. Karmakar and M. N. Mollah, "Investigations into nonuniform photonic-bandgap microstrip line filters," *IEEE Trans. Microwave Theory Tech.*, vol. 51, no. 2, pp. 564-572, Feb. 2003

[11] N. C. Karmakar and M. N. Mollah, "Microstrip lines on annular-ring photonic bandgap structures," *Microwave and optical Tech. Lett.* vol. 32, no. 6 pp., 431-433, March 20, 2002

[12] Nemai C. Karmakar and M. N. Mollah, "Investigations into planar photonic bandgap microstrip lines," *Electrical and Electronic Engineering Research,* pp. 36-37, Jan. 2002 School of EEE, NTU, Singapore 639798

C. International Conference Papers (Accepted/published)

[13] Nemai Chandra Karmakar and Md. Nurunnabi Mollah, "Novel Chirped *Chebyshev* EBGS," *IEEE-ICECE-2004,* Bangladesh

[14] Md. Nurunnabi Mollah and Nemai Chandra Karmakar, "Dumbbell Shaped DGS Assisted Bandpass Filter," *IEEE- ICECE-2004,* Bangladesh

[15] Md. Nurunnabi Mollah and Nemai Chandra Karmakar, "EBG Engineered Phased Array Antenna," *IEEE-ICECE-2004,* Bangladesh

[16] M. N. Mollah and N. C. Karmakar, "PBG Assisted Phased Array Antenna" *APMC-2004,* Delhi, India

[17] M. N. Mollah and N. C. Karmakar, "A Novel Hybrid Defected Ground Structure" *APMC-2004,* Delhi, India

[18] M. N. Mollah and N. C. Karmakar, "A novel hybrid defected ground structure as low pass filter," *IEEE APS-S International* 2004, Monterey, California, USA, June 20-26, 2004

[19] M. N. Mollah and N.C. Karmakar, "Effect of substrates on S-parameter performances of 1-D circular uniform photonic bandgap structures (uniform circular PBGS)," *IEEE APS-S International* 2004, Monterey, California, USA, June 20-26, 2004

[20] Mohammad N. Mollah and Nemai C. Karmakar, "Investigation into Planar Photonic bandgap Structures," *Asia-Pacific Microwave Conference (APMC)-2003,* Korea Nov. 4-7, 2003

[21] Mohammad N. Mollah and Nemai C. Karmakar, "Aperiodic Non-uniform Photonic bandgap Structures," *Asia-Pacific Microwave Conference (APMC)-2003,* Korea Nov .4-7, 2003

[22] Mohammad N. Mollah and Nemai C. Karmakar "A compact Photonic Bandgap Assisted Phased Array antenna," *APMC-2003,* Korea Nov. 4-7, 2003

[23] M. N. Mollah and N.C. Karmakar, "Investigation of matching into PBG assisted VSAT antennas," *ICICS-2003,* Singapore

[24] M. N. Mollah and N.C. Karmakar, "Effect of number of uniform photonic bandgap (U-PBG) elements on the performance of microstrip transmission lines," *PACRIM-2003,* Victoria, Canada

[25] M. N. Mollah and N.C. Karmakar, "Optimum filling factor and performance of a transmission line at x-band perturbed by Binomially distributed photonic bandgap structure," *PACRIM-2003,* Victoria, Canada

[26] Nemai C. Karmakar and Mohammad N. Mollah, "Harmonic suppression of bandpass filters with photonic bandgap structure," 2003 *IEEE* International Antennas and Propagation Symposium and URSI North American Radio Science Meeting, Columbus, Ohio, USA, June 22-27, 2003

[27] N. C. Karmakar, M. N. Mollah, and S. K. Padhi "Planar Electromagnetic Bandgap Structures - Paradigm Lowpass Filters," *Proceedings of Progress In Electromagnetic Research 2003*, 07-10 Jan. 2003, Singapore, pp. 135

[28] N. C. Karmakar, M. N. Mollah, and S. K. Padhi, "Novel Planar Photonic Bandgap Structures," *2002 Asia-Pacific Microwave Conference* (APMC 2002) *Proceedings*, vol. 2, pp. 1173-1176, Kyoto, Japan, 19-22 Nov. 2002

[29] N. C. Karmakar, M. N. Mollah, and S. K. Padhi, "Shared Aperture Photonic Bandgap Assisted Aperture Coupled Microstrip Patch Antenna For Satellite Communication," *Asia-Pacific Microwave Conference* (APMC 2002) *Proceedings*, vol. 2, pp. 1177-1180, Kyoto, Japan, 19-22 Nov. 2002

[30] Nemai C. Karmakar, Mohammad N. Mollah, and Shantanu K. Padhi, " Photonic bandgap assisted aperture coupled patch antennas," *IEEE* International Antennas and Propagation Symposium and URSI North American Radio Science Meeting, 2002, 16-21 June, vol. 3 pp. 772-775 Texas, USA

[31] N. C. Karmakar and M. N. Mollah, "Improved performance of a non-uniform ring patterned PBG assisted microstrip line," *IEEE* International Antennas and Propagation Symposium and URSI North American Radio Science Meeting, 2002, 16-21 June, vol. 2 pp. 848-851, Texas, USA

[32] Mohammad N. Mollah and Nemai C. Karmakar, "RF-MEMS switches: paradigms of microwave switching," *APMC,* 2001, vol. 3, pp. 1024-1027, Dec. 2001, Taiwan

[33] M. N. Mollah and N. C. Karmakar, "Planar PBG structures and their applications to antennas," *IEEE* International Antennas and Propagation Symposium and URSI North American Radio Science Meeting, *2001*, vol. 2 pp. 494-497, 10th July, Boston, USA

D. Submitted (Journal)

[34] Md. Nurunnabi Mollah and Nemai C Karmakar, Jeffrey Shiang Fu, "Filling factor controlled EBGS assisted phased array antenna," International Journal of *RFMiCAE, USA*

[35] Nemai Chandra Karmakar, Md. Nurunnabi Mollah, Shantanu Kumar Padhi and Rita Lim Li Ling, "Investigations into Planar Electromagnetic Bandgap," *IEEE-Transactions on Microwave Theory and Technique*

[36] Md. Nurunnabi Mollah, Nemai C Karmakar and Jeffrey S. Fu, "Investigation into Dumbbell Shaped DGS Assisted Bandpass Filter," *IEEE- Transactions on Microwave Theory and Technique*

[37] Jeffrey S. Fu, Md. Nurunnabi Mollah, and Nemai C Karmakar, "Investigation into Metallic Perturbed Photonic Bandgap (PBG) Structures," *IEEE-Transactions on Electromagnetic Compatibility*

[38] Nemai C Karmakar, Md. Nurunnabi Mollah, and Jeffrey S. Fu, "PBG Assisted Shared Aperture Dual-Band Aperture Coupled Patch Antenna For Satellite Communication," *Microwave and Optical Tech. Lett. USA*

[39] Md. Nurunnabi Mollah, Nemai C Karmakar and Jeffrey S. Fu, "Matching Improvement of VSAT Antennas by Non-uniform PBGS," *IEEE-Transactions on Vehicular Technology*

[40] Md. Nurunnabi Mollah and Nemai C Karmakar, Jeffrey Shiang Fu, " Investigation into DGS Assisted Phased Array Antenna," *IEEE-Transaction on Antenna and propagation*

[41] Jeffrey S. Fu, Mohammad Nurunnabi Mollah, and Nemai Chandra Karmakar "Electromagnetic Bandgap (EBG) Structures for Reconfigurable Antenna," *International Journal of Infrared and Millimeter waves, USA*

[42] Md. Nurunnabi Mollah and Nemai C Karmakar, Jeffrey Shiang Fu, "Developing Phased Array Antenna by Varying Number of 1-D EBG elements," *IEEE-Transaction on Vehicular Technology*

[43] Md. Nurunnabi Mollah and Nemai C Karmakar, Jeffrey Shiang Fu, "1-D DGS and its application in Antennas and Filters," *IEE Proceedings*

[44] Md. Nurunnabi Mollah and Nemai C Karmakar, Jeffrey Shiang Fu and A. Alphones, "Novel Phased array antenna by offsetting EBG elements," *IEEE – Transactions on Antenna and Propagation*

[45] Md. Nurunnabi Mollah and Nemai C Karmakar, Jeffrey Shiang Fu and A. Alphones, "Theoretical Investigation into Square Patterned 1-D PBG Assisted Phased Array Antenna," *APMC-2005*

References

[1] D. Sievenpiper, L. Zhang, R. F. J. Broas, N. G. Alexopolous, and E. Yablonovitch, "High-impedance electromagnetic surfaces with a forbidden frequency band," *IEEE Trans. Microwave Theory Tech.,* vol. 47, no.11, pp. 2059-2074, Nov. 1999.

[2] K-C.CHEN, C-K.C.TZUANG, Y. Qian, and T. Itoh "Leaky properties of microstrip above a perforated ground plane," *Microwave symposium digest. IEEE MTT-S Int.* vol. 1, pp. Page(s) 69-72, 1999.

[3] Y. Qian, D. Sievenpiper, V. Radisic, Y. Yablonovitch, and T. Itoh, "A novel approach for gain and bandwidth enhancement of patch antenna," *Radio and wireless conference, 1998, RAWCON98, 1998.*

[4] Y. Qian, R. Coccioli, D. Sievenpiper, V. Radisic, E. Yablnovitch and T. Itoh, "Microstrip patch antenna using novel photonic band-gap structures," *Microwave J.,* vol. 42, no. 1, pp. 66-76, Jan 1999.

[5] R. Coccioli, F-R. Yang, K-P Ma, and T. Itoh, "Aperture-coupled patch antenna on UC-PBG substrate," *IEEE Trans. Microwave Theory Tech.,* vol. 47, no. 11, pp. 2123-2130, Nov. 1999.

[6] R. Gonzalo, P. D. Maagt, and M. Sorolla, "Enhanced patch antenna performance by suppressing surface waves using photonic-bandgap substrates," *IEEE Trans. Microwave Theory and Tech.,* vol. 47, no. 11, Nov. 1999.

[7] E. Yamashita and Y. Qian, "Analysis of microwave circuits and planar antennas using the FDTD method," *Realize Inc., Tokyo, May 1996.*

[8] K.M. Shum, Q. Xue, C. H. Chan and K. M. Luck "Investigation of microstrip reflectarry using a photonic using a photonic bandgap structure." *Microwave and Opt. Tech. Lett.,* vol. 28, no. 2, pp. 114-116 Jan.20, 2001.

[9] P. S. Hui and A. Alphones, "Microstrip patch antenna with annular ring PBG," *APMC 2000*, Sydney Australia.

[10] R. Gonzalo, B. Martinez, P.D. Maagt, and M. Sorolla "Patch antennas on photonic crystal structures." http://www.ecs.umass.edu/ece/allerton/99/34/

[11] E. R. Brown, C. D. Parker, and E. Yablonovitch, "Radiation properties of a planar antenna on a photonic-crystal substrate," *J. Opt. Soc. Amer. B. Opt. Phys.*, vol. 10.no. 2, pp. 404-407, Feb.1993.

[12] S. K. Sharma and L. Shafai, "Enhanced performance of an aperture-coupled rectangular microstrip antenna on a simplified unipolar compact photonic bandgap (UC-PBG) structure," *IEEE-APS Digest 2001*, pp. 498-501.

[13] A. Byers, I. Rumsey, Z. Popovic, and M-P-May, "Surface-wave guiding using periodic structures," *APS-International symposium, 2000, IEEE,* vol.1, 2000, page(s): 342-345.

[14] D. Sievenpiper and E. Yablonovitch, "Eliminating surface currents with metallodielectric photonic crystals," *IEEE Int. Microwave Symp. Dig.,* Baltimore, MD. June 7-12, 1998. pp. 663-666.

[15] R. Kim and H.Y.D. Yang., "Surface waves and leaky waves in integrated circuit structures with planar periodic dipole loading," *APS-International symposium, 2000, IEEE*, vol. 1, page(s): 346-349.

[16] R. Coccioli and T. Itoh "Design of photonic band-gap substrates for surface waves suppression," *Microwave symposium digest. IEEE MTT-S Int.* vol. 3, pp. 1259-1262 1998.

[17] K-P. Ma, J. Kim, F-R. Yang, Y. Qian, and T. Itoh, "Leakage suppression in stripline circuits using a 2-D photonic bandgap lattice," *Microwave symposium digest, IEEE MTT-S Int.* vol.1, Page(s) 73-76, 1999.

[18] B. Elarman *et al.,* "A beam-steerer using reconfigurable PBG ground plane," *Microwave symposium digest,* 2000 *IEEE MTT-S Digest* pp. 835-838.

[19] Chul-Soo Kim, Jun-Seok Park, Dal Ahn, and Jae-Bong Lim, "A Novel 1-D Periodic Defected Ground Structure for Planar Circuits," *IEEE-MWCL,* vol.10, no. 4, pp.131-133, April 2000.

[20] Paul J. Schields, "Bragg's Law and Diffraction," Center for High Pressure Research, State University of New York, Stony Brook, NY 11794-2100. http://www.eserc.stonybrook.edu/ProjectJava/Bragg/

[21] K. Sato, K. Nishikawa, and T. Hirako, "Development and field experiment of phased array antenna for land vehicle satellite communications," *1992 IEEE MTT-S Digest*, pp. 1073-1076.

[22] P. C. Strickland, "Planar arrays for MSAT and INMARSAT land mobile satellite communications," 1995 *IEEE MTT-S Digest* pp. 1388-1391.

[23] R. S. Francian, H.H. Chung, and S. Y. Peng, "A hybrid scanned conformal planar array for mobile satellite communications," *APS-International symposium, 1989, IEEE*, vol.1, page(s): 686-689.

[24] J. D. Kraus, Antennas, 2nd Edition, McGraw Hill, New York, NY, 1988.

[25] D. M. Pozar, "Microstrip Antennas," *Proc. IEEE,* vol. 80, no.1, pp. 79-81, Jan. 1992.

[26] S. B. De Assis Fonseca and A. J. Giarola, "Microstrip disk antenna, Part II: The problem of surface wave radiation by dielectric truncation," *IEEE Trans. Antennas Propogat.,* vol.32, no. 6, pp. 568-573 June 1984.

[27] R. J. Mailoux, "On the use of mettalized cavities in printed slot array with dielectric substrates," *IEEE Trans. Antennas Propgat.,* vol. 35, no. 5, pp. 477-487, May 1987.

[28] J. T. Aberle and F. Zavosh, "Analysis of probe-fed circular microstrip patches backed by circular cavities," *Electromagnetics,* vol. 14, pp. 239-258, 1994.

[29] M. Qui and S. He, "High-directivity patch antenna with both photonic bandgap substrate and photonic band cover," *Microwave and Optical Tech. Lett.* vol. 30, no. 1, July 5, 2001.

[30] S. T. Jellet, A vehicle mounted antenna system for mobile satellite communications, Ph.D. Dissertation, The University of Queensland, March 1996.

[31] A. Kumar, Fixed and mobile terminal antennas, Artech House Inc., Boston, USA, 1991.

[32] F-R Yang, K-P Ma, Y. Qian and T. Itoh "A uniplanar compact photonic-bandgap (UC-PBG) structure and its applications for microwave circuits," *IEEE Trans. "Microwave Theory and Tech.*, vol. 47, no. 8, pp. 1509-1514, Aug. 1999.

[33] Dal Ahn, Jun-Seok Park, Chul-Soo Kim, Juno Kim, Y.Qian, and T. Itoh, "A design of the low-pass filter using novel microstrip defected ground structure," *IEEE Trans. Microwave Theory and Tech.*, vol. 49, no. 1, pp. 86-93, Jan. 2001.

[34] V. Radisic, Y. Qian, R. Coccioli, and T. Itoh, "Novel 2-D photonic bandgap structures for microstrip lines," *IEEE Microwave and guided wave lett.,* vol. 8 no. 2, pp. 69-71, Feb. 1998

[35] N.C. Karmakar and M. N. Mollah, "Investigations into nonuniform photonic-bandgap microstrip line filters," *IEEE Trans. Microwave Theory Tech.*, vol. 51, no. 2, pp. 564-572, Feb. 2003.

[36] Nemai C. Karmakar, and Mohammad N. Mollah, "Harmonic suppression of a bandpass filter using Binomially distributed photonic bandgap structures," *IEEE-APS,* Columbus, USA, July 2003.

[37] T. Akaline, M. A. G. Laso, T. Lopetgi, and O. Vanbesien, "PBG-type microstrip filters with one-end and two-sided patterns," *Microwave and Optical Tech. Lett.,* vol. 30, no. 1, July 5, 2001.

[38] D. Nesic and A. Nesic, "Bandstop microstrip PBG filter with sinusoidal variation of the characteristic impedance and without etching in the ground plane," Microwave *and Optical Tech. Lett.,* vol. 29, no. 6, June 20, 2001.

[39] Q. Xue, K. M. Shum and C.H Chan, "Novel 1-D photonic bandgap microstrip transmission line," *APS-International symposium, 2000, IEEE*, vol. 1, page(s), 354-356.

[40] W. Barnes, T. Priest, S. Kitson, and J. Sambles, "Physical origin of photonic energy gaps in the propagation of surface plasmas on gratings," *Phys. Rev. B. Condens. Matter*, vol. 54, pp. 6227–6244, 1996.

[41] S. Kitson, W. Barnes, and J. Sambles, "Full photonic band gap for surface modes in the visible," *Phys. Rev. Lett.*, vol. 77, pp. 2670–2673, 1996.

[42] A. Harvey, "Periodic and guiding structures at microwave frequencies,"*IRE Trans. Microwave Theory Tech.*, vol. 8, pp. 30–61, June 1959.

[43] S. Ramo, J. Whinnery, and T. Van Duzer, *Fields and Waves in CommunicationElectronics*, 2nd ed. New York: Wiley, 1984.

[44] Y. Qian *et al.* "Simulation and experiment of photonic band-gap structures for microstrip circuits," *1997 Asia pacific microwave conference,* pp. 585-588.

[45] N. C. Karmakar, M. N. Mollah, and S. K. Padhi, "Shared Aperture Photonic Bandgap Assisted Aperture Coupled Microstrip Patch Antenna For Satellite Communication," *Asia-Pacific Microwave Conference* (APMC 2002) *Proceedings*, vol. 2, pp. 1177-1180, Kyoto, Japan, 19- 22, November 2002.

[46] Y. Qian, R. Coccioli, F-R. Yang and T. Itoh "Passive and active component design using PBG," *Terahertz Electronics proceedings, 1998, IEEE sixth Int. Conf., pp.* 42-45.

[47] V. Radisic, Y. Qian, and T. Itoh, "Novel architectures for high-efficiency amplifiers for wireless applications," *IEEE Trans. Microwave Theory and Tech.* Vol.46. no. 11, pp. 1901-1909, Nov. 1998.

[48] F-R.Yang, Y. Qian, R. Coccioli, and T. Itoh, "A novel low-loss slow-wave microstrip structure," *IEEE Microwave and guided wave lett. v*ol. 8, no. 11, pp. 372-374, Nov. 1998

[49] C.Y. Hang, W.R Deal, Y. Qian, and T. Itoh "High efficiency transmitter front-ends integrated with planar antennas and PBG," *2000 Asia-Pacific Microwave Conf.* Australia.

[50] F-R. Yang, Y. Qian and T. Itoh, "A novel uniplanar compact PBG structure for filter and mixer applications," *Microwave Symposium Digest, 1999 IEEE MTT-S Int.,* vol. 3 page(s): 919-922.

[51] D. M. Pozar, *Microwave Engineering.* Reading, MA: Addison-Wesley, 1990.

[52] H. Shigesawa, M. Tsjui, and A. A. Oliner, "Conductor-backed slot line and coplanar waveguide: Dangers and full wave analyzes," *IEEE MTT-S Int. Microwave Symp. Dig.,* New York, May 25-27, 1988, pp. 199-202.

[53] J. Y. Park, C.-C. Chang, Y. Qian and T. Itoh, "An improved low-profile cavity-backed slot antenna loaded with 2D UC-PBG reflector," *IEEE-APS. Digest 2001,* pp. 194-197.

[54] C. Caloz, C.-C. Chang, Y. Qian, and T. Itoh, "A novel multilayer photonic band-gap (PBG) structure for microstrip circuits and antennas," *IEEE- APS. Digest 2001,* pp. 502-505.

[55] Y. Kown *et al.* "A 44-GHz monolithic waveguide plane-wave amplifier with improved unit cell design," *IEEE Trans. Microwave Theory Tech.* vol. 46, pp. 1237-1241, Sept.1998.

[56] M. Kim *et al.* "A rectangular TEM waveguide with photonic crystal walls for excitation of quasi-optical amplifiers," *IEEE MTT-S Microwave Symp. Dig.,* Anaheim, CA, June 13-19, 1999, pp. 543-546.

[57] F-R. Yang, K-P Ma, Y. Qian, and T. Itoh, "A novel TEM waveguide using uniplanar compact photonic bandgap (UC-BG) structures," *IEEE Trans. Microwave Theory and Tech.,* vol. 47, no. 11, pp. 2092-2098, Nov.1999.

[58] K.C. Gupta, "Design of frequency-reconfigurable rectangular slot ring antennas," *IEEE-APS Digest, pp.* 326, 2000.

[59] A. Fathy, A. Rosen, H. Owen, S. Kanamaluru, F. M. Ginty, D M. Gee and G. Taylor, "Silicon based reconfigurable antennas," *IEEE MTT-S Digest* 2001, pp. 377-380.

[60] J.T. Bernhard, R. Wang, R .Clark, and P. Mayes, "Stacked reconfigurable antenna elements for space-based radar applications," *IEEE MTT-S Digest* 2001, pp. 158-161

[61] M .N. Mollah and N. C. Karmakar, "A novel hybrid defected ground structure as low pass filter," Accepted for presentation in *IEEE APS-S International* 2004, Monterey, California, USA, June 20-26, 2004.

[62] Leltxu Garde, Miguel Javier Yabar, and Carlos del Rio, "Simple modeling of DGS to design 1D-PBG low-pass filter," *Microwave and Opt. Tech. Lett.,* vol. 37, no. 3, May 2003.

[63] H. W. Liu, Z. F. Li, and X. W. Sun, "A novel fractal defected ground structure and its application to the low-pass filter," *Microwave ant Opt. Tech. Lett.* vol. 39, no. 6 December 20, 2003.

[64] Y. Qian, F.R. Yang, and T. Itoh, "Characteristics of microstrip lines on a uniplanar compact PBG ground plane," *1998 Asia-Pacific Microwave Conf. Dig.,* pp.589-592, Dec. 1998.

[65] M. Rahman and M. A. Stuchly, "Transmission line-periodic circuit representation of planar microwave photonic bandgap structures," *Microwave and Opt. Tech. Lett.*, vol. 30, no. 1, July 5, 2001.

[66] I. J. Bahl and P. Bhartia, *Micorwave solid state circuit design*, Wiley, New York, 1998.

[67] Larkins, G. L Socorregut, R. Y.A. Vlasov, "Superconducting microstrip hairpin filter with BaTiO/sub 3/ patches," *IEEE Transactions* on *Applied Superconductivity,*, vol. 13 , no. 2 , pp. 724 – 726, June 2003.

[68] Chih-Ming Tsai, Sheng-Yuan Lee, Chin-Chuan Tsai, "Hairpin filters with tunable transmission zeros," *2001 IEEE MTT-S International Microwave Symposium Digest* vol. 3, pp. 2175 - 2178, May 2001.

[69] Bonetti, R. R. Williams A.E, "Preliminary design steps for thin-film superconducting filters," *IEEE MTT-S International Microwave Symposium Digest*, 1990, pp. 273-276, vol. 1, 8-10 May 1990.

[70] Yingjie Di, Gardner P, P. S Hall, H. Ghafouri-Shiraz, and Jiafeng Zhou, "Multiple-coupled microstrip hairpin-resonator filter," *IEEE Microwave and Wireless Components Letters, v*ol. 13 , no. 12 , pp. 532- 534, Dec. 2003.

[71] Deleniv, A.N. , Gashinova, M.S., Vendik, I.B., Eriksson, A., "Design of an interdigital hairpin bandpass filter utilizing a model of coupled slots," *IEEE*

Transactions on Microwave Theory and Techniques, vol. 50 , no. 9, pp. 2153 – 2158 Sept. 2002.

[72] Matthaei G.L., Fenzi N.O., Forse R.J., Rohfing S.M., "Hairpin-comb filters for HTS and other narrow-band applications," *IEEE Transactions on Microwave Theory and Techniques,* vol. 45 , no. 8, pp. 1226 -1231 Aug. 1997.

[73] Matthaei G.L., Fenzi, N.O., Forse R , Rohlfing S. , "Narrow-band hairpin-comb filters for HTS and other applications," *IEEE MTT-S International Microwave Symposium Digest*, 1996, vol. 2. pp. 457 – 460.

[74] Di, Y., Gardner P., Hall P.S., Ghafouri-Shiraz H., "Multiple-coupled microstrip hairpin-resonator filter," ICMMT 2002, 3rd International Microwave and Millimeter Wave Technology, pp. 1051 – 1054.

[75] M. A.G. Laso, T. Lopetegi, M .J. Erro, D. Benito, M. J. Garde, and M. Sorolla, "Novel wideband photonic bandgap microstrip structures," *Microwave and Opt. Tech. Lett*. vol. 24, no. 5, March 5, 2000.

[76] C.A. Balanis, *Antenna Theory Analysis and Design,* 2nd edition, John Wiley, New York, USA, 1997.

[77] M. N. Mollah and N. C. Karmakar "Optimum Filling Factor and Performance of a Transmission Line at X-Band Perturbed by Binomially Distributed Photonic Bandgap (PBG) Structure," *PACRIM-2003,* Canada.

[78] Mohammad Nurunnabi Mollah and Nemai Chandra Karmakar "Investigation into Planar Photonic bandgap Structures," *Asia-Pacific Microwave Conference (APMC)-2003,* Korea, Nov. 4-7, 2003.

[79] N. C. Karmakar and M N .Mollah, "Microstrip lines on annular-ring photonic bandgap structures," *Microwave and optical Tech. Lett.,* vol. 32, no. 6, pp. 431-433, March 20, 2002.

[80] Hai-Wen Liu, Xiao-Wei Sun, and Zheng-Fan Li, "A low-pass filter of wide stopband with a novel multilayer fractal photonic bandgap structure," Microwave *and Opt. Tech. Lett.,* vol. 40, no. 5, March 2004

[81] F.R. Yang, R. Coccioli, Y. Qian, and T. Itoh, "PBG assisted gain enhancement of patch antennas on high dielectric constant substrate," *IEEE-APS Digest 1999*, pp. 1920-1923.

[82] M. Fallah-Rad and L. Shafai, "Mode control in microstrip patch antenna using ground plane perforations," *Microwave and Opt. Tech. Lett.,* vol. 37, no. 2, pp. 103-107 April 20, 2003.

[83] Nanbo Jin, Ang Yu, and Xuexia Zhang, "An enhanced 2×2 antenna array based on a dumbell EBG structure," *Microwave and Opt. Tech. Lett.* vol. 39, no. 5, pp. 395-399 Dec. 5 2003.

[84] Yen- Liang Kuo, Tzung-Wern Chiou, and Kin -Lu Wong, "A dual- band rectangular microstrip antenna using a novel photonic bandgap ground plane of unequal orthogonal periods, " *Microwave and Opt. Tech. Lett.* vol. 30, no .4, pp. 280-283, Aug. 20, 2001.

[85] M. Rahman and M. A Stuchly, "Wide band microstrip patch antenna with planar PBG structure," *IEEE-APS Digest 2001*, pp. 486-489.

[86] Xiao-Hai Shen, Peter Delmotte, and Guy A. E. Vandenbosch, "Enhancing the gain of microstrip antennas at different frequencies with one substrate-supersubstrate structure," *Microwave and Opt. Tech. Lett.* vol. 27, no. 1, pp. 37-40, Oct. 5 2000.

[87] Hung-Yu David Yang, Nicolaos G. Alexopoulos, and Eli Yablonovitch, "Photonic bandgap materials for high-gain printed circuit antennas," *IEEE Trans. Antennas. Propgat.,* vol. 45, no.1, pp. 185-187, January 1997.

[88] Raman Gonzalo, Beatriz Martinez, Peter de Maagt, and Mario Sorolla, "Improved patch antenna performance by using photonic bandgap substrates," *Microwave and Opt. Tech. Lett.* vol. 24, no. 4, pp. 213-215, Feb. 20, 2000.

[89] J.S Colburn and Y. Rahmat-Samii, "Printed antenna pattern improvement through substrate perforation of high dielectric constant material: An FDTD evaluation," *Microwave and Opt. Tech. Lett.* vol. 18, no. 1, pp. 27-32, May 1998.

[90] Elliott R. Brown, "On the gain of a reconfigurable-aperture antenna", *IEEE Trans. Antennas. Propgat.,* vol. 49, no. 10, pp. 1357-1362, Oct. 2001.

[91] T.H. Liu, W. X. Zhang, M. Zhang, and K. F. Tsang, "Low profile spiral antenna with PBG substrate," *IEE Electronics Letters*, vol. 36, no. 9, pp. 779-780, April 2000.

[92] G. Poilasne, J. Lenormand, P. Pouliguen, K. Mahdjoubi, C. Terret, and Ph. Gelin, "Theoretical study of interactions between antennas and metallic photonic bandgap materials," *Microwave and Opt. Tech. Lett.,* vol. 15, no. 6, pp. 384-389, Aug.,1997.

[93] M. Thevenot, M.S Denis, A. Reineix, and B. Jecko, "Design of a new photonic cover to increase antenna directivity," *Microwave and Opt. Tech. Lett.* vol. 22, no. 2, pp.136-139, July 1999.

[94] Andrey S. Andrenko, Yukio Ikeda, and Osami Ishida, "Application of PBG microstrip circuits for enhancing the performance of high density substrate patch antennas," *Microwave and Opt. Tech. Lett.* vol. 32, no. 5, pp. 340-343, March 2002.

[95] Shun-Yun Lin, and Kin-Lu Wong, "A conical pattern annular ring microstrip antenna with a photonic bandgap ground plane," *Microwave and Opt. Tech. Lett.* vol. 30, no.3, pp.159-161, August 2001.

[96] C. Serier, C. Cheype, R. Chantalat, M. Thevenot, T. Monediere, A. Reineix, and B. Jecko, "1-D photonic bandgap resonator antenna," *Microwave and Opt. Tech. Lett,.* vol. 29, no. 5, pp. 312-315 June 5, 2001.

[97] A. Griol, D. Mira, J. Marti, and J. L. Corral, "Harmonic suppression in microstrip multistage coupled- ring bandpass filters using defected ground plane," *Microwave and Opt. Tech. Lett.* vol. 39, no. 5, pp. 351-354, Dec. 5, 2003.

[98] V. Radisic, Y. Qian, and T. Itoh, "Broad band power amplifier using dielectric photonic bandgap structure," *IEEE Microwave and guided wave lett.,* vol.8, no.1, pp. 13-14, Jan.1998.

[99] P.B. Katehi, and N. G. Alexopoulos, "On the modeling of electromagnetically coupled microstrip antennas-The printed strip dipoles," *IEEE Trans. Antennas. Propgat.,* vol. 32, no. 11, pp. 1179-1186, Nov. 1984.

[100] J. R. James, and P.S. Hall, *Handbook of microstrip antennas*, vols. 1 and 2, Peter Peregrinus, London, UK, 1989.

[101] G. Gronau and I. Wolff, "Aperture coupling of a rectangular microstrip resonator," *Electronics Letters*, vol. 22, pp. 554-556, May 1986.

[102] D. M. Pozar, and B. Kaufman, "Increasing the bandwidth of a microstrip antenna by proximity coupling," *Electronics Letters*, vol. 23, pp. 368-369, April 1987.

[103] D. M. Pozar, "Microstrip antennas," *Proc. IEEE*, vol. 80, no. 1, pp. 79-81, Jan. 1992

[104] T. Itoh, "Spectral domain immittance approach for dispersion characteristics of generalized printed transmission lines," *IEEE Trans. Microwave Theory Tech.,* vol. 28, no. 7, pp. 733-736, July 1980.

[105] Mohammad Nurunnabi Mollah, Nemai Chandra Karmakar and Jeffrey Shiang Fu, "Investigation Into Novel Tapered Hybrid Defected Ground Structure (DGS)," Accepted to be published in International Journal of RFMiCAE. Ref. No: B1779.

[106] A. K. Bhattacharyya, "A numerical model for multilayered microstrip phased array antennas," *IEEE Trans. Antennas. Propgat.,* vol. 44, no. 10, pp. 1386-1392, Oct. 1996.

[107] A. K. Bhattacharyya, "A modular approach for probe fed and capacitively coupled multilayered patch arrays," *IEEE Trans. Antennas. Propgat.,* vol. 45, no. 2, pp. 193-202, Feb. 1997.

[108] A. K. Bhattacharyya, "Analysis of multilayer infinite periodic array structures with different periodicities and axes orientations," *IEEE Trans. Antennas. Propgat.,* vol. 48, no. 3, pp. 357-369, March. 2000.

[109] N. I. Herscovici, and D. M. Pozar, "Analysis and design of multilayer printed antennas: A modular approach," *IEEE Trans. Antennas. Propgat.,* vol. 41, no. 10, pp. 371-1378, Oct. 1993.

[109] Robert W. Jackson, and D. M. Pozar, "Full wave analysis of microstrip open end and gap discontinuities," *IEEE Trans. Microwave Theory Tech.,* vol. 33, no.10, pp.1036-1042, Oct.1985.

[110] Raj Mittra, Chi H. Chan, and Tom Cwik, "Techniques for analyzing frequency selective surfaces- A review," Proceedings of the *IEEE,* vol. 76, no. 12, pp. 1593-1615, Dec. 1988.

[111] Rafael Pous, and D. M. Pozar, "A frequency selective surface using aperture coupled microstrip patches," *IEEE Trans. Microwave Theory Tech.,* vol. 39, no. 12, pp. 1763-1769, Dec. 1991.

[112] Elliot R. Brown, "RF-MEMS switches for reconfigurable integrated circuits," *IEEE Trans. Microwave Theory Tech.*, vol. 46, no. 11, pp. 1868-1880, Nov. 1998.

[113] M. E. Biakowski and N.C. Karmakar, "High performance L-band pin diode switches for base station antennas with reconfigurable sector capability," APMC *'01*, Taipei, Taiwan, December 3~6, 2001.

[114] Shyh-Chiang *et al.*, "Low actuation voltage RF MEMS switches with signal frequencies from 0.25 GHz to 40 GHz," *IEDM Technical Digest'99*, Electron Devices Meeting, 1999, pp. 689-692.

[115] Jeremy B. Muldavin *et al.*, "30 GHz tuned MEMS switches," *Microwave Symposium Digest*, 1999 *IEEE MTT-S International,* vol. 4, 199, pp. 1511-1514.

[116] Jeremy B. Muldavin *et al.*, "High-isolation CPW MEMS shunt switches-part 1: Modeling," *IEEE Trans. Microwave Theory Tech.,* vol. 48, no. 6, pp. 1045-1052, June 2000.

[117] Jeremy B. Muldavin *et al.*, "High-isolation CPW MEMS shunt switches-part 2: Design," *IEEE Trans. Microwave Theory Tech.,* vol. 48, no. 6, pp. 1053-1056, June 2000.

[118] Jad Rizk *et al.*, "High-isolation W-band MEMS switches," *IEEE Microwave and Wireless Components Letters,* vol. 11, no. 1, pp. 10-12, Jan. 2001.